IMPACT OF FAULTS AND FAULT DAMAGE ZONES ON LARGE OPEN PIT SLOPES

by

JORDAN MELVIN SEVERIN

B.Sc., The University of Waterloo, 2001

M.Sc., The University of British Columbia, 2004

A THESIS SUBMITTED IN PARTIAL FULFILLMENT OF

THE REQUIREMENTS FOR THE DEGREE OF

DOCTOR OF PHILOSOPHY

in

THE FACULTY OF GRADUATE AND POSTDOCTORAL STUDIES

(Geological Engineering)

THE UNIVERSITY OF BRITISH COLUMBIA

(Vancouver)

March, 2017

ABSTRACT

The demand for metals combined with diminishing near surface resources has prompted the increasing development of complex and unprecedented open pit designs to recover deeper resources. These designs include pushback extensions, intentional over-steepening of toes, or the transition to underground retreat or mass mining methods. While past designs rarely involved pit depths exceeding 500 m, steeper and deeper designs approaching or exceeding 1000 m are now considered. Experiences with large open pits demonstrate that complex failure mechanisms occur with higher propensity within these slopes.

New technologies used to monitor slope displacement, such as radar interferometry, along with increased real-time data processing have given engineers more data and faster tools to investigate the fundamental rock mechanics that occur within large slopes. Radar allows for the collection of large amounts of real-time data with millimeter precision. Emphasis is given in this thesis to the use of radar monitoring in resolving displacements in proximity to fault damage zones. Research was conducted to develop and execute a first of its kind 3-D radar experiment involving the simultaneous deployment of two radar systems. This experiment demonstrates that valuable knowledge, in the form of a 3-D displacement map, was used to resolve the influence of large fault zones in promoting complex slope deformation kinematics and failure mechanisms.

In parallel, numerical modelling continues to develop as a key tool in understanding deep-seated rock slope deformation mechanisms. Research was conducted to investigate the characterization and representation of key fault properties within sensitivity analyses used to provide guidance on the impact of simplification of these complex structures. Representative geometries and input parameters based on case studies were used to show the influence of fault location, orientation and complexity, on stress heterogeneity created by the interaction between faults and deepening large open pits, as well as the transition to underground mass mining. These interactions can create zones of plastic shear strain or extensional strain damage not typically accounted for in most stability analyses. The inclusion of stress heterogeneity and subsequent rock mass damage is shown to modify the observed mechanisms of slope movement and allow previously unviable kinematics to develop.

PREFACE

Chapter 3 “Detection of Differential Pit Slope Displacement near Fault Structures” was co-authored by Jordan Severin, Dr. Erik Eberhardt, Lorenzo Leoni of IDS (Ingegneria Dei Sistemi), and Sebastien Fortin of THVC (Teck Highland Valley Copper). As the lead author, Mr. Jordan Severin was responsible for the design and implementation of the radar experiment on site as well as the data analysis from the two radar instruments, and re-interpretation of pit slope displacement mechanics. Dr. Eberhardt provided guidance in the development of the experiment and reviewed the data interpretation as well as the manuscript and provided editorial comments. Mr. Leoni provided guidance in the set up and analysis of the radar data and provided editorial comments. Mr. Fortin provided access to the experiment site, overview to the slope displacement mechanics, and editorial guidance and permission to publish the data.

Chapter 4 “Variation of Stress Heterogeneity near Faults in Large Open Pits” was co-authored by Jordan Severin and Dr. Erik Eberhardt. Mr. Severin identified and designed the research program, which was developed in conjunction with a NSERC Collaborative Research and Development grant led by Drs. Eberhardt and Stead in partnership with Rio Tinto. Mr. Severin performed the numerical modelling, completed the analysis of the results and prepared the manuscript. Dr. Eberhardt, reviewed the manuscript and provided editorial comments.

Chapter 5 “Impact of Fault Characterization and Representation of Faults and Fault Damage Zones in Large Open Pit Slopes” was co-authored by Jordan Severin, and Dr. Erik Eberhardt. Mr. Severin designed the numerical analyses program, performed the research, data review and 3-D numerical modelling, and prepared the manuscript. Dr. Eberhardt provided review of the numerical modelling and provided editorial comments for the manuscript.

Chapter 3 has been published in the scientific journal “Engineering Geology” and Chapters 4 and 5 are currently in preparation for journal submission.

- Severin, J., Eberhardt, E., Leoni, L. & Fortin, S. (2014). Development and application of a pseudo-3D pit slope displacement map derived from ground-based radar. *Engineering Geology*: 181, 202-211.

- Severin, J. & Eberhardt E. (2017). Influence of stress heterogeneity on large open pit slopes. To be submitted.

- Severin, J. & Eberhardt E. (2017). Importance of characterization and representation of faults and fault damage zones in large open pit stability models. To be submitted.

Portions of the work included within Chapters 4 and 5 have been presented at the following technical conferences:

- Severin, J., Eberhardt, E., Ngidi, S. & Stewart, A. (2009). Importance of understanding 3-D kinematic controls in the review of displacement monitoring of deep open pits above underground mass mining operations. In *Rock Engineering in Difficult Conditions, Proceedings of the 3rd Canada–US Rock Mechanics Symposium, Toronto, 9-15 May 2009*. Edited by M. Diederichs & G. Grasselli. Canadian Rock Mechanics Association, e-Paper, 3914, 12 pp;

- Severin, J., Eberhardt, E. & Woo, K. (2010). Influence of major fault zones on 3D ground deformations caused by open pit block cave interactions. In *Caving 2010, Proceedings of the 2nd International Symposium on Block and Sublevel Caving, Perth, 20-22 April 2010*. Edited by Y. Potvin, Australian Centre for Geomechanics, Perth, pp. 205-216;

- Severin, J.M. & Eberhardt, E. (2012). Influence of stress path during the transition from open pit to block cave mine: A Palabora example. In *MassMin 2012: Proceedings of the 6th International Conference and Exhibition on Mass Mining, Sudbury, 10-14 June 2012*. Canadian Institute of Mining, e-Paper 6794, 9 pp.

TABLE OF CONTENTS

Abstract ii
Preface iii
Table of Contents v
List of Tables viii
List of Figures ix
List of Equations xvi
List of Principal Symbols and Abbreviations xvii
Acknowledgements xix
Dedication xx

CHAPTER 1 Introduction 1
1.1. Problem Statement 1
1.2. Research Objectives 4
1.3. Thesis Structure 6

CHAPTER 2 Background Information and Methodology 8
2.1. Open Pit Mining Slope Monitoring Techniques 8
2.1.1. Geodetic Prism Monitoring 9
2.1.2. Radar Monitoring 10
2.2. Stress Analysis and Stress Distribution 15
2.2.1. Near Open Pit Excavations 15
2.2.2. Near Geological Structures 17
2.3. Relevant Failure Criterion 19
2.3.1. Plastic Shear Strain and Strain Softening 20
2.3.1. Extensional Strain and Brittle Fracture Damage 21
2.4. Numerical Modelling – Current State of Practice 24
2.5. Research Methodology 27

CHAPTER 3 Detection of Differential Pit Slope Displacement near Fault Structures 29
3.1. Structural Control of Slope Displacements in Brittle Rock at Palabora* 29
3.1.1. Introduction 29

3.1.2. Interpretation of Geodetic Pit Slope Monitoring Data 30
3.2. Development and Application of a Pseudo-3D Pit Slope Displacement Map Derived from Ground-Based Radar* 33
3.2.1. Introduction 33
3.2.2. Slope Monitoring Techniques 34
3.2.3. Full Spatial Detection of a Slope 36
3.2.4. Data Analysis 39
3.2.5. Displacement Map Generation 42
3.2.6. Potential Sources of Error 42
3.2.7. Three-Dimensional Displacement Pattern 43
3.2.8. Pit Slope Kinematics 47
3.3. Radar Experiment Conclusions 50
3.4. Chapter Summary 51

CHAPTER 4 Influence of Stress Heterogeneity on Large Open Pit Slopes 52
4.1. Introduction 52
4.2. Induced Stresses and Open Pit Mining 54
4.3. Investigation of Regional-Scale Stress Heterogeneity Factors 57
4.3.1. In-Situ Stress Regime 57
4.3.2. Topography 61
4.4. Investigation of Pit Scale Stress Heterogeneity Factors 64
4.4.1. Pit Geometry 64
4.4.2. Pit Depth 67
4.5. Investigation of Wall Scale Stress Heterogeneity Factors 69
4.5.1. Rock Mass Strength and Lithology Variations 69
4.5.2. Faults and Tectonic Damage Zones 72
4.6. Case History – Influence of Stress Heterogeneity on Palabora Pit Slope Failure 82
4.6.1. Impact of Fault Representation on Scale Stress and Damage at the Pit Wall Scale 90
4.6.2. Local Pit Wall Response to Fault Representation 93
4.7. Discussion - Implications of Stress Heterogeneity 95
4.7.1. Open Pit Design 95
4.7.2. Mine Plan / Excavation Sequence 98
4.8. Key Findings and Design Recommendations 103

CHAPTER 5 Importance of Characterization and Representation of Faults and Fault Damage Zones in Large Open Pit Slope Stability Models 106
5.1. Introduction 106
5.2. Fault Representation in Numerical Analyses 108
5.2.1. Fault Characterization and Properties 110
5.2.2. Representation of Fault Zone Composition 112
5.2.3. Representation of Fault Complexity 114
5.2.4. Influence of Fault Strength Contrast with Host Rock 115
5.2.5. Influence of Fault Thickness 119
5.2.6. Influence of Fault Location Relative to its Intersection with the Pit Wall Face 123
5.2.7. Influence of Fault Angle 127
5.2.8. Summary of Sensitivity Analyses 129
5.3. Modelling of Fault Development within a Numerical Slope Stability Analysis 130
5.3.1. Modelling Procedure 130
5.3.1. Stage 1: Modelling of Fault Development 131
5.3.1. Stage 2: Modelled Stress Heterogeneity and Influence on Modelled Slope Performance 133
5.4. Case History - Teck Highland Valley Copper Mine 136
5.4.1. Background and Pit Slope Behaviour 136
5.4.2. Fault Properties and Potential Damage 137
5.4.3. Lornex Modelling Results 139
5.5. Chapter Summary and Key Findings 147

CHAPTER 6 Conclusions and Recommendations for Further Work 150
6.1. Summary of Conclusions 150
6.2. Future Work 156
References 157

LIST OF TABLES

Table 4.1. FLAC3D properties used for in-situ stress sensitivity modelling 59
Table 4.2. FLAC3D properties used for topography sensitivity modelling 62
Table 4.3. FLAC3D model input parameters for comparative analysis of pit geometries and in-situ stress ratios 66
Table 4.4. FLAC3D properties used for pit depth sensitivity modelling 68
Table 4.5. FLAC3D Lithological stiffness sensitivity model parameters 71
Table 4.6. FLAC3D Fault model properties 74
Table 4.7. FLAC3D properties used to evaluate stress development near faults for different fault stiffnesses 77
Table 4.8. UDEC plan section model properties (THVC) 81
Table 4.9. 3DEC rock mass and caved rock input properties for the Palabora case study analysis 87
Table 4.10. 3DEC input properties for the major faults explicitly represented in the Palabora case study analysis 87
Table 5.1. UDEC fault composition sensitivity model parameters 113
Table 5.2. FLAC3D input properties used in sensitivity analyses investigating fault strength contrast 116
Table 5.3. FLAC3D fault strength sensitivity results 116
Table 5.4. FLAC3D input properties for investigation of model sensitivity to fault zone thickness 121
Table 5.5. FLAC3D model properties used in modelling of tectonic structures present in the Lornex west wall, and subsequent modelling of fault interaction with pre-mining stress initialization and pit slope excavation 133
Table 5.6. FLAC3D model rock mass parameters used in the tectonic stability models 135
Table 5.7. UDEC model input rock mass parameters for the THVC Lornex pit case study (based on Piteau, 2005) 138
Table 5.8. UDEC rock mass properties for blocks in the Voronoi modelling of the Lornex Pit (THVC) case study 142
Table 5.9. UDEC joint properties for discontinuities in the Voronoi modelling of the Lornex Pit (THVC) case study. The random discontinuities represent Voronoi segments along which intact rock bridge fracturing can be simulated 142

LIST OF FIGURES

Figure 1.1. Frequency and depth of current and proposed open pit mines based on contributing Large Open Pit (LOP) project participating companies. 1

Figure 1.2. Quickbird image of 2004 North wall failure at Palabora. Note the proximity of access shafts to the crest of the East wall to the right of the image. 3

Figure 2.1. Examples of typical geodetic monitoring data including: a) cumulative displacement rate plot, and b) wander (x-y) plot used at the Palabora Mine 10

Figure 2.2. Resolution concept of IBIS-L synthetic aperture radar. 13

Figure 2.3. Comparison of site photo and recorded displacement from radar. a) Photo of IBIS-L monitoring displacements in a quarry, Dieburg. b) Mean amplitude of observed scene. . 14

Figure 2.4. Generalized distribution and orientation of stress around an open pit: a) section view of a 300m open pit, b) section view of a 900m depth open pit, c) plan section through an elliptical shaped open pit at mid-slope and d) a kidney shaped open pit..... 16

Figure 2.5. Fault separated in-situ stress domains at the URL (from Martin, 1990) including changes in a) orientation, b) magnitude and c) stress ratio between maximum and minimum horizontal stress. 18

Figure 2.6. Composite failure envelope for damage initiation and spalling (from Diederichs 2007) proposed for tunneling and underground mining environments. 22

Figure 3.1. 3-D structural model of the Palabora open pit with regional faults indicated. North is towards the top. The outline of the 2004 pit wall failure is shaded red..... 30

Figure 3.2. Prism data review indicating both spatial and temporal control of faults on rock mass displacements. a) West wall displacement vectors before block caving (shown in green) and after (shown in red); b) Relative timing of displacement of prism toward failure zone (red = crown de-stressing, green = +3 months, orange = +6 months). 32

Figure 3.3. Geographic location of study site, Teck Highland Valley Copper mine (left) with aerial view of Lornex and Valley Pits (right) [online image]. Retrieved December 5, 2009 from http://www.trcr.bc.ca/report-33rd-annual-mine-reclamation-awards. 36

Figure 3.4. West wall of the Lornex Pit at the Teck Highland Valley Copper mine, showing the location of the Lornex Fault Zone, and graben-like backscarps and toe bulging that has developed with pit wall movements..... 37

Figure 3.5. Location of operational geodetic prisms on the northwest wall Lornex and the radar monitoring experiment sites 38

Figure 3.6. Site preparation and installation of the IBIS-M radar unit for the 3-D radar experiment, showing: leveling and grading of gravel site pad, lifting of concrete filled drums for radar base, fitting of leveled radar guide rail, and radar positioning for pit wall monitoring. 39

Figure 3.7 Determination of pseudo-3D vector (green) resolved from the line-of-sight vectors (A and B) and a weighted elevation assumption along the line of intersection between planes normal to A and B. Also shown is the average elevation option. 41

Figure 3.8. Measured line-of-sight displacement patterns from experiment site locations. Note that a minimum cut-off value of 30cm was used to reduce the background noise..... 44

Figure 3.9. Displacement pattern of data set combined from Sites A and B. Several distinct zones are identified (i, ii and iii), as described in the text. 46

Figure 3.10. Vector map of the data combined from Sites A and B, with vectors scaled to displacement magnitudes to show direction of movement. Left diagram shows an enlarged view of the lower slope (approximately 125 × 125 m)..... 47

Figure 3.11. Oblique view of the Lornex Pit northwest corner, highlighting areas of higher displacement and movement directions. a) displacement magnitude, b) average azimuth (trend) of displacement vector, c) average plunge of displacement vector, and d) interpreted pit kinematics of the northwest corner of the Lornex Pit. 48

Figure 3.12. Schematic diagram of interpreted kinematics for the northwest wall of the Lornex Pit. Note that the measure displacement vectors have been overlaid on the pit slope surface. 49

Figure 4.1. Generalized stress distributions and orientations for a 600-m high, 45°, homogeneous, open pit slope, showing maximum principal stress (top), minimum principal stress (middle) and principal stress trajectories (bottom)..... 55

Figure 4.2. Factors identified as contributing to stress heterogeneity near open pits ranging from regional scale to local wall scale. 56

Figure 4.3. Compilation of measured principal stress magnitudes in terms of: a) horizontal to vertical stress ratio for several mining-focused countries (Hoek and Brown, 1980), and b) maximum principal stresses for the Canadian Shield (Mahoney, et al., 2006)..... 58

Figure 4.4. Fault separated in-situ stress domains at the URL (from Martin, 1990) including changes in a) orientation, b) magnitude and c) stress ratio between maximum and minimum horizontal stress..... 59

Figure 4.5 FLAC3D model geometries and finite difference meshes used for in-situ stress sensitivity modelling with slope heights of 300, 600, and 900m. 60

Figure 4.6. Deviatoric stress magnitudes with varying in-situ stress regime and pit depth. Note that the increase in deviatoric stress is greater with increased pit depth compared to increased horizontal stress ratios. 61

Figure 4.7. Oblique plan view (top) and section view (middle) of FLAC3D analyses comparing maximum principal stresses (bottom) for an excavated pit within a flat topography and undulating topography..... 63

Figure 4.8 FLAC3D deviatoric stresses for topographic sensitivity analyses, oblique (top) and section (bottom) views. Note the similarity in deviatoric stress patterns at the bottom of the pit and the variation near the pit crest. Compression is negative. 64

Figure 4.9. Modelled stress distributions (in plan) relative to the geometries and in-situ stress field orientation for several actual open pit geometries. These include: a) HVC's Lornex pit, b) preliminary Mine A open pit design, c) Palabora, and d) preliminary Mine B design. Cooler colors reflect relaxation stresses and the warmer colours reflect stress concentrations..... 65

Figure 4.10. Stress heterogeneity near elongated and circular pits for varying in-situ stress regimes. The relative increase in stress development is greater for the elongated pit geometry with changes in the direction of the principal stresses. Compression is negative. 67

Figure 4.11. Maximum principal stresses (σ_1) calculated for a 300 m (top), 600 m (middle) and 900 m (bottom) open pit slope height. Mining induced stress concentration at the toe of the slope is shown. Note that compression is negative. 68

Figure 4.12. Induced mining stress (i.e., stress change above the pre-mining stress state) located at the toe of the slope as a function of pit depth..... 69

Figure 4.13. Model set up to determine sensitivity of stress heterogeneity development to relative lithological stiffness. Models were run with either weaker or stiffer materials in the bottom half of the slope..... 70

Figure 4.14. Deviatoric stresses created within slopes containing varying lithological stiffness as a function of pit depth. Slopes with stiffer material within the toe developed significantly higher stresses. 72

Figure 4.15. Areas of low and high stress modelled around natural fault systems (after Tanno, 2010). 73

Figure 4.16. Model set-up to review stress development with and without the presence of a 60m wide fault zone bisecting the slope..... 74

Figure 4.17. Minimum principal stresses (above) and extensional strains (below) around an open pit slope for a homogenous rock mass (left) and one bisected by a 60 m wide fault zone (right). Note that compression is negative..... 76

Figure 4.18. Maximum principal stresses (above) and plastic shear strains (below) around an open pit slope for a homogenous rock mass (left) and bisected by a 60 m wide fault zone (right). Note that compression is negative..... 76

Figure 4.19. Example of minimum principal stresses showing areas of low confinement (purple) arising due to fault stiffness contrast with surrounding rock mass and excavation of the open pit. Compression is negative..... 78

Figure 4.20. Maximum stress observed at the toe of the slope for a 600m high pit slope, and its variation as a function of deformation modulus of a fault zone bisecting the slope wall. 79

Figure 4.21. Depth of low confinement stress within the hanging wall and footwall of a 600m high pit slope as a function of fault zone stiffness..... 80

Figure 4.22. UDEC modelled stress contours plotted for a plan section view through the mid-slope elevation of the Lornex Pit without (left) and with (right) the inclusion of tectonic faults explicitly included in the model. Compression is negative. 81

Figure 4.23. a) 3-D spatial relationship between the underground operations, open pit, and Mica Fault; and b) 2008 Quickbird image of Palabora northwest wall failure. 83

Figure 4.24. 3-D structural model of the Palabora open pit with regional faults indicated. North is towards the top. The outline of the 2004 pit wall failure is shaded red..... 84

Figure 4.25. 3DEC Palabora model geometry shown as an oblique view (top), and cross-section (bottom). Shown are the key rock units and structures explicitly included in the model. Location of plan section view shown in subsequent figures is indicated. 85

Figure 4.26. Cave propagation geometries developed for implementation in the 3DEC Palabora case study model. 86

Figure 4.27. Maximum shear stresses (Pa), without and with the inclusion of the mapped faults, plotted for a horizontal plan view through the upper half of the pit slope (150 m below surface). The plan section location is shown in Figure 4.25. 88

Figure 4.28 3DEC results for the Palabora case study showing the minimum principal stresses (in Pa) for a cross-section view, comparing the influence of including the mapped faults to the base case without faults. Shown are the results for three time intervals from the end of the pit life, to cave breakthrough in 2004, to the cave extent in 2010. Note that compression is negative. 89

Figure 4.29. 3DEC modelled displacement magnitudes (in m) projected in plan view onto a plane at 50 m depth (left) and onto a cross-sectional view through the North pit face (right), for the Palabora case study at its 2010 cave extent. Shown are results for both the base model without faults (top) and model with faults included (bottom). 90

Figure 4.30. Section views of the pit, fault and cave geometries modelled in 3DEC for the following geometries: A) without faults (continuum treatment), B) faults as distinct breaks, and C) fault zones, either represented by an equivalent continuum of weaker material or as a discontinuum of multiple fractures..... 91

Figure 4.31. Stress history location points within north wall of the Palabora mine model. 92

Figure 4.32. Response of stress orientation to block cave mining, comparing modelling of the faults as zones as in Figure 4.30c (above) and as discrete discontinuities as in Figure 4.30B (below) for the 3DEC mine-scale case study models of Palabora. Stress orientation histories are those for the north wall, showing direction of maximum (σ_1) and intermediate (σ_2) stress, with minimum stress (σ_3) estimated as vertical. 93

Figure 4.33. 10x10x10m 3DEC blocks used to estimate the amount of rock damage within the Palabora Pit north wall for the following joint conditions; A) GSI=75 Random, B) GSI = 50 Random, C) GSI=75 Anisotropic, D) GSI=50 Anisotropic. 94

Figure 4.34. Maximum shear stress and % volume of yielded elements within the 10x10x10m blocks (as shown in Figure 4.33). Line graphs are shown with maximum shear stress observed in the model. Bar graphs are shown for the volume of rock yielded in shear (bar) for models with faults composed of weakened materials and those including a thick blocky fault zone. 95

Figure 4.35. Areas of damage caused by excavation dilation within a 900m pit 97

Figure 4.36. Mine excavation strategies modelled to investigate the impact of mine pushback direction including a) vertical excavation without interim mine phase, b) excavation perpendicular to fault intersection within interim phases developed away from fault, c) excavation parallel to fault with interim phases developed toward fault, and d) excavation toward fault without further deepening. 99

Figure 4.37. Section view of the temporal evolution of open pit mining induced stress heterogeneity near a fault. Plotted are the minimum principal stresses, with compression negative. Note purple region denotes area of low confinement. 100

Figure 4.38. Comparison of deviatoric stresses (σ_1-σ_3) arising due to fault-pit interactions using previously identified mine sequencing strategies (see Figure 4.36) as modelled in FLAC3D. 101

Figure 4.39. Comparison of maximum depth of extensional strain arising from fault-pit interactions using different mine sequencing strategies for a 900-m high pit slope. 102

Figure 5.1. Examples of how faults are typically represented in continuum analyses (in this case using FLAC3D): a) as a zone of weak elasto-plastic rock, or b) as rock with a preferential direction of weakness via a ubiquitous joint model. 109

Figure 5.2. Examples of how faults can be represented in discontinuum analyses (in this case UDEC): a) as a zone of contrasting rock mass properties like that used in continuum analyses, b) as a discrete discontinuity that can open, close or slip, and c) as a combination of discrete fractures and yieldable blocks that represent a central discontinuity (i.e., fault) and adjacent tectonic damage zones. 109

Figure 5.3. Critical fault elements investigated with numerical analysis considered as fault characteristics (as identified in the field), typical numerical simplifications made during modelling, and potential design changes that can be adapted based on modelled wall performance. 111

Figure 5.4. UDEC model results plotting maximum principal stresses (σ_1), indicating influence of fault material representation on stress heterogeneity. The example shown here is from the Palabora Mine. Note that only the representation of the Mica Fault material was modified in this model. Compression is negative. 113

Figure 5.5. Shear displacement (in m) along the faults for a UDEC model treating the fault as an equivalent continuum zone (left) and as a discontinuum zone (right). 114

Figure 5.6. Influence of fault shape complexity (non-planarity) on maximum principal stress (σ_1) perturbations developing around a network of faults. Example shown here is from the Palabora Mine. Note that all faults were modified in this model. Compression is negative. 115

Figure 5.7. Potential extensional damage area within a 600-m high pit slope, for the bounding cases of a strong fault (GSI =55, light blue trace) and weak fault (GSI = 15, dark blue trace). 117

Figure 5.8. Side by side comparison of extensional damage regions, for pit slope heights of 300, 600, and 900 m, associated with upper bound (GSI = 55, blue) and lower bound (GSI = 15, red) fault strengths. 118

Figure 5.9. Depth of potential extensional (dashed line) and plastic shear (solid line) damage areas with respect to pit height as a function of relative fault strength and pit height. 119

Figure 5.10. FLAC3D model set up for sensitivity analysis of fault zone thickness. 120

Figure 5.11. Minimum principal stresses (top) and maximum shear stress (below), in Pa, for a 600 m high pit slope comparing different fault thicknesses (10, 40m and 80m). Note that compression is negative. 121

Figure 5.12. Minimum principal stress (top) and maximum shear stress (below), in Pa, for a 900 m high pit slope comparing different fault thicknesses (10, 40m and 80m). Note that compression is negative. 122

Figure 5.13. Depth of potential extensional strain (dashed line) and plastic shear (solid line) damage zones with respect to fault thickness for 600 and 900 m slope heights. 123

Figure 5.14. Model geometry for the FLAC3D fault intersection sensitivity analysis, showing the locations of the intersecting fault at either 0, 25, 50, or 75% of the slope height. 124

Figure 5.15. Minimum principal stress (left) and maximum shear stress (right) distributions, in Pa, with respect to fault intersection location (75, 50 and 25% slope height) for a 600m high pit slope. 125

Figure 5.16. Depth of potential extensional strain (dashed line) and plastic shear (solid line) damage areas with respect to fault intersection location sensitivity and pit depth. 126

Figure 5.17. Ratio of depth of potential extensional strain damage in the footwall relative to the hanging wall, as a function of fault intersection location and pit slope height. 126

Figure 5.18. Minimum principal stress (left) and maximum shear stress (right), in Pa, with respect to fault incidence angle (50°, 80°, and 110°) for a 600 m high pit slope. 128

Figure 5.19. Depth of potential extensional strain (dashed line) and plastic shear (solid line) damage areas with respect to fault angle incidence and pit depth. 128

Figure 5.20. Relative impact of key fault properties on the development of stress heterogeneity within a pit slope intersected by a fault. 129

Figure 5.21. Procedure and fault generation results for modelling of fault development within the model prior to stress initialization and modelling of the open pit excavation.Contours shown are shear strain rate contours (relative contour interval 2.5 units). 131

Figure 5.22. FLAC3D results of modelling of initiation and development of fault zones present in the west wall of the Lornex Pit (above), and comparison to the interpreted geotechnical section (below) reported by Piteau Associates (2005). Note that the two main faults, the Lornex and W1-1, are clearly reproduced in the modelling of fault initiation and development carried out here. 132

Figure 5.23. Modelled maximum principal stress field generated using a conventional numerical stress initialization approach (upper), and that where the tectonic faults are first explicitly modelled as part of the stress initialization procedure (lower).Note that the location of the Lornex Fault Zone is outlined in black for reference in both models. Compression is negative. 134

Figure 5.24. FLAC3D shear strength reduction comparative analysis of fault implementation methods. Factor of Safety (FOS) results for the THVC Lornex pit when using a conventional fault representation (above) and when using a more complex fault structure based on one that is first modelled (below). 136

Figure 5.25. Location of Teck Highland Valley Copper mine (left) and a view of the north and west walls of the Lornex pit with the trace of the Lornex Fault Zone superimposed (right). 137

Figure 5.26. Initial UDEC model results indicating increased damage in the footwall of the fault during excavation at THVC Lornex west wall. 139

Figure 5.27. Damage (represented by yielded elements) with respect to mining stage for the footwall (above) and hanging wall (below) of the UDEC modelled Lornex Pit west wall. Results compare models that include the Lornex Fault (solid line) and those assuming a homogenous rock mass (dashed line). 140

Figure 5.28 UDEC model set-up showing joint sets (red and blue) including random joints representing intact rock bridges (i.e., potential brittle fracture pathways) using voronoi tessellation (black). 143

Figure 5.29 Depth of failure indicated by black line and reduced properties for strain softening model (above) and strain softening model with inclusion of reduced properties caused by extension (below) in UDEC. 144

Figure 5.30 Depth of failure indicated by yielded material (pink and green) for strain softening model (above) and strain softening model with inclusion of reduced properties caused by extension (below) in UDEC. 145

Figure 5.31. THVC Lornex pit model results indicating x-displacements (bottom) from Model 1 – Strain Softening (above) and Model 2 – Strain Softening with extensional strain (below). 146

Figure 5.32. Open joints (blue) and joints undergoing shear displacement (red) for strain softening model (left) and strain softening with extensional strain (right). 147

LIST OF EQUATIONS

Equation 2.1 11
Equation 2.2 12
Equation 2.3 13
Equation 2.4 13
Equation 2.5 21
Equation 2.6 23
Equation 3.1 40
Equation 3.2 40

LIST OF PRINCIPAL SYMBOLS AND ABBREVIATIONS

3-Dimensional Universal Distinct Element Code 3DEC

Coefficient of Determination R2

Cohesion c

Disturbance Factor . . . . . D

Extension strain critical value . . . . . ε_{crit}

Factor of Safety . . . . . FS

Fast Lagrangian Analysis of Continua in 2 Dimensions FLAC2D

Fast Lagrangian Analysis of Continua in 3 Dimensions FLAC3D

Finite Difference Method . . . . . FDM

Finite Element Analysis . . . . . FEA

Finite Element Method . . . . . FEM

Friction angle (degrees) . . . . . φ

Geological Strength Index . . . . . .GSI

Hoek-Brown failure criterion . . . . . H-B

Generalized Hoek-Brown material constant "m" for intact rock . . . . . m_i

Generalized Hoek-Brown reduced value of "m" material constant . . . . . m_b

Generalized Hoek-Brown rockmass constant "a" . . . . . a

Generalized Hoek-Brown rockmass constant "s" . . . . . .s

Gravitational stress component (MPa) . . . . . σ_{grav}

Horizontal in-situ stress (MPa) . . . . . σ_h

Horizontal to vertical stress ratio . . . . . k

Intermediate Principal stress (MPa) . . . . . σ_2

Maximum Principal stress (MPa) . . . . . σ_1

Material density (kg/m^3) . . . . . ρ

Minimum principal stress (MPa) . . . . . σ_3

Mohr-Coulomb failure criterion . . . . . .M-C

Normal stress (MPa) . . . . . σ_n

Poisson's ratio . . . . . ν

Residual friction angle (degrees) . . . . . φ_{res}

Rock Mass Rating . . . . . RMR

Rock Quality Designation . . . . . RQD

Shear strength (MPa) . . . . . τ

Synthetic Rock Mass . . . . . SRM

Tensile stress (MPa) . . . . . σ_{ten}

Uniaxial Compressive Strength . . . . . UCS

Uniaxial compressive strength of intact rock sample (MPa) . . . . . σ_{ci}

Uniaxial compressive strength of rock mass (MPa) . . . . . σ_c

Universal Distinct Element Code . . . . . UDEC

Vertical in-situ stress (MPa) . . . . . σ_v

Young's modulus (GPa) . . . . . E

ACKNOWLEDGEMENTS

First and foremost, I would like to thank Dr. Erik Eberhardt for giving me the opportunity to work on such a variety of interesting projects. This dissertation would not have ever been completed if it were not for his help and his continued patience.

I also offer my heartfelt gratitude to my supervisory committee: Dr. Oldrich Hungr, Dr. Ken Hickey, and Dr. Doug Stead.

This work was funded in part through a Collaborative Research and Development grant from the Natural Science and Engineering Research Council of Canada (NSERC), in partnership with Rio Tinto, together with a grant from the B.C. Natural Resources and Applied Sciences (NRAS) Endowment. I would like to thank these organizations for their financial support.

I would also like to thank my employer, SRK Consulting (Canada) Ltd. for giving me the time required to finish my research, especially during troubling economic times.

I would also like to thank Teck Highland Valley Copper Mine as well as Rio Tinto and the Palabora mine staff for providing data, Dr. Andre van As (Rio Tinto Technical Services), Mr. Sebastien Fortin (THVC), and Mr. Nick Rose (Piteau Associates) for their technical guidance.

My thanks also go to Dr. Kyusoek Woo, Dr. Scott McDougall, David Hewlett, Tony Pullano, Vlad Kobiljski, Masoud Rahjoo, and Dr. Tom Styles for their assistance in developing the theories and concepts used in this thesis; Dr. Reza Taghavi, Dr. Mark Christianson, and Dr. Loren Lorig for their advice on modelling techniques. Much appreciation is given to my friends for keeping me sane and taking me golfing every so often. Thanks Boys!

Lastly but most importantly, I cannot thank enough my loving family for sacrifices they have made throughout my studies. Their continued love and support have kept me surviving and moving forward.

DEDICATION

This thesis is dedicated primarily to my loving and supportive wife who has seen me through this experience and somehow still loves me. You are my light at the end of this tunnel and I can never thank you enough. You have given me the strength, direction, and vision I needed to finish this. This thesis is more yours than mine.

To my children, Jack Elias and Charlotte Grace, “Thank you for making life worth living. You are and will always be my greatest achievements. All else pales in comparison. I know you each will do something special and amazing”

CHAPTER 1 INTRODUCTION

1.1. Problem Statement

The global demand for base metals combined with a diminishing number of near surface resources has required the mining industry to develop an increasing number of complex and unprecedented open pit mine designs to access and recover deeper ore resources. These designs can include pushback extensions (laterally and to depth) of existing open pits as well as the transition to a variety of underground or mass mining methods. While past open pit designs rarely involved depths exceeding 500 m, many mining companies are now considering steeper and deeper designs approaching or exceeding 1000 m (Figure 1.1). Experiences with large open pits such as Bingham Canyon (Pariseau et al., 2007) and Betze-Post (Rose and Hungr, 2007) in the U.S.A. and Batu Hijau in Indonesia (Leech and McGann, 2008), demonstrate that slope failures with complex failure mechanisms are occurring with these deeper pits and higher, steeper slopes.

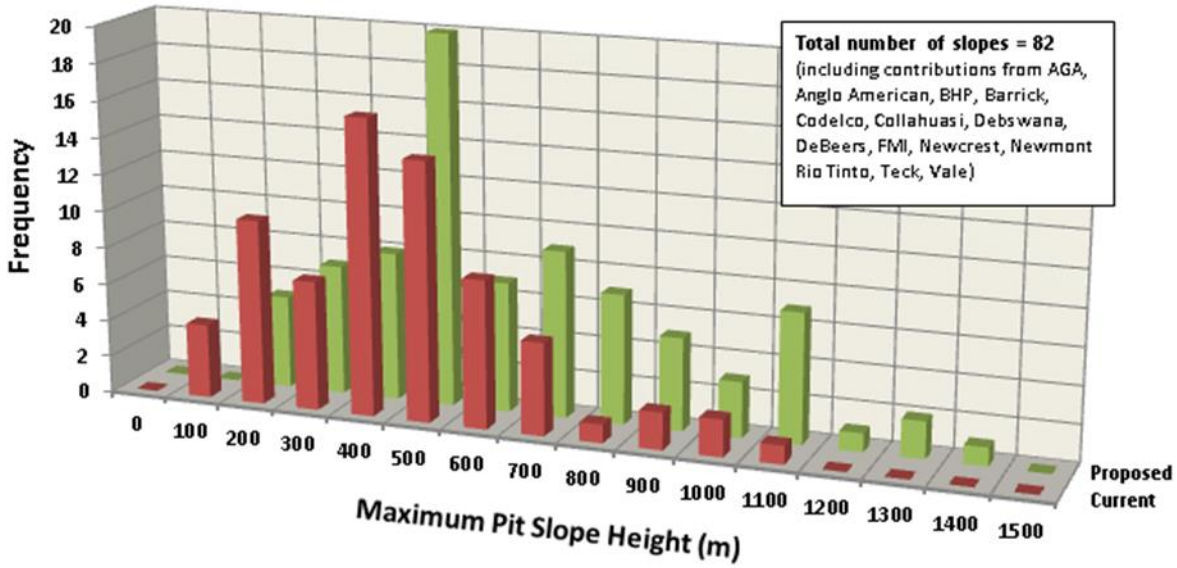

Figure 1.1. Frequency and depth of current and proposed open pit mines based on contributing Large Open Pit (LOP) project participating companies. From Robotham (2011).

Simultaneous to the deepening of large open pits, lower cost mining methods such as block, panel, and sub-level caving are increasingly being favored to target low-grade ore bodies at depth. Several open pits have transitioned into caving operations; examples include the Palabora Mine in South Africa, Cadia-Ridgeway

Mine in Australia and Grasberg in Indonesia, with others like Chuquicamata Mine in Chile and Udachny in Russia being in the process of transitioning or are considering similar plans.

As the boundaries of mine design are pushed, the tools which engineers use to review the geotechnical feasibility of these designs must also advance. Hoek et al. (2000) state that the determination of rock mass strength was a major deficiency in rock slope design practice. Stacey (2007) echoes this sentiment when he concluded that conventional approaches for the evaluation of the stability of rock slopes in high stress, hard rock environments are of questionable validity. As the majority of pit slope designs to date have involved depths of 300 m or less, geotechnical analyses have generally focused on low stress environments and the influence of geological structures is considered to be primarily kinematic and on bench to multi-bench scale stability. Engineers involved in the design of open pits in the past have in large part favoured the use of empirical design charts and kinematic wedge analyses to assess and design around the day-to-day practical engineering problems faced on site. Designs are now more commonly checked using a variety of numerical analyses, including limit equilibrium and finite element analyses.

With pushbacks and expansions to deeper and more complex open pit operations, and transitions to underground mass mining, the potential for rock deformation to evolve into large pit wall scale failures gives cause for both safety and economic concerns. Failure mechanisms within the open pit environment are no longer confined to low stress structurally controlled kinematic failures, but are evolving to incorporate more complex stress-strain rock damage related phenomena. The transition to an underlying mass mining operation adds further complexity to the induced stress conditions within and near the bottom of the large slopes.

Numerical modelling has emerged as a key tool for improving our understanding of slope deformation processes and can be used to help identify areas or situations where the stability of the slope may be compromised. Current use of numerical modelling has largely focused on 2-D analyses, requiring simplification of the geology and geological structures present. Complex 3-D analyses are often conducted by major mining companies; however, these are often continuum based and the impact of the simplifications required to conduct such analyses are not well understood. Geological structures, anisotropy and rock mass heterogeneity can significantly influence the stress field within a large rock slope or around a developing cave, and therefore the 3-D kinematics of the slope. The exclusion of these features can lead to a misleading or incorrect understanding of the stability state and potential slope failure mechanisms. A second key deficiency lies with the constitutive relationships adopted in these models, which in most cases involve elasto-plastic shear-based yield criteria (e.g., Mohr-Coulomb or Hoek-Brown). How such constitutive

models are used to model the stress path and response of the rock mass to the stress path is a topic that has not been fully studied.

The current limitations in open pit design are clearly demonstrated by the unexpected pit slope failure at Palabora in 2004 (Figure 1.2). Poor understanding of the rock mass response to the presence of a developing block cave beneath the deep pit led to the triggering of a large rock slope failure, and subsequently, to a situation where dilution from the failed rock entering the block cave from the collapse structure in the bottom of the pit is severely impacting the economics of the mine. If the failure had developed elsewhere around the pit, it could have possibly led to the loss of critical infrastructure (e.g., the production and/or ventilation shafts), which in turn would have led to the shutdown or major re-investment of the mine.

Figure 1.2. Quickbird image of 2004 North wall failure at Palabora. Note the proximity of access shafts to the crest of the East wall to the right of the image.

Palabora represents the deepest open pit (800 m depth) associated with an operating underground block cave mine. However, similar transitions to underground mass mining are planned or in development for at least four open pits with greater depths. Based on experiences at Palabora, Brummer et al. (2006) have emphasized the need to better understand the role of structures, water, and stresses and related deformations that develop through more complex mine designs to better protect mine infrastructure and minimize environmental impacts.

1.2. Research Objectives

The research outlined in this thesis aims to address the challenges of mining deeper large open pits with focus on furthering the understanding of the influence of stress heterogeneity on stability as it arises from the influence of the open pit geometry, in-situ stress field, and specifically the presence of major geological structures. Damage related to these stress imbalances is investigated to determine what potential impact the reduced rock mass strength and the extension and dilation of existing structure (joints, foliation, faults, etc.) can have on the performance of large open pit slopes. To do so, several research objectives have been defined, as described below, which investigate the use of state-of-the-art monitoring and numerical modelling techniques to identify pit slope deformation patterns related to: i) large geologic structures that transect a large pit slope; and ii) the complex interactions that can develop between these structures and the development of an underlying mass mining operation. The results from the interpretation of monitoring data are then used as a basis to understand the corresponding rock mass responses and to calibrate and constrain advanced 3-D numerical models. As part of this research, a critical investigation of stress path and rock mass constitutive behaviour is undertaken. These results will then be applied to two case studies to aid and further the understanding of the influence of geological structures on the rock mass behaviour of large open pit slopes.

The research conducted in this thesis focusses on the following principal research objectives:

I. Determine if differential behavior of a rock mass, near or separated by faults, can be detected and/or characterized using both conventional monitoring and new, state-of-the-art techniques in the form of terrestrial radar.

This objective includes:

- Review data typically collected by current monitoring techniques such as geodetic prisms during pit deepening, cave start up, and caving operation. This data will be used to identify and quantify large scale patterns (spatially and temporally) of displacements within the pit

and will be evaluated to determine if any association can be made with large scale geological structures, such as faults.

- Develop and conduct a unique "first of its kind" 3-D radar experiment in a working mine involving the simultaneous deployment of two terrestrial radar systems to collect continuous, line-of-sight displacement data and merging these data sets to construct a 3-D displacement vector map.

- Identify the complex 3-D rock mass deformation patterns within two separate pit slopes, one composed of hard, brittle rocks and another within softer, more deformable tectonically disturbed rocks, both influenced by large geological structures.

II. Identify the critical factors controlling stress heterogeneity around open pit mines and determine their effect on the design, stability, and operation of large open pit slopes.

This objective includes:

- Identify regional to local scale factors that affect stress distribution around large open pits, and develop a series of conceptual numerical models that test the relative impact of these in creating stress heterogeneity around open pits at increasing depths.

- Review the current design standards in the mining industry and determine the potential impact that stress heterogeneity can have on designs.

- Test push back strategies to determine which sequencing methods reduce the impact of stress development, both during mining and at the end of the mine life.

III. Identify the critical fault characteristics which influence the development of stress heterogeneity and determine the best means to represent these in numerical modelling of rock mass damage and slope stability.

This objective includes:

- Summarize the current industry practice for including rock mass damage associated with faults within slope stability numerical analyses, and develop a series of numerical models within increasing depths to determine the impact that faults and select properties can have on plastic shear and extensional strain damage development.

- Create a novel alternative to stress development and fault evolution within a numerical model to highlight the potential for stress heterogeneity to develop in the pre-mining environment (e.g., tectonic damage).

- Apply this knowledge to two detailed case studies, the Palabora mine in South Africa and Highland Valley Copper mine in British Columbia. These will incorporate the damage observed in the field and in conceptual models and demonstrate the effect of large, persistent geological structures on the development of stress heterogeneity and destabilizing slope damage.

1.3. Thesis Structure

This thesis is presented through six chapters, with Chapters 3, 4 and 5 presenting the main research results and contributions. The present chapter, Chapter 1, provides an introduction, outlining the research motivation and primary objectives. Chapter 2 provides an in-depth literature review, given to provide the reader with the appropriate background information to understand the main methodologies used. Included within this chapter is a brief discussion of the current state of practice in open pit design involving numerical modelling for slope stability analyses as typically conducted by mining consulting companies.

Chapter 3 describes the use of monitoring data in the observation and detection of differential behavior of a rock mass bisected by large geological structures in the open pit environment. The chapter includes a review of geodetic monitoring data within an open pit excavated in hard, brittle rock mass, but primarily focusses on a unique experiment that has since been published in Engineering Geology (2014, vol. 181, pp. 202-211) entitled "Development and application of a pseudo-3D pit slope displacement map derived from ground-based radar". This published paper describes the experiment and results obtained relative to the research objectives of this thesis.

Chapter 4 describes numerical modelling undertaken to investigate the impact of various factors that affect the stress distribution around open pits, in particular major geological structures. The chapter includes a review of the current state of knowledge with respect to mining induced stresses around open pits and the impact that geometry and pit depth can have on the mining-induced stresses. The conceptual models described in this chapter review the spatial and temporal distribution of stresses that are created by varying the sequencing of the pit excavation relative to the interactions between the faults and open pit slope and the degree of slope weakening damage generated. A detailed 3-D numerical model of the progressive deepening of the Palabora Mine open pit followed by the development of the underlying block cave. This chapter explores the changes in 3-D stress magnitudes and orientations experienced by areas proximal and

distal to the fault zones and demonstrates the effect of changing stress conditions on highly anisotropic rock.

Chapter 5 describes the applicability of current numerical methods in modelling the potential damage arising from stress heterogeneity in a large open pit slopes. Several critical aspects of fault representation are investigated and the potential for developing tectonic stresses within a model prior to pit excavation are explored. Two case studies are given in this chapter to aid in the explanation of the concepts. A detailed 2-D model of the Lornex Pit at the Teck Highland Valley Copper is developed which shows the development of damage and the need to include extensional strain within a numerical model.

Finally, Chapter 6 summarizes the findings provided in Chapters 3 to 5 and lists the key conclusions and contributions arising from this research, and proposes topics for further research.

CHAPTER 2 BACKGROUND INFORMATION AND METHODOLOGY

2.1. Open Pit Mining Slope Monitoring Techniques

Monitoring programs are used to record slope displacements in open pit mine slopes and form a key component of most slope stability programs in modern open pits. These programs are generally geared toward the tactical objective of identifying slope hazards that pose an immediate threat to mine workers and equipment, and subsequently, to provide early warning of an impending failure. As a secondary use, the monitoring equipment can provide strategic insights into quantifying the nature and extent of a hazard and the kinematics and mechanics of a slope. Issues of uncertainty relating to the geological conditions, slope kinematics, and failure modes provide obstacles that contribute to a lack of understanding of the potential for failure. In practice, monitoring data is not routinely used to evaluate slope mechanics and potential failure modes due to the obstacles listed above, high staff turnover rates lead to a lack of continuity of the data set, and a generally perceived lack of time to review the data. Often monitoring data is used only once a large-scale failure has already been identified or as a tool used for back analysis, rather than as a tool used in future mine design.

Techniques used for monitoring and forecasting impending slope failures are largely reliant on surface-based point measurements of displacements monitored over time to establish the overall behaviour of the slope. The use of investigative monitoring has been shown to facilitate a greater understanding of the behaviour and mechanics of both natural (Willenberg et al., 2008) and open pit mine slopes (Walker et al., 2006), thus enabling the correct mitigation approach to be chosen or to confirm that the correct approach has been taken.

Commonly used techniques for open pit slope monitoring are categorized as either involving surveying or geotechnical methods (Jarosz and Wanke, 2003). Surveying techniques include total station/geodetic monitoring of prisms, use of GPS receivers, slope stability radar, LiDAR, etc., used to determine absolute positions. Geotechnical methods employ specialized instrumentation to measure differential displacements over a short distance, and include extensometers, tiltmeters, inclinometers, etc. Examples of strategies employed at different mines based on these methods include those by Logan et al. (1993), Laubscher (1993), Little (2006), Brown et al. (2007), and Seery (2007), amongst others. The surveying of geodetic prisms remains the most commonly employed monitoring method in open pit environments, however, emerging technologies such as real aperture and synthetic aperture radar are quickly becoming commonplace on mine sites as well.

2.1.1. Geodetic Prism Monitoring

Due to its lower cost, reliability, and ease of collection, the surveying of geodetic prisms remains the most commonly used slope monitoring method in open pit mining. The geodetic monitoring of numerous prisms installed throughout the pit is now routinely undertaken using robotic total stations, with more recent efforts being to combine these systems with global navigation satellite systems (Brown et al., 2007). Monitoring through GPS receivers has also been considered an answer to large open pit projects where the pit diameter exceeds 1 km and refraction and pointing errors start to limit the effectiveness of total station measurements. Bond et al. (2007) list the advantages of GPS monitoring over other geodetic technologies as: i) providing temporally continuous and high accuracy displacement detection, ii) not requiring line of sight between stations, iii) providing 3-D position information, and iv) making millimetre-level data possible for baselines up to 10 km in length.

Most the slopes within an open pit environment are monitored to ensure the safety of workers and equipment, and to evaluate the effectiveness of any mitigative measures undertaken (e.g. slope drainage). Figure 2.1 shows some common techniques for visualizing prism data, which include: incremental and cumulative displacement plots, daily rate plots, and wander plots (movement direction in plan view or section). Early warning thresholds are usually set by trial and error, or over time, the experience of those involved. In turn, the data is assessed by extrapolating the measured displacement-time series to detect accelerations that exceed set thresholds. One such example is the inverse velocity method (Fukuzono, 1985; Rose and Hungr, 2007). It must be noted that these approaches are generally applied independent of the acting slope failure mechanism or its kinematic controls. As such, the triggering of faulty alarms or uncertainty over misleading instrument readings is a frequent problem. Once an alarm is triggered, the mine will shut down operations in the unsafe area: if a failure is realized, the procedure is deemed a success (Seery, 2007); if a failure is not realized, the procedure results in costly down time, delays to production schedules and diminished confidence in the system.

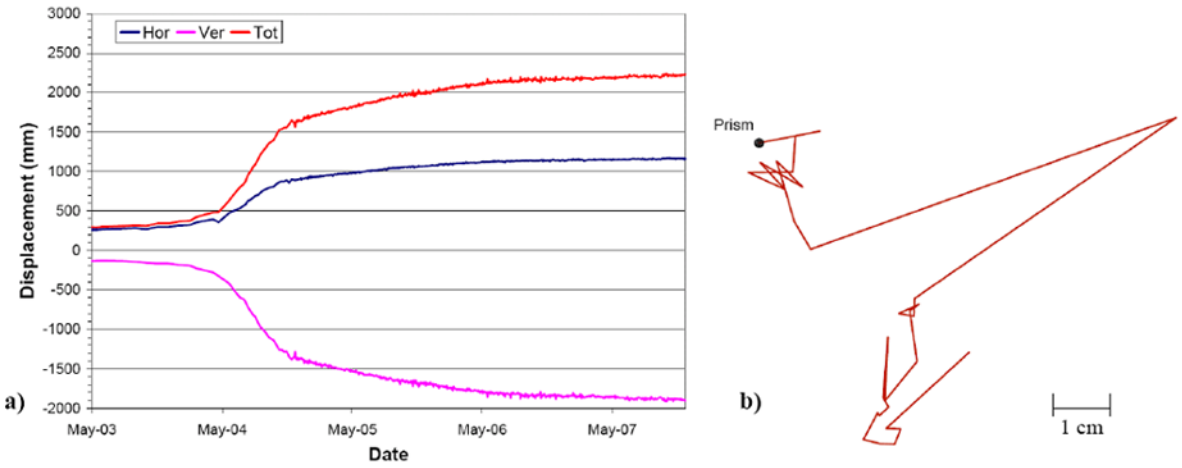

Figure 2.1. Examples of typical geodetic monitoring data including: a) cumulative displacement rate plot, and b) wander (x-y) plot used at the Palabora Mine After Piteau (2005).

As noted by Dunnicliff (1988) and Eberhardt et al. (2008), instrument reliability is of paramount importance, especially if it is part of a system being relied upon for early warning monitoring. One key limitation of using geodetic monitoring to interpret slope stability failure mechanisms within the open pit is that the monitored points are represented by point-based data on the slope surface. These prisms are often located based on accessibility. Prisms located on benches of limited accessibility are often not maintained and have a limited operational time frame. Movement and deformation located within the pit wall between the points must be extrapolated and some key deformation along geologic structures may be missed or misinterpreted. Slope displacement patterns based on geodetic data can provide a generalized pattern of slope movement. Although new advancements (as described below) have been made, a well thought out prism network is fundamental to a slope monitoring program and can further be used to calibrate and validate other monitoring campaigns.

2.1.2. Radar Monitoring

In the last decade, several terrestrial instruments based on microwave interferometry have been developed for the monitoring of displacements at large structures and slopes (e.g. Farrar et al., 1999; Tarchi et al., 2003; Pieraccini et al., 2005; Harris et al., 2006). These instruments provide high-resolution, full area spatial coverage as opposed to relying on geodetic point measurements. Radar works by continuously scanning and comparing highly accurate and precise measurements made from up to 4 km from the slope face to detect sub-millimetre movements (0.1 to 1 mm, depending on distance). The two main methods of collecting the terrestrial radar data are the use of real aperture radar (RAR) and synthetic aperture radar (SAR).

2.1.2.1. Ground-Based Real Aperture Radar (RAR)

A scanning radar system was designed specifically for monitoring mine slopes using differential interferometry by researchers at the University of Queensland, Australia (2002). The system, known as the Slope Stability Radar (SSR), commercially available from Ground Probe Pty Ltd., uses real aperture radar to scan a slope in both the vertical and horizontal directions. Scanning occurs at 10°/second over a range of ±60° vertically and 340° horizontally leading to typical scan repeat times of about 15 minutes. The system continuously monitors the slope face for deformations. The return signal phase is recorded for each pixel in the resulting image and phase unwrapping is used to remove ambiguity over deformation changes greater than the signal wavelength (Reeves et al., 1997). The trailer-mounted unit features a 0.92 m diameter scanning parabolic dish antenna, mounting, controlling/data collecting computer, remote area power supply, warning siren and lights, CCD camera, communication links, and internet compatibility. The system can operate at a range of 450 m from the target slope. Line of sight displacement can be measured to ±0.2 mm without the use of reflectors. In operation, the system produces an image showing spatial deformation relative to a reference image for the entire scanned slope. The displacement history of each point in the image can be plotted.

2.1.2.2. Ground-Based Synthetic Aperture Radar (SAR)

Interferometric Synthetic Aperture Radar (InSAR) is a radar technique that uses two or more Synthetic Aperture Radar (SAR) images to generate maps of surface deformation. This is achieved using differences in the phase of the waves returning to the satellite. Synthetic aperture radars using microwave interferometry were developed for remote static and dynamic monitoring of rock and soil displacements and as a means of overcoming the limitations of real aperture radars. The general principle of microwave interferometry is the detection of amplitude and phase of an electromagnetic wave transmitted by the sensor and reflected from the slope. The interferometric phase φ (i.e. the phase difference between two different time epochs) of the target slope can only be observed within the range $-\pi$ to π, and is expressed as:

Equation 2.1

$$\varphi = \varphi_{Disp} + \varphi_{atm} + \varphi_{diel} + \varphi_{noise} - 2 * \pi * n$$

with *n* being the phase ambiguity (i.e. integer number of full phase cycles). The left side of the expression is the observed value, while the right side contains the unknown parameters:

- φ_{Disp}: displacements of the target in line of sight (LOS) of the radar;
- φ_{atm}: changes of atmospheric properties between sensor and target;
- φ_{diel}: changes in the dielectric properties of the target;

- φ_{noise}: measurement noise.

For displacement monitoring, only φ_{Disp} is of interest which is related to the LOS displacement Δr_{disp} in the following way:

Equation 2.2

$$\varphi_{Disp} = -\frac{\lambda}{4\pi} * \Delta r_{Disp}$$

where λ is the wavelength of the transmitted microwave.

For the experiment reported in Chapter 3, the IBIS system manufactured by Ingegneria Dei Sistemi (IDS) was used, which is based on the synthetic aperture radar technique. The IBIS system was originally developed as a joint research project between the University of Florence and IDS (Pieraccini et al., 2005) and is offered in two different configurations:

- IBIS-S: Microwave interferometer
- IBIS-FM: Ground-based Synthetic Aperture Radar (GB-SAR)

The IBIS-FM is based on: i) Stepped Frequency Continuous Wave (SF-CW), allowing resolution in the range direction, ii) Synthetic Aperture Radar (SAR), allowing the system to resolve the monitored region in the cross-range direction, and iii) differential interferometry, which allows the measurement of displacements by comparing phase information of the back scattered electromagnetic waves collected at different times. The IBIS-FM sensor can perform real-time, near-continuous (5-minute repeat interval), line-of-sight (1-D) monitoring of large areas, day or night and in all weather conditions (-50°C to 50°C). These abilities are helping to establish radar as a key tool for managing unstable pit slopes, quickly identifying the size and extent of a developing failure (see Harries et al., 2006; Harries and Roberts, 2007; Seery, 2007).

Range resolution is obtained by sampling in the frequency domain using the Stepped Frequency Continuous Wave (SF-CW) technique (Taylor, 2001, see Figure 2.2). The sensor continuously transmits a stepped frequency signal. For each frequency step the returned echo delivers amplitude and phase. By means of an inverse Fourier Transform the sampled values can be transformed into the range domain. This step is called focusing and results in a phase and amplitude information for each range resolution cell. The resolution in the range domain δr is related to the bandwidth B of the transmitted stepped frequency signal by:

Equation 2.3

$$\delta_r = \frac{c}{2B}$$

with c being the velocity of light. With a bandwidth of 200 MHz, the maximum range resolution obtained is 0.75 m. At each discrete step while moving along the rail, the sensor transmits the stepped frequency signal and records the echo. Thus, the phase is a function of the sensor position as the distance to each target is slightly altered. By that the physical radar antenna is synthetically elongated. The cross range (azimuth) resolution δc is directly related to the synthetic antenna length L by:

Equation 2.4

$$\delta_c = \frac{\lambda}{2L} r$$

with λ being the wavelength and r the distance. The equation for the cross-range resolution equals the cross-range resolution of real aperture radar (RAR) except for the factor 2. In the case of IBIS-FM with a rail length of 2 m, a RAR with the same cross-range resolution would need an antenna of 4 m length.

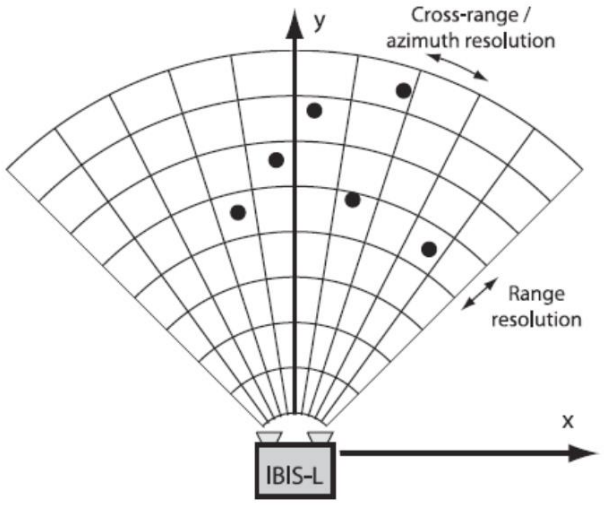

Figure 2.2. Resolution concept of IBIS-L synthetic aperture radar. By moving along the x-axis, IBIS-M can distinguish targets at the same range and different azimuth.

Rödelsperger et al. (2010) describe the advantages and disadvantages of the IBIS-M unit as compared to other forms of monitoring; one key disadvantage of the system, as with all radar systems, is that it can only

provide line-of-sight displacement meaning that important 3-D information of the displacement kinematics may be missed (Figure 2.3).

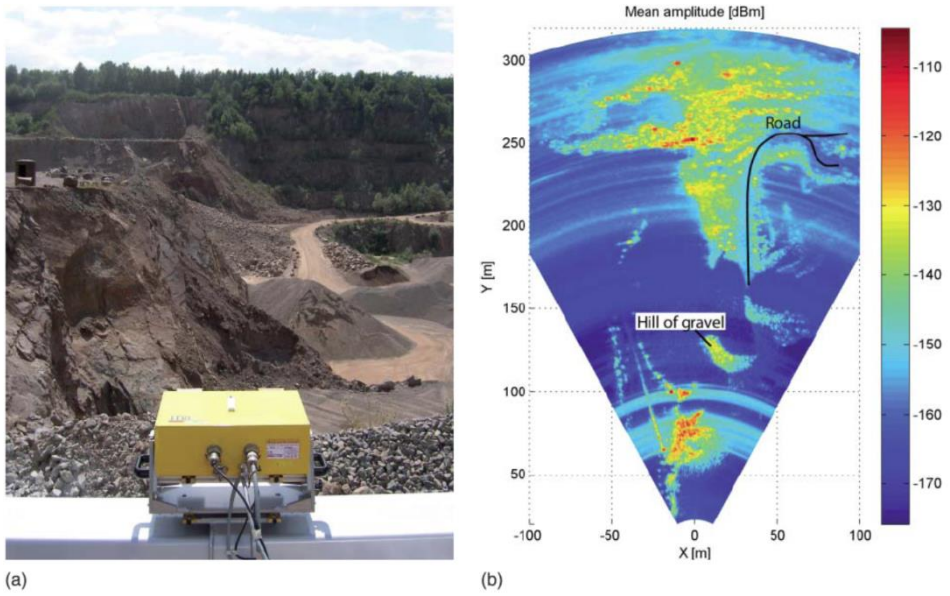

Figure 2.3. Comparison of site photo and recorded displacement from radar. a) Photo of IBIS-L monitoring displacements in a quarry, Dieburg. b) Mean amplitude of observed scene.

2.1.2.3. Satellite-Based Synthetic Aperture Radar

Satellite-based synthetic aperture radar is similar to that described in the above section; however, the images used to generate the surface deformation maps are retrieved via satellite. Jaroswz and Wanke (2003) have shown that satellite-based InSAR can play an important role as an initial method to determine the subsidence active area and further plan for other monitoring methods employing usually "classical" surveying techniques. It can be also used as complementary method providing accurate monitoring of vertical component of rock strata movements.

One of the earliest applications of radar interferometry for change detection was accomplished at the site of the Landers earthquake of 1992 in the Mojave Desert of California (Massonet et al., 1993; Massonet et al., 1994). Similar applications of radar satellite data have been used to map and monitor landslides, ice movement, and volcano deformation (Fruneau et al., 1996), and subsidence caused by the extraction of ground water, oil and gas, or minerals (Carnec et al., 1996; Stow, 1997; Cigna et al., 2012). These pioneering studies have generated enormous interest in the Earth science community because they point to an entirely new way to study the surface of the Earth.

One major drawback affecting satellite InSAR is the longer repeat frequency related to satellite orbit times, together with other limitations related to the satellite look angles, path coverage and decorrelation (e.g., from snow cover and vegetation).

2.2. Stress Analysis and Stress Distribution

2.2.1. Near Open Pit Excavations

Historically, the investigation of mining induced stresses and stress migration has focused on underground mining where rock mass failures such as rock bursting and pillar collapses occur where compressive and confining stresses have been shown to contribute to mine instability. Relationships between in-situ and mining induced stress have been investigated through analytical techniques (Kirsch, 1898; Love, 1927; Muskhelishvili, 1953; and Savin, 1961) as well as numerical methods (Lorig and Brady, 1984). Stresses around open pits are generally considered to be gravity driven and mostly dilationary within a homogenous rock mass (Read and Stacey, 2009); however, the effect of pit excavation on the redistribution of the in-situ stress magnitudes and orientations with respect to material properties, such as deformation modulus, and in-situ stress ratios has clearly been demonstrated by Stacey et al. (2003) and has been observed in the buckling of laminated rock at the base of the slope in several instances. The mining induced stress field within a homogenous material is shown for an open pit depths of 300 and 900 m in Figure 2.4a and b, respectively. Principal stresses wrap around the excavation and the magnitude of the maximum stress increases near the toe of the slope. The relative increase of stress concentrations is similar between the pit heights (2x the initial stress condition for 300 m and 2.5x for 900 m); however, the absolute stress increase becomes important when the open pits reach greater depths. For the case of a 900-m deep pit, the maximum stress increases from a background stress value of 25 MPa to an induced value of 55 MPa in a geostatic stress environment. A 30 MPa stress increase may be enough to create damage within even a moderately strong rock mass. Stress orientation of the maximum principal stress was found to be approximately parallel to the inter-ramp slope angle in the slope and to progressively rotate to be parallel with the pit floor near the toe of the slope (Smith, 2013). The excavation of a large open pit has been shown to affect both the magnitude and orientation of the principal stresses within homogenous rock masses.

Pit geometry has also been shown to affect the stress distribution within the rock mass behind the pit face. The stress contours around a circular pit within a homogenous rock mass are evenly distributed and highly affected by the in-situ stress field. Modifying the open pit shape (even to a simplified ellipse), creates a stress concentration along the short axis of the pit (Figure 2.4c) and corresponding lower stress values along the long axis where there is less confinement. Regions of relatively high or low stress can be observed

(Figure 2.4d) with local variations of stress orientation for open pits with irregular shapes like bullnoses or sharp changes in pit slope direction.

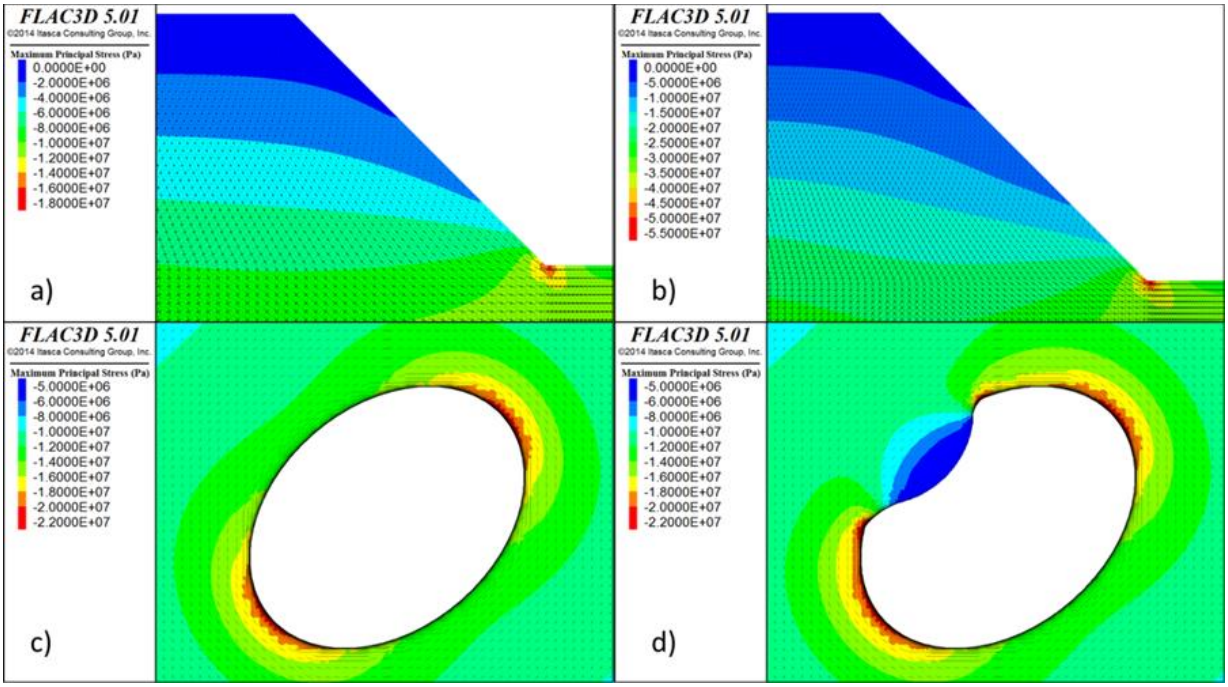

Figure 2.4. Generalized distribution and orientation of stress around an open pit: a) section view of a 300m open pit, b) section view of a 900m depth open pit, c) plan section through an elliptical shaped open pit at mid-slope and d) a kidney shaped open pit.

Stresses around open pits are often depicted as being relatively static with the excavation being the single source of loss of confinement; however, in practice this is rarely the case. The dynamic nature of principal stresses was clearly shown during the excavation of the Bjørnevatn mine in northern Norway (Myrvand et al., 1993). At Bjørnevatn, in-situ stress measurements were taken at two locations (at approximately 100 and 300 m below ground surface) in both 1971 and 1990, during which time the open pit had been excavated by roughly 120 m. The subsequent measurements were taken approximately 1 m away from the earlier measurements. Readings from the measurements showed that during the 19 years of mining, the magnitude of the maximum horizontal stress had tripled at the shallower location due to stress concentrations near the edge of the pit.

Recent investigations of seismicity around open pit mining activities at both the Mt. Keith Open Pit Mine in Australia (Wesseloo and Sweby, 2008) and the Navachab Mine in Namibia (Lynch and Malovichko, 2006) have highlighted the potential of both the stress state and the response to stress to be dynamic around pits. The micro-seismic activity is attributed to fracture growth in low stress environments; therefore, the

excavation of the open pit leads to the development of new areas that can rupture demonstrating the migratory nature of stresses. Massive rock slope failure processes have been shown to be largely driven by the initiation and propagation of brittle fractures driven by extensional strain, which interact with natural pre-existing discontinuities to eventually form basal and internal shear planes (Eberhardt, 2004). Determining the interaction between the excavation, in-situ stress, and the faults can help identify regions of high stress as well as those regions where extensional strain can occur. Lynch and Malovichko (2006) could demonstrate that a focal point of the seismic activity was near a weak group of geological structures and that the seismic activity was the result of stress changes brought about by the excavation of rock within the pit.

Wesseloo and Dight (2009) conclude that stress changes during the open pit mining process are much more complex with zones of comparatively low and high stresses. Generally, near surface in situ horizontal stresses are higher than the vertical stress. In the open pit mining environment, horizontal stresses can rotate and concentrate around the bottom of the pit and the toe of the slope leading to higher stresses. What is often regarded as a de-stressed slope may in fact be a slope with a comparatively low minimum principal stress, σ_3 (aligned vertical) but a comparatively high intermediate, σ_2 (circumferential to the pit) and maximum, σ_1 (slope-parallel) principal stresses. Wesseloo and Dight (2009) conclude that the influence of σ_2 is important under bi-axial loading conditions (such as pit excavation) and is therefore important to develop appreciation of the true 3-D stress fields around an open pit.

2.2.2. Near Geological Structures

Many of the deposits exploited by large pits and mass mining are low grade porphyries, skarns, and other large scale deposits. Ore emplacement within these deposits are often associated with existing structures in the rock mass. Applying generalized tectonic conditions to these deposits is extremely difficult due to the variety of emplacement methods and geological histories at each individual deposit as well as the potential influence of post-depositional faulting; however, the presence of faulted rock near the deposit is often common (Cox et al., 2001; Sibsone, 2001). Deposit extents and the potential weakening of the host orebody by mineralization processes often means that these large-scale deposits are intersected by a series of regional to mine-scale fault systems as well as other smaller scale or pervasive geological structures such as veins and joints. Characterization, mechanics, and fluid flow near faults within the geological context as well as the petroleum industry have been undertaken for which many summaries exist (Faulkner et al., 2010; Evans and Chester, 1995). As faults often have a controlling nature on the placement and extent of ore bodies (Cooke et al., 2005; Sillitoe, 2010), the review of the mining interaction with faults is also warranted.

Faults have been shown to damage the rock mass on a regional scale though the development of secondary faults (Maerten et al., 2002) as well as to create stress pockets (Tanno et al., 2010) in natural systems. Martin (1990) demonstrated through in-situ stress monitoring and numerical modelling that a compartmentalization of in-situ stress has occurred within the Lac du Bonnet granite. Distinct in-situ domains were defined with variance in both magnitude and principal direction delineated by major fault structures at the underground research laboratory (URL) in the Canadian Shield (Figure 2.5).

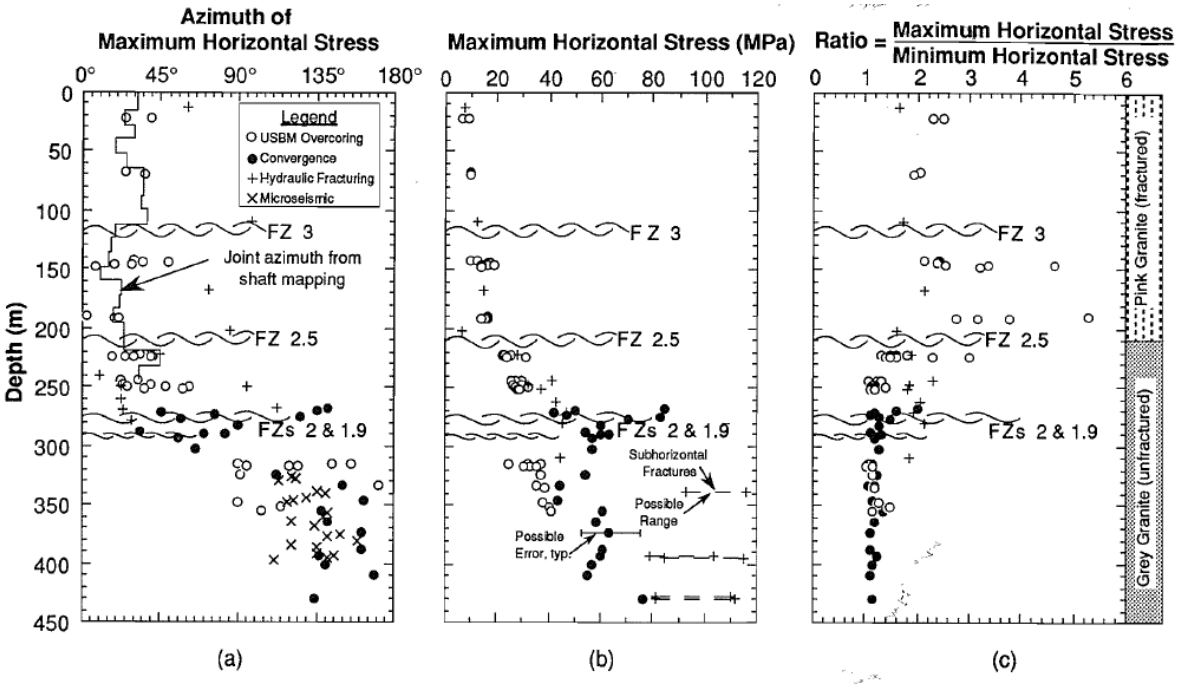

Figure 2.5. Fault separated in-situ stress domains at the URL (from Martin, 1990) including changes in a) orientation, b) magnitude and c) stress ratio between maximum and minimum horizontal stress.

Studies of stress perturbations conducted using discrete element numerical modelling (Su and Stephansson, 1999; Su, 2004, Harrison et al., 2010) have shown that changes in both orientation and magnitude of in-situ stresses can be expected near fault systems. The key factors which affect the stress variation around a fault identified from the numerical modelling were the mechanical properties of the faulted rock, such as stiffness and friction angle, as well as the boundary stress ratio. Sassi and Faure (1997) highlighted that major structural features can control the local variations of the stress regime and influence the deformation modes of faulting and fracturing which can take place at a smaller scale.

These stress regimes or local perturbations have proven to be a controlling factor of stability in many instances in tunneling (Diederichs et al., 2004) and underground mining (Beck et al., 1996; Martin et al., 2003) but have largely been ignored in open pit mine designs.

2.3. Relevant Failure Criterion

Many modern mining operations define a geotechnical model for their operations which acts as a fundamental basis for future mine designs and decisions. This geotechnical model is generally composed of the local lithological or geology model, a structural geology model, rock mass testing, and a hydrological model. From the geotechnical model, geotechnical domains are created to group together similar behaving rock masses and these domains are assigned strengths and associated failure criterion. The most commonly used failure criteria are the Mohr-Coulomb and the Hoek-Brown shear strength criteria, which are defined by testing rock strengths under varying confining stress levels to determine at what combination of stresses, shear failure of the rock occurs.

The strength of rock is often characterized with respect to shear-driven failure. Uniaxial and triaxial compressive strength testing are used to establish the intact rock strength values. Multiple samples of each rock type (of significance) are tested, with average or mean values being determined. Scaling of these intact strength values is then carried out using empirical relationships based on field mapping and various rock mass rating systems, to determine the field-scale rock mass shear strength properties. These are generally expressed in the form of a shear-based failure criterion, with the linear Mohr-Coulomb and non-linear Hoek-Brown relationships being the most common.

The tensile strength of rock is also often tested using methods like the Brazilian indirect tensile test. However, this is restricted to intact rock, and again, empirical relationships like the GSI-Hoek-Brown system (Hoek et al., 2002, 2013) are used to estimate the rock mass tensile strength, although the values in this case are more questionable than those derived for shear strength using the same system. This is primarily due to the heterogeneous nature of rock masses which include previous fractures (zero tensile strength joints and faults), which make the direct scaling of the tensile strength more difficult.

In between, and even more problematic (with respect to established experience) is the assessment of extensional strength. Although this can take the form of tensile strength in the presence of tensile stress gradients, extensile strength also comes into play in cases of low confinement where the maximum principal stress may be compressive, but the absence of confinement and the freedom to deform, leads to a Poisson's ratio effect where the strains in the direction of low confinement are negative (tensile). This can play an important role locally where brittle fracture propagation and intact rock bridges are a key factor, and where

the maximum principal stress is high, for example in the case of large pit slopes. On a rock mass scale, the extensional strength is determined using the scaled compressive shear strength failure criterion described earlier. This is due to the absence of an established criteria or methodology specific to extensional strain.

2.3.1. Plastic Shear Strain and Strain Softening

Conventional numerical slope stability analyses generally rely on elasto-plastic yield criteria that assume a plastic shear failure mode. The post-peak behavior in these cases is often treated as perfectly plastic. Yet experiences with large rock slope failures often point to a more complex failure mode which can incorporate or even be dominated by brittle fracture and progressive development of a rupture surface through a combination of localized slip along non-persistent geological structures and fracturing through intact rock bridges (Eberhardt et al., 2004; Stead and Eberhardt, 2013). Brittle failure is often used to describe the post-peak behaviour in a stress strain curve; however, it is also used to refer to the physical process of failure involving extensional or tensile failure of the rock (Kaiser and Kim, 2015). Shear failure has been noted as the dominant mode of macroscopic brittle failure in compression with high confining pressures; however, as confinement in reduced, the failure mechanism transitions to one that is more influenced by extensional brittle fracturing and cohesion loss (i.e., brittle fracture damage) rather than shear failure and friction mobilization. These effects cannot be fully modelled employing the shear based Mohr-Coulomb or Hoek-Brown criteria. A review of the importance of brittle failure has been undertaken with respect to underground mining and tunneling by Diederichs (2003), Diederichs et al. (2004), Kaiser and Kim (2008, 2015), and Kwasniewski and Takahashi (2010). However, the importance of stress-induced brittle damage on slope stability has largely gone ignored.

While the conventional application of Mohr-Coulomb and Hoek-Brown is considered appropriate for estimating the shear strength of rock masses around tunnels and slopes where strength is homogenous and dictated by friction mobilization (i.e., highly jointed), there is growing evidence that for brittle rock masses where failure is driven by cohesion loss (i.e., massive to moderately jointed), these shear based criteria are not suitable for estimating the strength of rocks in high stress settings (Martin et al., 1999). The fundamental difference in behavior is that in jointed rock, slip along discontinuities dominates the failure process, while at depth (i.e., high stresses) but under low confinement, the process is controlled by stress-induced brittle fracturing (Cai et al., 2001). Yet the use of the GSI-Hoek-Brown relationships for scaling rock mass properties (Hoek et al., 2002) is so prevalent and straightforward to use, notably in the absence of alternative relationships, that even when using a Mohr-Coulomb constitutive model, many practitioners will first calculate the scaled rock mass properties using the GSI-Hoek-Brown system and then convert these to equivalent Mohr-Coulomb properties. The quantitative conversion of Hoek-Brown to Mohr-Coulomb

parameters is done by fitting an average linear relationship to the non-linear Hoek-Brown envelope for a range of minimum principal stress values defined by $T_o < \sigma_3 < \sigma'_{3max}$ (Eberhardt, 2012).

The modification and application of the Mohr-Coulomb and Hoek-Brown criteria to predict the onset of brittle failure has met with limited success (Diederichs, 2007). Using Mohr-Coulomb, brittle failure is modelled to force peak cohesion to mobilize before friction; in doing so, brittle fracturing is simulated as being dominated by cohesion loss (Martin, 1997; Martin and Chandler, 1994). Under this assumption, Martin et al. (1999) proposed an adapted version of the Hoek-Brown criterion for representing brittle behavior. In this form of the criterion, the strength envelope is based only on equivalent cohesion ('s' parameter), and the equivalent frictional strength ('m' parameter) is assumed to be zero. Specifically, the extent of brittle failure around underground excavations in massive to moderately fractured rock has been calibrated through field observations of overbreak as m =0 and s =0.11. This reduces the Hoek-Brown strength criterion for brittle failure to Equation 2.5.

Equation 2.5

$$\sigma_1 = \sigma_3 + \sigma_{ci} 0.11^{\alpha}$$

This brittle Hoek-Brown criterion has shown good agreement with field observations when predicting the depth of brittle failure and rock mass fracturing around tunnels (Martin, 1997), where the traditional Hoek-Brown criterion greatly under predicts the occurrence of fractures. However, this approach is not adequate for representing post-peak behavior since it ignores the increase in frictional strength mobilization with higher damage levels within the rock mass (Hajiabdolmajid and Kaiser, 2002).

Alternatively, strain softening constitutive models in numerical analyses allow representation of nonlinear post-peak strength loss with increasing plastic shear strain to simulate strength degradation with increasing brittle fracture damage. Strain softening behavior is more widely applied based on prescribed variations in terms of Mohr-Coulomb (i.e., cohesion, friction, dilation and tensile strength) as a function of the deviatoric plastic shear strain. A reduction of rock strength is applied to the properties after the onset of yielding. Using this method, additional damage can be accounted for within a numerical model, however, this is an implicit not explicit representation of brittle fracture.

2.3.1. Extensional Strain and Brittle Fracture Damage

Through research conducted mainly for underground mining and tunneling in brittle rock under high in-situ stress conditions (Kaiser and Kim, 2015; Kwasniewski and Takahashi, 2010; Kaiser and Kim, 2008;

Diederichs et al., 2007; Kaiser, 2006; Diederichs et al., 2004; Diederichs, 2003; Martin, 1999), findings have led to a better understanding of stress driven failure involving brittle fracturing under low confinement. These have not been fully replicated using standard failure criteria. Diederichs (2007) proposed a composite s-shaped failure envelope to be used to identify areas of potential spalling in tunneling and underground mine infrastructure. At lower confining stresses, the failure envelope for damage of massive rocks was found to be limited in tension by the true tensile strength of the rock (Figure 2.6). Below the lower bound field strength envelope, damage did not occur within the rock, whereas above the envelope, micro-cracks began to initiate at the grain scale. The upper bound strength was found to be controlled by shear fractures formed by micro-crack coalescence. At low confinement, rock that was stressed above the lower bound envelope incurred spalling damage as new extension cracks and old cracks could propagate.

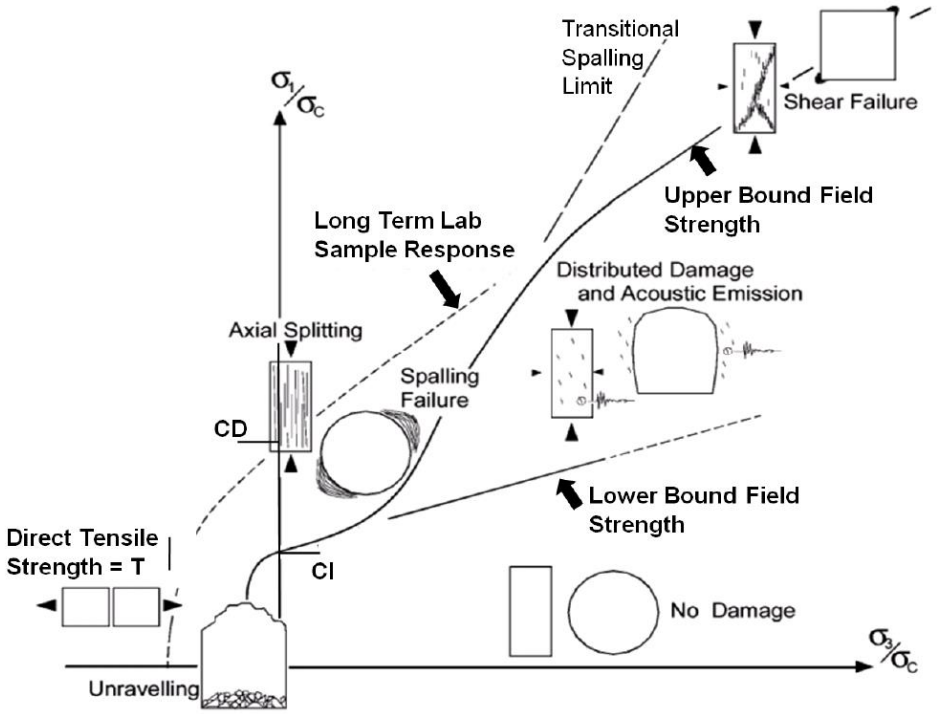

Figure 2.6. Composite failure envelope for damage initiation and spalling (from Diederichs 2007) proposed for tunneling and underground mining environments.

After recognizing the difficulty of estimating rock mass strength in brittle conditions, Stacey (1981) proposed an extensional-strain criterion based on laboratory testing of intact rock to interpret sidewall slabbing and tunnel face spalling in hard rock. This criterion states that brittle fracturing of the rock will initiate when the extension strain exceeds a critical value εcrit which is dependent on the properties of the

rock. In a numerical analysis, this can be applied as a failure criterion to be compared against an elastic stress analysis to assess the potential depth of brittle fracture damage. The extensional strain is defined as the minimum principal strain σ3 (in a compression positive convention) and is calculated from the principal stresses using the three-dimensional elastic equation (Equation 2.6)

Equation 2.6

$$\varepsilon_{crit} = (\sigma_3 - \upsilon * (\sigma_1 + \sigma_2))/E$$

In the previous equation, σ_1, σ_2 and σ_3 are the three principal stresses, ν is Poisson's ratio and E is the modulus of elasticity. The extensional strain magnitude εcrit depends on all three principal stresses, including the out-of-plane direction in a 2-D analysis. As it can be deducted from Equation 2.2 that strains can be extensional even in a triaxial compressive stress field. This means that it is not necessary for the rock mass to be in tension, but simply one in which confinement loss is experienced resulting in extensional strain in the direction of σ_3. The onset of extensional strain zones around an open pit implies that the rock mass has deformed in at least one direction, which can lead to brittle fracturing. The extensional strain criterion provides an explanation for the development of brittle fractures observed under low confinement levels, like near an excavation. The criterion seems to work well in predicting fracture initiation in brittle rocks, where it has shown better agreement with the stress-induced spalling observed in many deep tunnels and ore passes compared to the Mohr-Coulomb or Hoek-Brown elasto-plastic (frictional) constitutive models. It can also predict the orientation of induced fractures, which will occur in the plane normal to the minimum principal stress σ_3. Stacey's criterion is only intended to predict potential zones of extension fracturing representing rock mass damage. It does not account for material weakening due to these fractures, or attempt to represent post-peak behavior.

Stacey (1981) suggested a critical value of extensional strain was suggested at a stress level of approximately 30% of the ultimate strength of the rock, which corresponds to very small strains, ranging from 0.0073 to 0.0175% strain. Further research conducted by Sukurai (1981), Fuji et al. (1994 a, b), Li et al. (2000), and Kwasniewski and Takahashi (2010) have furthered the definition of an extensional strain failure criterion primarily focusing on underground mining and tunneling environments.

For rock slopes, although largely ignored, Stacey et al. (2003) introduced the idea of extensional strain as a control on brittle rock mass failure affecting slope stability, and illustrated the importance of in-situ stress on the localization of extensional strain behind the pit wall in a homogenous rock mass. Stacey et al. (2003) also showed that the orientations of extensional fractures are expected normal to the minimum principal stress. Within a homogenous rock mass, extensional strain was shown to largely occur at the toe of the slope or with its contact with the pit floor, whereby new fractures align to the free face of the open pit.

Within the open pit mining environment, much of the near surface rock mass is gradually subjected to low confinement conditions during the excavation of the pit. As such, it becomes very difficult to determine the effect of low confinement extensional strain as compared to the gravity driven kinematics and shear strain along the discontinuities within the rock mass and how far ahead of the excavation face that extensional strain can have an effect.

Several case examples reviewing the potential damage created extensional strain around open pits were reviewed by Dight (2006). The results indicate that structures and lithological changes may influence the location of fracture growth created by extensional strain leading to the breakage of rock bridges or unknown features within the slope.

2.4. Numerical Modelling – Current State of Practice

Numerical modelling methods are used to investigate numerous open pit and underground mining operations, and represent the state-of-the-art in geotechnical analysis tools used within the industry. Hamman and Coulthard (2007) describe the current uses of numerical modelling in the mining industry as being: 1) a predictive tool, given detailed and accurate input data and appropriate calibration, and 2) a method to undertake parametric studies, given uncertain or qualitative data on the rock units and geologic structure. Numerical modelling also serves as an investigative tool to explore and better understand mechanisms.

Once a numerical analysis is deemed necessary, the user must make several choices which affect the ways the engineering problem and the inputs used are addressed. These choices include the use of 2-D or 3-D analyses, limit equilibrium or advanced numerical techniques, use of continuum or discontinuum codes, etc.

Currently, much of the work done within the industry for open pit analyses is completed using 2-D numerical analyses. Cross sections through the problem geometry are chosen with representative lithologic boundaries and geologic structures. Two-dimensional codes generally provide quicker solution times and are simpler to develop due to the reduced dimensional needs for defining the problem geometry, together with required inputs regarding the in-situ stresses and geological structures present in the rock mass. Recent advances in computing technology have allowed for higher-level 3-D analyses to be undertaken; however, they are mostly conducted by only the md to upper level mining companies and not yet widely used by smaller or junior companies due to limitations in computing power and time required to set up a problem

involving complex 3-D geometries. Three-dimensional codes allow the models to incorporate varying stresses as well as changing slope angles, slope directions and discontinuity orientations within the slope.

Continuum codes, such as RS^2 and RS^3, formerly Phase2 (by Rocscience) or FLAC and FLAC3D (by Itasca Consulting Group) involve structured meshes which allow the user to develop detailed numerical models with respect to mining excavations and major geological changes. Faults can be included within continuum numerical codes through a variety of methods, the most prominent being through the assignment of specialized constitutive models (for example the ubiquitous joint model) or reduced input properties to a grouping of elements representing the fault. Other techniques include the use of interfaces that allow the mesh to separate, although these are not as commonly used as they negate the simplicity of the continuum framework. Each of these methods may be used if the geology and slope failure mechanism can be appropriately represented; however, continuum treatments also come with some major drawbacks that also need to be considered. For example, the ubiquitous joint method will only allow the user to add a single plane of weakness within a single element and cannot be made to be continuous through several elements. While this may be enough to replicate a failure mechanism at the onset of failure, if continued movement is expected, this method will not appropriately capture the stresses and displacements that will occur.

Discontinuum methods, such as the distinct-element codes UDEC and 3DEC (by Itasca Consulting Group), model a rock mass as an assemblage of discrete blocks that allows for internal sliding along and opening/closure between blocks to occur. The discontinuities are treated as boundary conditions between blocks allowing for large displacements along discontinuities and rotations of blocks are allowed without severely distorting the entire model. The blocks within the assemblage can be set as rigid or deformable. Deformable blocks are subdivided into a mesh of finite-difference elements, and each element responds per a prescribed linear or nonlinear stress-strain law. Linear or nonlinear force-displacement relations for movement in both the normal and shear directions also govern the relative motion of the blocks.

Discontinuum methods used to analyze the stability of large open pit mine slopes are particularly well suited to problems involving jointed media or when structures are believed to play a significant role in the stability of the slope. The approach shows the importance of joints in enabling slip to occur between blocks as well as yielding and deformation of the blocks in contributing to the kinematics and development of the failure mechanism (e.g., flexural toppling). Rose and Scholz (2009) provide four examples of the use of UDEC to approximate the 2-D stress-strain paths of a large open pit slope by simulating bench-by-bench mining with a strain softening constitutive criterion. The results attained from this study were compared and calibrated against geodetic monitoring data to allow for predictive modelling of the pit slope walls. One of the important limitations of discontinuum modelling, especially in 3-D, is the need to simplify the geometry of

the fault surfaces. The simplifications chosen by the user may have a significant effect on the stresses, strains and rock damage produced within a model.

One commonality to both continuum and discontinuum methods as well as 2-D and 3-D models is the method in which stress is treated within the model. In contrast to analyses involving underground excavations, the initial in-situ stress conditions in slope stability analyses are thought to be less important to the eventual result. Within advanced codes, in-situ stresses are applied throughout the model as either constant boundary conditions assigned to the edges of the model or by applying constant values of stress within the models based on geodetic loading or generalized tectonic in-situ stress ratios. Generally, in-situ stresses at the beginning stages of a mine-scale numerical model are set out in a depth-dependent fashion (i.e., gravity loading) with a stress ratio multiplier assigning either higher or lower horizontal stresses relative to the gravity dependent vertical stresses. Weaker units within the models will accept a lesser amount of stress relative to adjacent stiffer units; however, in general, it is only once mining is simulated within the model that stress heterogeneity begins to develop. This is done for several reasons including: i) the need to set up the geometry of the problem prior to running the model, ii) the lack of perceived information on the structural or tectonic history of the site, iii) the low confidence in material properties and their impact on stress heterogeneity; and iv) budgetary and time constraints in creating practical numerical models used in decision making.

Due to the expense of collecting appropriate data and the natural variability of geological systems, the fact that numerical modelling for geomechanical analysis of mining operations suffers from a lack of information should not be a surprise. This in fact emphasizes the need to use numerical modelling as an investigative tool to explore potential risks and hazards related to geological uncertainty, constrained for practical purposes by field observations. Geomechanical characterization of a rock mass is very much simplified in terms of rock behavior and potential failure mechanisms. Strain-softening of a rock mass is one method in which the user of the numerical analysis can simulate brittle behavior, test post-peak strength, and to allow for early on-set of failure if the critical strain limit is set appropriately. In practice, very few sites have enough information to properly group and characterize the peak or residual strength and behavior of the rock. With numerical models, the user can explore potential outcomes of mining decisions based on engineering judgement; however, the properties and behaviors used must be justified to allow decision makers to have confidence in the potential outcomes they are presented with. As such, most peak strengths are simplified and post-peak behavior ignored.

2.5. Research Methodology

For Objective 1, to "*Determine if differential behavior of a rock mass, near or separated by faults, can be detected and/or characterized …*", the methodology adopted includes first analyzing two unique monitoring data sets. This entails an in-depth review of historical geodetic prism data collected by the Palabora Mining Company Ltd. (Palabora), prior, during, and after a massive pit wall failure that occurred in 2004. The type of data collected at Palabora is typical of that collected at an active mine site; however, a focused analysis of monitoring data will be performed to determine the influence of large and persistent faults on the recorded displacements during the mine's transition from open pit mining to underground block caving. Results link geodetic displacements to the influence of faults on slope deformations. These demonstrate that the point measurements require much of the rock mass response to be interpolated.

Based on the limitations experienced during the review of the Palabora data set, a "first of its kind" experiment was proposed and carried out in which two terrestrial InSAR units are simultaneously deployed to collect continuous, line-of-sight displacement data for a large, moving open pit slope. The slope selected for this experiment was at the Teck Highland Valley Copper (THVC) mine near Kamloops, B.C., and involved a weak rock mass transected by a large fault zone that separates zones of rock mass yielding near the toe and toppling kinematics near the crest. This experiment was designed to determine if emerging technologies in slope monitoring can be improved on to provide both full spatial coverage as well as a real-time 3-D slope displacement map.

For Objective 2, to "*Identify the critical factors controlling stress heterogeneity around open pit mines…*", several potential factors will be investigated with 2-D and 3-D numerical models. The impact of these factors on slope stability will be evaluated, ranging from regional, pit, and local slope scales. Both continuum and discontinuum modelling methods, as previously described, and utilized where their strengths prove advantageous. The model geometries are largely conceptual, but these and the input parameters used are based in part on actual open pit examples.

For Objective 3, to "*Identify the critical fault characteristics which influence the development of stress heterogeneity and determine the best means to represent these in numerical models…*", several aspects of geological structures (i.e., faults and fault zones) will be analyzed using detailed 2-D and 3-D numerical models. These will examine the effect of faults on stress development and rock mass deformation as an open pit is progressively excavated. The numerical analyses will be used to show that failure mechanisms can transition from one that is primarily structurally controlled to a more complex mechanism that incorporates stress-strain rock mass damage near an adjacent fault. Fault aspects to be examined include: width, representation of faulted rock (i.e. discrete plane or fractured zone), and surface complexity. The

role of in-situ stresses and 3-D mine geometry, relative to the discontinuities, will also be investigated. A similar approach as for Objective 2 is used with respect to employing both continuum and discontinuum modelling methods, and basing models in part on actual large open pit cases. These models will be calibrated and constrained by the monitoring sets developed from the first objective. A comparative analysis of linear and non-linear elasto-plastic, bi-modal and strain softening constitutive models is conducted through numerical modelling of the HVC case study.

CHAPTER 3 DETECTION OF DIFFERENTIAL PIT SLOPE DISPLACEMENT NEAR FAULT STRUCTURES

Synopsis

This chapter investigates the ability of current and emerging monitoring technologies to detect differential behavior of a rock mass within an open pit intersected by large geological structures. Faults within a rock mass can be expected to control or at least affect the displacement magnitudes and patterns within open pit slopes. Depending on the rock mass strength and deformability, the faults may act to constrain rigid block movement or may influence rock mass deformation within a fault-bounded block. This chapter focuses on: 1) typical insights that can be achieved through current and emerging displacement monitoring techniques, 2) the structural control of faults on displacement within large open pits, 3) the advancement of a state-of-the art monitoring technique, and 4) the ability to assess pit slope kinematics using these techniques. The primary component of this chapter (Section 3.2) has been published as a journal paper in *Engineering Geology* (2014, vol. 181, pp. 202-211). Parts of Section 3.1 have been published as a technical paper presented at the Caving 2010 Symposium in Perth.

3.1. Structural Control of Slope Displacements in Brittle Rock at Palabora*

* Sections extracted from Severin, J., Eberhardt, E. & Woo, K. (2010). Influence of major fault zones on 3D ground deformations caused by open pit block cave interactions. In *Caving 2010, Proceedings of the 2nd International Symposium on Block and Sublevel Caving, Perth*, 20-22 April 2010. Edited by Y. Potvin, ACG, Perth, pp. 205-216.

3.1.1. Introduction

The Palabora Copper Mine is located approximately 500 km northeast of Johannesburg, South Africa. Mining commenced in 1964 as an open pit operation, producing a pit measuring approximately 800 m in depth and 1650 m across by the end of the pit life in 2002. Inter ramp angles ranged from 37 degrees in the upper weathered rock to 58 degrees in the competent lithology at the base of the pit (Moss et al., 2006). The mine successfully transitioned to a block caving operation with underground production commencing in April 2001 and increasing gradually until full production was achieved in May 2005. The geology of the ore body at Palabora involves a sub-vertical volcanic pipe emplaced within pyroxenite. Late stage dykes with steeply dipping northeast trends are also present as are several northwest and northeast trending faults. Figure 3.1 shows the four main faults transecting the pit. Amongst these, the Mica Fault is described as a 60-m wide shear zone comprised of large rock blocks, fault breccia and fault gouge.

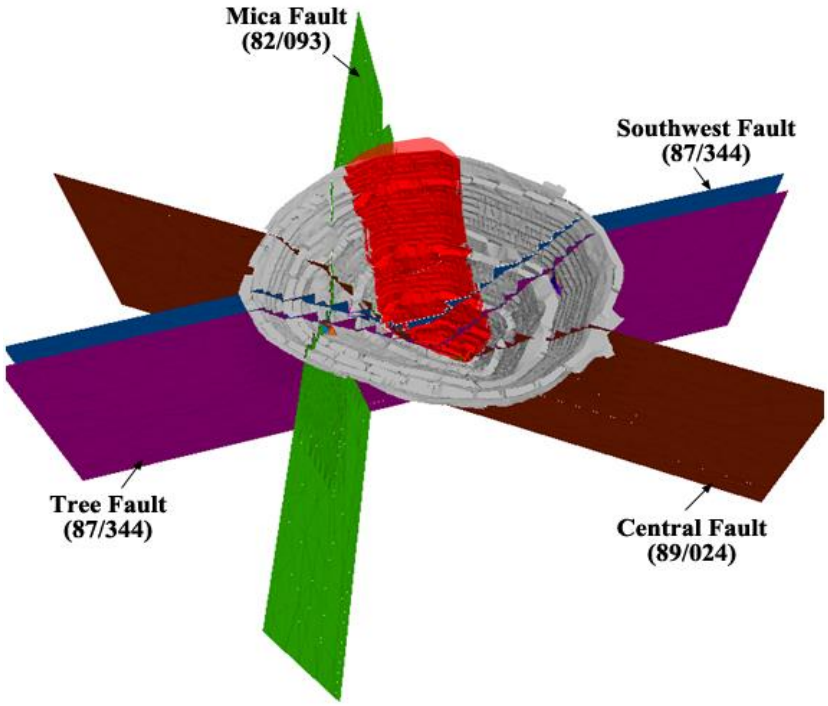

Figure 3.1. 3-D structural model of the Palabora open pit with regional faults indicated. North is towards the top. The outline of the 2004 pit wall failure is shaded red.

3.1.2. Interpretation of Geodetic Pit Slope Monitoring Data

A review of available geodetic monitoring data at Palabora was conducted to investigate how the transecting faults can affect the spatial and temporal response of a hard, brittle rock mass to mining activities. Slope behaviour was reviewed using displacement rates, cumulative displacement, and direction of displacement with respect to these major features. The assessment includes all geodetic data collected between 1984 and 2004, during pit deepening, block cave initiation, crown break through, and eventually, pit wall failure. Focus was placed on the west wall and northwest wall of the pit.

Generally, both displacement rates and direction of prism movement during pit deepening appear to be consistent with normal rebound associated with the excavation of the open pit. The displacement vector directions for the Palabora mine from 1998 to 2005 are plotted in Figure 3.2a), differentiating those before (green) and those after (red) the initiation of caving. Inspection of the incremental displacements showed that before caving, displacement rates were constant and in a common direction and the vertical component was dominant suggesting that both strain relief (rebound) and downward relaxation of the slopes towards the pit were active components in response to mining. In general, the displacement rates increased with pit deepening, with the displacement vectors prior to caving pointing towards the bottom of the west wall and

middle of the pit. Prisms located near the Mica and Southwest faults show movement toward the faults, likely due to the compression of broken rock within the brecciated fault zones. Minor movements along the Mica Fault in a strike-slip direction during pit deepening can also be observed in the data.

After the initiation of caving operations in April 2001 and progressing up to the 2004 pit wall failure, the pattern of displacement in the west wall began to noticeably change. Displacement data collected from most prisms on the west wall indicate that the rock slopes are being drawn towards a location beneath the northwest wall (red arrows in Figure 3.2a), roughly corresponding with the location of the eventual failure. Microseismic data collected at Palabora (Glazer, 2003) supports the displacement data interpretation that the caving front migrated from beneath the centre of the pit, as planned, to beneath the north wall.

Most prisms located on the west side of the Mica Fault underwent a sharp, distinct movement to the southwest during January to February 2002. This movement did not correlate well to any pit or underground development activities and is therefore interpreted as a strike slip motion along the Mica Fault, possibly induced by the growing caving front. Prisms located on the east side of the Mica Fault did not experience this movement.

The temporal changes in the West wall resolved from the analysis of the geodetic data further reveal several important that are key to understanding the 3-D slope kinematics in response to block caving. A review of the timing at which the prisms began to move toward the base of the north wall show that the displacements occurred in stages. Figure 3.2b indicates the location of the prisms reviewed and their relative start date of displacement toward the north wall. The red dots show areas of consistent movement of the surrounding rock mass as early as January 2003, roughly the same time as the cave breakthrough occurred in the bottom of the pit, while prisms located to the west of the Mica Fault (main north-south fault) began to displace 3 to 6 months later (green and orange dots, respectively). Prisms to the west of the Mica Fault did not begin to displace until June 2003, suggesting that the fault may have partially shielded the rest of the west wall from movement during these early stages of cave migration. The Mica Fault consists of a zone of brecciated rock, which would allow most of the extensional strains caused by the advancing cave to be diffused through dislocation and opening rather than transferred across to the west side of the fault.

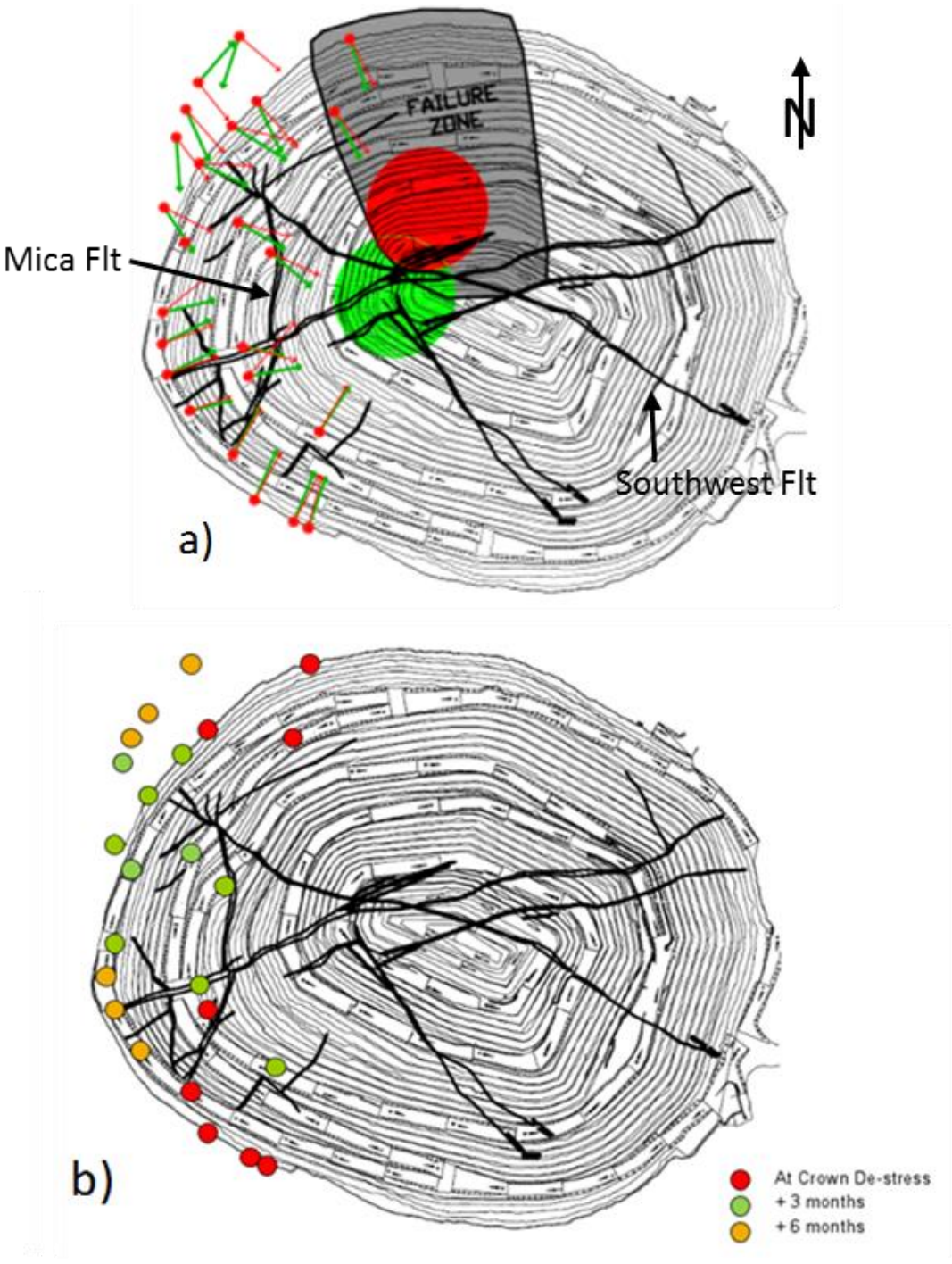

Figure 3.2. **Prism data review indicating both spatial and temporal control of faults on rock mass displacements. a) West wall displacement vectors before block caving (shown in green) and after (shown in red); b) Relative timing of displacement of prism toward failure zone (red = crown de-stressing, green = +3 months, orange = +6 months).**

In summary, the analysis of the monitoring data from Palabora relative to the pit wall failure has led to several important observations that provide insight into the kinematics of the west wall. From these, the following working findings were derived: a) the caving front acted as the dominant control for the pit slope movements observed, but the major fault zones crossing the pit also had a notable influence, b) the sub-vertical nature of the geologic structures tend to promote vertical movements, damp those that are horizontal and extensional, and have little to no effect on those that are horizontal and compressional, c) the Mica Fault shielded the West wall from induced strains during breakthrough of the cave and failure of the northwest wall, d) the location of the cave front along with the vertical nature of the geologic structures interacted to promote subsidence of the northwest wall with a feedback that promoted migration of the cave back towards the northwest wall, and e) the cave back does not appear to migrate up and along one of the major faults, but rather along the dominant joint set in the north wall.

3.2. Development and Application of a Pseudo-3D Pit Slope Displacement Map Derived from Ground-Based Radar*

* Severin, J., Eberhardt, E., Leoni, L., and Fortin, S. 2014. Development and application of a pseudo-3D pit slope displacement map derived from ground-based radar. *Engineering Geology*, Vol. 181, October 2014, pp 202-211.

3.2.1. Introduction

Slope monitoring using radar, geodetic prisms, visual observations, and other geotechnical instruments forms a key component of modern open pit slope management programs for most mining companies. The management programs are designed to focus on providing an early warning of an impending slope failure so that personal risk to mining staff is minimized while mine production is maximized by reducing downtime of the mine. Standard slope monitoring practices typically involve the periodic measurement of geodetic prisms by a survey crew or robotic total station to identify and quantify the nature and extent of pit slope movements. The prism data, being point measurements, are susceptible to uncertainty relating to the geological conditions and slope kinematics controlling the instability mechanism. The detection of accelerating behavior may either be an early warning of impending failure or a false alarm related to highly localized movements in the immediate vicinity of the prism or atmospheric conditions in the pit. Similarly, the interpolation of slope behavior between prism locations may result in displacements influenced by large-scale geological structures being misinterpreted or missed all together. Increasingly, the geodetic data is collected in collaboration with radar instruments to help delineate the region of increased slope displacement and collect data between the geodetic prisms on the slope. Radar data is collected near

continuously in real time, which creates a massive amount of data over a short period. Thus, it is often only used for early warning monitoring using vendor-provided software, even though it also contains useful information on the slope instability kinematics.

This paper outlines a novel experiment which may be repeated in cases where mine staff is required to investigate and gain a better understanding of the 3-D kinematics and dynamics of pit slope displacements which have been identified as representing a threat to mine operations and safety. The experiment involves the simultaneous deployment of two ground-based interferometric synthetic aperture radar systems which were used to collect continuous, line of sight displacement data in "stereo" of a large, moving open pit slope bisected by a large fault. The data and results presented demonstrate that an improved understanding of the 3-D kinematics of the slope and influence of large scale geological structures can be achieved using advanced state-of-the-art monitoring techniques. This understanding can be used to help mitigate the current risk presented by a slope or be used to design the next phase of an open pit layout (e.g. pushback).

3.2.2. Slope Monitoring Techniques

Investigative Monitoring

For slope monitoring to be most effective, the data should first be used to gain a baseline understanding of the slope behavior before using it for predictive purposes and defining early warning alarm thresholds. Thus, the function of the monitoring network is serving two purposes (Moore et al., 1991):

(i) Investigative monitoring: To provide an understanding of the slope behavior over time and typical responses to external events (e.g. precipitation and seasonal fluctuations).

(ii) Predictive monitoring: To provide a warning of a change in behavior, enabling the possibility of limiting damage or intervening to prevent hazardous sliding.

Investigative monitoring has been shown to facilitate a greater understanding of the behavior of both natural (Willenberg et al., 2008) and engineered slopes (Walker et al., 2006), thus enabling the correct mitigation measures to be selected or to confirm that the slope is performing as expected. Ultimately, pit slope monitoring is carried out to ensure the safety of workers and equipment with the added benefit of calibrating geotechnical models. Alarm thresholds are usually set based on experience, extrapolating measured displacement time series to detect accelerations that exceed set thresholds. Rose and Hungr (2007) demonstrated further utility by extrapolating the inverse velocity time series introduced by Fukuzono (1985). It must be noted that these approaches are generally applied independent of the failure mechanism or monitoring method (e.g., geodetic point measurement and tension crack opening). As such, false alarms

or uncertainty over misleading instrument readings is a frequent problem. Once an alarm is triggered, the mine may shut down operations around potential instability. If a failure occurs, the procedure is deemed a success (Seery, 2007); if not, the procedure results in costly downtime, delays to production schedules and diminished confidence in the system.

Geodetic Monitoring

Geodetic monitoring represents the most common method employed in pit slope management due to its general reliability, relative low cost, and ease of execution. The geodetic monitoring of numerous prisms installed on multiple benches is now routinely undertaken using robotic total stations, with recent efforts to combine these systems with global navigation satellite systems (Brown et al., 2007). Monitoring through GPS receivers has also been seen as an answer to large open pit projects where the pit diameter exceeds 1 km and refraction and pointing errors start to limit the effectiveness of total station measurements.

Outside of potential safety concerns during the deployment of the prisms, an important limitation of data collected from geodetic monitoring is that movement and deformations between prisms must be interpolated. This may result in: i) the boundaries of areas with high displacement rates being poorly defined, ii) smaller scale structurally controlled movements such as wedge or planar sliding to be overlooked, and/or iii) the kinematics behind larger and more complex pit-scale failures being misinterpreted. Another major limitation is the interruption of monitoring of prisms due to the physical loss of the prism or due to dust causing a disruption.

Radar Monitoring

New developments in slope monitoring include the use of remote sensing technologies like terrestrial radar, which provide high resolution, full area spatial coverage as opposed to relying on geodetic point measurements. Radar works by continuously scanning and comparing highly accurate and precise measurements made from up to 4 km from the slope face to detect sub-millimeter movements (with an accuracy of 0.1 to 1mm, depending on distance). Radar units can collect real-time, near-continuous (5-minute interval), line-of-sight (1-D) monitoring data of large areas in all weather conditions (Farina et al., 2012). Such capabilities are helping to establish radar as a key tool for managing unstable pit slopes, quickly identifying the size, extent and temporal behavior of a developing failure (e.g., Harries et al., 2006; Seery, 2007; Harries and Roberts, 2007). Rödelsperger et al. (2010) describe the advantages and disadvantages of radar data as compared to other forms of monitoring. The precise measurement of displacement from far distances allows radar data to be used by researchers in several state-of-the-art applications such as

monitoring volcanic activity (Di Traglia et al., 2014), concrete dam displacement (Talich et al., 2014), and natural slope stability (Martino and Mazzanti, 2014).

Ground based synthetic aperture radar was initially applied to measurement of natural slope movements in the Italian Alps (Tarchi et al., 2003) in 2000 and since has been validated during multiple investigations of landslides (Noferini et al., 2007; Monserrat et al., 2013) and has been used as a predictive tool to forecast slope displacement (Herrera et al., 2009; Casagli et al, 2010).

One key limitation of all radar systems is that it can only provide line-of-sight displacement meaning that important 3-D information of the displacement kinematics may be missed. The collection of large amounts of data in combination with a shrinking and overly specialized work force has had the unintended effect of reducing the mine geotechnical engineer to either a radar system trouble shooter or a data archive manager.

3.2.3. Full Spatial Detection of a Slope

Teck Highland Valley Copper Mine

The Teck Highland Valley Copper (THVC) mine is located near Kamloops in south-western British Columbia, Canada (Figure 3.3). THVC is a truck and shovel operation comprised of several open pits. The experiment described within this paper was carried out in the Lornex Pit (Figure 3.4).

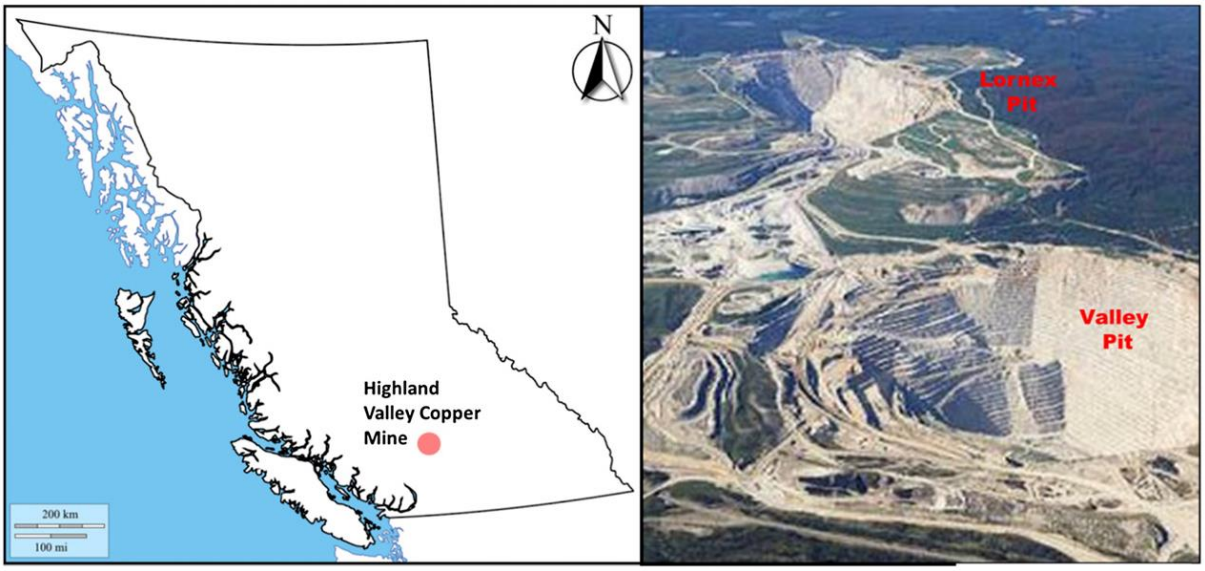

Figure 3.3. Geographic location of study site, Teck Highland Valley Copper mine (left) with aerial view of Lornex and Valley Pits (right) [online image]. Retrieved December 5, 2009 from http://www.trcr.bc.ca/report-33rd-annual-mine-reclamation-awards.

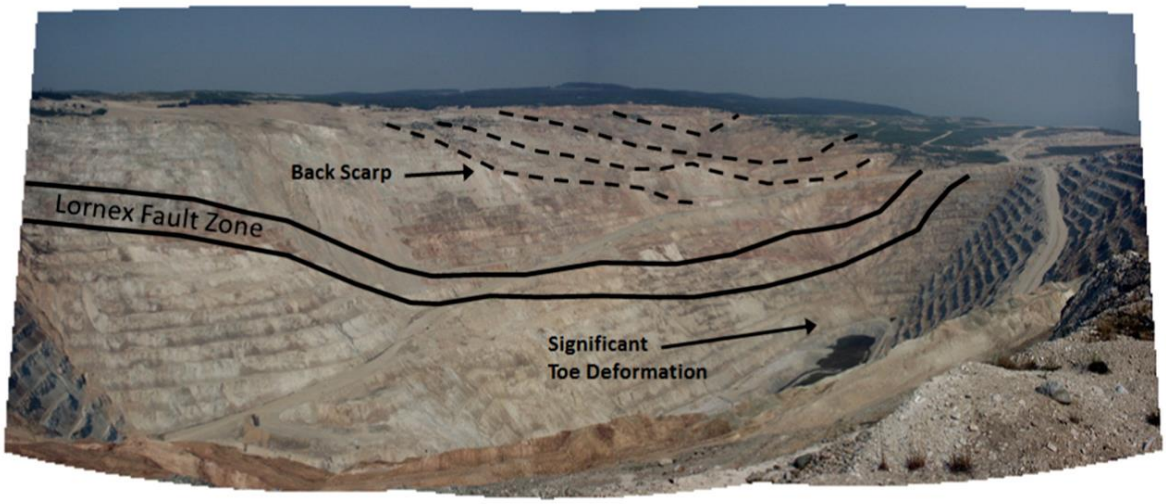

Figure 3.4. West wall of the Lornex Pit at the Teck Highland Valley Copper mine, showing the location of the Lornex Fault Zone, and graben-like backscarps and toe bulging that has developed with pit wall movements.

The west wall of the Lornex Pit is a 400m high slope with an overall angle of 29° (Figure 3.4). The rock is relatively competent but is altered near the fault zones. The west wall is bisected by the Lornex Fault Zone (LFZ), a zone of highly fractured and intensely altered rock ranging between 40 and 80 m that dips approximately 75° into the slope. The LFZ in conjunction with the other faults in the slope is interpreted as playing a critical role in controlling the kinematics of the upper slope movement (Rose and Scholz, 2009).

Other moderately to steeply dipping faults that trend northeast–southwest occur intermittently throughout the hanging wall of the LFZ. Movement within the hanging wall of the LFZ (upper slope) is reported as being caused by a complex toppling mechanism with a historical maximum daily velocity of greater than 300 mm/day (Rose and Scholz, 2009). At the time of the writing of this paper, the west wall of the Lornex Pit was well instrumented with over 75 geodetic prisms installed; however, the northwest portion of the pit wall is relatively void of prisms (Figure 3.5, left), primarily because of safety concerns, lack of access preventing their installation, or slope displacements that rendered them inoperative. The Lornex Pit is currently undergoing a pushback around its entire circumference.

Experiment Set-up and Instrument Positioning

The radar system used in this study was an IBIS-M (manufactured by IDS Ingegneria Dei Sistemi). The system is based on: i) Stepped Frequency Continuous Wave (SF-CW), allowing resolution in the range direction, ii) Synthetic Aperture Radar (SAR), allowing the system to resolve the monitored region in the

cross-range direction, and iii) differential interferometry, which allows the measurement of displacements by comparing phase information of the back scattered electromagnetic waves collected at different times. The first radar unit (Site A) was located near the top of the northeast pit wall (Figure 3.5, right). The distance of the monitored points here ranged between approximately 800 and 1500 m.

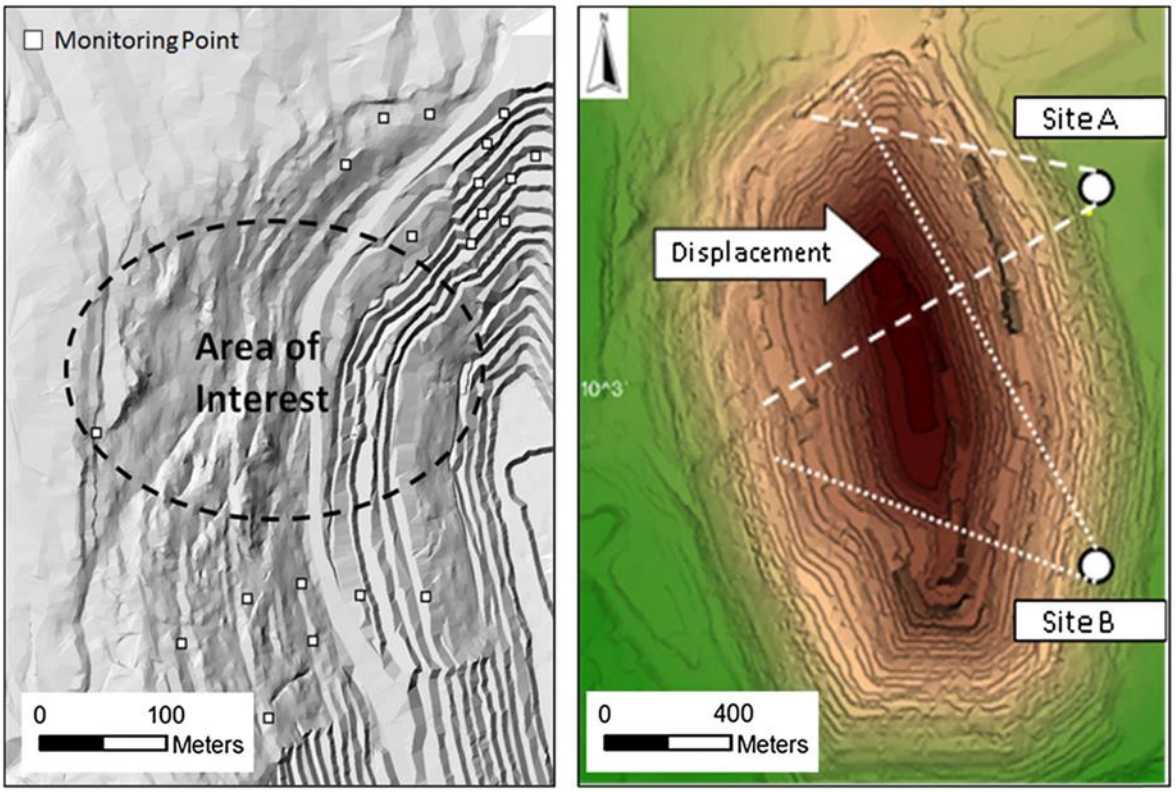

Figure 3.5. Location of operational geodetic prisms on the northwest wall Lornex and the radar monitoring experiment sites (right) with respect to the portion of the wall undergoing the highest rates of displacement (within dashed lines).

At this distance, the resolution of the monitored pixels was 1.5 × 4.3 m. This site was chosen for being roughly parallel to the general direction of slope movement. Site B was located at the top of the southeast pit wall, providing good spatial overlap with Site A and an oblique angle to the projected direction of slope movement. The distance of the monitored points ranged between 1200 and 2500 m, which correlates to a monitored pixel size of 1.5 × 8.6 m. Both monitoring sites were selected as their locations were stable (minimal displacement) and outside the range of any fly-rock generated from production blasts in the pit. Power to the radar units was provided by batteries and a portable power generator. The timing of the data collection scans was set to collect data simultaneously within the internal clock of the radar units with scan time intervals of approximately 6 min. The data were then collected for a 5-day overlap time. As the

distances between the monitoring point and the wall of interest were different, the frequencies used to collect the data were not the same and no interference occurred. A typical radar setup is shown in Figure 3.6. A full description of the IBIS-M system is given by Farina et al. (2012).

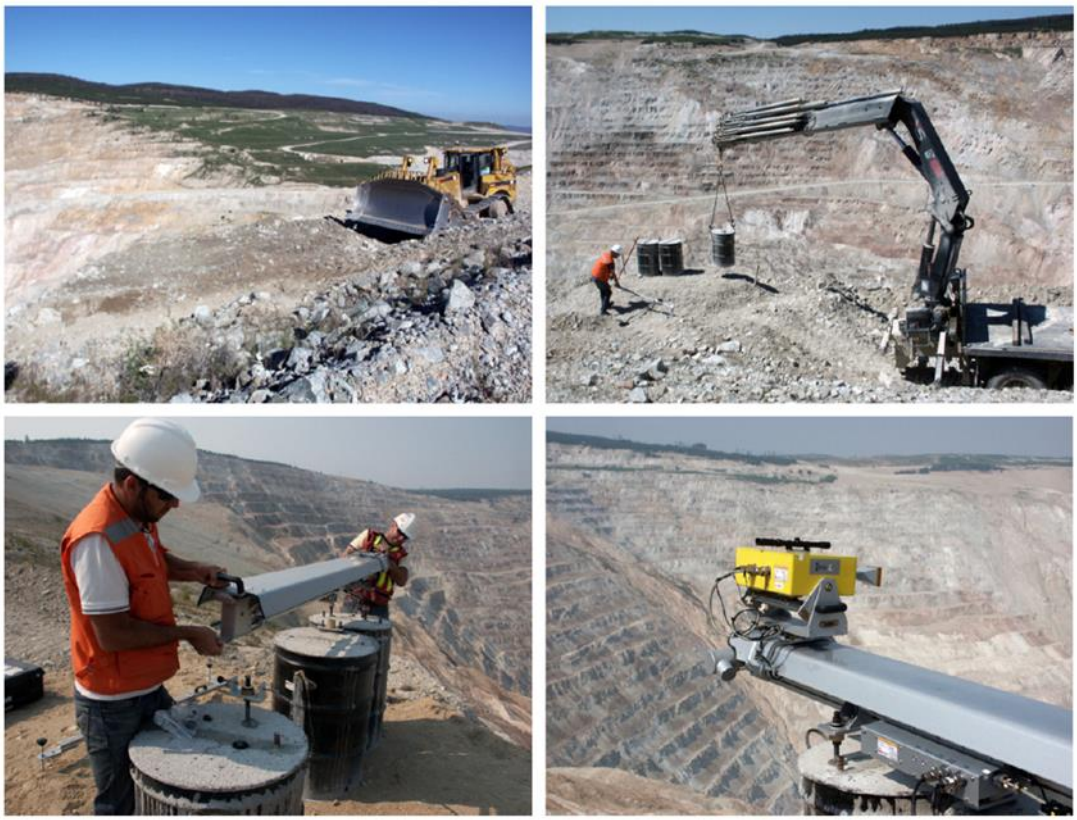

Figure 3.6. Site preparation and installation of the IBIS-M radar unit for the 3-D radar experiment, showing: leveling and grading of gravel site pad, lifting of concrete filled drums for radar base, fitting of leveled radar guide rail, and radar positioning for pit wall monitoring.

3.2.4. Data Analysis

Resolving 3-D Displacement Vectors

The monitoring data was collected and processed using the software IBIS Controller® and IBIS Guardian® to remove the atmospheric artifacts, in both range and cross-range, from the phase information with a mathematical algorithm that can automatically discern stable points from those that are moving. This avoids the need to manually select ground control points. Two independent displacement maps in raster format for each of the installation points were created over the selected time frame. Using ArcGIS, the raster data set were combined with a digital elevation model (DEM) of the mine site and converted into global coordinates

with displacement values. The slope was pixelated into a grid of between 30,000 and 40,000 monitoring points by each radar unit. The locations of the center points of the pixels were compared and matched, and approximately 25,700 points were found to be common between the two data sets.

Based on the original location common to each raster set (X_{A1}, Y_{A1}, $Z_{A1} = X_{B1}$, Y_{B1}, Z_{B1}), the corresponding line-of-sight displacement magnitude and the location of each radar instrument, a displacement vector for each direction of movement was created (X_{A2}, Y_{A2}, Z_{A2} and X_{B2}, Y_{B2}, Z_{B2}) using the formula:

Equation 3.1

$$(x_2, y_2, z_2) = (x_1, y_1, z_1) + R * [(x_1, y_1, z_1) - (x_0, y_0, z_0)]$$

where x_0,y_0,z_0 is the instrument location, and R is the ratio of the measured displacement and distance from the instrument.

For each of the new vectors created, the equation of the plane perpendicular to that vector at the new point (X_{A2}, Y_{A2}, Z_{A2} and X_{B2}, Y_{B2}, Z_{B2}) was determined. The actual displacement of each raster cell must exist on both planes; therefore, the end of the combined displacement vector exists on the line created by the intersection of these two planes.

In the absence of a third radar unit to allow for true 3-D triangulation, one of the values of the new vector was assumed. In this case, an estimated value for the elevation was evaluated by using two techniques: an average Z value and a weighted Z value based on displacement. For the weighted Z value, the elevation of the new vector was determined using the following relationship:

Equation 3.2

$$\frac{Disp\ A}{Disp\ B} = \frac{\Delta Z_A}{\Delta Z_B}$$

Inspection of the results using this relationship suggested that the weighted Z value (i.e., weighted elevation values) produced a unique solution for the combined A + B vectors (X_{Comb}, Y_{Comb}, Z_{Comb}).

An idealized example is shown in Figure 3.7. In this example, two vectors are created from the respective line-of-sight displacements (Sites A and B) with corresponding planes perpendicular to the vectors. The two planes are plotted with a resultant line of intersection.

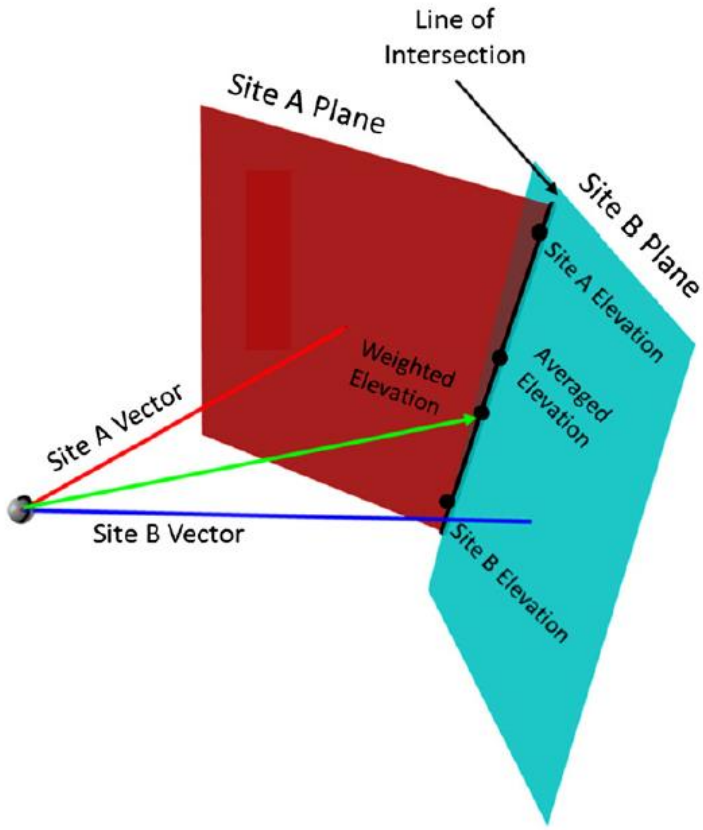

Figure 3.7 **Determination of pseudo-3D vector (green) resolved from the line-of-sight vectors (A and B) and a weighted elevation assumption along the line of intersection between planes normal to A and B. Also shown is the average elevation option.**

For a given elevation value entered into the equation representing the line of intersection, both X and Y values can then be determined. In this case, when a larger amount of displacement is recorded by one instrument, it is assumed that the direction of movement for that cell is more like the direction parallel to the line of sight of that instrument and a weighted value for the elevation (Equation 2.2) is used. In individual cases, geological features such as the fault or joints can be used to help interpret the direction of movement; however, these assumptions would not be able to be used over the entirety of thousands of points making up the displacement map. Caution should be used when trying to apply specific knowledge to the displacement map as the precise location of the vector and the digital elevation model may lead to the interpretation of an incorrect structure.

3.2.5. Displacement Map Generation

The newly created vectors and corresponding points were imported into the CAD software Rhino© (Rhino Software, 2010), and sorted by magnitude. These points/vectors were then draped over a DEM of the Lornex Pit and the Lornex Fault Zone to determine the patterns of movement.

Displacement maps based on the individual instruments (Sites A and B) were also created for individual comparison. Unfortunately, no geodetic prisms were operational at the time of the experiment to help calibrate the creation of the 3D displacement map (as seen in Figure 3.5, left). A further validation experiment was not attempted as the condition of the prisms was not disclosed at the time of the experiment.

3.2.6. Potential Sources of Error

Several potential sources of error during the creation of these maps were identified. Rounding errors may be introduced as the CAD software used can handle up to 8 significant digits. This error is expected to only be significant where very small displacements are recorded.

To create a true 3-D displacement map, three radar units would be required; however, with the use of two units, a pseudo-3D map can be produced. The result of the combination of the two vectors created from each individual unit is the equation of the line of intersection of the two planes. Therefore, the end displacement vector direction can be influenced by the end elevation assumed. If the displacements in the pit wall were predominantly vertical, a larger source of error would be incorporated in the vector direction. In this case, the two radar units were placed at roughly equal elevations and the direction of suspected movement was largely horizontal based on site observations, historical prism data and previous numerical modelling, meaning that the methods for determining the end elevation did not greatly influence the direction of the vector. If the direction of movement is suspected to contain a larger vertical component, then a different configuration of radar placement would have been required.

As both radar units were located near the crest of the opposite slope, much of the pit wall being monitored was below the elevation of the instruments. This means that all movements were recorded in near horizontal or an upward line-of-sight direction. The principal direction of movement in some areas above the Lornex Fault Zone is expected to be gravity driven and move downward toward the toe of the pit wall; therefore, only a portion of the displacement was resolvable.

To achieve a more realistic vector, at least one of the instruments should be located nearer to the bottom of the pit; however, this presents logistical and safety problems in an operating mine environment and possible interference with pit operations.

Another potential source of error was the displacement of the monitoring units during the data collection. The end and center points of both units were surveyed at the start, mid-point, and completion of the monitoring period to capture any movement and/or rotation of the radars.

3.2.7. Three-Dimensional Displacement Pattern

Line of Sight Displacement Magnitudes

The pattern of total cumulative displacements observed from Sites A and B during the monitoring period is shown in Figure 3.8. At Site A, displacement values ranged between +26 and −220 mm/day, while at Site B, displacement values ranged between +35 and −275 mm/day. Negative values represent movement toward the instrument, while positive values represent movement away from the instrument.

Although the instruments were focused upon the same slope segment, the displacement patterns recorded from Sites A and B were found to be similar with slightly different boundaries and, in some cases, magnitude. This confirms the presence of absolute movement occurring in distinct areas of the pit wall and that the different perspectives of the instrument can capture different components of that movement. The comparison between the two displacement patterns highlights the importance of the investigative processes used in understanding the failure or displacement mechanism within a slope prior to setting thresholds used to set monitoring alarms. If a single (often arbitrary) position is picked for slope monitoring, the nature of the pit wall movement may not be observed.

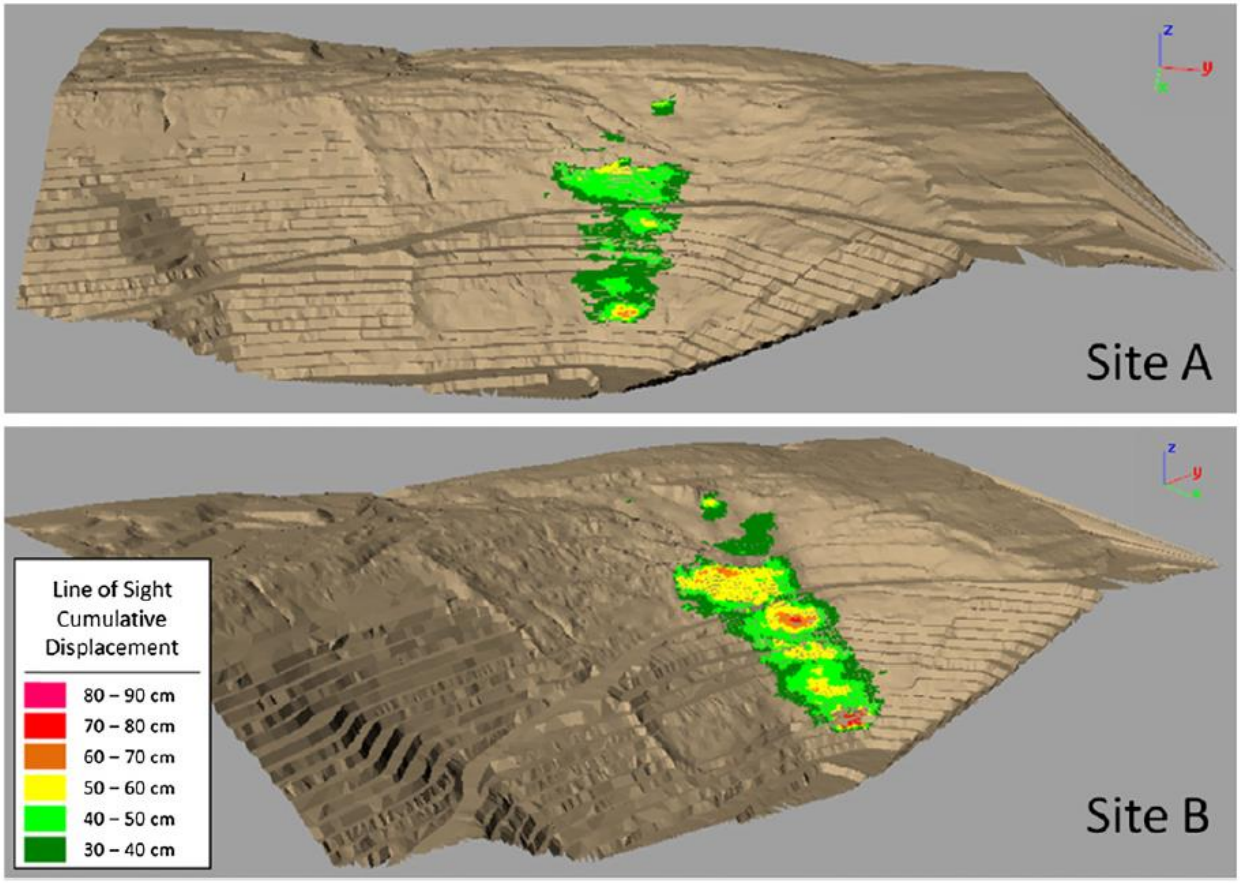

Figure 3.8. Measured line-of-sight displacement patterns from experiment site locations. Note that a minimum cut-off value of 30cm was used to reduce the background noise.

Combined Displacement Magnitudes

The combined displacements measured from the two radar systems lead to the pattern observed in Figure 3.9. Displacement values ranged between 0 and 307 mm/day and as much as 750 mm cumulative displacement over the monitored 4-day period. As the vectors, have been combined, displacements no longer must be referenced as being toward or away from the instruments as in line-of-sight monitoring techniques but rather an absolute value. These results show maximum displacement values that are higher than the 100 mm/day average reported for the geodetic prisms (Rose and Scholz, 2009). Likely explanations for this discrepancy include the large number of points being measured, the opportunity to measure near vertical rock faces and areas moving too rapidly to install stable prisms, and the mining activities at the time of the experiment which may have influenced activity along the LFZ.

By creating the pseudo-3D displacement map, a more complete representation of the location and pattern of displacements in the slope can be achieved. Based on the combined displacement pattern, several distinct zones of displacement can be observed in Figure 3.9, including: i) below the Lornex Fault near the base of the pit, ii) just above the LFZ near a former access ramp, and iii) in the upper reaches of the slope. The full extent of these lobes can be determined as well as smaller zones within the pit wall. The zones of concentrated displacements resolved by combining the individual radar line-of-sight displacements highlight several smaller areas of localized displacement otherwise not discernible in either of the individual displacement plots. These displacement zones can then be used, in combination with the conventional geodetic data, to aid the creation of a conceptual model used to interpret the measured displacements and the underlying kinematics of the slope, the limits of movement within the slope, and to help calibrate future 2D and 3D numerical deformation models.

Displacement Vectors

The displacement direction of each monitoring point can be resolved into a vector from the individual sets of radar monitoring data from monitoring sites A and B (Figure 3.10). The enlarged region in Figure 3.10 shows an example of an area with higher displacement rates in the slope. By plotting the displacement vectors, several independent lobes of movement within the slope are observed which are likely controlled by separate structures within the rock mass as well as changes in lithology and constitutive behavior of the rock mass.

The vectors indicate toppling movements in the upper slope above the Lornex Fault, which agrees with the presence of a persistent discontinuity set that dips steeply into the slope.

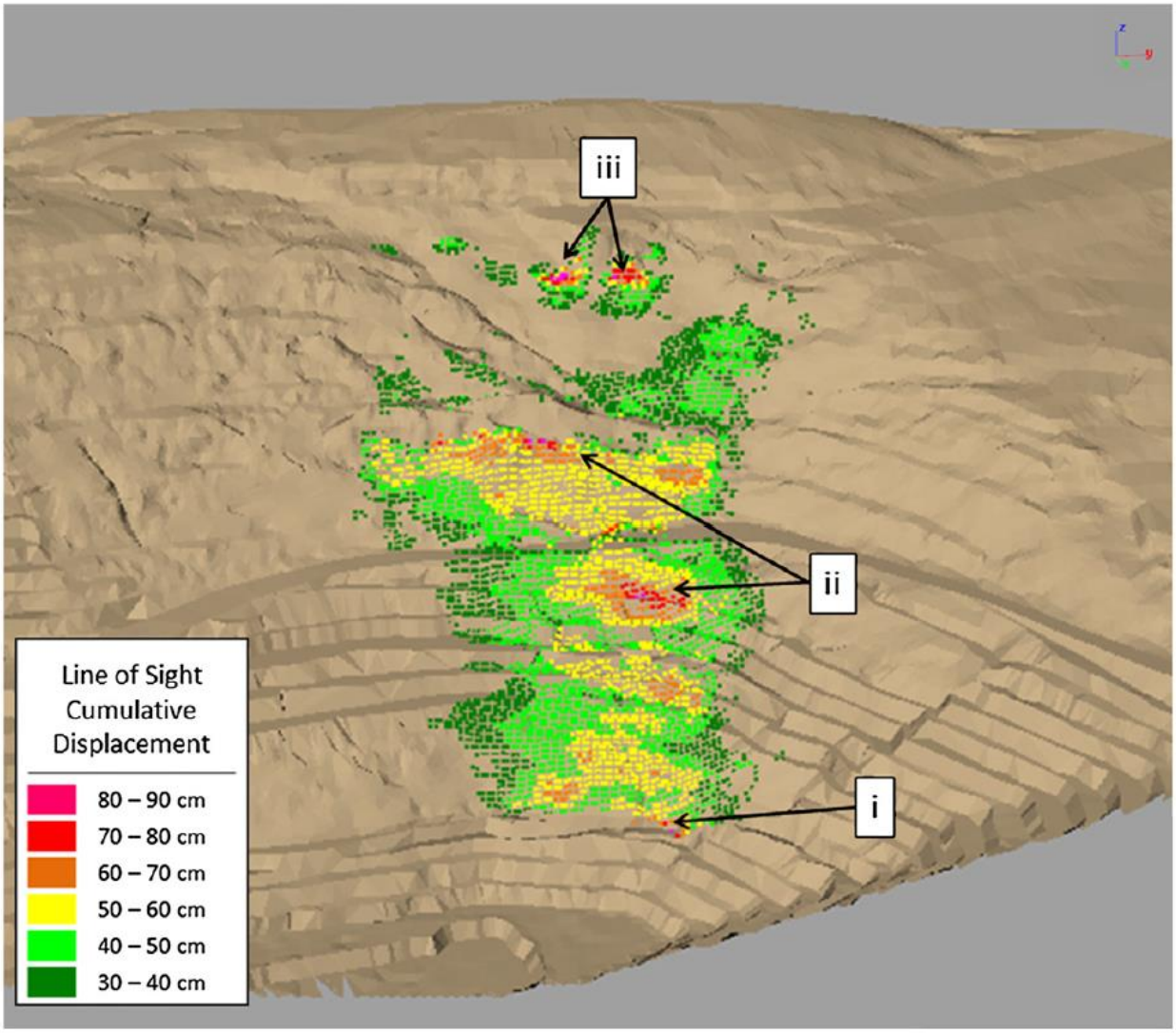

Figure 3.9. Displacement pattern of data set combined from Sites A and B. Several distinct zones are identified (i, ii and iii), as described in the text.

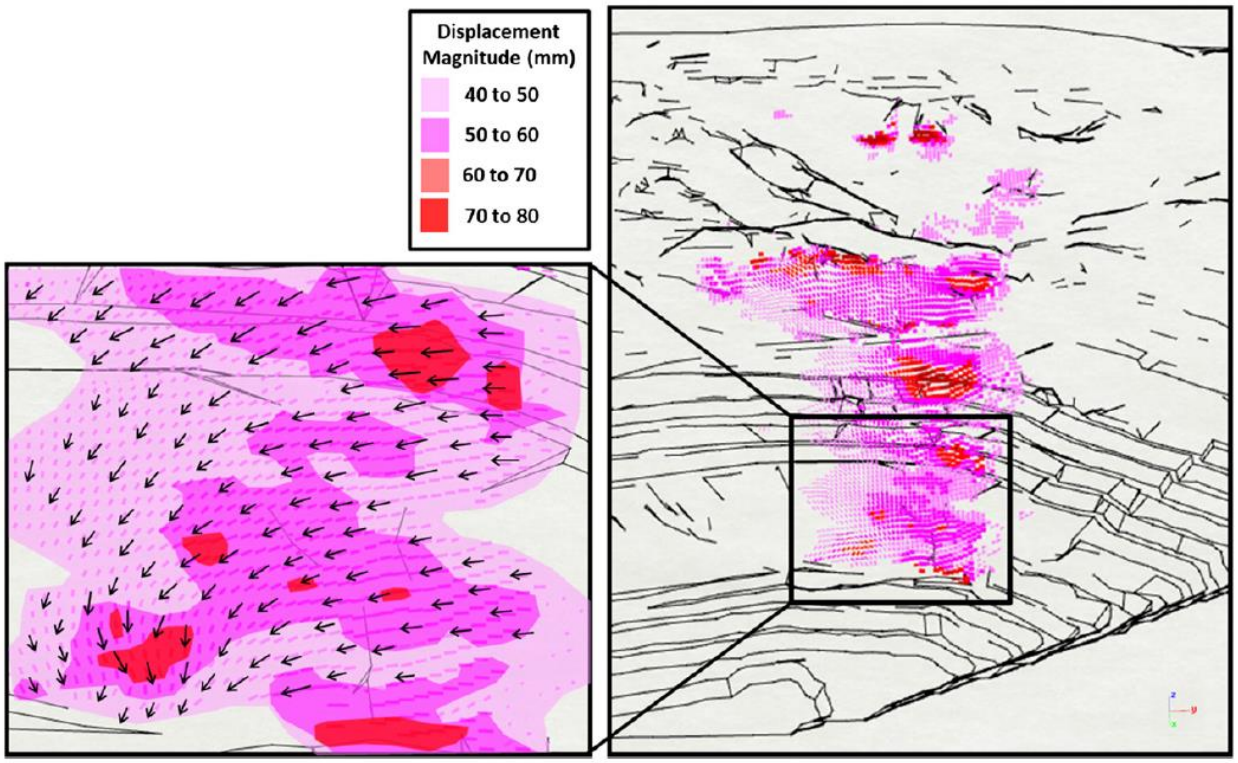

Figure 3.10. Vector map of the data combined from Sites A and B, with vectors scaled to displacement magnitudes to show direction of movement. Left diagram shows an enlarged view of the lower slope (approximately 125 × 125 m).

3.2.8. Pit Slope Kinematics

Review of the combined radar displacement data (magnitude, direction, and plunge) allows for an expansion of earlier slope kinematic models (Tosney et al., 2004; Piteau Associates Ltd, 2008; Rose and Scholz, 2009), which were created to describe the observed displacements within the Lornex Pit based on field observations and geodetic data, complemented by 2-D numerical analyses. Figure 3.11 shows projections of the 3-D radar data in terms of cumulative displacement magnitude, trend, and plunge taken directly from the displacement vectors with the mapped geologic structures plotted on the slope (Black lines) (Figure 3.11 a through c). Each of the aspects of the displacement vectors was reviewed in detail to identify potential failure mechanisms, abrupt changes in the values were concluded to be controlled by structural features within the slope.

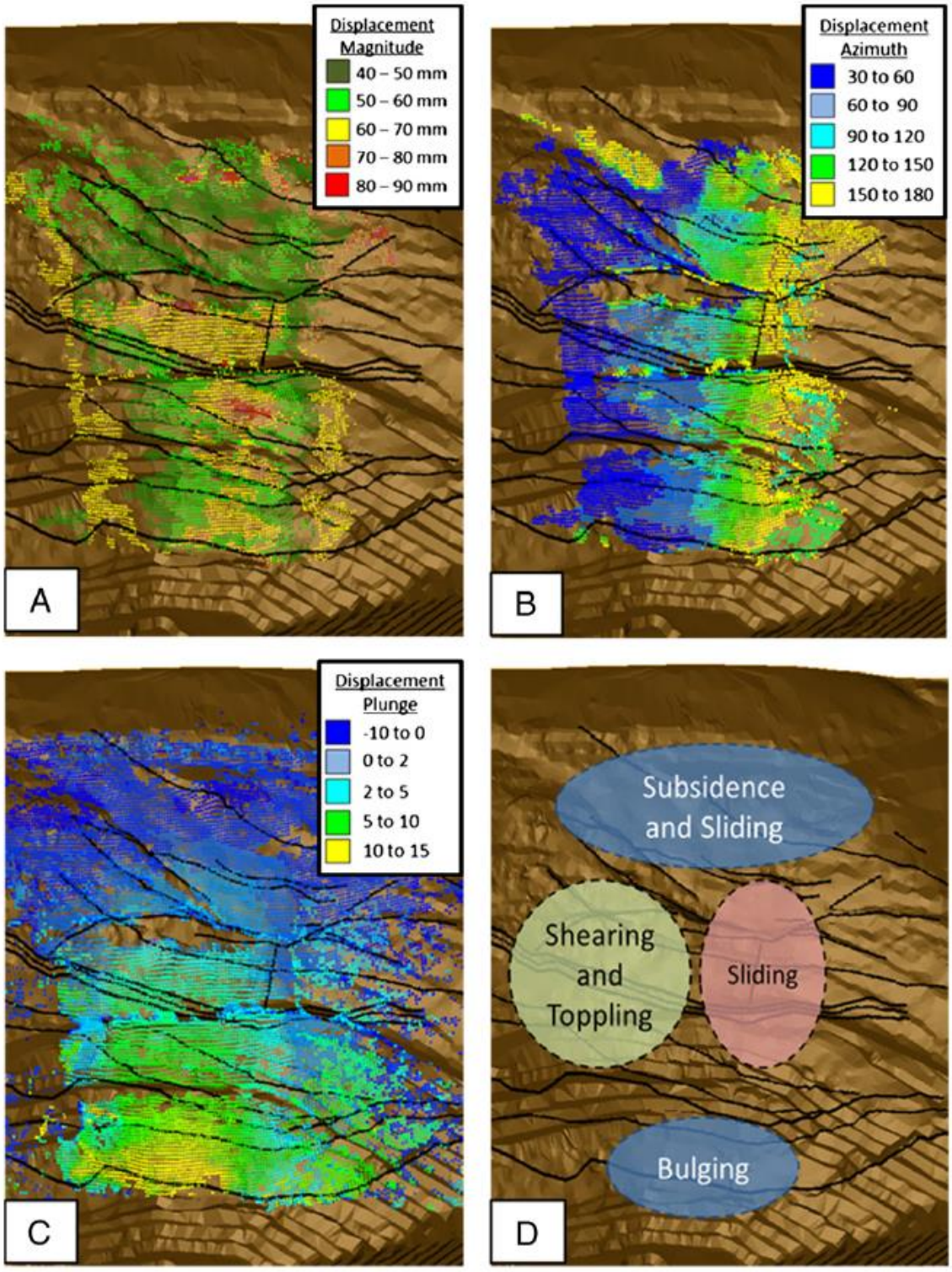

Figure 3.11. Oblique view of the Lornex Pit northwest corner, highlighting areas of higher displacement and movement directions. a) displacement magnitude, b) average azimuth (trend) of displacement vector, c) average plunge of displacement vector, and d) interpreted pit kinematics of the northwest corner of the Lornex Pit.

A bias within the plunge data exists as the setup locations of both radars were placed near the pit rim, giving rise to an upward plunge in the line of sight displacement. The plunge values should only be used as a tool to help guide in the identification of possible rock displacement kinematics and to determine areas of relative upward movement. Figure 3.11d shows the interpreted kinematic modes based on the 3-D radar data, which were then used to develop the engineering geology model of the interpreted pit wall deformation mechanisms in Figure 3.12.

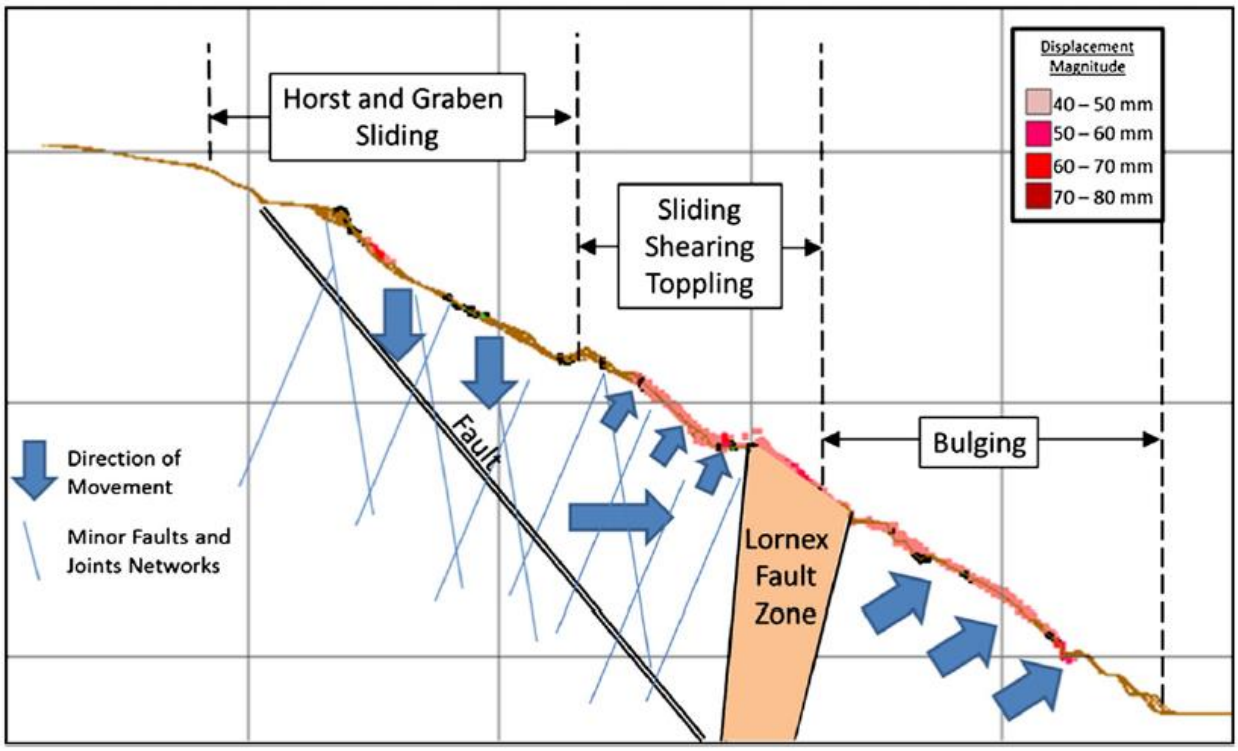

Figure 3.12. Schematic diagram of interpreted kinematics for the northwest wall of the Lornex Pit. Note that the measure displacement vectors have been overlaid on the pit slope surface.

Several key observations with respect to displacement patterns and slope kinematics can be observed within the plots in Figure 3.11. Within a continuum environment, displacement within the pit arising from the excavation would tend to show a gradual change in magnitude, azimuth and plunge as the rock responds to the changes in stress. The discontinuous nature of the measured displacement indicates that rock mass response can be partially or fully controlled by large scale structures such as faults. Both small variations

and abrupt changes can be detected within both the displacement data suggesting not only movement or separation along structures but also yielding of the rock mass in between the faults.

Comparison between the displacement magnitude and azimuth indicates that the areas with the highest total displacement above the Lornex Fault tend to move toward directions between 120° and 150°. Movement within the northwest corner between the Lornex Fault and the pit access ramp is interpreted as being predominantly sliding controlled by a shallow dipping fault(W1-1) sub-parallel to the slope or shear structures parallel to theW1-1 Fault. The sliding allows for the development of graben-like blocks to form and drop into the space created by the translational sliding (Figure 3.12). The presence of a basal fault controlling sliding in the upper slope agrees with the kinematic model developed by Rose and Scholz (2009). In the western half of the upper slope, these displacements decrease in magnitude and become more sporadic in terms of direction. Together they suggest that the movement within this region is dominated by toppling and shearing of the rock mass induced by the dilation of the rock mass and loss of confinement within the slope. Significant sliding may not be observed within the west wall due to the angle of incidence between the fault and the pit wall. As the pit wall direction curves toward the south, sliding along the fault is enabled.

The lower line of sight displacements within the upper portion of the slope and interpretation that these are being dominated by vertical downward movements of graben-like blocks are supported by geodetic data that exists outside of the area monitored by the experiment. The lack of directional correlation in the 3-D radar data below the LFZ suggests that the rock mass below the fault (altered Skeena Quartz Diorite) is undergoing bulging through shearing and dilation of the rock. Thus, the 3-D radar data shows a clear and distinct difference in slope behavior from that of the complex sliding–shearing–toppling mechanism interpreted in the upper slope. This corresponds with the presence of weaker, more tectonically disturbed rock below the Lornex Fault combined with higher shear stresses at the toe of the slope.

3.3. Radar Experiment Conclusions

A novel experiment involving the simultaneous deployment of two ground-based radar systems was conducted to collect continuous, line of sight displacement data in “stereo” of a large, moving open pit slope bisected by a large fault. The simultaneous monitoring with two synthetic aperture radar units has led to the construction of a high resolution, pseudo-3D displacement map of a large open pit rock slope. Analysis of the corresponding displacement vector map allowed an interpretation of the overall slope kinematics to be resolved. The 3-D radar experiment could identify localized movements related to smaller-scale geological structures and changes in pit wall slope orientation.

The radar monitoring clearly provided a significant increase in coverage above that possible using geodetic prism, with over 25,000 common displacement points. The need to extrapolate displacements between prisms is avoided and small areas of high displacement that may pose potential safety concerns can be better identified and monitored.

Furthermore, areas which cannot be monitored due to poor or dangerous access can be covered by the radar without the need to install prisms. For the 3-D radar experiment reported here, the monitoring could identify localized movements related to smaller-scale geological structures and changes in pit wall slope orientation.

Understanding of the pit slope kinematics was significantly improved with the pseudo 3-D radar data. This has the potential to add significant value to a mine project where the mine plan is considering a pit wall pushback to deepen the pit. In such cases, the influence of the controlling nature of any major faults and smaller structures on the pit wall movements can be investigated and better understood with respect to pit geometry, slope deformation kinematics, evolving failure mechanisms, and ultimately geo-risk. This is the subject of ongoing research, and involves the integration of the 3-D slope deformation map with advanced 3-D numerical modeling. Preliminary modeling using the distinct element code 3DEC has been carried out to further investigate and validate the kinematic model derived from the 3-D radar data. In parallel, the 3-D radar data is being used to calibrate the model with respect to the controlling influence of important fault and joint properties, including location, persistence, and strength characteristics. These can then be projected for future deepening of the pit and pushback of its slopes.

3.4. Chapter Summary

The review of both commonly used and emerging monitoring technologies has shown that large scale geological structures, such as faults, can affect deep-seated rock slope behaviour within a large open pit. The potential influences of a fault on pit slope stability observed through the review of monitoring date in this study include:

- acting as a sliding service and prompting kinematic controls;
- influencing the vertical and/or horizontal slope displacements;
- acting as a focal point for damage to occur in the surrounding rock mass (or propagation of a cave);
- shielding the rock mass from stress or strain increases generated by nearby mining; and
- creating areas of potential extensional strain and brittle rock fracturing.

CHAPTER 4 INFLUENCE OF STRESS HETEROGENEITY ON LARGE OPEN PIT SLOPES

Synopsis

This chapter investigates the development of stress heterogeneity and potential damage at and behind large open pit rock slopes. Several factors ranging from regional scale, such as stress regime, to more local scale, such as changes in lithology, are investigated to determine their relative impact on the stability of large open pits. Of primary interest is the interaction that develops between the existing faulted rock (and/or fault damage zones) and the incremental deepening of a large open pit. This interaction has the potential to create pockets of high localized stresses in the adjacent rock mass several times greater than the typical stresses arising from the mining process or those calculated in numerical slope stability analyses. Similarly, these damage zones can also produce zones of extensile strain that help to promote brittle fracture propagation and the development of tension cracks. This stress heterogeneity is amplified as the pit depth increases, which can influence slope displacements or failure mechanisms especially at critical times in the pit's operation where deepening is required to further access valuable ore (e.g., via a pushback) or plans are to transition to underground mining beneath the pit. This chapter reports the findings for a numerical investigation examining the potential for and influence of stress heterogeneity, a topic that has received some attention in the context of underground mining, but has not been addressed yet in research on large open pits. The numerical analyses within this paper summarizes a series of conceptual 2-D and 3-D numerical models. The analyses and results highlight: 1) the identification of the key factors in creating stress heterogeneity within a pit wall, 2) the impact of selected fault properties on mining-induced stress development, 3) the evaluation of increasing pit depth and mining-induced stresses on amplifying the damage state around faults and the resulting effects on pit slope performance, and 4) potential design/mitigation strategies that mines can employ to reduce the adverse effects of stress heterogeneity in the pit wall. This chapter is in the process of being submitted to a peer-review journal.

4.1. Introduction

Recent mining trends have shown an increase toward the proposal of deeper and more complicated open pit mine designs either within difficult or unique ground conditions, or incorporating a future transition to underground mining, via open stoping, sub-level or block caving. Many of these challenging open pit designs push our empirical knowledge base, which has largely been founded on smaller pits and structurally-controlled failures. Unexpected multi-bench failures or hazardous acceleration events have

occurred at several of the largest open pit mines in current operation including Bingham Canyon Copper Mine (Newcomen and Dyck, 2016), Chuquicamata Copper Mine (Lorig and Calderón Rojo, 2009), Palabora Copper Mine (Brummer et al., 2006), Cuajone Pit (Hormazabal et al., 2013), Betze-Post Pit (Rose, 2011), Grasberg Mine (Ginting et al., 2011), and the Gold Quarry Mine (Yang et al, 2011). Within these deeper open pits, the response of the pit slopes to higher stresses is not well understood, thus significantly increasing the mines exposure to the consequences of a major pit slope failure. These potential consequences include worker injury and loss of life, loss of equipment and production, loss of economic value due to sterilization of ore or increased dilution, and the forced deviation from the mine design, or ultimately force majeure and closure of the mine.

A key knowledge gap is the importance and influence of the pre-mining in-situ stress state. In-situ stress has been identified as being a potentially important factor in the development of failure and unexpected displacement in larger open pits (Sjoberg, 2013; Noorani et al., 2011; Robotham; 2011; Dight 2006). Pre-mining in-situ stress fields can deviate from simple gravity loading to a highly heterogeneous stress state due to the presence of tectonic stresses, topography, geological contacts, rock lithology/stiffness contrasts, rock mass anisotropy, and major faults. This potentially complex pre-mining stress field is then further altered as the mine is developed and the ore is extracted. As open pits extend to deeper depths and stress levels increase, the relative importance of deeper seated shear or compressive brittle fracture failures is also increased, leading to unexpected damage of the rock mass behind the pit face. Both observation and understanding of these complex failure mechanisms are limited with respect to past experiences, which instead have primarily focussed on low stress, joint-controlled kinematics. These stress changes may influence the response of the intact rock at a small local scale, for example intact rock bridges between non-persistent discontinuities, but also affect larger volumes of the rock mass when the structures contributing to stress heterogeneity intersect at the mine scale, for example major faults.

Experiences with large open pit slope failures along with awareness that the industry is pushing knowledge boundaries (as mining progresses deeper), has increased the need to assess potential failure mechanisms not routinely considered in slope design. Conventional slope design is dominated by limit equilibrium analyses where the failure mechanism is assumed *a priori*. In many the recent failures, previously listed, tectonic faults have been shown to play a key role in the development of failure, either through influencing slope kinematics or by weakening the rock mass. Damage of rock bridges from brittle fracture propagation leading to complex step path or progressive failure mechanisms, has also been shown to be a significant factor affecting the stability of both natural slopes (Eberhardt et al., 2004) and open pit mine slopes (Sjoberg, 1996; Sainsbury, 2007; Elmo et al., 2007). Localized plastic shear strain and extensional strain, hypothesized here as being generated in pockets of low and high stresses induced during pit deepening

(referred to herein as stress heterogeneity), has been shown to play an important role in the development of large slope failures (Eberhardt et al., 2003; Stacey et al., 2003; Rose, 2011).

In the sections that follow, a series of conceptual numerical models are developed and presented which begin by examining the mining-induced stresses that develop in a large open pit slope based on conventional treatments of the pre-mining in-situ stress conditions. These are then contrasted with models that incorporate the influence of regional to local scale stress heterogeneity, with a focus on heterogeneity resulting from the presence of tectonic faults and damage zones. The complex interactions that develop with increasing slope height and the factors shown to affect local stress heterogeneity are then discussed as well as possible mining strategies that may reduce the development of adverse stress conditions near faults within a pit wall.

4.2. Induced Stresses and Open Pit Mining

The pre-mining in-situ stress state is the single most important boundary condition influencing the calculation of mining-induced stresses. Historically, the investigation of in-situ stresses has largely been restricted to underground deep mining studies where mining-induced stresses and stress-induced failures such as squeezing, spalling, and rock bursting might impact mine safety and production. Relationships between in-situ and mining-induced stress have been investigated through analytical techniques (Kirsch, 1898; Love, 1927; Muskhelishvili, 1953; and Savin, 1961) as well as numerical methods (Lorig and Brady, 1984).

Despite being a fundamental concern in the design of deep underground excavations, in-situ stresses for large open pit projects are generally treated using simplified assumptions of gravity loading and homogeneity (Read and Stacey, 2009). An example of the mining-induced stresses calculated for a 600-m high, 45° slope based on these assumptions is provided in Figure 4.1. Within a homogenous rock mass, the stresses developed in the model are guided by continuum mechanics and are shown to increase with depth, redistributing and concentrating at the toe of the slope. Even though the model is highly simplified, the results provide a useful basis for understanding the impacts of pit excavation on an in-situ stress field for a continuum-based numerical analysis of slope stability. Smith (2013) gives a detailed account of stress trajectories around an open pit assuming a homogenous rock mass material and notes that principal stresses rotate to be approximately parallel to the inter-ramp slope angle and that stresses near the toe of the slope progressively rotate to be parallel with the pit floor.

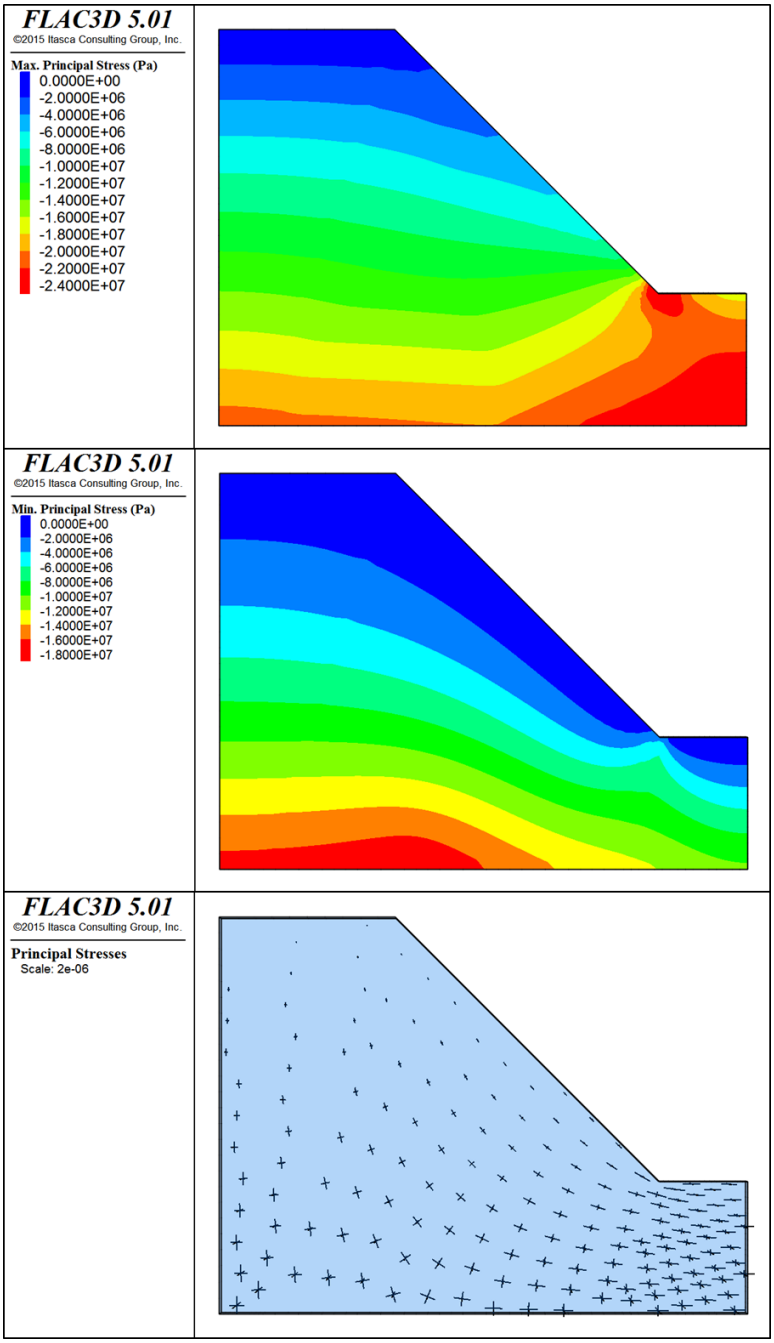

Figure 4.1. Generalized stress distributions and orientations for a 600-m high, 45°, homogeneous, open pit slope, showing maximum principal stress (top), minimum principal stress (middle) and principal stress trajectories (bottom).

It is argued here, however, that the in-situ stresses affecting pit slope stability are far from being the simple homogeneous, gravity driven conditions typically assumed. Instead, several factors have been noted to affect the in-situ stress field within a rock mass ranging in scale from regional to local effects. Thus, the

key factors contributing to the development of stress heterogeneity in an open pit slope can be classified per the scale at which they impact stress development (Figure 4.2).

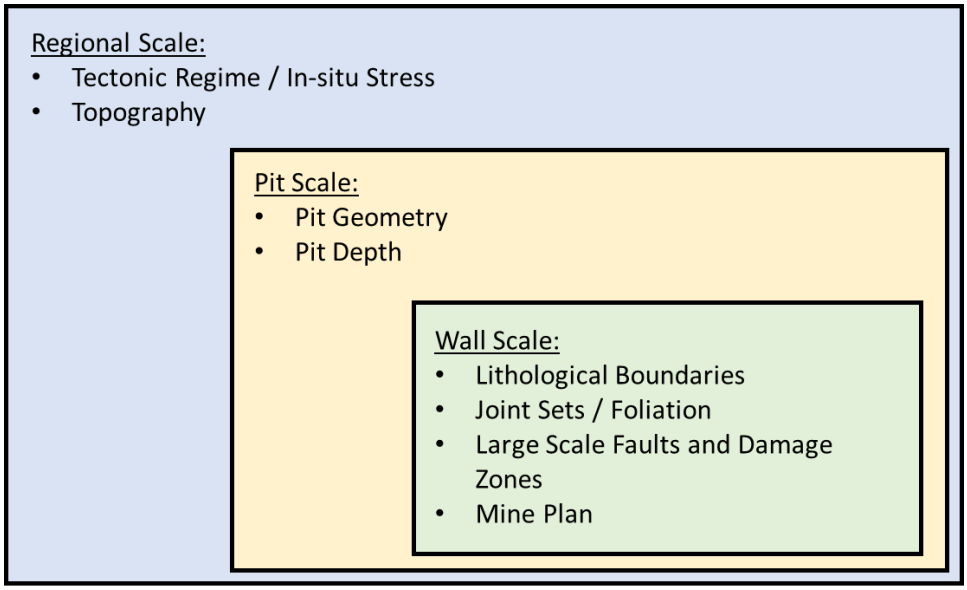

Figure 4.2. Factors identified as contributing to stress heterogeneity near open pits ranging from regional scale to local wall scale.

Many of these factors are geological in nature and therefore represent the fixed conditions the mine design must account for. Others, such as global economics, govern the price of the commodity being mined (e.g., gold, diamonds, copper, etc.), which when combined with the mine's development and operating costs, control the cut-off grades required to make the mine profitable. When combined with the orebody type, these factors usually determine the shape and depth of the open pit. Mine development plans and local geometry details are often refined based on operating factors such as equipment selection, pit dewatering and surface water diversion efforts, mill feed requirements, ore grade variability, and others. Pit slope designers are often left with only a few options for creating optimization opportunities to improve the mine economics or reduce geotechnical risks.

Mining companies are required to make a series of compromises which balance operational, geotechnical, and ore grade considerations in developing their mine plan and slope designs. Some of these are well understood. For example, if the mill does not receive a specific grade of ore, the economic impact is immediate and easy to quantify, but also easy to mitigate (e.g., stockpiling of different ore grades). In contrast, many of the consequences of uncertainty related to pit slope design and stability are poorly understood or unrecognized. This either introduces risk to the operations, or requires added conservatism

in the slope design. Chief amongst these uncertainties is the pre-mining in-situ stress state, which despite its importance as a boundary condition in numerical analyses, or its complete absence in limit-equilibrium safety factor-calculations, often does not get reviewed in sufficient detail due to time and staff constraints.

It should be cautioned, however, that the assumption of gravity loading and stress homogeneity, as is commonly adopted in many slope stability analyses, is also the most favorable for returning a stable slope answer. The influence of stress heterogeneity on slope stability is investigated in the following sections. Unless otherwise stated, the numerical analyses performed are based on 3-D finite difference modelling using the commercial code FLAC3D (Itasca, 2012). Also, it should be noted that FLAC3D calculates stresses with compression negative.

4.3. Investigation of Regional-Scale Stress Heterogeneity Factors

4.3.1. In-Situ Stress Regime

Natural formations of rock have been subject to complex stress histories through various geologic processes (e.g. plate tectonics, uplift, intrusion emplacement, erosion, glacial loading and unloading, etc.), which result in an in-situ stress state that is highly heterogeneous and very difficult to measure or predict, both in terms of magnitudes and orientations of the principal stresses. For this reason, together with skepticism regarding their importance near surface, in-situ stress measurements are rarely included in most open pit mine site investigation programmes. Nevertheless, it is a required boundary condition for any numerical analysis. The input is typically assigned assuming a constant vertical stress gradient and setting the horizontal stress as a ratio to this. The horizontal to vertical stress ratio is commonly denoted as K. Common assumptions include: i) gravity loading, where the horizontal stresses are calculated during numerical time stepping based on the Poisson's ratio (this typically results in a K of 0.33 to 0.5); ii) an extensional or normal faulting stress regime ($0.5 < K < 1$); iii) a hydrostatic stress regime, where the in-situ stresses are equal in the vertical and two horizontal directions ($K = 1$); and iv) a thrust faulting stress regime ($K>1$, often up to $K = 2$). During the feasibility and design stages of a proposed mine, the influence of the in-situ stress assumption is sometimes compared through a sensitivity analyses involving two or more of these in-situ stress assumptions.

In contrast to the prevalent modelling assumption that the in-situ stresses are gravity controlled ($K = 0.3$ to 0.5), regional stress data compiled by various authors suggests otherwise. Hoek and Brown (1980) compiling data from several countries with significant mining activity show that the horizontal stresses down to 1000 m depth tend to be 1.5 to 2.5 times the vertical (Figure 4.3a). A similar example is given by Mahoney et al. (2006) for the Canadian Shield (Figure 4.3b). The latter further shows that the stress gradient with depth is not necessarily constant, in this case changing at several hundred metres depth to a less steep

K ratio. Martin (1990) demonstrated through an intensive in-situ stress measurement campaign at the AECL Underground Laboratory, supported with numerical modelling, that changes in the in-situ stress field with depth can be compartmentalized and change in gradient in response to major tectonic features. This involved the differentiation of distinct in-situ stress domains that varied both in magnitude and principal stress direction on either side of major sub-horizontal thrust fault structures (Figure 4.4).

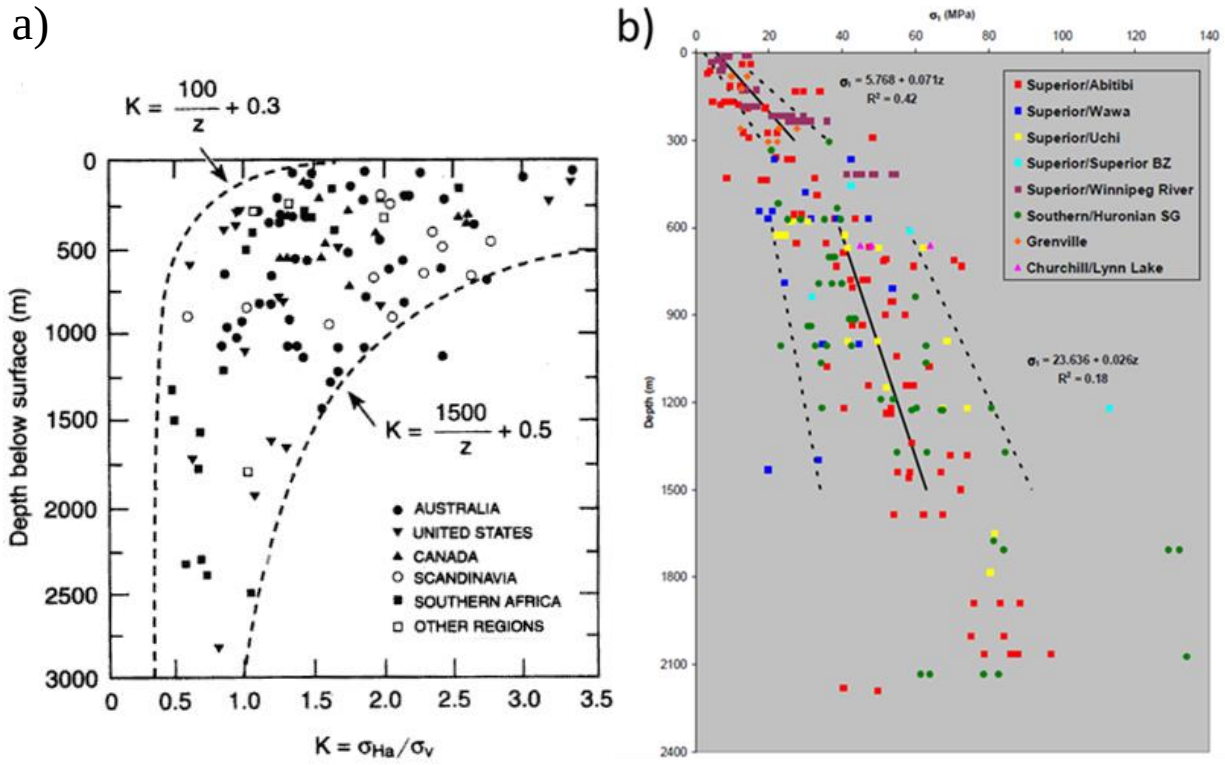

Figure 4.3. Compilation of measured principal stress magnitudes in terms of: a) horizontal to vertical stress ratio for several mining-focused countries (Hoek and Brown, 1980), and b) maximum principal stresses for the Canadian Shield (Mahoney, et al., 2006)

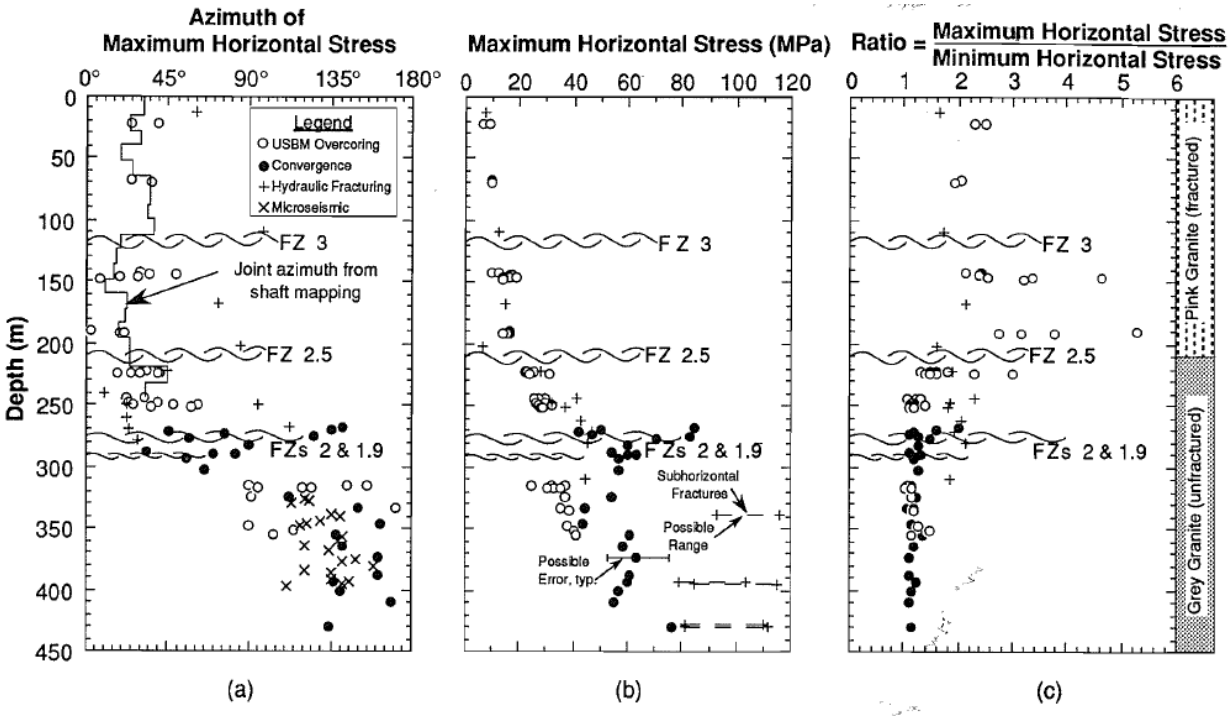

Figure 4.4. Fault separated in-situ stress domains at the URL (from Martin, 1990) including changes in a) orientation, b) magnitude and c) stress ratio between maximum and minimum horizontal stress.

To illustrate the effect that the in-situ stress ratio has on stress concentrations at the toe of a 45º slope, a series of FLAC3D models were constructed comparing pit slope heights of 300, 600, and 900 m. The models assumed elastic properties for a weak rock mass to demonstrate the potential of stress accumulation. Properties for the models are given in Table 4.1.

Table 4.1. FLAC3D properties used for in-situ stress sensitivity modelling

Pit Slope Height (m)	Host Rock E_{rm} (GPa)	Host Rock Poisson's Ratio	Density (kg/m^3)	Stress Regimes Tested (K_0)
300, 600, 900	5.87	0.25	2500	0.5, 1.0, 2.0, 3.0

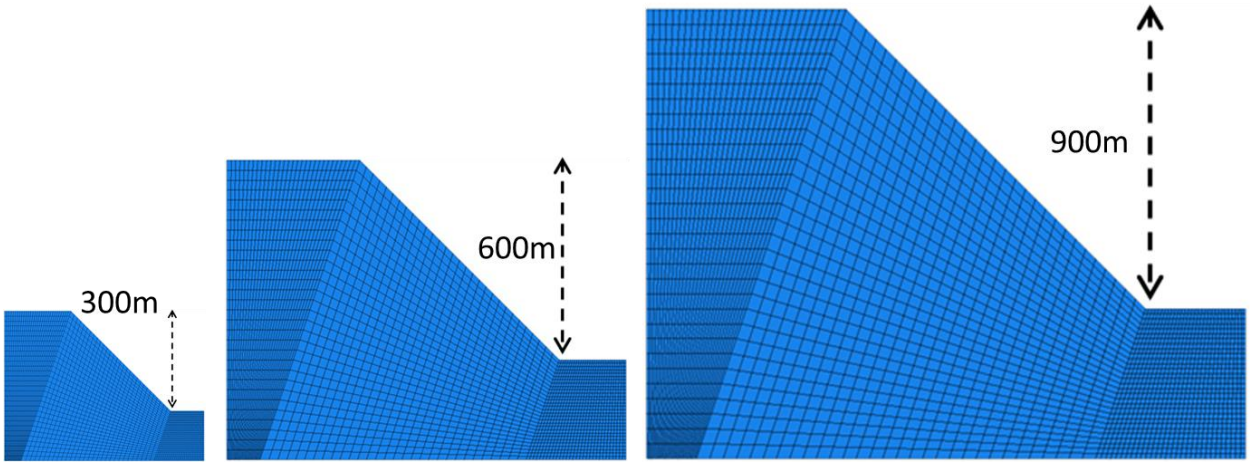

Figure 4.5 FLAC3D model geometries and finite difference meshes used for in-situ stress sensitivity modelling with slope heights of 300, 600, and 900m.

Figure 4.6 illustrates the affect of increasing horizontal stress ratios on the development of deviatoric stress at the toe of the 300, 600, and 900 m high slopes. Deviatoric stresses represent the difference between the maximum and minimum stresses and are used here to illustrate high stress conditions with low confinement areas of the pit. In this low confinement condition, deviatoric stress can also be used as a proxy for maximum shear stress. The results of this sensitivity analysis illustrate that the deviatoric stresses are shown to increase at a dramatically increased rate for higher in-situ stress regimes as the pit depth increases. This suggests that deeper pits in high in-situ stress environments would be far more susceptible to yielding and shear failure at the toe while still being subject to low confinement stress.

Historically, open pit designs have largely been limited to depths of up to 500 m where stresses are generally lower and those arising from the excavation of the pit are considered dominant. In shallower pits, for example a 300-m deep pit, the increase in deviatoric stress at the toe of a slope may range in the order of 10 to 20 MPa, depending on the K stress ratio; these magnitudes are generally within the strength capacity of a moderately competent rock mass. As the horizontal to vertical stress ratio K increases, the calculated stress concentrations in the toe of the slope similarly increase but with an increasing gradient as the slope height increases. Thus, the modelling results in Figure 4.6, show that the deviatoric stresses for a 300-m pit with an initial K stress ratio of 3 is much less than a 900-m pit slope with a K stress ratio of 1, even though the initial stress magnitudes are approximately the same (note that the difference is in the orientation of the maximum principal stress).

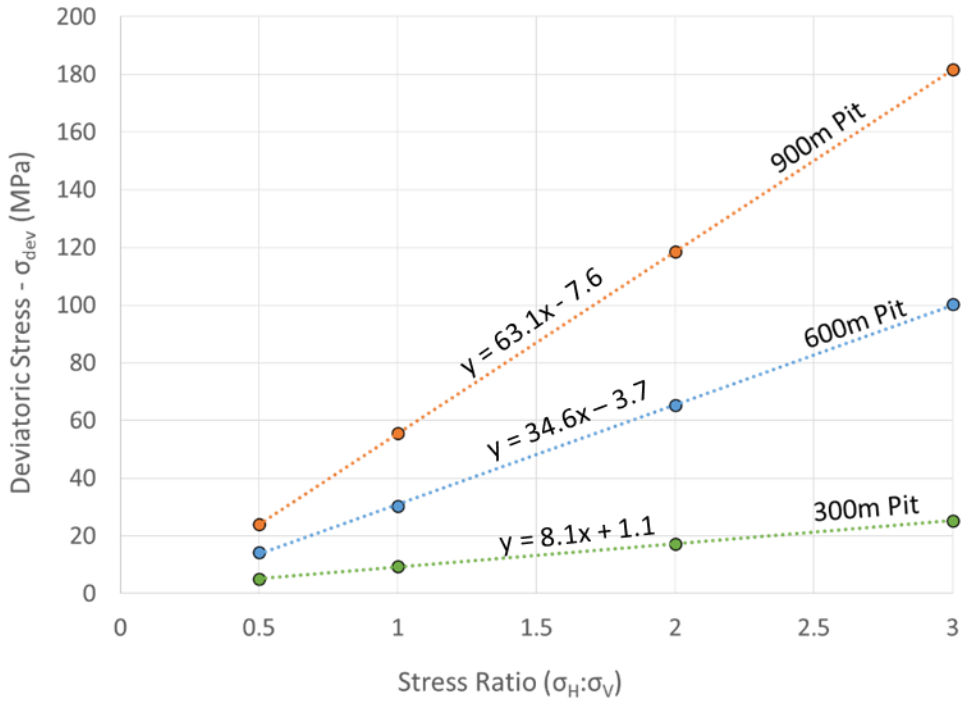

Figure 4.6. Deviatoric stress magnitudes with varying in-situ stress regime and pit depth. Note that the increase in deviatoric stress is greater with increased pit depth compared to increased horizontal stress ratios.

4.3.2. Topography

The effect of topography (without the influence of tectonic forces) on the in-situ stress state is significant, but also straight forward and easily accounted for in numerical analyses. Where the ground surface contains a series of hills and valleys, the rock stresses under gravity loading will result in principal stresses near the surface that are parallel and normal to the undulating topography. However, with depth, the influence of topography on the stress trajectories diminishes and eventually approaches the same orientations as when the ground surface above is flat. Slopes and valleys create unbalanced stress concentrations in their troughs, like those at the toe of an open pit slope (Figure 4.1). Figueiredo et al. (2012) demonstrated the effect of topography on the distribution of in-situ stresses at the Paradela Dam site in Portugal in which the orientation and magnitude of the near-surface principal stresses were found to deviate significantly (up to 35%) from stresses expected from gravity loading alone.

The effect of local topography was investigated using FLAC3D, comparing a 600 m high pit slope excavated into a flat lying topography with one involving a sloping topography with an elevation change difference of 300 m near the pit crest. Elastic rock mass properties are assumed, as outlined in Table 4.2,

together with hydrostatic stress conditions (K=1). Figure 4.7 shows the two 3-D model geometries developed (top), together with the continuum mesh along a section cut through the highwall of the pit (middle), and maximum principal stresses (σ_1) along the section (bottom). Regionally, the stress contours follow the topography, however, upon final excavation, the stress contours around the pits for both cases were found to be generally similar. However, although the highwall, stresses appear to be similar, local variations of 2 to 5 MPa are present. This example suggests that minor variations in maximum and minimum stresses can be expected if topography changes exist around the pit. Extreme topographic changes (i.e. mountainous environments) in which topographic changes are more significant are expected to have a larger effect on the stress distribution around the pit.

Table 4.2. FLAC3D properties used for topography sensitivity modelling

Host Rock E_{rm} (GPa)	**Host Rock Poisson's Ratio**	**Density (kg/m^3)**	**Stress regimes tested (K_0)**
5.87	0.25	2500	1.0

Although the maximum principal stress showed only minor variation in magnitude, the influence of topography can be observed by examining the deviatoric stress around the pit. Figure 4.8 shows the deviatoric stresses within the two models using an oblique plan view and a section view along the red line in Figure 4.7. While the pattern and magnitude of deviatoric stresses at the bottom of the pit remains similar between the models, the topographic influence is shown to clearly control the deviatoric stress closer to the surface and may affect potential failure mechanisms that initiate in the upper portions of the pit walls.

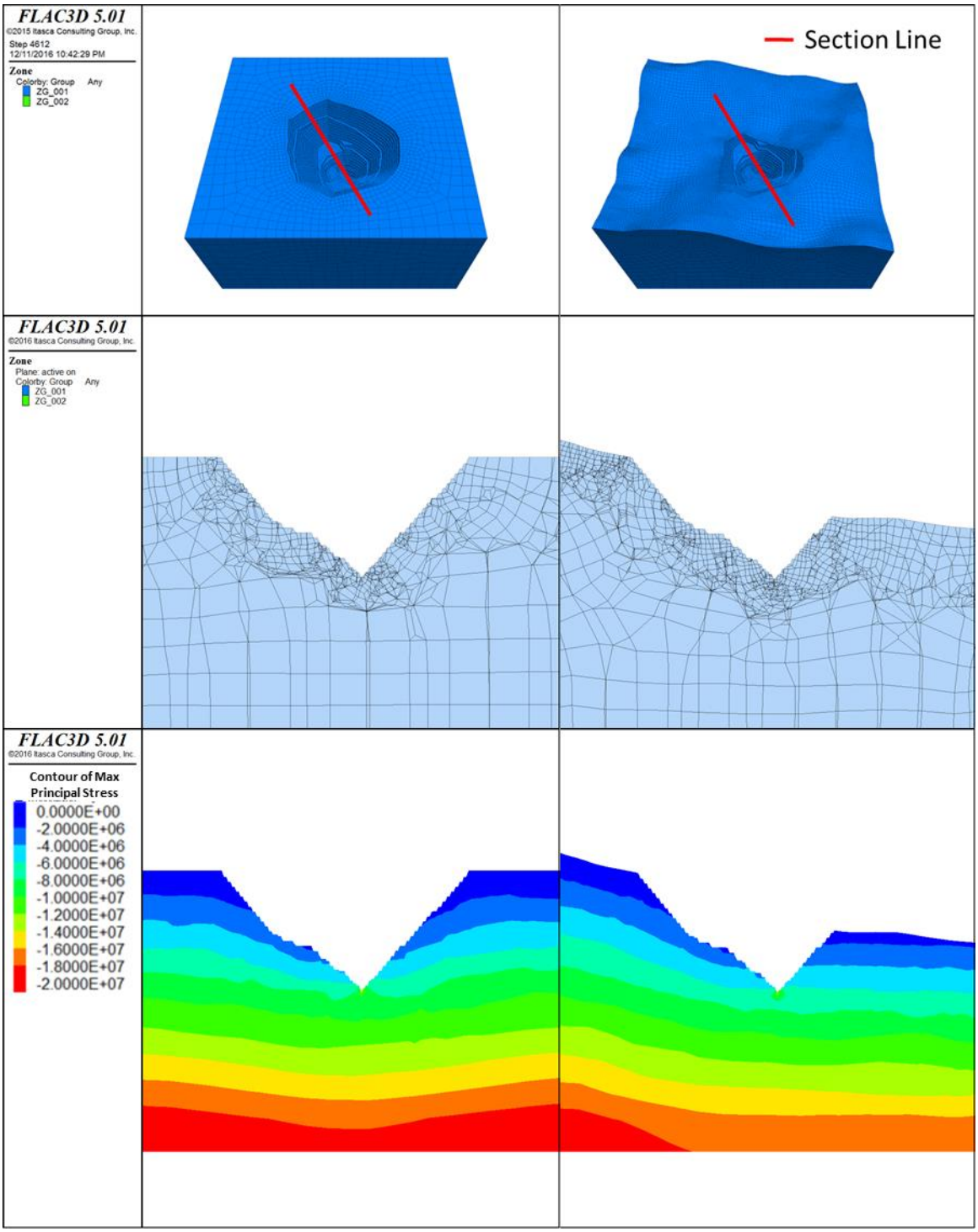

Figure 4.7. Oblique plan view (top) and section view (middle) of FLAC3D analyses comparing maximum principal stresses (bottom) for an excavated pit within a flat topography and undulating topography

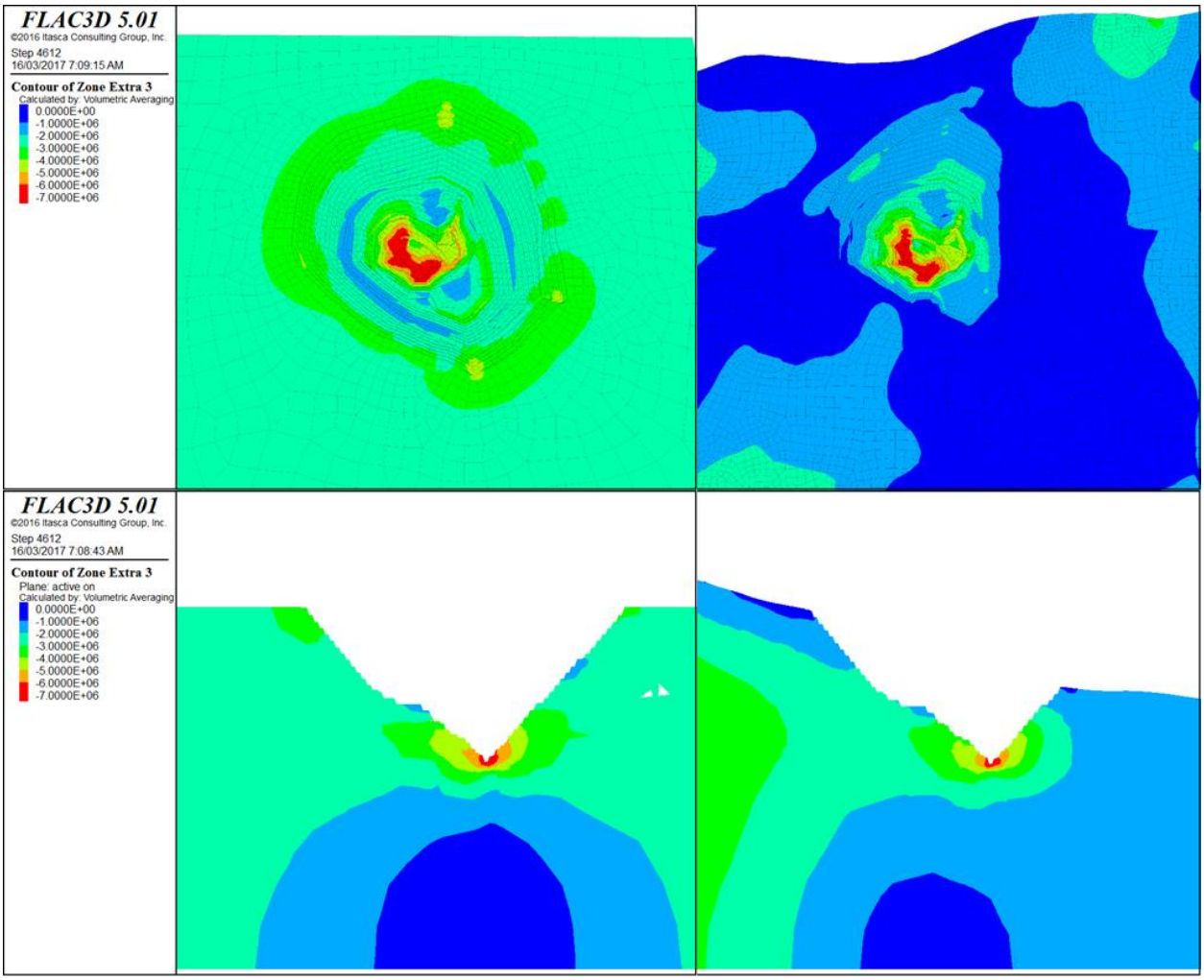

Figure 4.8 **FLAC3D deviatoric stresses for topographic sensitivity analyses, oblique (top) and section (bottom) views. Note the similarity in deviatoric stress patterns at the bottom of the pit and the variation near the pit crest. Compression is negative.**

4.4. Investigation of Pit Scale Stress Heterogeneity Factors

4.4.1. Pit Geometry

Although many slope stability analyses adopt the simplifying assumption of 2-D plane strain, the geometry of an open pit has a major impact on the 3-D stress redistribution surrounding the open pit. Stress contours around a circular pit within a homogenous rock mass are evenly distributed; however, around an elliptical shaped pit, greater stress concentrations exist along the short axis of the pit with lower stress values (involving relaxation) occurring along the long axis. Zones of smaller pockets of stress heterogeneity can be observed locally with small-scale irregularities in the pit shape, for example bullnoses or sharp/tight

corners. To illustrate this, plan views were cut at mid-slope heights through several different FLAC3D models analyzing different open pit geometries, as shown in Figure 4.9.

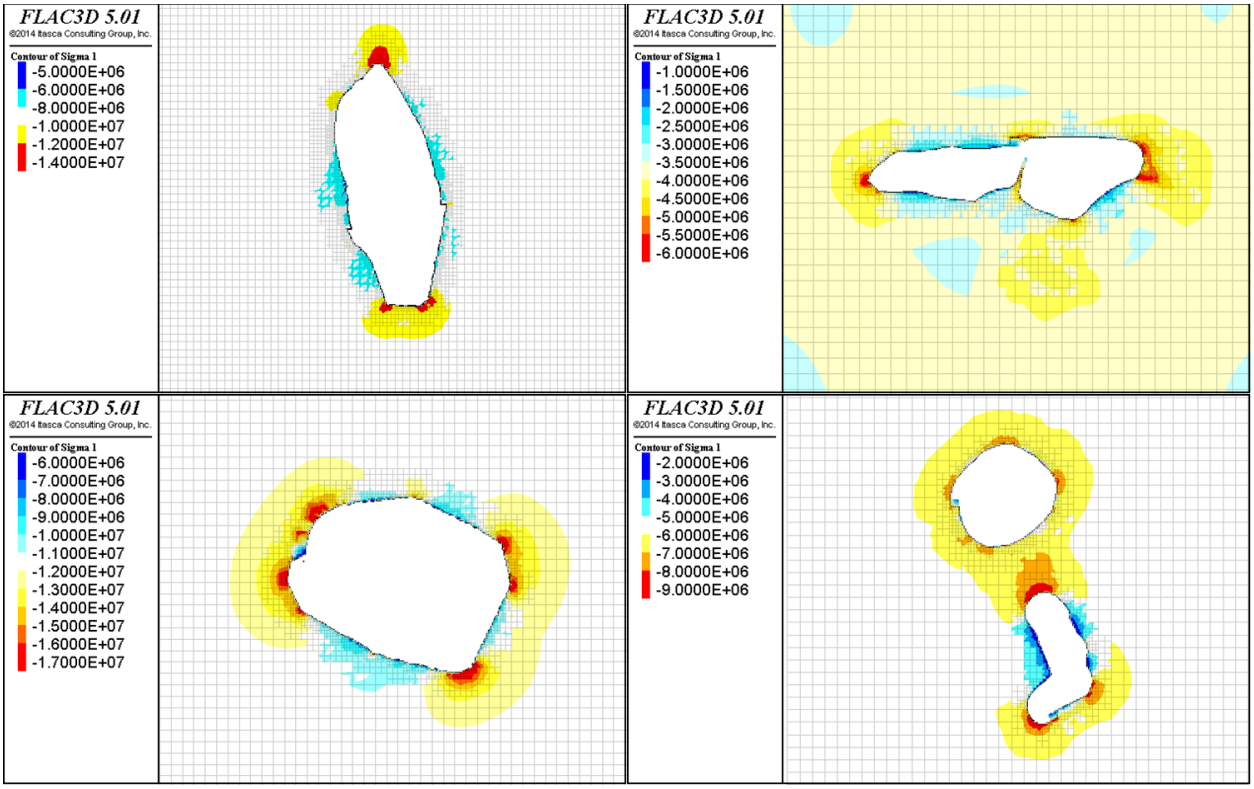

Figure 4.9. Modelled stress distributions (in plan) relative to the geometries and in-situ stress field orientation for several actual open pit geometries. These include: a) HVC's Lornex pit, b) preliminary Mine A open pit design, c) Palabora, and d) preliminary Mine B design. Cooler colors reflect relaxation stresses and the warmer colours reflect stress concentrations.

These models incorporated variable pit depths (ranging from 300 to 800 m) and rock strengths; however, the in-situ stress conditions for each model was assumed to be hydrostatic (K=1). The plots show areas in which low (blue) or high (red) stress concentrations have developed beyond that of the expected lithostatic condition (white).

Given that the geometry of an open pit can affect the stress distribution behind a pit face, the combination of pit geometry and in-situ stress regime is expected to drastically affect the distribution of the low and high stress regions around a pit. To further investigate the impact of high horizontal stresses on the development of stress heterogeneity surrounding the pit, two end member geometries were selected for further review in FLAC3D, the roughly circular shaped pit at Palabora in South Africa and the elongated Lornex pit at Teck's Highland Valley Copper mine in British Columbia. Each of these pit geometries were subjected to either:

a) hydrostatic stress conditions (K=1), b) high E-W horizontal stresses (aligning with the model's x-x axis, or c) high N-S horizontal stresses (aligning with the model's y-y axis). Rock strength and deformation modulus input values were kept consistent between the different model simulations (Table 4.3).

Table 4.3. FLAC3D model input parameters for comparative analysis of pit geometries and in-situ stress ratios

Pit Geometry	Host Rock E_{rm} (GPa)	Host Rock Poisson's Ratio	Density (kg/m^3)	Stress Regime (K_0)
Elongated	58	0.25	2500	$K_0 = 1$
				$K_0 = 2$ (xx)
				$K_0 = 2$ (yy)
Circular	58	0.25	2500	$K_0 = 1$
				$K_0 = 2$ (xx)
				$K_0 = 2$ (yy)

The results for the elongated open pit geometry indicate that relative to pit slope behavior, the presence of narrow ends or abrupt changes in circumferential pit wall shape will lead to areas more susceptible to shearing and crushing (in tight corners), compared to kinematic block movements (sliding and toppling) in the destressed long axes of the pit. For many open pit projects without stress information or with inconclusive stress data, a stress sensitivity analysis can be run using 3-D numerical modelling to determine the risk of very high or low stress regions on slope stability. In pits that are elongate in shape, a change in the in-situ stress ratio and magnitudes (either through tectonic stress or depth) may affect the mining induced stress more so than pits that are roughly circular in shape.

For the circular pit shape, the 3-D numerical modelling results (plan view) show that the increase in mining-induced stress is roughly the same for the different pre-mining in-situ stress scenarios, although the location of the stress concentrations depend on the orientation of the pre-mining maxiumum principal stress axis, as expected. For the elongated pit shape, the effect on the magnitudes of the redistributed mining-induced stresses is more significant. This is highlighted in Figure 4.10, where the maximum stress for the elongated pit shape is 40% greater (28 MPa vs 20 MPa) in the regions of high stress when the maximum principal stress is orientated perpendicular instead of parallel to the long axis of the pit.

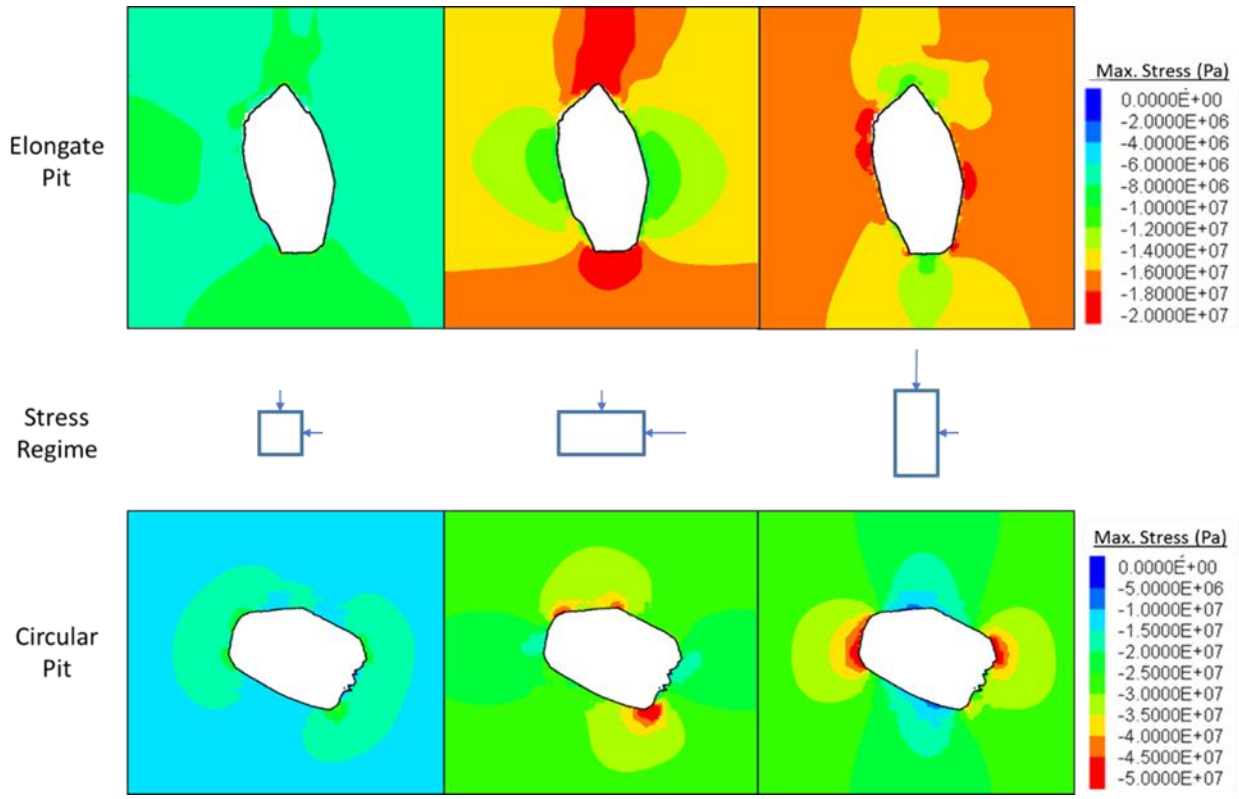

Figure 4.10. Stress heterogeneity near elongated and circular pits for varying in-situ stress regimes. The relative increase in stress development is greater for the elongated pit geometry with changes in the direction of the principal stresses. Compression is negative.

During back analyses, the interaction between pit geometry and in-situ stress regime is often tested by changing the boundary conditions in a numerical model; the pit geometry is given and the in-situ stress ratio K is varied. This often reflects the most important unknown in an open pit mine design and stability analysis. This was exemplified by experiences at the Palabora block cave mine where detailed 3-D numerical back analyses first required a modification of the in-situ stress conditions from what was originally measured (Itasca, 2007), and then only 8-months later, required the maximum horizontal stress direction be rotated 90 degrees to further improve the model calibration (Itasca, 2008).

4.4.2. Pit Depth

As pit depths continue to deepen, understanding of the in-situ and mining-induced stresses occurring within the slope become ever more important. A FLAC3D model (as Figure 4.5) of an extruded (2x slope height) 45° open pit slope section was developed to determine the increases in maximum principal stress. For illustrative purposes, an elastic model is assumed using the properties outlined in Table 4.4.

Table 4.4. FLAC3D properties used for pit depth sensitivity modelling

Host Rock E_{rm} (GPa)	Host Rock Poisson's Ratio	Density (kg/m^3)	Stress regimes tested (K_0)
5.87	0.25	2500	1.0

Figure 4.11 shows the maximum principal stresses under hydrostatic stress conditions (i.e., gravity loading) at increasing slope heights of 300, 600 and 900 m. and the value of estimated mining induced stress, which is the maximum stress at the toe of the slope -subtracting the pre-mining value at the same location.

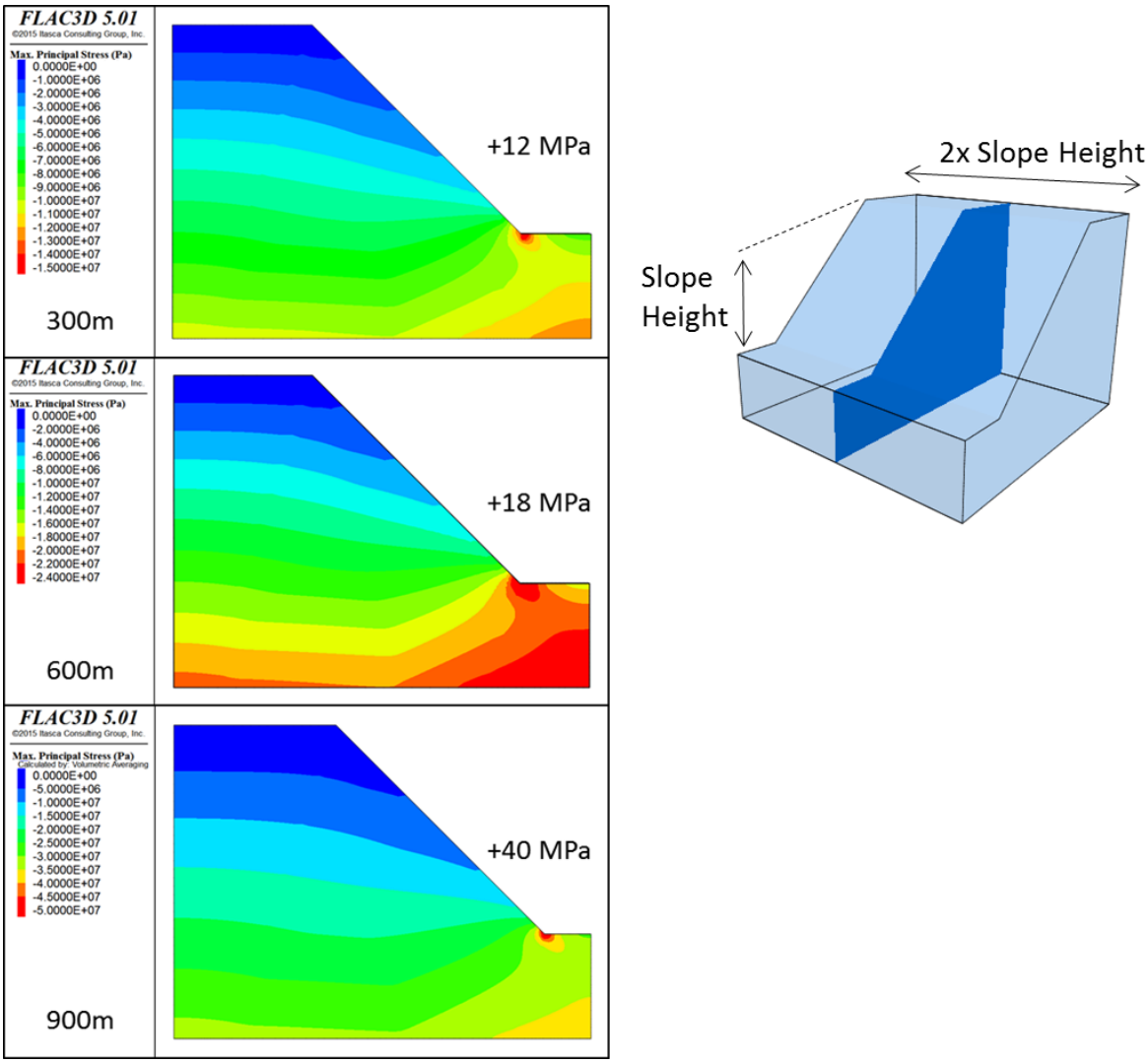

Figure 4.11. Maximum principal stresses (σ_1) calculated for a 300 m (top), 600 m (middle) and 900 m (bottom) open pit slope height. Mining induced stress concentration at the toe of the slope is shown. Note that compression is negative.

As the slope height increases, the observed concentration of induced stresses increases in a linear relationship (Figure 4.12). Concentrated stress increases at the toe of the slope (in this case increasing by more than 20 MPa) may prove significant in weaker ground conditions or in promoting the progressive failure of rock bridges that in turn contribute to internal shearing and localization of failure at the toe of the slope.

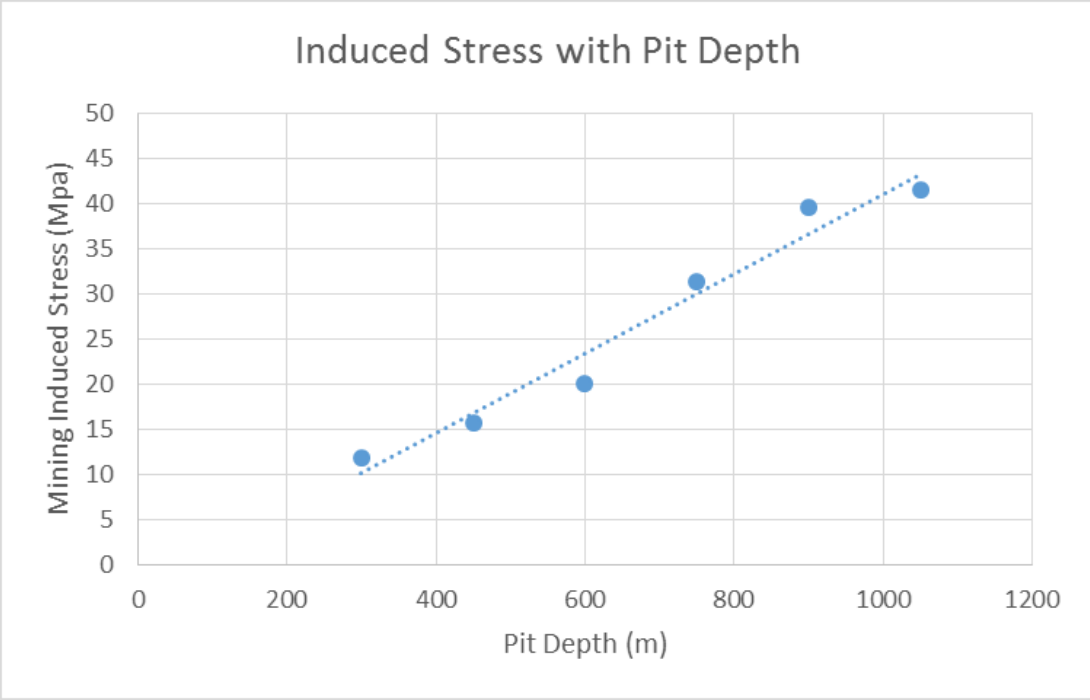

Figure 4.12. Induced mining stress (i.e., stress change above the pre-mining stress state) located at the toe of the slope as a function of pit depth.

4.5. Investigation of Wall Scale Stress Heterogeneity Factors

4.5.1. Rock Mass Strength and Lithology Variations

At the pit wall scale, rock mass properties such as deformation modulus have been shown to affect the mining-induced stresses (magnitudes and orientations), and thus the expected behavior of the rock near the toe and crest of an open pit slope (Stacey et al., 2003). Stacey et al (2003) varied the Young's modulus and Poisson's ratio for a homogeneous open pit slope, and determined that the magnitude of extensional strain is inversely proportional to the Young's modulus and directly proportional to the Poisson's ratio. However, the assumption of a homogenous slope is an over-simplification, as most pit slopes contain multiple

geological or geotechnical units that can be locally significant. The effect of stratification and changes in lithology on the in-situ stress state has been reviewed by multiple authors and in most cases, vary in response to contrasts in stiffness in the rock units, with stiffer rocks carrying a higher share of the overall stress than more compliant rock units (Warpinski et al., 1985; Haimson and Rummel, 1982; Whitehead et al., 1987).

To investigate the impact that changes in lithology have on stress development within open pit slopes, a series of conceptual FLAC3D models were created in which a slope of increasing height (300 to 900 m) includes a lithological unit in the lower half of the slope that is either two to five times more or less stiff than the adjacent lithological unit (Figure 4.13 and Table 4.5). The models were run with elastic properties and hydrostatic stress conditions to demonstrate the potential stress build up in the toe (i.e., stress shedding due to yielding is negated).

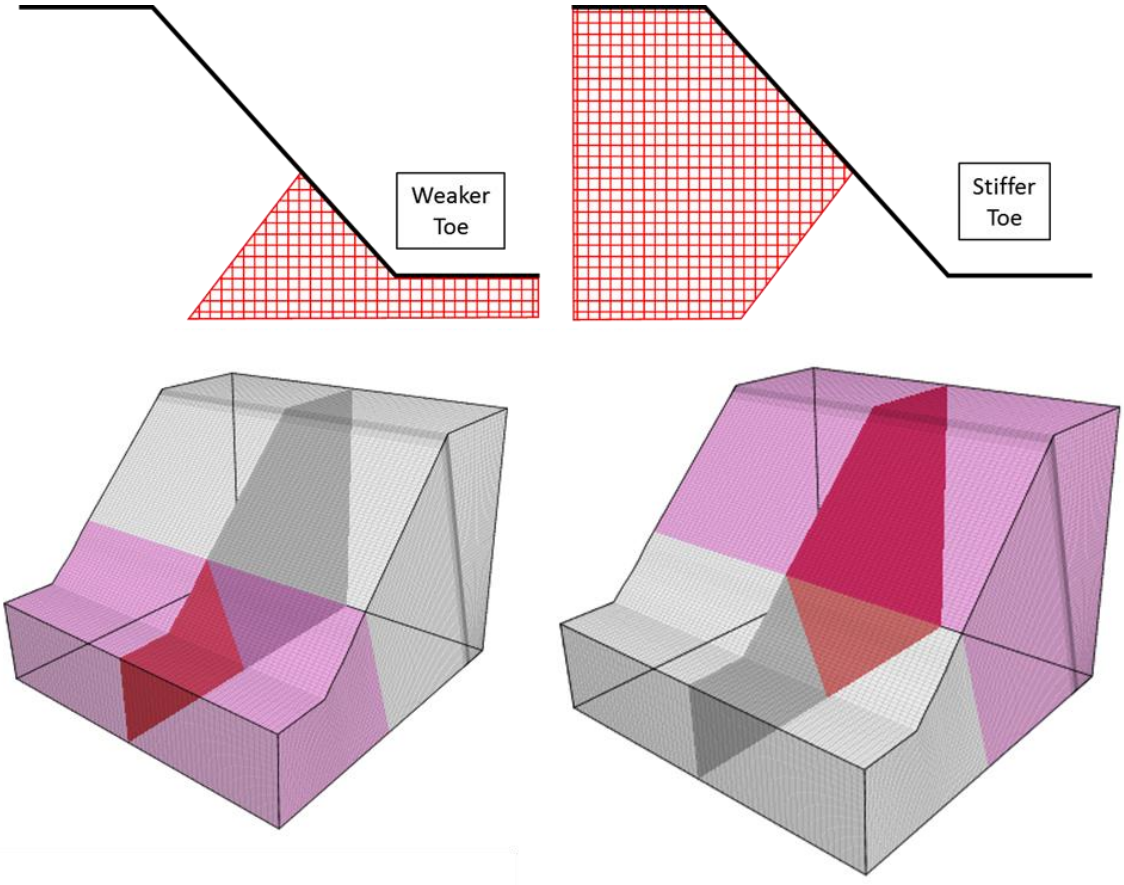

Figure 4.13. Model set up to determine sensitivity of stress heterogeneity development to relative lithological stiffness. Models were run with either weaker or stiffer materials in the bottom half of the slope.

As expected, the results indicate that higher deviatoric stresses concentrate in the toe of the slope with the presence of a stiffer lithological unit at the toe (Figure 4.14). As the pit deepens (slope height increases), the variance in stress concentrations at the toe of the slope increases. For example, the increase in deviatoric stress is almost double at the toe of a 900-m slope compared to a 600-m slope when the lithological unit is five times stiffer (24 MPa compared to 13 MPa). With increasing depth, changes in lithology or rock mass strength are compounded due to the overall increase in mean stress, and for these deeper pits, an increase of 10 MPa may be the difference between rock bridges failing and shear failure localizing. Many rock masses exhibit a stiffness and strength anisotropy, and rock mass fabric is known to influence the distribution of in-situ stresses, both in magnitude and orientation (Amadei, 1996).

Table 4.5. FLAC3D Lithological stiffness sensitivity model parameters

Pit Geometry	E_{rm} (GPa)	Poisson's Ratio	Density (kg/m^3)	Pit Depths (m)	Stress Change with Stiff Toe (%)	Stress Change with Stiff Crest (%)
Stiff Material (x5)	29.0	0.25	2500	300 600 900	+40% +43% +45%	-20% -22% -25%
Stiff Material (x2)	11.6	0.25	2500	300 600 900	+15% +17% +18%	-9% -10% -11%
Base Material	5.8	0.25	2500	300 600 900	-- -- --	-- -- --

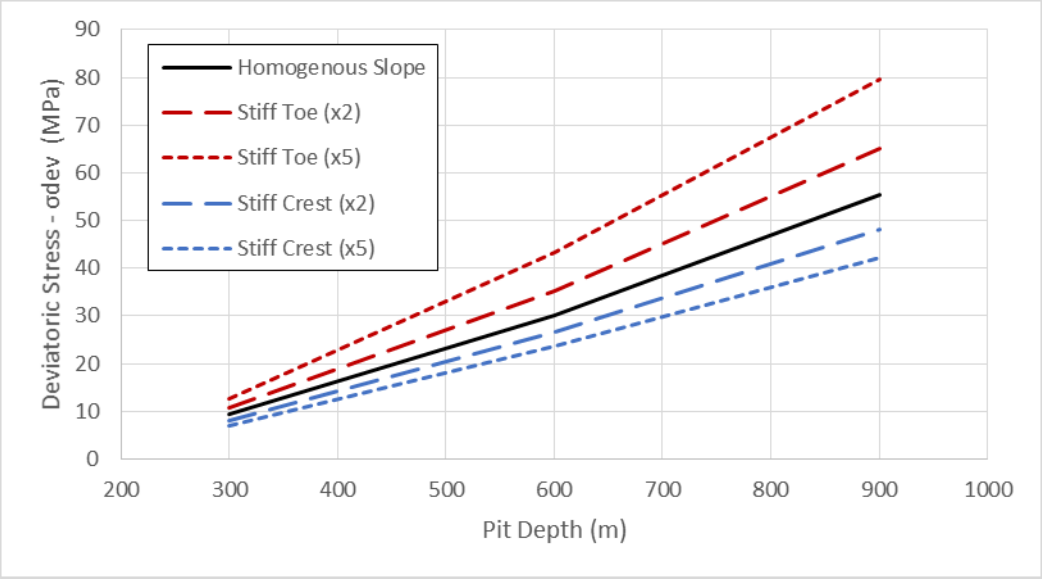

Figure 4.14. Deviatoric stresses created within slopes containing varying lithological stiffness as a function of pit depth. Slopes with stiffer material within the toe developed significantly higher stresses.

4.5.2. Faults and Tectonic Damage Zones

Characterization of individual fault zones show significant variation in complexity along strike or down dip, even over short distances (Schulz and Evans, 2000; Imber et al., 2008; Faulkner et al., 2010). On a regional scale, the complexity of tectonic damage includes the intersection of secondary faults (Maerten et al., 2002), which acts to create areas of low and high stress (Figure 4.15) with the faults effectively bounding stress domains (Tanno et al., 2010).

Large faults have been shown to create both local stress perturbations (Katterhorn and Marshall, 2006), preferential paths for strain (Reusch et al., 2009), as well as compartmentalization of in-situ stresses within a rock mass (Martin, 1990). Wesseloo and Dight (2009) concluded that stress changes during the mining process (induced stresses) are equally complex, with zones of comparatively low and high stress. What is often regarded as a de-stressed slope may in fact be a slope with a comparatively low minimum principal stress, σ3 (aligned normal to the slope face), but comparatively high intermediate, σ2 (circumferential to the pit) and maximum, σ1 (slope-parallel) principal stresses.

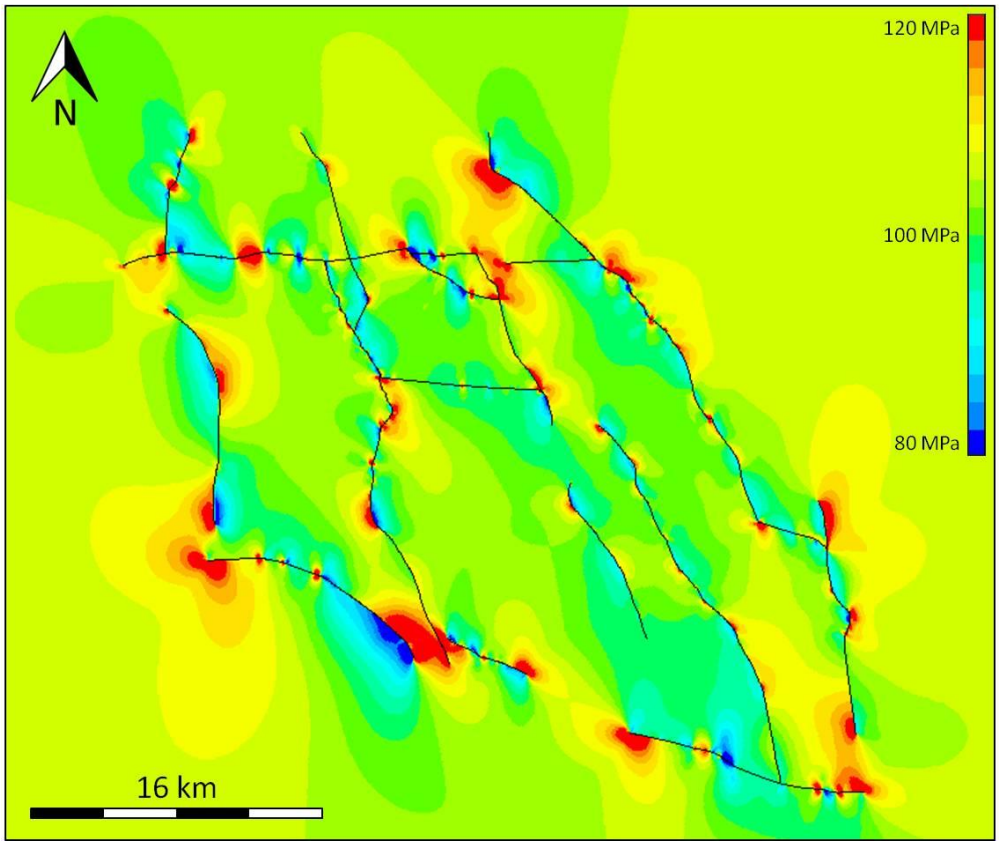

Figure 4.15. Areas of low and high stress modelled around natural fault systems (after Tanno, 2010).

To investigate the impact of faults and stress heterogeneity damage within an open pit, a series of numerical models were constructed using FLAC3D involving a 900-m high pit slope with an overall angle of 45° intersected by a fault dipping into the slope. This was compared to a base model, conducted assuming a homogenous rock mass. The fault zone was modeled as being 60 m wide, which bisects the slope at 70° (Figure 4.16). A hydrostatic in-situ stress condition was assumed and the input properties used in the models are given in Table 4.6.

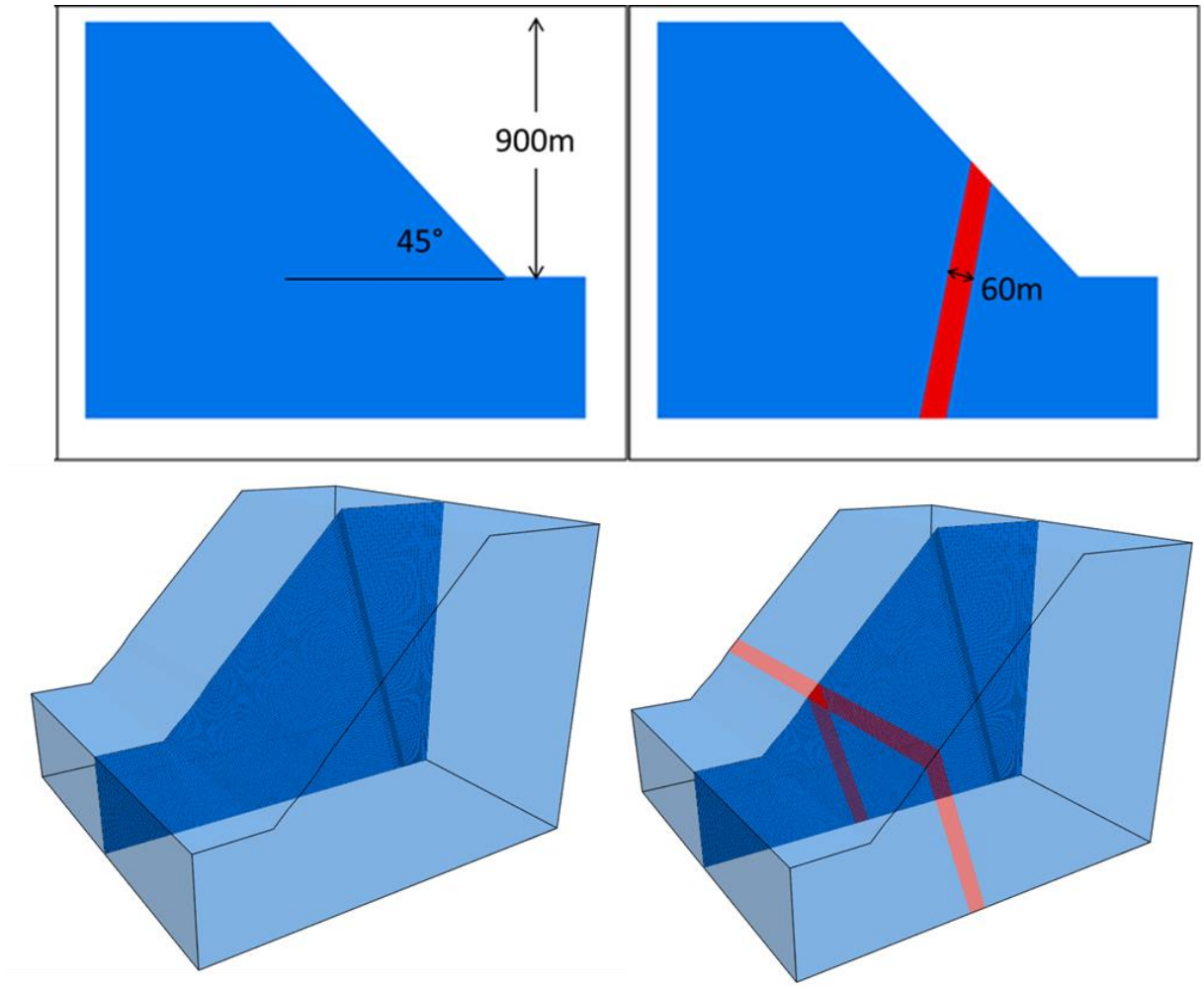

Figure 4.16. Model set-up to review stress development with and without the presence of a 60m wide fault zone bisecting the slope.

Table 4.6. FLAC3D Fault model properties

Material	Host Rock E_{rm} (GPa)	Host Rock Poisson's Ratio	Density (kg/m^3)
Host Rock	35.8	0.25	2500
Fault	0.5	0.3	2200

The models were run assuming an elastic behaviour to evaluate the potential for the development of extensional strain as defined by Stacey (2003). The effect of the more compressible fault on the distribution of both the minimum principal stress (σ_3) and the extensional strain is shown in Figure 4.17. Extensional strain within FLAC3D was calculated using Equation 2.6 and plotted through the program's internal *FISH* programming language, which allows the user to plot user-defined parameters. The homogenous rock mass case (Figure 4.17, left) exhibits elevated extensional strains near the base of the slope, which agrees with the findings from Stacey et al. (2003). The fault zone within the rock mass (Figure 4.17, right) causes the minimum principal stress magnitudes to be reduced on the footwall side of the fault and elevated within the faulted rock. The stress response at the toe of the slope is a loss of confinement toward both the free face of the slope and the fault, which can allow dilation near the fault and the resultant development of extensional strain in the footwall to occur. The footwall rock would be expected to undergo increased damage as extensional cracking occurs in directions normal to both the pit face and the fault.

The weak fault zone bisecting the slope has the effect of decoupling the principal stresses, as the pit floor rebounds from the excavation of the overlying rock (Figure 4.17). At the same time, the largely gravitational driving force from the upper slope is concentrated within the weaker fault material as it deforms as well as altering the magnitude and orientation of the stresses in the footwall (Figure 4.18). Plastic shear can develop within the footwall as the stresses are redistributed near the areas shown to be affected by extensional failure (Figure 4.17). The combination of increased extensional and plastic shear strain can result in a reduction in rock mass strength, which may allow for an unplanned rock mass failure or excessive bulging within the toe of the slope. The conditions created may also have the effect of promoting damage to rock bridges which can develop into complex failures involving non-daylighting planes or wedges.

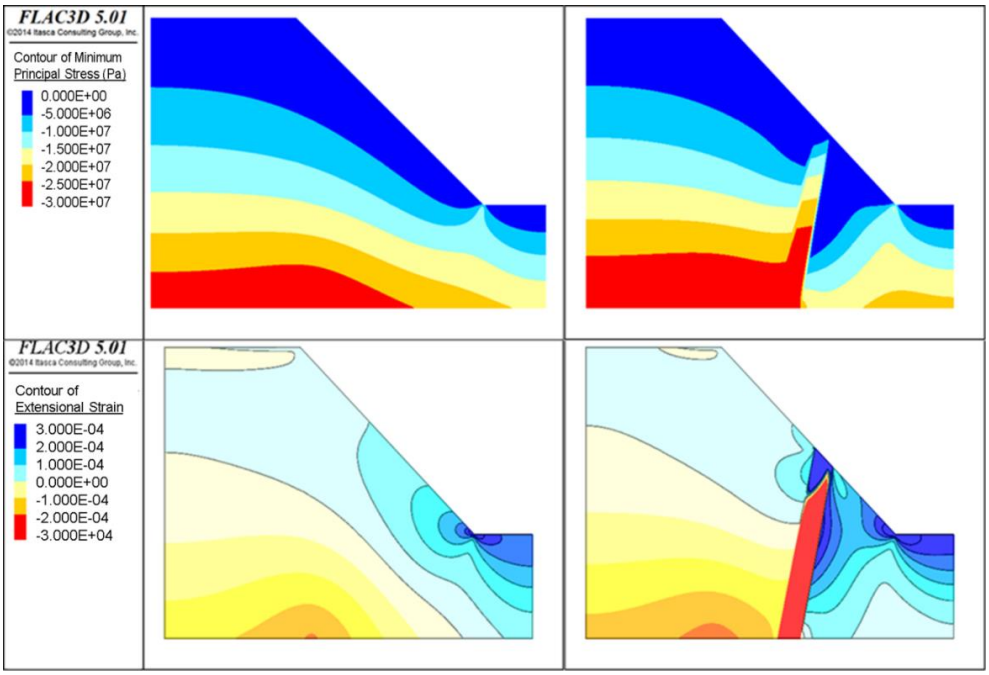

Figure 4.17. Minimum principal stresses (above) and extensional strains (below) around an open pit slope for a homogenous rock mass (left) and one bisected by a 60 m wide fault zone (right). Note that compression is negative.

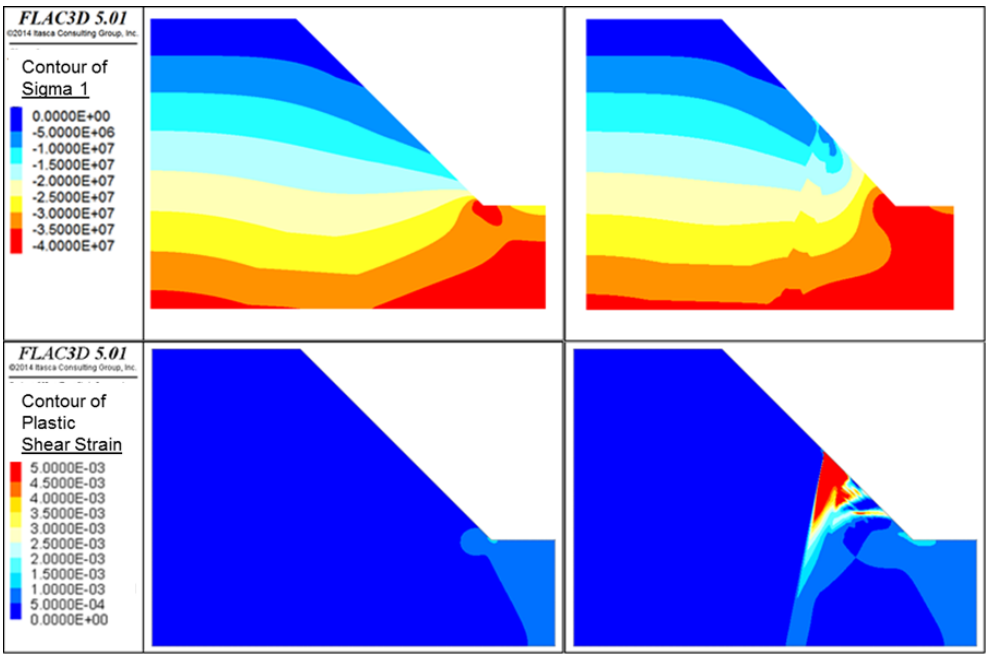

Figure 4.18. Maximum principal stresses (above) and plastic shear strains (below) around an open pit slope for a homogenous rock mass (left) and bisected by a 60 m wide fault zone (right). Note that compression is negative.

4.5.2.1. Influence of Fault Zone Stiffness on Stress Heterogeneity

The FLAC3D conceptual models developed to demonstrate the effect of a thick fault zone on pit wall stresses and damage (Figure 4.16) were modified to test the sensitivity to different fault stiffness relative to a stiffer host rock mass. The deformation modulus of the fault was varied between 1 and 50% of that for the surrounding rock mass. The end conditions of the parametric models were set to replicate conditions in which the contrast between the surrounding rock mass and fault zone is relatively minor (e.g., a weak or ductile sedimentary or saprolite host rock mass) to conditions where the stiffness contrast strength is reduced sharply (e.g., a harder more brittle host rock mass). The model was run with elastic properties as shown in Table 4.7.

Table 4.7. FLAC3D properties used to evaluate stress development near faults for different fault stiffnesses

Model Run	Host Rock E_{rm} (GPa)	Host Rock Poisson's Ratio	Fault E_{rm} (GPa)	Fault Poisson's Ratio	Ratio of Fault:Host Rock E_{rm}
1	35.8	0.25	17.9	0.3	50%
2	35.8	0.25	8.9	0.3	25%
3	35.8	0.25	3.6	0.3	10%
4	35.8	0.25	1.8	0.3	5%
5	35.8	0.25	0.4	0.3	1%

Stress heterogeneity in each of the models was assessed by comparing the maximum principal stress magnitudes and distributions modelled as well as the measurement of depth of confinement loss into the pit wall (i.e., minimum stress < 0; see Figure 4.19). Confinement is an important factor in rock failure as it helps to arrest brittle fracture propagation and the degradation of cohesive rock strength.

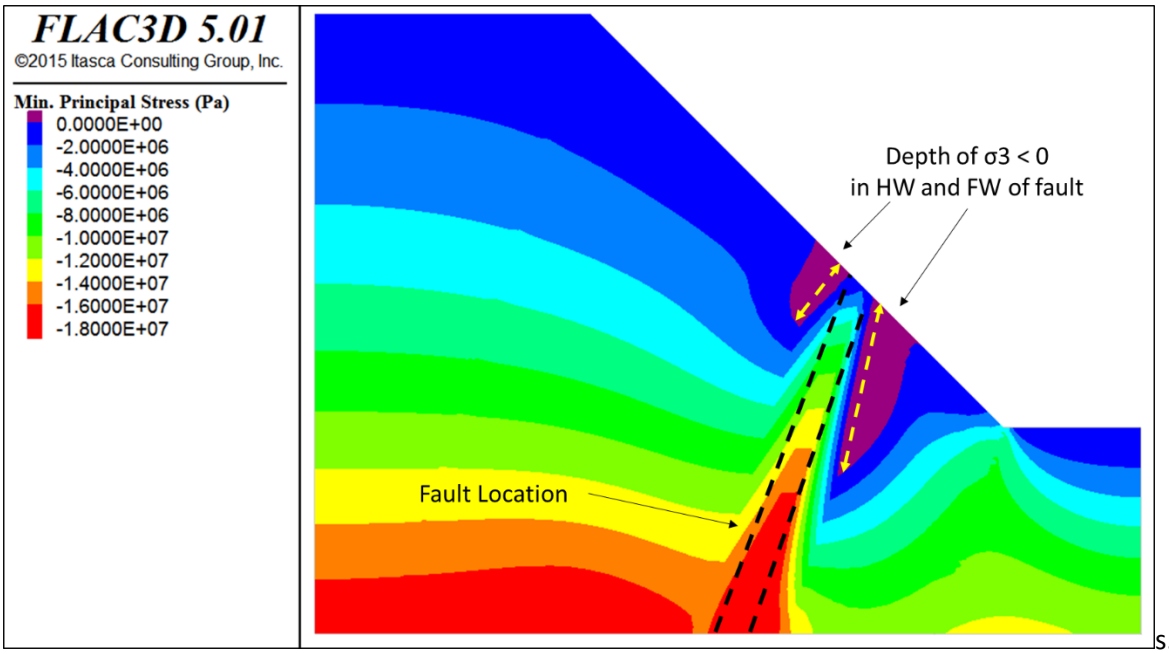

s.

Figure 4.19. Example of minimum principal stresses showing areas of low confinement (purple) arising due to fault stiffness contrast with surrounding rock mass and excavation of the open pit. Compression is negative.

Results from these models first show that without the presence of a fault, the mining-induced stresses wrap around the pit resulting in a homogeneous stress state and a relatively more stable slope condition. In contrast, the presence of a fault zone within the model de-couples the pit slope and inhibits the wider redistribution of induced stresses that develop in the toe of the slope. The mining induced stress is effectively focused at the base of the slope, with an increase in the maximum principal stresses within the toe of the slope. These stresses were seen to dramatically increase as the deformation modulus of the fault material was reduced, especially for the case of 10% relative to the deformation modulus of the host rock (Figure 4.20).

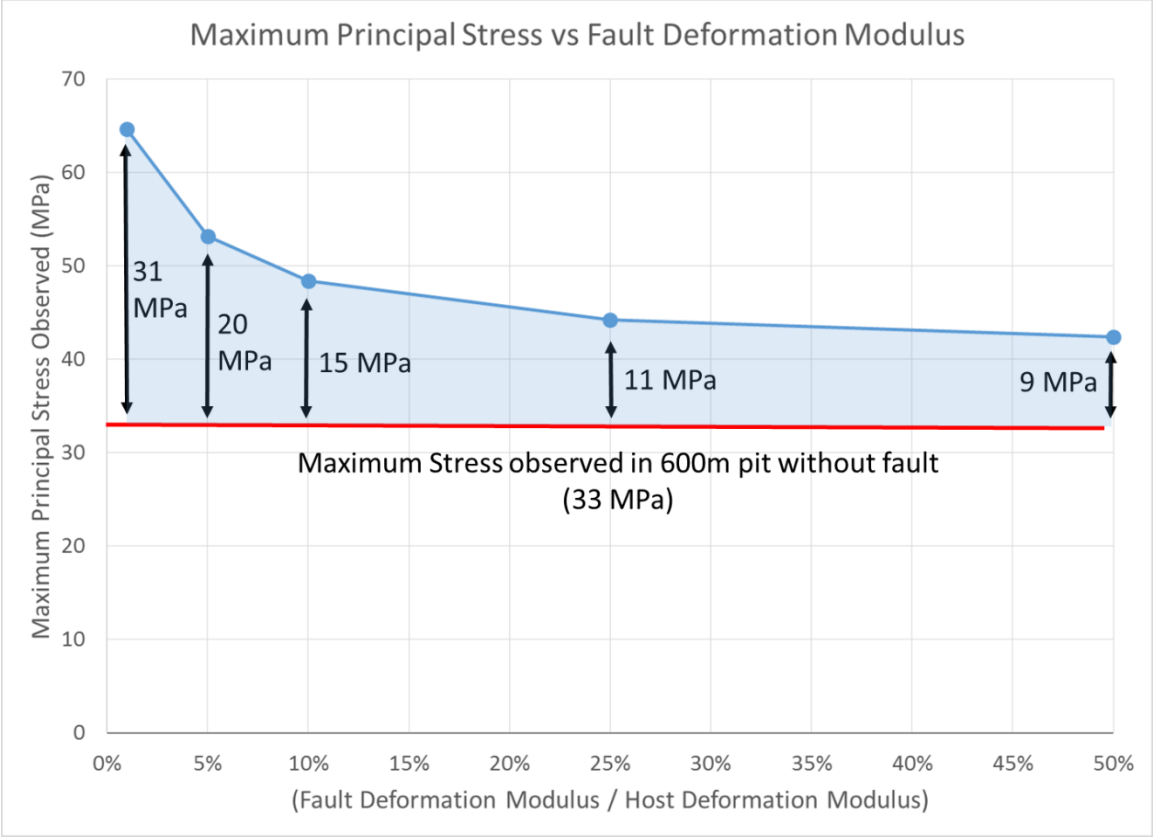

Figure 4.20. Maximum stress observed at the toe of the slope for a 600m high pit slope, and its variation as a function of deformation modulus of a fault zone bisecting the slope wall.

Similarly, the minimum principal stresses within the modelled slope are significantly affected by the presence of the fault zone in combination with the excavation of the pit. This creates neighboring regions behind the pit face of increased compressive stresses, which promote yield and mobilization of the rock mass in the direction of the fault, and zones of unconfined rock which at depth would otherwise normally be confined (Figure 4.19). The latter would facilitate kinematic slip of blocks. The depth into the pit slope of the unconfined zone that develops, where the minimum principal stress is tensile, was determined for each of the model cases outlined in Table 4.7.

Table 4.7Minimum stresses within the footwall of the fault were found to be particularly sensitive to the deformation modulus of the fault zone (Figure 4.21). For the modelling results obtained, when the deformation modulus of the fault is less than 10% of that for the surrounding rock mass, the depth of the tensile region increases significantly and to depths well below the bottom of the pit. Again, this tensile

region would promote extensional failure together with the degradation of rock mass strength in the toe of the slope.

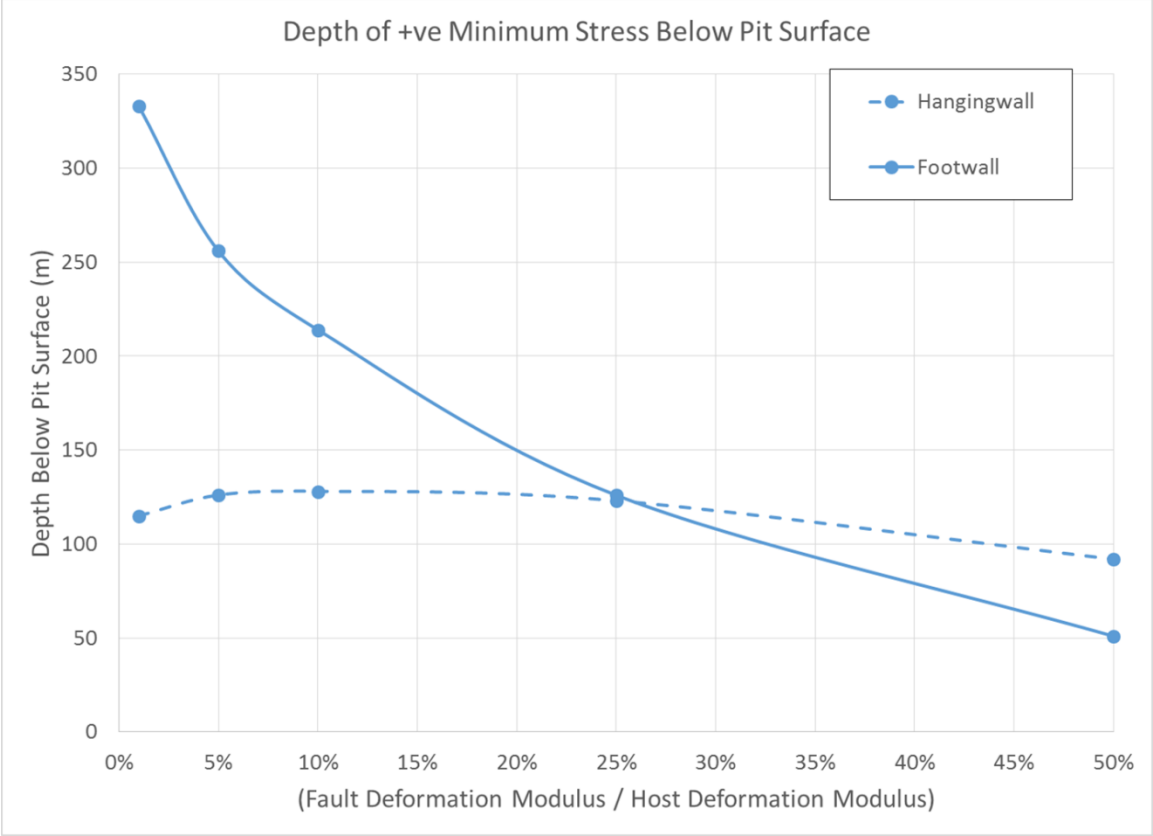

Figure 4.21. Depth of low confinement stress within the hanging wall and footwall of a 600m high pit slope as a function of fault zone stiffness. Note the steep slope of the footwall side indicating that this portion of the slope is particularly sensitive to fault stiffness.

4.5.2.2. Influence of Discontinuum Representation of Faults on Stress Heterogeneity

The previous analyses were based on 3-D finite difference representations of a fault zone where the continuum formulation forces its connectivity with the adjacent lithology. To further investigate the impact that faults can have on stress heterogeneity within an open pit, discontinuum-based modelling using the distinct-element software UDEC (Itasca, 2011) was used. The distinct-element formulation allows for the modelling of slip, opening and closing along interfaces used to represent faults in the model. The model geometry was based on Teck's Highland Valley Lornex Pit, and was taken as a 2-D plane cut through the mid-slope height. Analysis on the plan section included the outline of the open pit excavation with and without a network of intersecting faults (Figure 4.22). A hydrostatic in-situ stress state was assumed and the rock mass properties used assumed a Mohr-Coulomb elasto-plastic constitutive model to allow for rock

mass yield in between fault segments. The faults were modelled using a Coulomb slip model. The input properties are provided in Table 4.8.

Table 4.8. UDEC plan section model properties (THVC)

Unit	Density (kg/m^3)	RMR/ GSI	σ_{ci} (MPa)	Cohesion (MPa)	Friction Angle (°)	Tensile Cut-off (kPa)	Joint Normal Stiffness (Pa/m)	Joint Shear Stiffness (Pa/m)
Skeena Quartz Diorite (SQD)	26	43	37.9	0.261	38.4	75	-	-
Bethsaida Granodiorite (BGD)	26	51	55.5	0.372	46.7	125	-	-
Faults	-	-	-	0.1	30	0.01	1e10	1e9

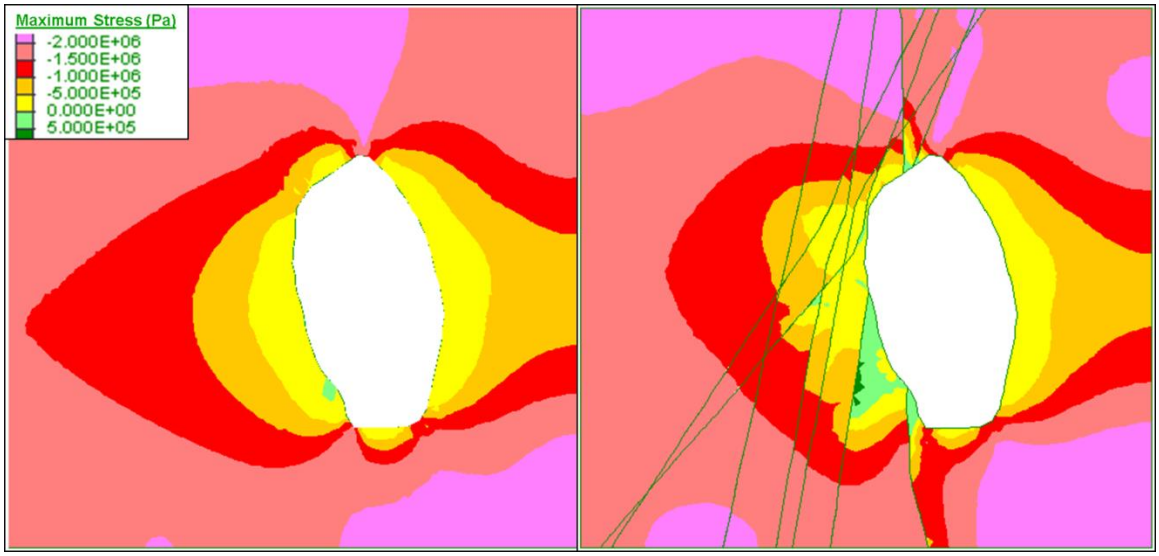

Figure 4.22. UDEC modelled stress contours plotted for a plan section view through the mid-slope elevation of the Lornex Pit without (left) and with (right) the inclusion of tectonic faults explicitly included in the model. Compression is negative.

By explicitly including the faults in the model as a discontinuity, the stress patterns are similar to those where the faults are represented implicitly in a continuum framework. However, localized heterogeneity within the wall develops as well as local areas of tension between several of the sub-vertical faults and the pit wall (light green, right). These results further indicate that as the open pit deepens, the magnitude of the

deviatoric stresses will likewise increase. This would indicate that the zones of stress concentration may involve higher stresses, promoting yield and shear localization, and that the zones of relaxation will involve increased unconfined stress conditions around the faults facilitating kinematic block movements and wedge failures. By including the third dimension within these models, side wall stresses may vary over the pit height, which may also locally effect the concentration of stress.

4.6. Case History – Influence of Stress Heterogeneity on Palabora Pit Slope Failure

The Palabora Copper Mine, as described in Section 3.1 successfully transitioned into a block caving operation with underground production with current production level of the underground mine is located approximately 1,200 m below surface and 400 m below the final pit bottom (Figure 4.23a). Shortly after breakthrough of the cave into the floor of the mined-out open pit in 2004, the northwest wall experienced a slowly evolving, multi-bench failure (Figure 4.23b). The failure mechanism likely involved a combination of slip along existing structures and brittle failure of the rock mass in response to the undermining of the slope toe by the developing block cave. Prior to the failure, a series of complex slope movements occurred in 2003 in response to the crown pillar (pit floor) becoming de-stressed. Movement of the pit walls increased substantially upon cave breakthrough into the bottom of the pit with the largest deformations being observed in the North wall. Failure of the northwest wall was gradual and continued to develop slowly over a period of 18 months. Brummer et al. (2006) observed that within the main zone of movement on the northwest wall, most of the visible deterioration of the rock mass was along the western and eastern boundaries, and that the central portion of the slide mass appeared to remain relatively "intact".

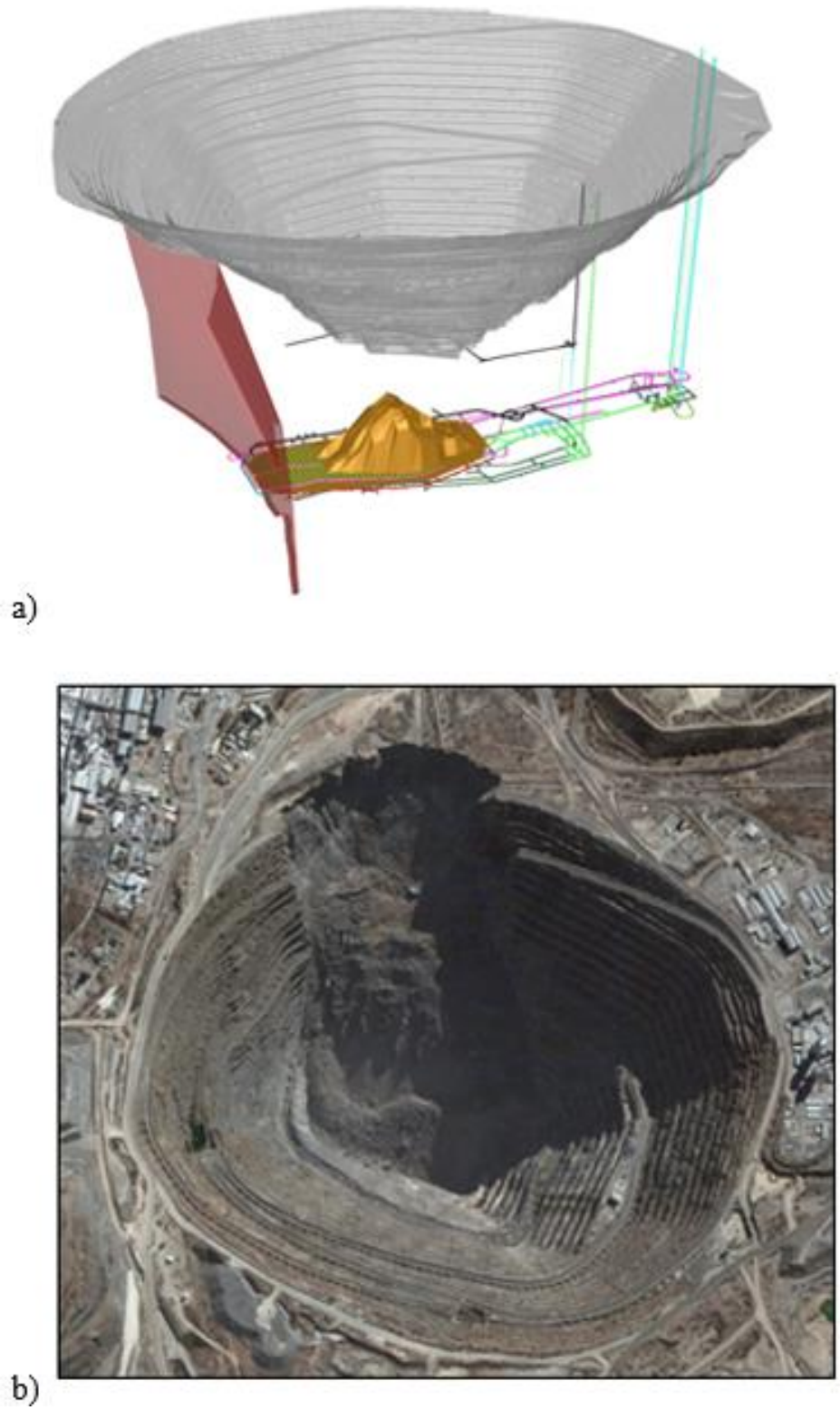

Figure 4.23. a) 3-D spatial relationship between the underground operations, open pit, and Mica Fault; and b) 2008 Quickbird image of Palabora northwest wall failure.

The development of an underlying caving operation or other underground workings adds further complexity to the induced stress changes observed within a large open pit slope. At the Palabora Mine, there are four regional faults transecting the pit (Figure 4.24), including the Mica Fault described as being a 60-m wide shear zone comprised of large rock blocks, fault breccia and fault gouge. The influence of fault structures in the creation of a heterogeneous stress field and its interaction with the mining induced stress are further studied using the discontinuum code 3DEC (Itasca, 2013) to develop two similar numerical models, a base model which included lithological boundaries, and a faulted model which included the four main faults, as shown in Figure 4.25. The objective of the model was to identify the magnitudes and orientations of the principal stresses within the north and west pit walls and to study the effect that large faults have on local stress distributions in the area where a massive pit wall failure eventually occurred in 2004.

A Mohr-Coulomb elasto-plastic constitutive model was used to determine the stresses and stress paths in the north wall. Estimates of the rock mass and fault properties were based on estimates derived from laboratory testing and field mapping data (i.e. RMR), as reported by Sainsbury et al. (2008).

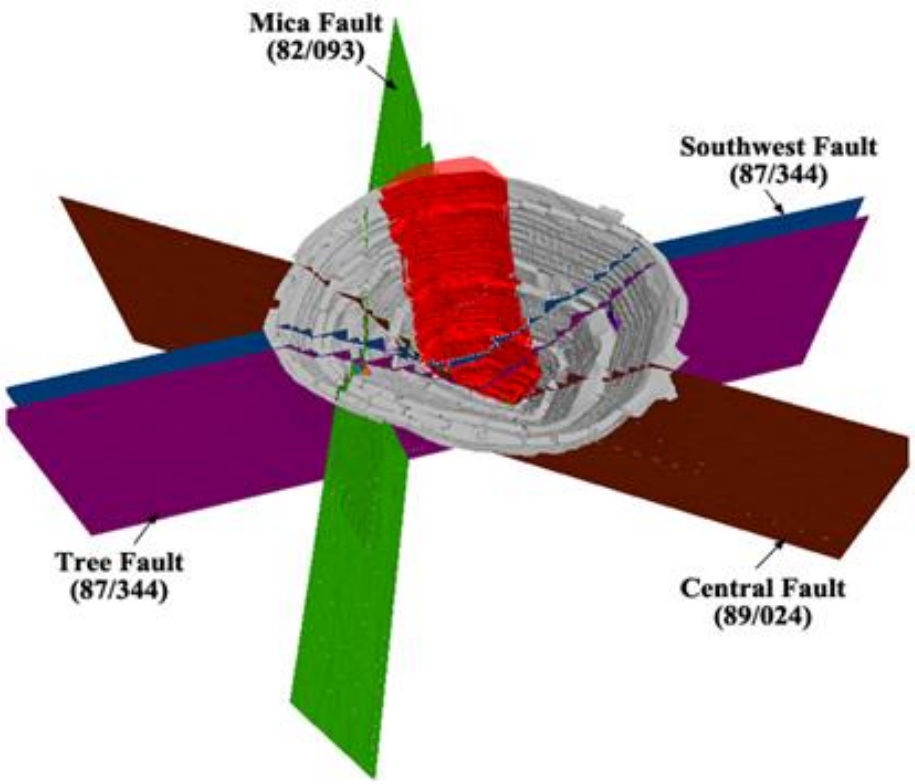

Figure 4.24. 3-D structural model of the Palabora open pit with regional faults indicated. North is towards the top. The outline of the 2004 pit wall failure is shaded red.

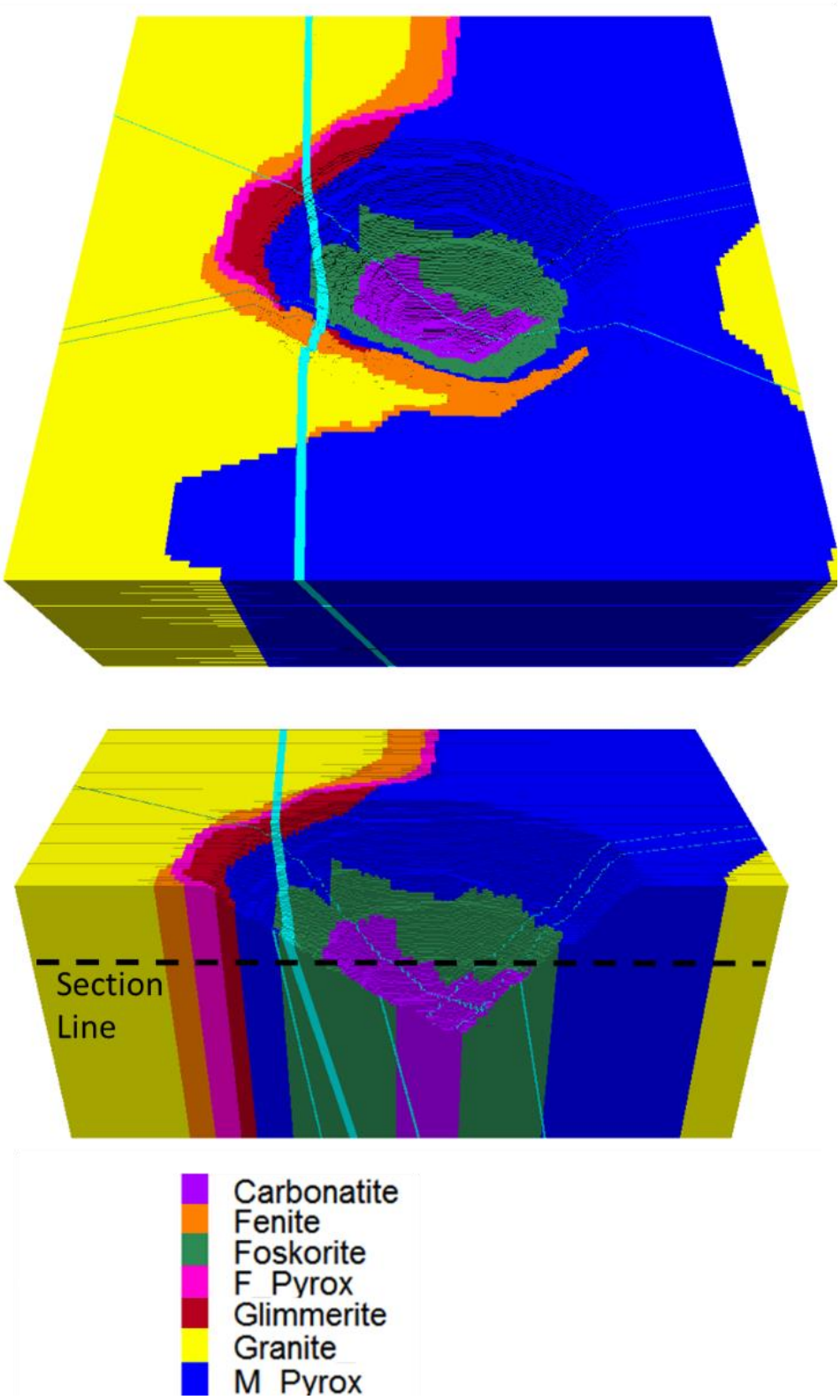

Figure 4.25. 3DEC Palabora model geometry shown as an oblique view (top), and cross-section (bottom). Shown are the key rock units and structures explicitly included in the model. Location of plan section view shown in subsequent figures is indicated.

The cave propagation was projected for each year, between the start of caving in 2002 to 2010 (Figure 4.26). The cave fronts were derived based on: 1) monthly tonnage production data reported for each draw point adjusted for bulking for localized cave heights; 2) geotechnical monitoring data, such as TDR cables; 3) a series of aerial images detailing the increase in surface expression of the cave break through; and 4) first-hand accounts from mine staff detailing hydraulic connection between the surface and cave break through. Table 4.9 and Table 4.10 present the input properties used. Groundwater conditions within the pit were assumed to be dry in accordance with the semi-arid climate of the region and dewatering work carried out for the block cave mine (Glazer, 2003; Sainsbury et al., 2008).

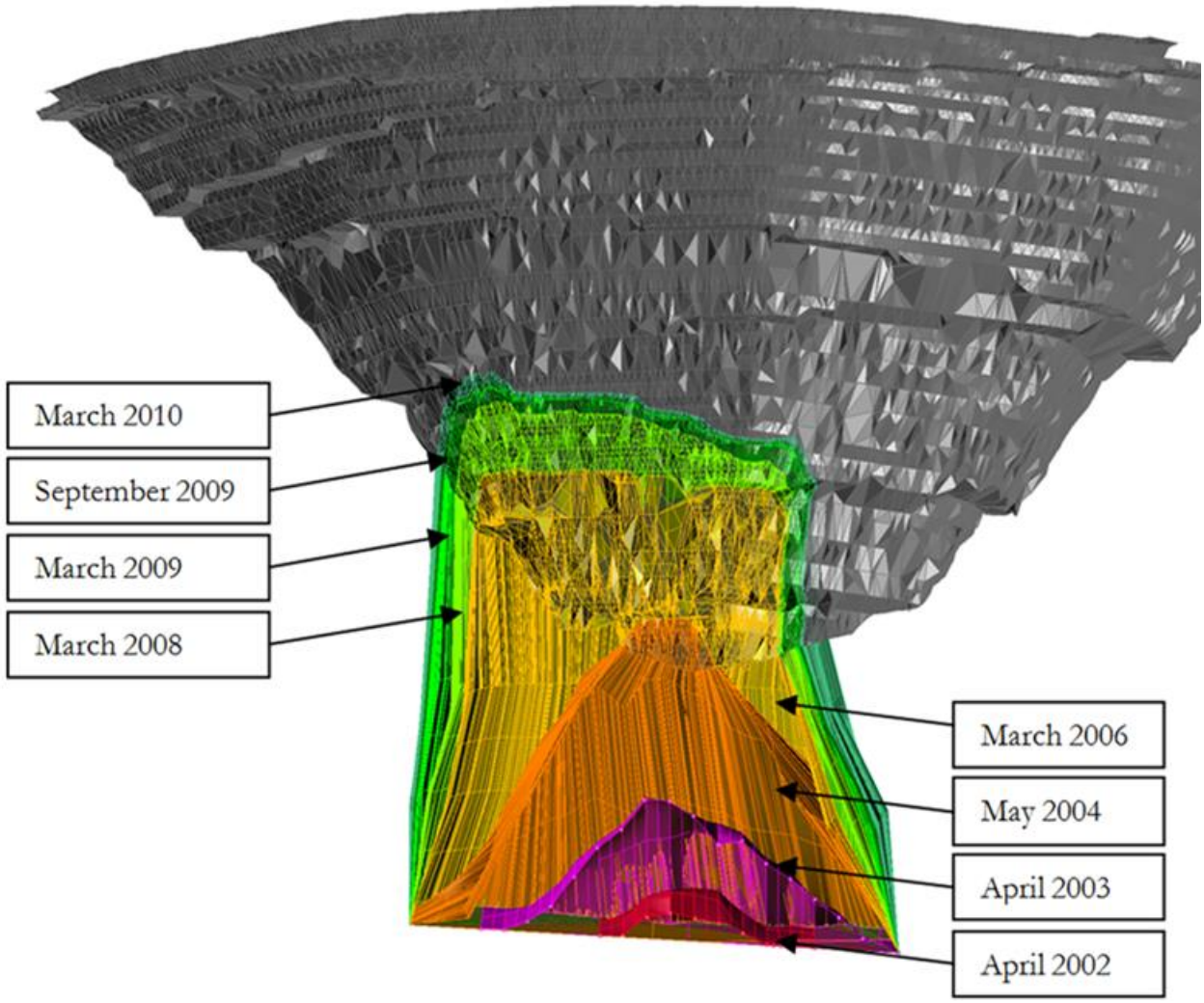

Figure 4.26. Cave propagation geometries developed for implementation in the 3DEC Palabora case study model.

Table 4.9. 3DEC rock mass and caved rock input properties for the Palabora case study analysis

Model Units	Density (kg/m3)	Cohesion (MPa)	Friction Angle (degree)	Bulk Modulus (GPa)	Shear Modulus (GPa)	Tension (MPa)
Rock mass	2700	6.1	55	37.2	22.0	1.2
Caved Material	2300	0	30	0.42	0.19	0
Faulted Rock	2500	1.0	35	0.85	0.59	0.1

Table 4.10. 3DEC input properties for the major faults explicitly represented in the Palabora case study analysis

Structure	Dip (degree)	Dip Direction (degree)	Cohesion (MPa)	Friction Angle (degree)	Normal Stiffness (GPa/m)	Shear Stiffness (GPa/m)	Tension (MPa)
Mica Fault	82	093	0	10	8.0	0.4	0
Southwest Fault	87	344	0.005	25	8.0	8.0	0
Central Fault	89	024	0	10	8.0	8.0	0
Tree Fault	87	344	0.005	25	8.0	8.0	0

Figure 4.27 is a plan section view at mid-slope height of the 3-D model (as shown in Figure 4.25) which shows the influence of major geological features on maximum shear stress distributions in the north wall at the 2010 cave stage. Both pit excavation and cave propagation were shown to influence the stresses within the model and an increase in shear stress was shown to extend behind the pit face when the known sub-vertical faults are included in the analysis. The concentration of shear stresses coincides with the area of an eventual pit slope collapse in the North Wall. Without faults, the shear stresses around the pit ranged to approximately 20 MPa. However, with the inclusion of the faults, shear stresses range up to more than 30 MPa around the eventual failure.

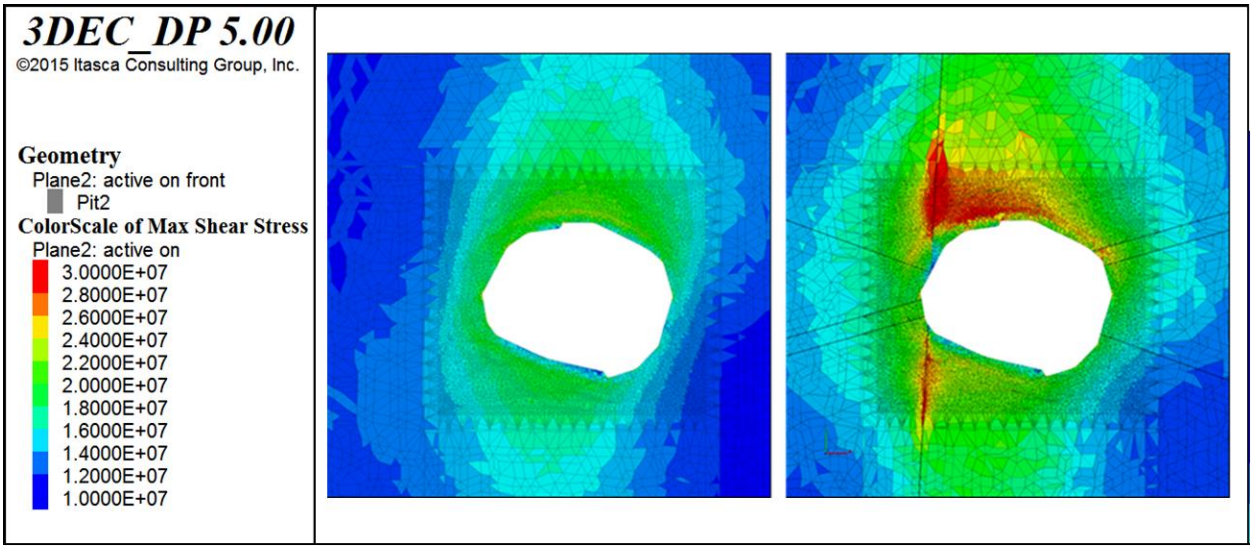

Figure 4.27. Maximum shear stresses (Pa), without and with the inclusion of the mapped faults, plotted for a horizontal plan view through the upper half of the pit slope (150 m below surface). The plan section location is shown in Figure 4.25.

The increased shear stress within this portion of the wall is enough to promote shear and fracture of intact rock, and the stress heterogeneity arising from the fault interaction between the open pit and propagating cave below the pit combines to promote an adverse stress condition promoting instability. The presence of shear failure behind the face of the pit is corroborated by the relative intact pit face and quick disintegration of the rock mass observed in the north wall.

The development of stress heterogeneity around the open pit and block cave mine at Palabora is considered to have a significant influence in promoting brittle failure behind the pit face leading to the eventual instability of the north wall. Stresses were reviewed from the end of the pit life to the point of instability in 2004 and carried onward until 2010. Figure 4.28 shows the confining stresses plotted along a cross-section cutting through the north wall at the eventual location of the pit wall failure for 3-D modelling without and with the explicit inclusion of the mapped faults. The faults are shown to reduce the minimal principal stress (i.e., confinement) adjacent to the pit wall around the failure to a much greater extent than the base case without faults included. The initiation and growth of the cave further reduces the stress in the north wall in the upper third of the pit, as well as increases the stresses locally where the fault intersects the wall. Displacement patterns surrounding the pit were altered significantly, both in the north and west walls in the location of the thick Mica Fault (Figure 4.29) through both relaxation of the host rock material into the cave as well as the stress cut-off created by the Mica Fault.

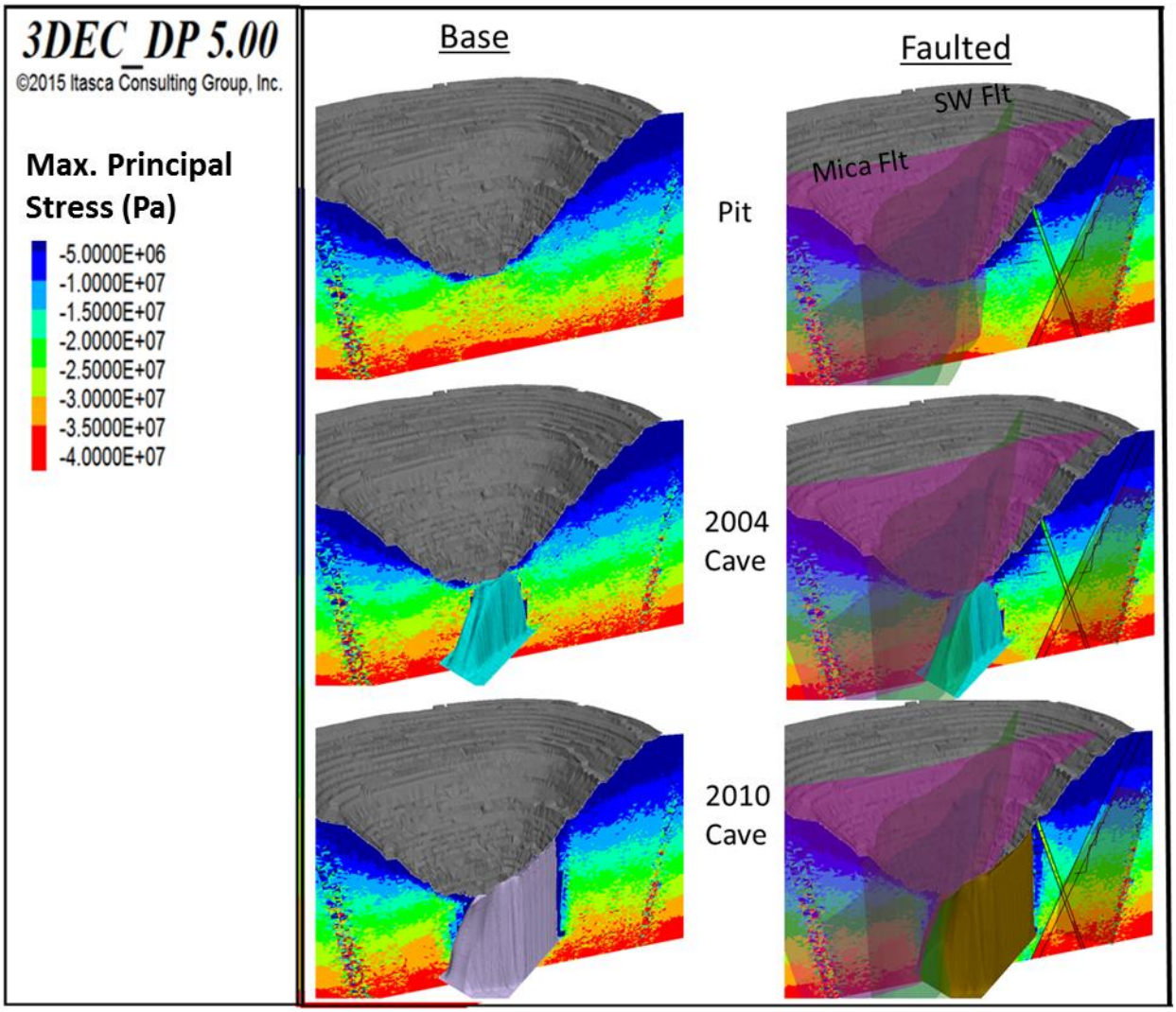

Figure 4.28 **3DEC results for the Palabora case study showing the minimum principal stresses (in Pa) for a cross-section view, comparing the influence of including the mapped faults to the base case without faults. Shown are the results for three time intervals from the end of the pit life, to cave breakthrough in 2004, to the cave extent in 2010. Note that compression is negative.**

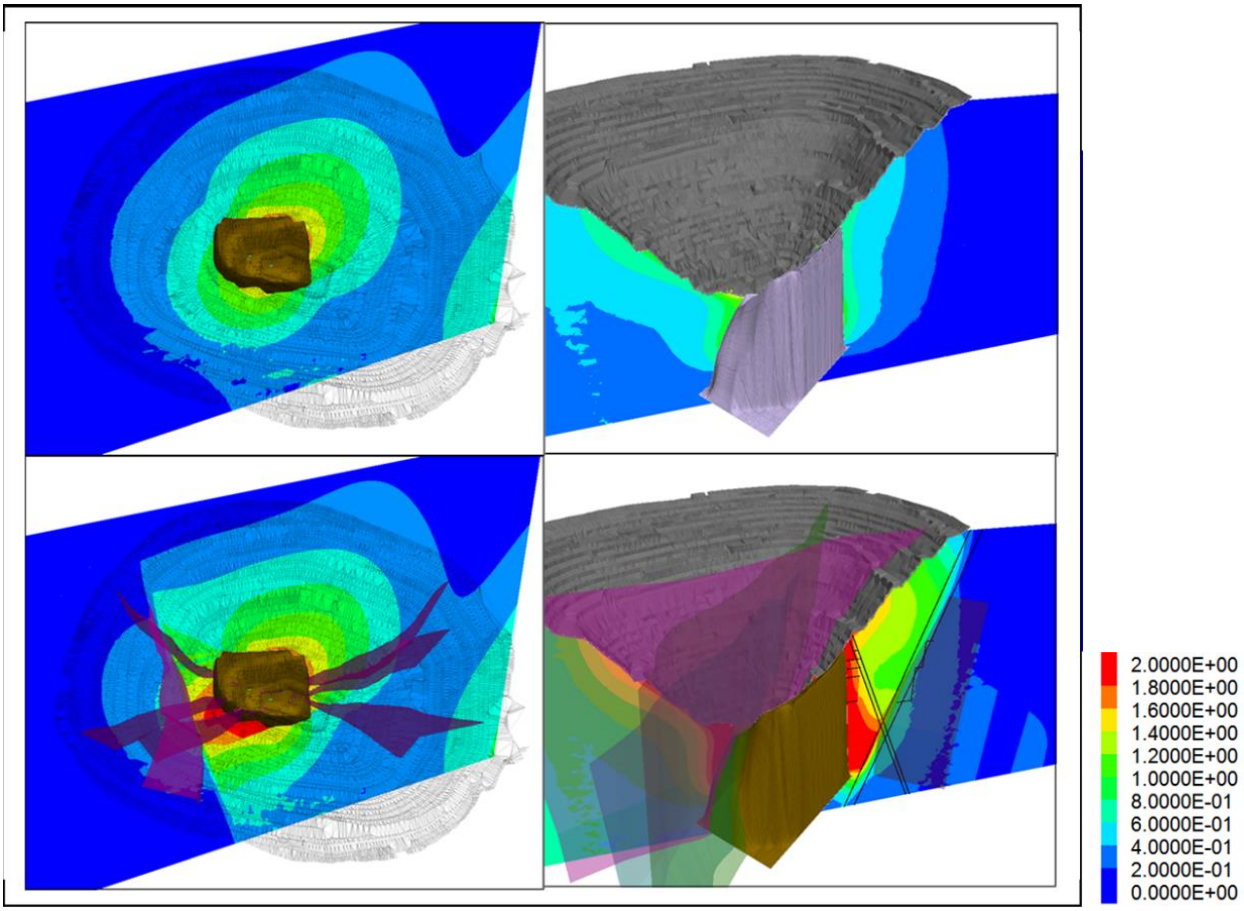

Figure 4.29. 3DEC modelled displacement magnitudes (in m) projected in plan view onto a plane at 50 m depth (left) and onto a cross-sectional view through the North pit face (right), for the Palabora case study at its 2010 cave extent. Shown are results for both the base model without faults (top) and model with faults included (bottom).

Stress heterogeneity created through the interaction between natural stress perturbations and mining induced stresses has been shown to create both increased shear stress near the faults and a reduced confining stress near the upper portion of the cave. This creates a highly variable stress condition to which the rock was subjected. It is postulated that these distinct changes in stresses conditions created an environment in which extensional and plastic shear damage could occur. This damage enabled a weakening of the rock mass and the fracturing of natural bridges within the north wall.

4.6.1. Impact of Fault Representation on Scale Stress and Damage at the Pit Wall Scale

The impact of fault representation on the development of stress in the 3DEC model was investigated through the development of four mine scale 3DEC models. Figure 4.30 shows three of the model geometries used to represent the four cases reviewed: A) no faults included (i.e. equivalent continuum), B) faults modelled

as discrete contacts, C-1) faults modelled as a 2 to 20 m continuum zone (based on their mapped true thickness) with properties equivalent to a highly fractured rock mass, and C-2) thick faults (2 to 20 m) explicitly modelled as distinct broken rocks (i.e. tectonically disturbed, blocky rock mass). This was done to investigate the variance in stress path experienced by a block of rock (at several chosen locations), depending on the representation of the faults within the model.

Lithological boundaries were simplified within this model to isolate the effect of the faults on the stress field and focus the model results on the influence of the major faults; it should also be noted that the range of properties derived for the two rock masses overlap, and therefore are approximately similar. The shape of both the pit and the cave were simplified to allow for additional detail within the fault of the blocky fault model. Cave propagation between the undercut and surface breakthrough was then divided into several intermediary stages.

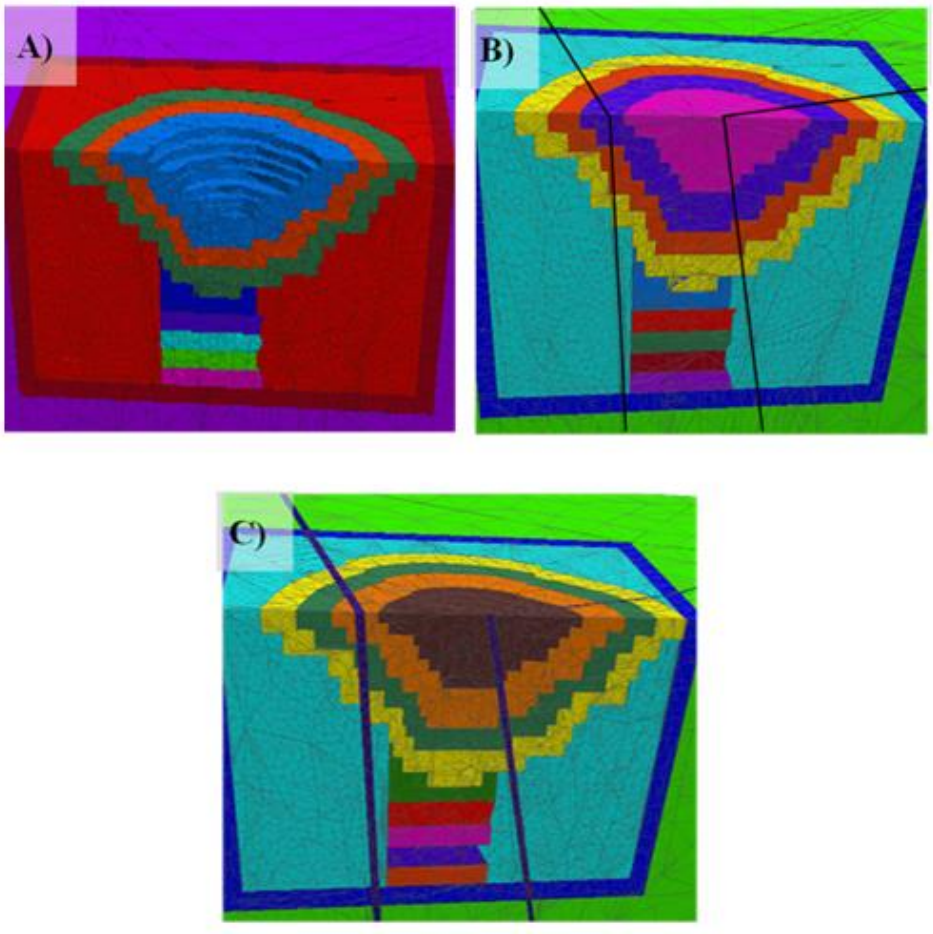

Figure 4.30. Section views of the pit, fault and cave geometries modelled in 3DEC for the following geometries: A) without faults (continuum treatment), B) faults as distinct breaks, and C) fault zones, either represented by an equivalent continuum of weaker material or as a discontinuum of multiple fractures.

Estimates of the rock mass and fault properties were based on estimates derived from laboratory testing and field mapping data (i.e. RMR), as reported by Sainsbury et al. (2008). Table 4.9 and Table 4.10 present the input properties used. Groundwater conditions within the pit were assumed to be dry in accordance with the semi-arid climate of the region and dewatering work carried out.

Several monitoring points were specified within the model positioned along planes parallel to the Mica Fault at 50, 100, and 200 m distances (Figure 4.31), and at elevations roughly equal to the bottom of the pit, and one- and two-thirds of the pit wall height. These were used to determine the importance of proximity to the fault to the source of the mining-induced stress change (i.e. propagating cave). As an example of how the inclusion of the faults can change the stress paths and states within a numerical model, Figure 4.32 shows the changes observed in the azimuth and magnitude of the principal stresses observed in the models during the excavation of the pit (in 5 incremental stages) and the propagation of the cave (in 5 incremental stages). The respective changes in the direction of the principal stresses show that significant differences in the stress paths generated are obtained simply by changing how the faults are modelled.

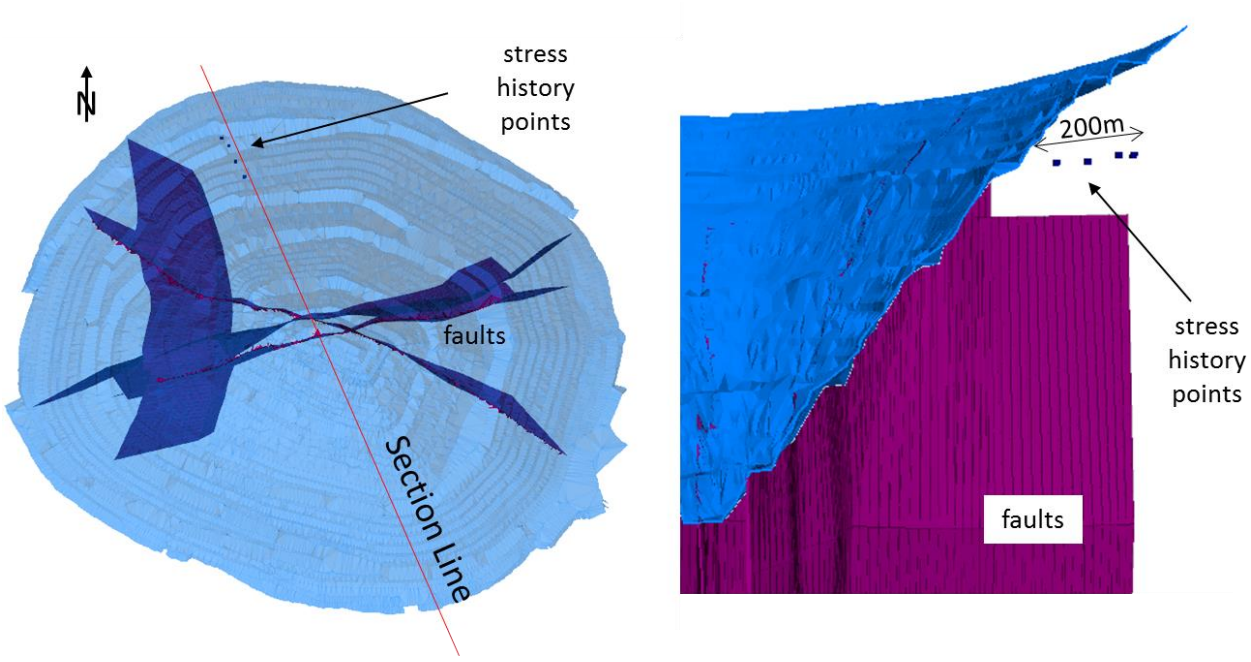

Figure 4.31. Stress history location points within north wall of the Palabora mine model.

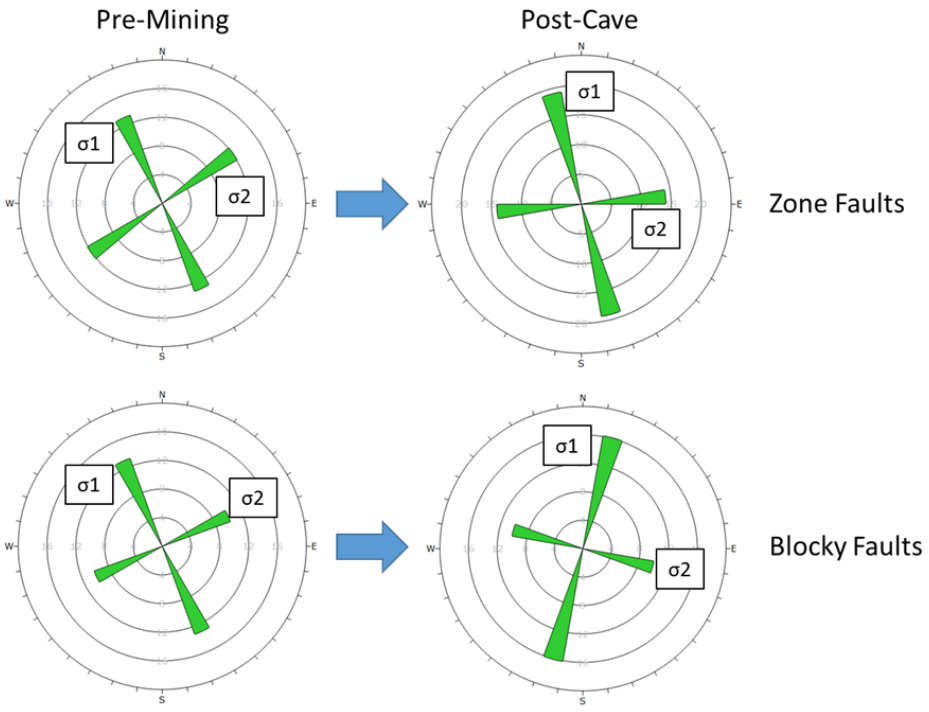

Figure 4.32. Response of stress orientation to block cave mining, comparing modelling of the faults as zones as in Figure 4.30c (above) and as discrete discontinuities as in Figure 4.30B (below) for the 3DEC mine-scale case study models of Palabora. Stress orientation histories are those for the north wall, showing direction of maximum (σ_1) and intermediate (σ_2) stress, with minimum stress (σ_3) estimated as vertical.

4.6.2. Local Pit Wall Response to Fault Representation

The stress histories achieved from the mine scale model were retrieved from each of the 4 cases; Model 1 – No Faults, Model 2 – Discrete Faults, Model 3 - Thick Continuum Fault Zones, and Model 4 – Thick Crushed Rock Faults (explicitly modelled). The monitored stress histories were applied to a local scale 3DEC model of a 10 x 10 x 10m block at each of monitored stress history points within the northwest portion of the pit wall. Each block contained the mapped joint sets, as mapped at Palabora and reported by Sainsbury et al. (2008) were applied to these blocks to represent the following configurations, A) GSI = 75 with random jointing, B) GSI = 50 with random jointing, C) GSI = 75 with anisotropic jointing, and D) GSI = 50 with anisotropic jointing. The blocks bound by the joint sets were made deformable and given the properties of the rock mass, as per Table 4.9.

The block models were loosely based on the joint sets mapped in the micaceous pyroxenite host rock at Palabora, which shows three near-vertical joints with one sub-horizontal set (Figure 4.33). Blocks with random joints allow a variance of 45° (+/- 10°) to these.

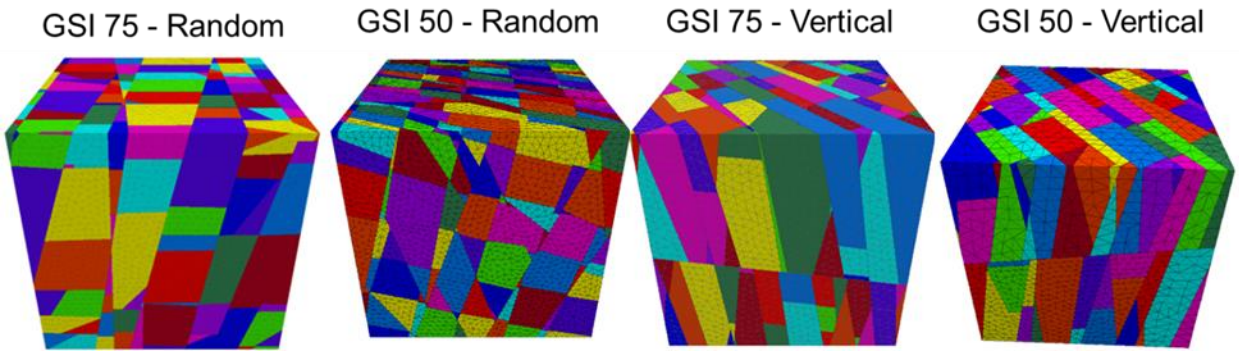

Figure 4.33. 10x10x10m 3DEC blocks used to estimate the amount of rock damage within the Palabora Pit north wall for the following joint conditions; A) GSI=75 Random, B) GSI = 50 Random, C) GSI=75 Anisotropic, D) GSI=50 Anisotropic.

To model the rock response, a strain-softening elasto-plastic constitutive model was used to represent the individual blocks in the model to allow for the brittle failure of rock bridges between the joints. The faults were assigned a Coulomb slip constitutive model. Estimates of the intact rock and fault properties were based on estimates derived from laboratory testing and field mapping data (i.e. RMR), as reported by Piteau Associates (2000; 2005).

The results of the numerical analyses show that if large-scale structures are included explicitly within the model, the corresponding change in stresses within that model lead to higher percentages of the surrounding rock mass yielding in shear and tension. As seen in Figure 4.34, the maximum recorded shear stress in each of the block models is higher with stresses transposed from mine-scale models incorporating a blocky discontinuum fault zone rather than those with no faults included. This is an expected result as the mine-scale model also indicated elevated shear stresses. In all block models, up to 20% more volume of elements is recorded as being yielded in shear for the stresses based on the blocky models. An increase of yielded elements occurs during the cave stages (7 through 10).

The excavation of rock, whether during open pit or subsequent underground mining, along with the presence of large scale geological structures, has been shown to significantly affect the stress path experienced by the rock mass. The extent of the perturbations caused by geological structures is poorly understood and the features are often simplified in numerical models which can misrepresent the local stress state of the rock. By including a more complex representation of the Mica and Southwest Faults, an increase in maximum shear stresses within the north wall of the Palabora pit wall were achieved, and a higher percentage of rock mass yielding occurred within smaller representative block models. This increase of yielded units may represent the breaking of intact rock bridges within the highly anisotropic rock.

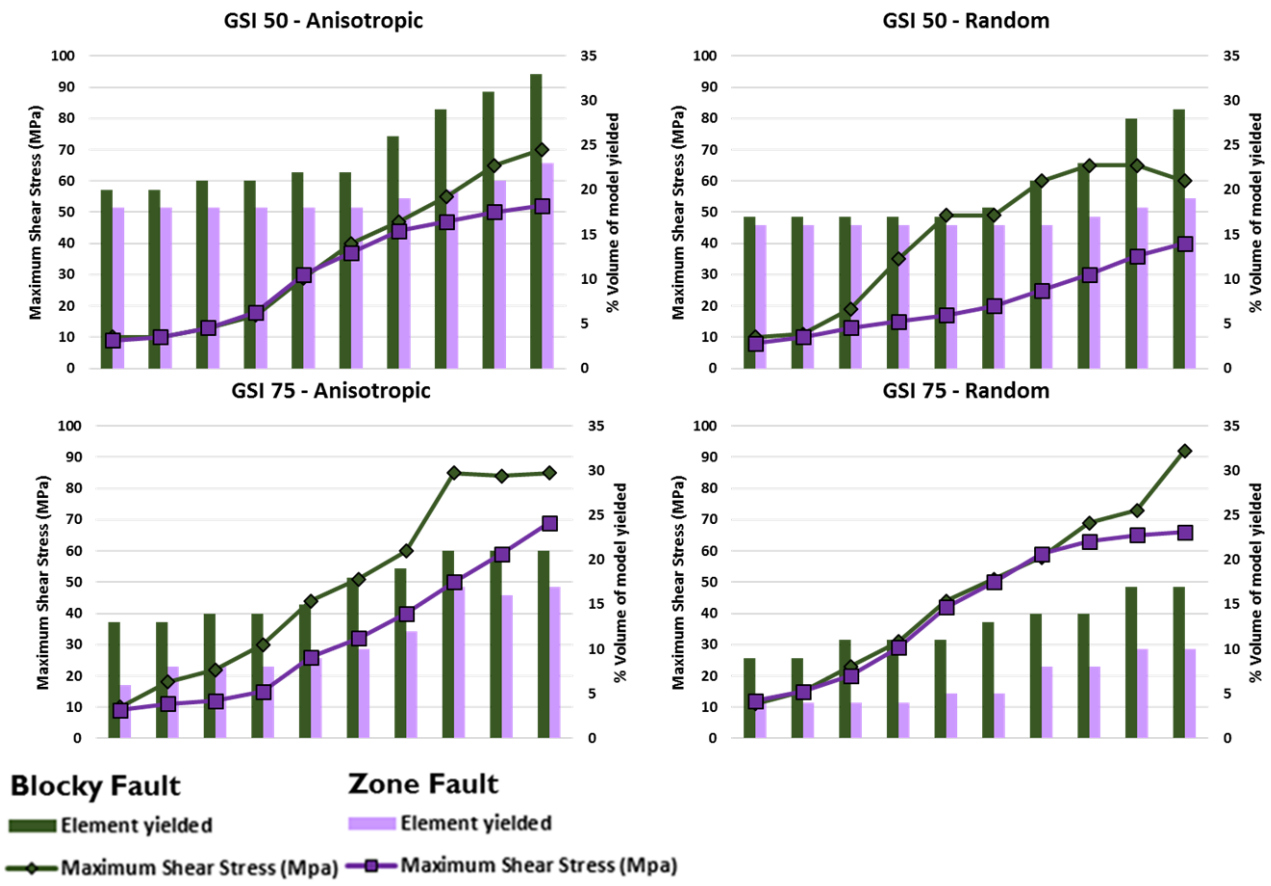

Figure 4.34. Maximum shear stress and % volume of yielded elements within the 10x10x10m blocks (as shown in Figure 4.33). Line graphs are shown with maximum shear stress observed in the model. Bar graphs are shown for the volume of rock yielded in shear (bar) for models with faults composed of weakened materials and those including a thick blocky fault zone.

4.7. Discussion - Implications of Stress Heterogeneity

4.7.1. Open Pit Design

Current industry standards in mine design have clear guidelines as to the inclusion of factors such as lithological changes, structural geology, hydrological conditions, and rock mass strength in the creation of a geotechnical model (Read and Stacey, 2009). One of the key considerations that remains unclear is the inclusion of rock mass strength degradation due to the excavation of the overlying rock. Several methods have been proposed to account for this effect which generally include the following sequence:

1. Create a continuum model of the slope;

2. Reduce the rock mass strengths within the model to a limited slope depth to account for blast damage and stress relaxation (usually done by applying a D = 0.7 factor using the Hoek-Brown failure criterion);
3. Excavate the model in stages elastically;
4. Determine a boundary of expected dilation or joint extension;
5. Include this boundary within the final model and reduce the strength in the boundary by the D = 0.7 factor (or similar).

The major limitations of this approach are the justification of Step 4, which leads to issues of repeatability between practitioners and the appropriate determination of a generally accepted criterion used to model this boundary. Several different criteria have been used for this purpose including vertical or total displacement, volumetric strain, extensional strain (Stacey et al., 2003), minimum principal stress (Stilwell and Gonzales Shand, 2015), and yielded elements within a strain-softening model (Lorig, 2009). Regardless of which of these methods selected, the induced stress state around the pit will significantly impact the region in which the strength reduction will occur, which in turn impacts the stability of the slope during the pre-feasibility to design level review of the slope.

Factors that increase the stresses on a regional or pit scale can be masked by the choice of the boundary selected to represent the increased damage caused by excavation as the values selected do not have to conform to an industry accepted limit. The use of yielded elements does not have this restraint; however, the values of residual parameters and the strain softening rates can be modified to represent the desired boundary effect.

Pit wall scale factors, for example lithological changes and faults, can have a significant effect on the expected excavation affected regions. As an example, various criteria were applied to the 900m pit depth FLAC3D models used to determine the impact of the inclusion of a fault (Section 4.2.3.2). Regardless as to which criterion is chosen, the inclusion of a fault bisecting the surface is readily observed in Figure 4.35. In all cases, the impact of the fault can be seen in both the footwall (right) and hanging wall (left) side of the fault. The footwall side of the fault experiences a reduction in the minimum stress leading to increased extensional and volumetric strain. This in turn results in yielding of the rock mass, which promotes increased displacements. The decreased stress on the footwall side results from two sources of confinement loss (the fault and the pit). The fault acts as a barrier to cut off the stress from the pit bottom.

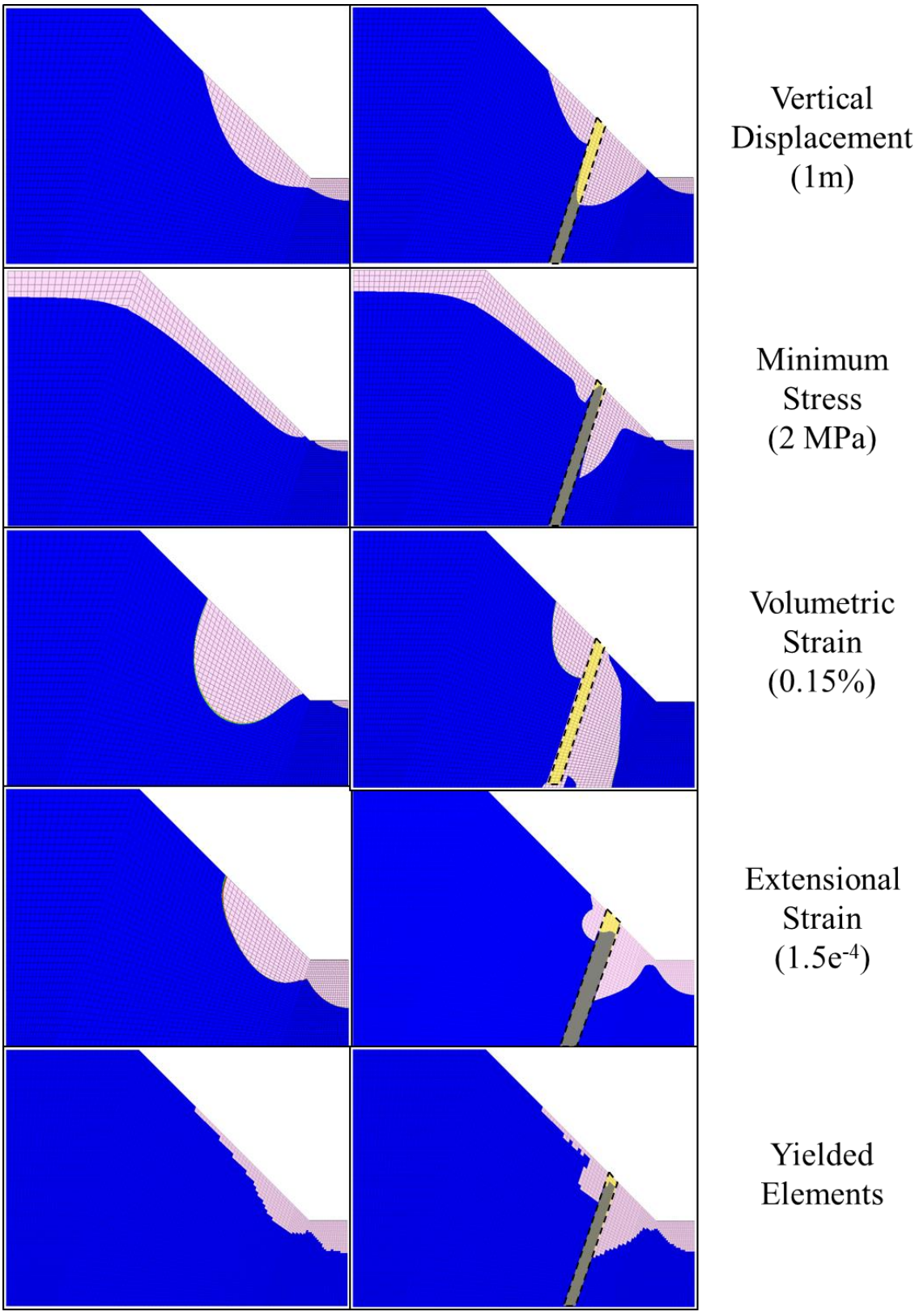

Figure 4.35. Areas of damage caused by excavation dilation within a 900m pit based on selected criteria in a homogenous material (left) and with the inclusion of a fault (right).

Based on the results of the numerical modelling. the use of extensional strain is recommended as criterion to be used to determine potential damage arising from excavation as appear to provide the best fit with the expected results from the yielded elements and are thus considered to be the more appropriate and repeatable depth of damage criterion.

The impact of fault damage zones on the expected damage areas associated with excavation of the pit could lead to increased damage at the toe of the slope. For a circular or oval shaped pit (in plan), the toe would likely be confined and expected displacements would be minimal. In an elongated pit where confinement at the slope toe would be reduced, decreased rock mass strength and fragmentation at the toe could allow for additional deformation and displacements to occur.

4.7.2. Mine Plan / Excavation Sequence

Stability analyses of large open pits often focus on the maximum pit depth (i.e., maximum slope height) relative to the overall slope angle, for which stability can be assured. However, to reduce computation times, the mining excavation process is sometimes modelled as a single step in which confinement is suddenly lost; however, this is not the case. The dynamic nature of the stress path experienced by a slope was clearly shown through stress measurement studies at the Bjørnevatn mine in northern Norway (Myrvand et al., 1993). At Bjørnevatn, in-situ stress measurements were taken at two locations (at approximately 100 and 300 m below ground surface), first in 1971 and then in 1990 after the open pit had been deepened by roughly 120 m. Spatially, the repeat measurements in 1990 were taken within approximately 1 m of the initial measurements. Readings from the measurements showed that during the 19 years of mining, the maximum horizontal stress had tripled at the shallower location at the end of the open pit life.

Recent investigations of micro-seismicity around open pit mining activities at both the Mt. Keith Open Pit Mine in Australia (Wesseloo and Sweby, 2008) and the Navachab Mine in Namibia (Lynch and Malovichko, 2006) have confirmed that both the stress state and the response to stress is dynamic around pits. Although the micro-seismicity is attributed to brittle fracture initiation and propagation in low confining stress environments (with high deviatoric stresses), the development of environments in which new areas can rupture shows the migratory nature of stresses. Massive rock slope failure processes have been shown to be largely driven by the initiation and propagation of brittle fractures driven by extensional strain, which interact with natural pre-existing discontinuities to eventually localize and form basal and internal shear surfaces (Eberhardt et al., 2004). Determining the interaction between the in-situ stress field, the presence of stress heterogeneity arising from faults, and the changing stress path due to pit deepening

can help identify regions of high stress as well as these regions where extensional strain can occur. Lynch and Malovichko (2006) could demonstrate that a focal point of the seismic activity was a weak group of geological structures and that the seismic activity was the result of stress changes brought about by the excavation of rock within the pit.

Final mine design layouts are governed by ore grade locations with pit walls determined by kinematics, rock strength and economics. While there are opportunities to modify these basic parameters (layout and pit wall angle), they generally remain constant through the life of the mine unless critical issues arise. In contrast, the mine sequencing and interim pit wall designs can vary greatly depending on mill requirements and current ore prices. Mine sequence is often changing and generally thought to be of minor importance if the pit wall angles do not exceed the final design. To investigate this, a series of FLAC3D numerical analyses (based on the properties used in Table 4.7 and the FLAC3D mesh in Figure 4.16 and 4.39) was carried out testing the sensitivity of the mining-induced stress path to mine sequencing in the presence of a large tectonic fault intersecting the slope. Four open pit sequencing strategies (Figure 4.36) were investigated using a pit wall geometry of 45°. The large bisecting fault zone was assigned using a strength of 1% of the host rock from Table 4.7.

Table 4.7with focus placed on determining the transient effect of stress migration near the fault.

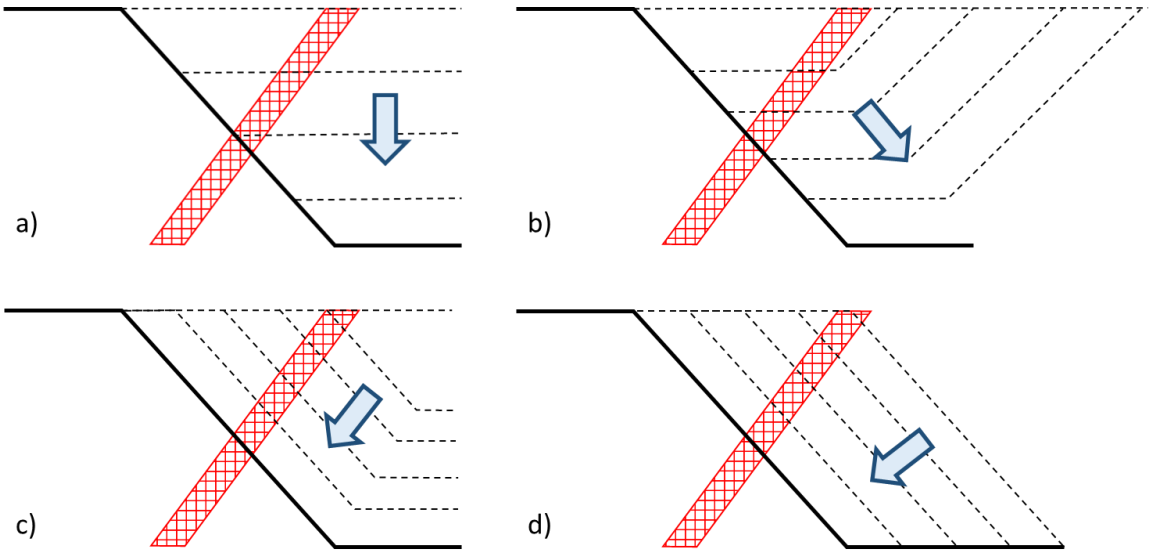

Figure 4.36. Mine excavation strategies modelled to investigate the impact of mine pushback direction including a) vertical excavation without interim mine phase, b) excavation perpendicular to fault intersection within interim phases developed away from fault, c) excavation parallel to fault with interim phases developed toward fault, and d) excavation toward fault without further deepening.

The results show that as the pit is deepened, zones of low stress (confinement loss) are created adjacent to the fault on both the hanging wall and footwall sides in roughly equal amounts (Figure 4.37). As the fault is increasingly exposed in the floor of the pit, the rock adjacent to the fault in the hanging wall experiences a decrease in stress level as the weaker fault material becomes unconfined, allowing for increased dilation and displacements within the fault to occur. Once the pit is further deepened and the dipping fault intersects the slope, the floor of the pit and rock in the fault's footwall is then exposed to a loss of confinement due to both the excavation of overburden and the displacements that concentrate in the weaker fault. Thus, the rock mass within the toe of the slope experiences both a reduction in minimum stress as well as a change in the orientation of minimum stress due to the change in the pit geometry as its excavated.

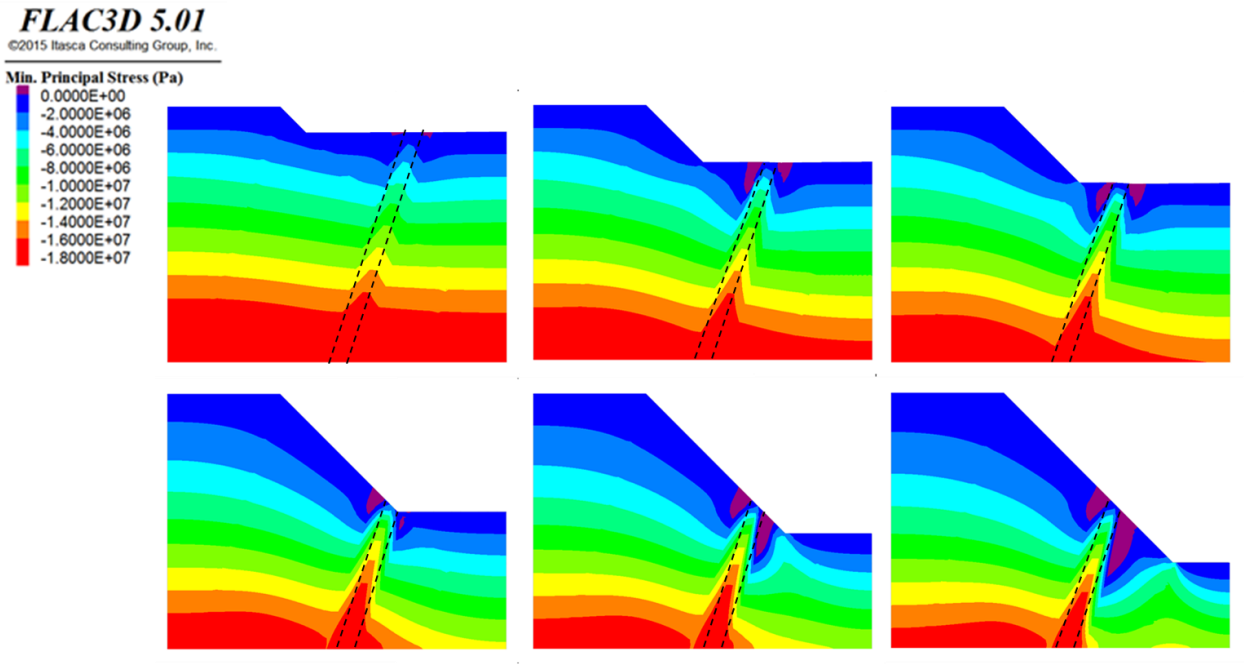

Figure 4.37. Section view of the temporal evolution of open pit mining induced stress heterogeneity near a fault. Plotted are the minimum principal stresses, with compression negative. Note purple region denotes area of low confinement.

In a homogenous rock mass, the maximum deviatoric stresses observed within each pushback strategy generally shows similar values with only minor variations in stresses during pit excavation (Figure 4.38, right). However, it is hypothesized here that the presence of a large tectonic damage zone that intersects the final pit wall can lead to important localized stress increases and decreases that depend both on the fault characteristics and mine sequencing. Figure 4.38 (left) shows the maximum deviatoric stresses for the same pushback strategies with the bisecting fault zone included. The results indicate that even though the final stress states may be similar in these elastic models, the variation in stress conditions between the pushback

strategies as the pit is excavated are significantly different in creating local conditions in which rock may yield. A clear distinction can be denoted in these mine sequencing scenarios as two of the strategies mine away from the fault (A and B), which keeps the stress low near the beginning of the mine life, and two of the strategies were developed to mine towards the fault (C and D), for which higher stresses and potentially more rock shearing and brittle fracture are observed early on. Mining is shown in Figure 4.38 as a percentage of full extraction to directly compare the sequencing strategies. As extraction occurs, the strategies which employed mining away from the fault induce smaller deviatoric stresses within the pit wall, either at the toe of the slope or near the fault. Strategy D, which employs a final pit depth early in the design using a series of pushbacks extending the full final pit slope height showed a distinct increase in deviatoric stress for the interim pit walls suggesting that excessive damage may be expected during mining.

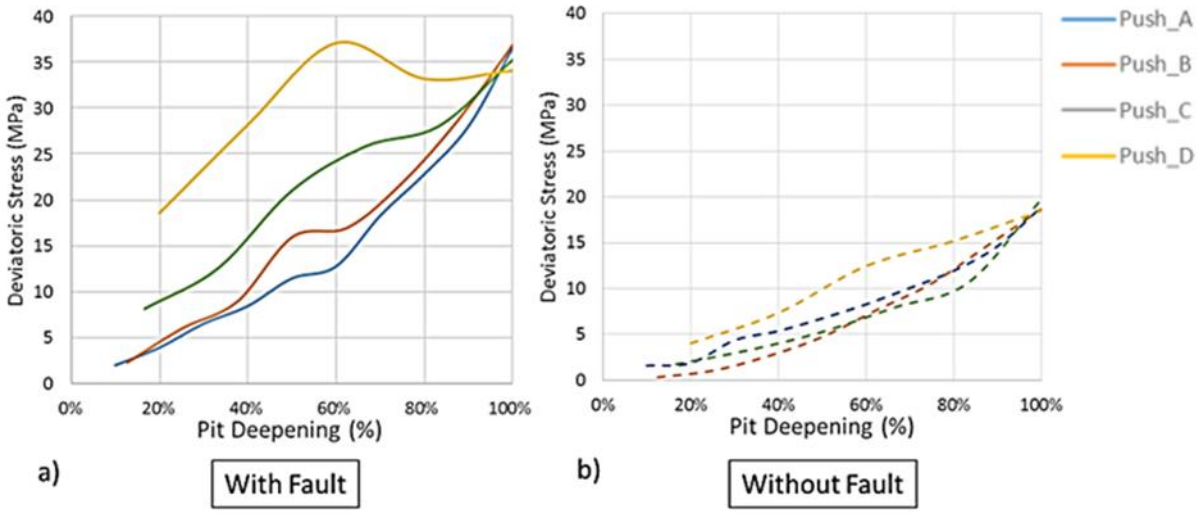

Figure 4.38. Comparison of deviatoric stresses (σ_1-σ_3) arising due to fault-pit interactions using previously identified mine sequencing strategies (see Figure 4.36) as modelled in FLAC3D.

The extensional damage limits observed within the models created by the outlined pushback strategies are shown in Figure 4.39. Based on the results of the modelling, pushback strategies 3 and 4 were found to offer the least amount of both plastic shear and extensional strain damage in the hanging wall but much more damage in the footwall. Pushback strategies A and B created a significant amount of damage in the floor and in the final pit wall as the pit is excavated, giving rise to the increased amount of damage observed in the hanging wall. This damage makes the long-term stability in the hanging wall an issue if the rocks are near their strength limit, as well as would make production blast holes difficult to keep open. Excessive damage also makes it difficult for the blast engineers to create clean benches close to the design

requirements. As the pit is excavated below the fault, the amount of damage observed in the slope grows deeper leading to the development of a possible active-passive wedge. As the pit deepens below the fault, extensional strain damage continues to develop in the hanging wall. One clear benefit to strategy B is the reduced damage in the floor during excavation, although this would leave more competent rock in the bottom of the pit, making it more difficult to efficiently blast and excavate. Strategies C and D are the most beneficial for the HW as the final wall does not experience the pit floor and fault stress interactions that occur in Strategies A and B, and therefore less extensional damage. However, the damage in the footwall is much deeper than strategies A and B.

The results suggest that all other circumstances being equal, the most favourable pit sequencing involves those that mine away from the fault and the final pit wall. These strategies lead to lower deviatoric stresses in the pit, which lowers the probability of shear damage and localization, as well as reduces the depth of extensional stress (confinement loss) near the fault which will help to reduce brittle fracture damage to rock bridges.

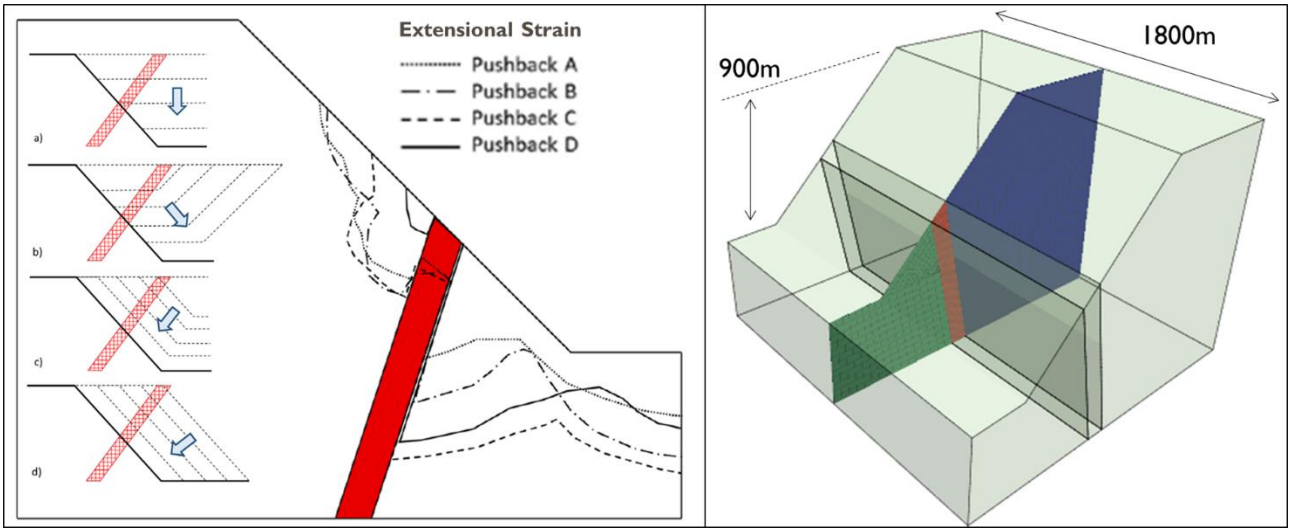

Figure 4.39. Comparison of maximum depth of extensional strain arising from fault-pit interactions using different mine sequencing strategies for a 900-m high pit slope. Note that the FLAC3D model used to compare these mine sequencing strategies involved an extruded model with a width of 1800 m.

The results in Figure 4.37 to 4.39 show that pit deepening and its interaction with existing faults has a pronounced influence on stress heterogeneity, as well as the stress path as the stress state changes with each excavation sequence. It should be noted that excavation sequencing is dictated by the mine plan and design layouts, which are governed by the ore grade distribution and pit wall stability requirements. Understanding

the potential impacts of the faults allows the mine an opportunity to plan for potential conditions and have options to modify the mine layout or pit wall angles in the early stages of design, whereas current pit optimization remains as a reactionary response to encountered conditions once critical issues arise. In contrast, the mine sequencing and interim pit wall designs are more flexible and the lessons learned here can more easily be implemented. The results presented here indicate that although mine sequencing is generally thought to be of minor importance, it can create optimization opportunities with respect to reducing the degree of strength reducing damage a pit slope experiences if intersected by a fault.

4.8. Key Findings and Design Recommendations

Stress conditions behind a pit wall can be affected by several factors, ranging from those present on a regional scale to wall scale. In-situ stresses, topography, pit geometry, and increased depth can play an important role in the development of the pit-wide induced stresses experienced by the surrounding rock mass. This can lead to areas in the pit that are more prone to specific types of kinematic failures or more complex stress-induced failures requiring shearing through rock or brittle fracturing of intact rock bridges. Relative to more homogeneous conditions, combinations of fault geometries and stress heterogeneity can incur stress increases of 40% or more around the pit. As a pit deepens, these localized concentrations of stress only increase further.

Wall scale factors such as changes in lithology and presence of large structures can influence both kinematic controls (as potential release planes) contributing to large, multi-bench slope failures, as well as influence the stresses within the slope. Most the empirical experience in open pit design and the influence of tectonic faults involves pit slopes that are less than 300 m in height. However, as the next generation of open pits are designed to greater depths (i.e., higher stress environments), faults and fault damage zones should also be recognized for their ability to affect the regional and local stress conditions. Numerical modelling results presented in this chapter have demonstrated that faults can create stress heterogeneity, which when combined with mining induced stress and relaxation, can promote slope instability.

Based on results from the different 3-D numerical models reported, the following conclusions can be drawn:

1. Stress heterogeneity around an open pit can be affected by several factors ranging from a regional to open pit to pit slope scale, particularly once the pit depth is increased past 300 m;

2. The plan view geometry of an open pit design can have a dramatic impact on the concentration of stress around an open pit (up to 40%) which can influence the potential failure mechanisms observed in these areas;

3. Deviatoric stresses increase dramatically in deeper open pits, suggesting these designs are more susceptible to yielding and dilation at the toe of the slope. The increase in deformation should be evaluated and where applicable, presented to the mining operation to allow for a potential modification in the design (such as a step-out or buttress), a change in the risk map of the open pit, or to plan for increased monitoring in this portion of the pit;

4. Mining induced stresses generated during the excavation of a large open pit are heavily influenced by faults, whether they are relatively large faults zones or more narrow, discrete structures was the case for the faults other than the Mica Fault at the Palabora mine;

5. The stress heterogeneity created during the excavation of an open pit and its interaction with any fault zones present can extend well behind the immediate face of the open pit slope, up to 75% of the pit diameter;

6. Faults with deformation moduli less than 10% of those for the adjacent host rock mass, can have a significant impact on the principal and deviatoric shear stresses generated within a slope;

7. Anisotropic rock masses are particularly sensitive to these changes in stress orientation and magnitude;

8. Small variations in stress orientations and magnitudes can have a critical effect of the yielding and shearing in the nearby roc mass, as shown through the modelling of the 10m x 10m x 10m cubes at the Palabora mine. Additional damage due to changes in stresses can lead to slope failure in some situations by connecting structures, especially in anisotropic rock;

9. Stress heterogeneities created by local pit wall conditions, such as faults, can affect the expected excavation and damage response of the pit. Depending on the pit design, these areas should be evaluated through numerical modelling to determine the potential effect on pit wall stability and appropriately designed for within the feasibility and design level review stages of a project if necessary. This may include reducing the inter-ramp angle of the pit, reduction of bench size, or the addition of rockfall protection systems; and

10. Mine sequencing strategies should be employed, where possible, that involves establishing the ultimate pit wall location which intersects the fault and mining away from that location. This will help to reduce the amount of stress heterogeneity experienced by the rock mass in the final pit wall.

CHAPTER 5 IMPORTANCE OF CHARACTERIZATION AND REPRESENTATION OF FAULTS AND FAULT DAMAGE ZONES IN LARGE OPEN PIT SLOPE STABILITY MODELS

Synopsis

This chapter investigates the impact of several key characteristics of major fault zones and the choice of representation within a numerical model on the resultant stress heterogeneity and associated damage created during the interaction between the fault and open pit mining. Damage associated with highly localized plastic shear and extensional strains are reviewed and applied to determine the potential impact on the failure mechanisms observed within the pit. This chapter will focus on the incremental excavation of a large open pit through 2-D numerical analyses using the discontinuum-based distinct-element software, UDEC. These will be supported in part by 3-D continuum analyses using FLAC3D and discontinuum analyses using 3DEC. The numerical modelling conducted will focus on the implications for rock slope behavior, displacements, and damage created in response to the inclusion and characterization of the faults within the models. The numerical analyses within this paper begin with a series of conceptual 2-D and 3-D numerical models, and then extends to consideration of observations related to faults intersecting the pit walls at the Teck Highland Valley Copper Mine in Canada and the Palabora Copper Mine in South Africa. The analyses and results highlight: 1) the identification of the key fault properties in creating stress heterogeneity and damage within a pit wall, 2) the impact of fault representation within a numerical model on the resulting mining-induced stress distributions calculated, 3) the evaluation of increasing pit depth and mining-induced stresses on amplifying the damage state around faults and the resulting effects on pit slope performance, and 4) potential methods on stress development within numerical models. This chapter is in the process of being prepared for submission to a peer-review journal.

5.1. Introduction

Many of the world's largest, deepest open pits, such as Palabora, OK Tedi, Chuquicamata, Grasberg and Bingham Canyon, have approached or are approaching their original design limit depths. The companies which run these and similar operations must assess the remaining options to extract any remaining reserves within the deposit which may include scavenging the ramps and leaving the deeper resources behind, deepening the pit through pushbacks and over-steepening the toe, or transitioning to underground mass mining methods (i.e., block and panel cave mining). To fully and properly assess these options, an

understanding of current and potential mining-induced damage behind the pit face can be invaluable to considering the viability of future excavations. Pit slope movements arising from unexpected damage can adversely affect mine infrastructure causing both safety and economic concerns as well as increased dilution of the target orebody and possibly sterilization of ore in extreme cases.

Large-scale geological structures can control the kinematics and stability of pit slopes as well as subsidence around block caves (Stacey and Swart, 2001). Depending on the complexity of the fault system, pit slope deformation patterns can be difficult to interpret with respect to identifying failure kinematics as well as how it will evolve. This leads to uncertainty in assessing the stability of large pit slopes and establishing early warning alarm thresholds, and/or determining setback distances for mine infrastructure located near the crest of the slope. Further complexity is added where new or old underground workings may be present, or similarly, the transition to underground mass mining. A number of cases exist where sudden collapses of cave backs, crown pillars, etc., have occurred due to unknown geological structures or unexpected rock mass behavior, including the hanging wall wedge failure at the Kidd Creek mine in Canada that propagated from 610-m depth to surface (Board et al., 2000), the 800-m high pit wall failure at Palabora in South Africa (Brummer et al., 2006), and the fatal air blast caused by the sudden collapse of the cave back at the Northparkes mine in Australia (Hebblewhite, 2003).

Interactions between mining-induced stresses from open pit mining and geologic structures (faults, damage zones, etc.) create pockets of very high shear stress as well as regions of tension behind the slopes of these large open pits. The localized damage created by this stress heterogeneity can weaken the rock mass behind the pit face leading to complex slope failures previously thought to be kinematically unviable. These are conceptualized as involving the degradation and localized failure of intact rock bridges (separating non-persistent structures) through shear or brittle fracture. Anisotropic rock masses with a dominant foliation are particularly sensitive to changes in stress magnitude and/or orientation with respect to the stability of rock bridges between existing discontinuities. The evolution of localized damage created due to stress heterogeneity behind a pit face is investigated within this paper through numerical modelling of conceptual slope geometries, based in part on actual cases, involving a large open pit slope bisected by a weak fault zone.

Lessons learned regarding rock mass behaviour near the fault are then applied to two case studies, which are used to further explain the potential for unexpected slope displacements. The first example is based on Teck's Highland Valley Copper Mine in central British Columbia, Canada, and follows the excavation of an open pit through a thick and complex fault zone. This example serves as an important lesson of the complex interactions and rock mass damage that may develop between the progressive deepening of the pit

floor with mining and the presence of an intersecting major geological structure. The second example is based on the Palabora Mine in South Africa and illustrates the need to represent key geological features in a 3-D numerical model to reproduce observed pit wall kinematics and key stress-strain interactions. Results of a detailed modelling study that compares the stresses generated during the excavation of the open pit and followed by the response to block cave mining are presented which investigate the effects that large scale fault systems can have on the smaller scale rock bridge strength which can affect caving-induced subsidence and pit slope deformations.

5.2. Fault Representation in Numerical Analyses

In practice, the representation of faults in most slope stability analyses and open pit designs tends to be highly simplified. Implementation is dependent in part on the numerical method used, which generally involves either continuum-based approaches (e.g., finite-difference and finite-element codes, such as FLAC3D or ABAQUS), or discontinuum-based approaches (e.g., distinct-element codes, such as UDEC or 3DEC). Continuum codes utilize a structured mesh of connected elements, which forces the user to represent faults and fault zones in the model as a zone of elements that are assigned weaker or softened rock mass properties via an elasto-plastic constitutive model (Figure 5.1). Faults in continuum codes can also be represented as a preferential direction of weakness using a ubiquitous joint model (Sainsbury et al., 2008), or in some cases as a limited number of discrete interfaces, although the latter partly negates the numerical efficiencies users are seeking when choosing a continuum-based approach.

The benefit of using continuum codes is the flexibility in creating larger and often more detailed models which can include more geometric detail, while requiring less computing power and providing faster solution times relative to discontinuum methods. Depending on the factors influencing the stability of the rock mass, the inclusion of a weaker zone of elements to represent a fault may be sufficient in assessing the stability state of the slope and analyzing the expected displacements and behaviour.

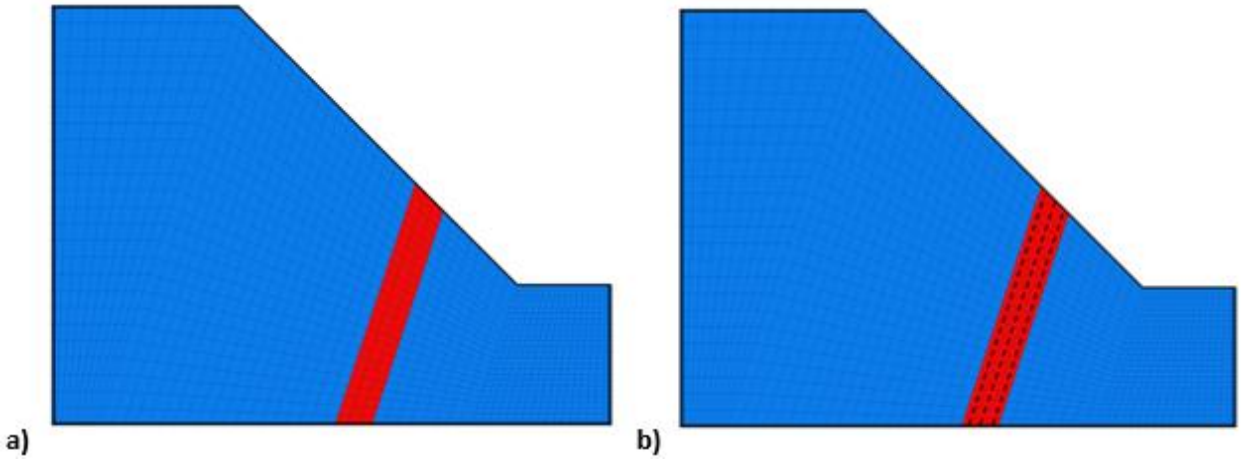

Figure 5.1. Examples of how faults are typically represented in continuum analyses (in this case using FLAC3D): a) as a zone of weak elasto-plastic rock, or b) as rock with a preferential direction of weakness via a ubiquitous joint model.

In contrast, discontinuum codes can model faults and other discontinuities as a series of contacts separating a grouping of rigid or deformable blocks. These contacts can open, close or slide, enabling a range of block movements and rotations relative to the contacts. In doing so, discontinuum codes can represent a fault as a single distinct plane that can slip in shear or open in extension, as well as incorporate zones of blocks assigned as a softer material to simulate adjacent tectonic damage zones of broken rock (Figure 5.2).

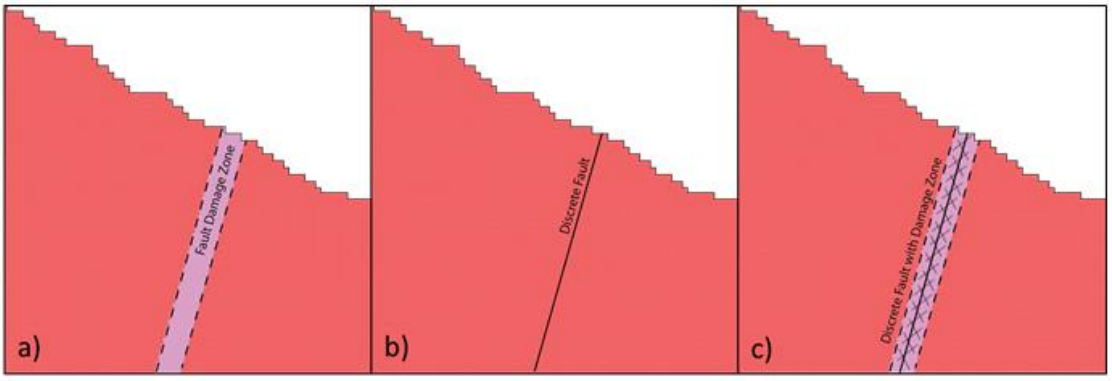

Figure 5.2. Examples of how faults can be represented in discontinuum analyses (in this case UDEC): a) as a zone of contrasting rock mass properties like that used in continuum analyses, b) as a discrete discontinuity that can open, close or slip, and c) as a combination of discrete fractures and yieldable blocks that represent a central discontinuity (i.e., fault) and adjacent tectonic damage zones.

Studies of stress perturbations conducted using distinct-/discrete-element methods show that the key factors affecting stress heterogeneity around a fault are its stiffness and friction angle (Su and Stephansson, 1999; Su, 2004, Harrison et al., 2010). Sassi and Faure (1997) further highlighted that major regional-scale faults can control local stress variations and influence the deformation modes of faulting and fracturing which can take place at a smaller more local scale.

The added need to track and solve the contact interactions in a discontinuum analysis makes this technique more computationally demanding. Thus, the choice between utilizing a continuum or discontinuum method becomes an important decision between balancing computational demand and the importance of modelling the fault interaction with the open pit with regards to its stability state and deformation response. The representation of faults in a model using either of these numerical methods is left to the geotechnical engineer (often without consultation of a structural geologist) on a case by case basis. It is hypothesized here that the choice of how to represent the fault with respect to its strength, structural complexity, and material behavior can greatly affect the interaction between the mining induced stress and the natural perturbations created by the faults. This is demonstrated in the following sub-sections using a series of conceptualized numerical models based on representative pit slope geometries. It should be noted that the FLAC3D, UDEC and 3DEC software used calculates stresses with a compression negative notation.;

5.2.1. Fault Characterization and Properties

The effect of faults and fault damage systems on the development of stress heterogeneity in rock is poorly understood in both the underground and surface mining environments. This is largely due to insufficient attention being given to the fundamental fault characteristics and nature of the faults present, including not only the type and architecture of the fault but the underlying conditions required for its development. An improved understanding on the development of stress heterogeneity around faults can lead to improved slope designs and reduced risk for mining personnel working in the pits. This section investigates several critical elements to the representation of fault architecture in numerical analyses and their interaction with open pit deepening, which can lead to pockets of stress heterogeneity and rock mass damage. These are outlined in Figure 5.3.

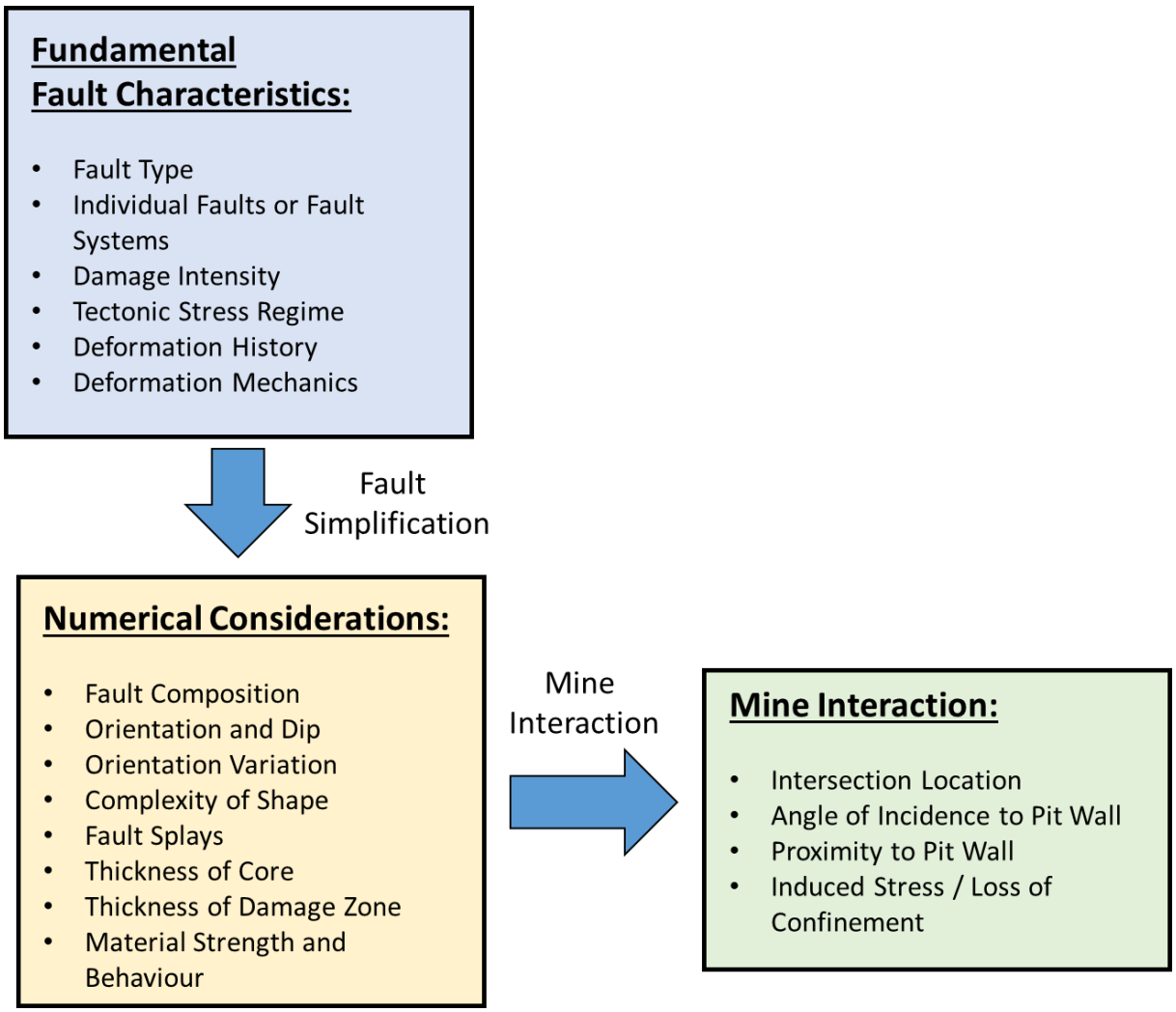

Figure 5.3. Critical fault elements investigated with numerical analysis considered as fault characteristics (as identified in the field), typical numerical simplifications made during modelling, and potential design changes that can be adapted based on modelled wall performance.

Large faults have been shown to create both local stress perturbations (Katterhorn and Marshall, 2006), preferential paths for strain (Reusch et al., 2009), as well as compartmentalization of in-situ stresses within a rock mass (Martin, 1990). Wesseloo and Dight (2009) concluded that stress changes during the mining process (induced stresses) are equally complex, with zones of comparatively low and high stress. What is often regarded as a de-stressed slope may in fact be a slope with a comparatively low minimum principal stress, σ_3 (aligned normal to the slope face), but comparatively high intermediate, σ_2 (circumferential to the pit) and maximum, σ_1 (slope-parallel) principal stresses.

5.2.2. Representation of Fault Zone Composition

In hard rock masses, fracturing associated with the failure process may be more brittle and faults may present themselves as distinct breaks in the rock or as a zone of broken material. In softer rock masses, the deformation may be more ductile and a zone of weakened rock may be more representative of the fault. Fault parameters within numerical modelling are often selected based on averaged properties of faults interpreted from drilling intersections or from surficial mapping. Field observations are then applied to appropriately characterize the fault at the mine-scale for analysis purposes.

To investigate the effect of fault composition on the development of stress heterogeneity, several distinct-element models were created based on faults mapped at the Palabora Mine. The commercial distinct-element program UDEC (Itasca, 2011) was used. The models depict a horizontal section divided by a network of faults, each varying in how the fault zone composition of a major north-south fault, the Mica Fault, is represented. The host rock mass at the mine is characterized as being very strong and brittle; the Mica Fault is characterized as being bounded by adjacent zones of tectonically damaged rock. The first model representation of the Mica Fault involved the most commonly used and simplest realization of a fault in a discontinuum analysis, that of a brittle, distinct break (Figure 5.4, left). The complexity of this fault was then increased to model it as a zone of weakened material based on a reduction of strength parameters (Figure 5.4, middle). Finally, the full complexity of the mapped fault was modelled by explicitly including both the continuous fault and the adjacent zones of tectonically damaged rock represented by a network of smaller discrete fractures (Figure 5.4, right). The input parameters, based on values determined from the Palabora mine (Sainsbury et al., 2008, used for the fault composition sensitivity analysis is given in Table 5.1. An initial uniform stress of 20 MPa was assumed, with the horizontal stresses being equal in both directions which is representative of natural stress state that is expected to occur mid-slope of the Palabora pit.

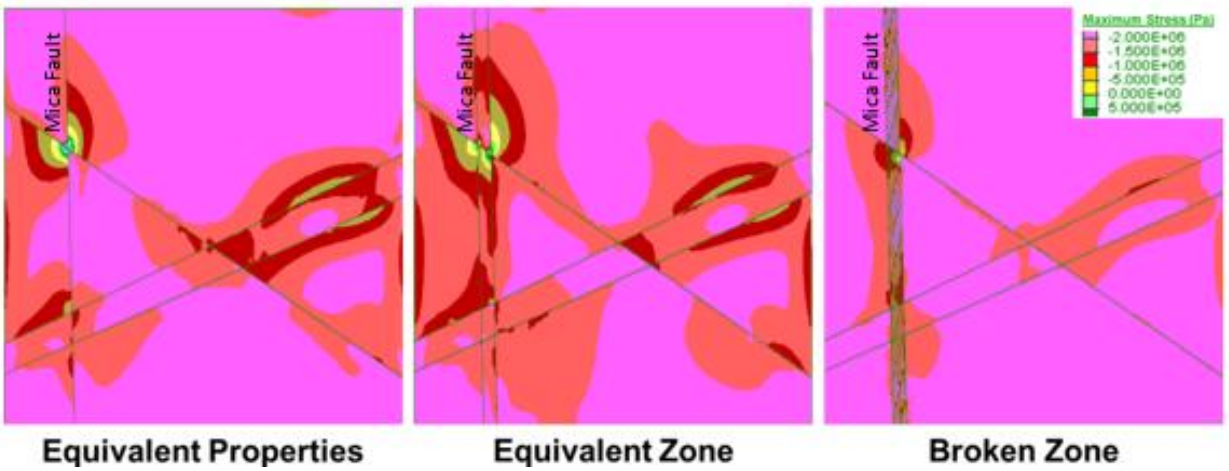

Figure 5.4. **UDEC model results plotting maximum principal stresses (σ_1), indicating influence of fault material representation on stress heterogeneity. The example shown here is from the Palabora Mine. Note that only the representation of the Mica Fault material was modified in this model. Compression is negative.**

Table 5.1. **UDEC fault composition sensitivity model parameters**

Model	Material Properties					Fault Properties			
	Density (kg/m³)	Deformation Modulus (GPa)	Friction Angle	Cohesion (MPa)	Tension Strength (MPa)	Normal Stiffness (Pa/m)	Shear Stiffness (Pa/m)	Friction Angle	Cohesion (MPa)
Host	2700	50	51	4.3	0.6	-	-	-	-
Discrete Fault Zone	-	-	-	-	-	1e9	1e9	35	0.1
Equivalent Fault Zone	2400	6.5	27	1.7	0.1				
Broken Fault Zone	2700	50	51	4.3	0.6	1e9	1e9	35	0.1

The model results demonstrate that how a fault is represented can affect the magnitude and distribution of stress heterogeneity surrounding the faults, although the general location of high and low pockets of stress remains somewhat consistent in several places. This suggests a minor to moderate model sensitivity with respect to how fault zone composition is represented as the stress distribution is similar with magnitudes being the only variable. This is likely due to the increased number of degrees of freedom in the broken fault system which dissipates the stress through increased shear displacement within the broken fault (Figure 5.5).

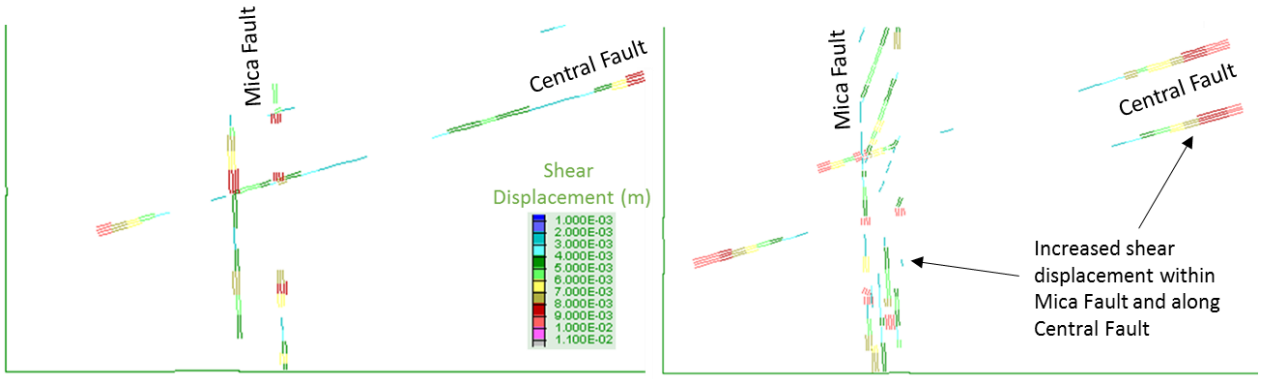

Figure 5.5. Shear displacement (in m) along the faults for a UDEC model treating the fault as an equivalent continuum zone (left) and as a discontinuum zone (right).

5.2.3. Representation of Fault Complexity

In most cases, faults in a numerical analysis are modelled as a single persistent plane (i.e., a single segment). However, in nature, faults are complex structures that are comprised of multiple segments representing a non-planar feature. A series of UDEC distinct-element models were constructed to test the impact of fault shape simplification on stress heterogeneity. The models were created to represent a horizontal section through the Palabora Mine in which the faults modelled were varied in geometric complexity (Figure 5.6). These include modelling the different faults present as 1, 3 or 10 segments per fault. The input properties used for these models are given in Table 5.1 as Host and Discrete Fault Zone. Similarly, to the model above, a constant boundary stress of 20 MPa was applied, with the horizontal stresses being equal in the x and y directions.

The model results indicate that the number of fault segments used to represent the fault can create local variations in the maximum principal stress distribution and increased magnitudes. These stress perturbations surrounding the faults can in turn influence the variation of strain and damage, and therefore stability state of the modelled rock slope. This suggests a moderate to high model sensitivity with respect to representation of the fault shape as the location, magnitude, and orientation are all greatly affected by the shape and location of the faults.

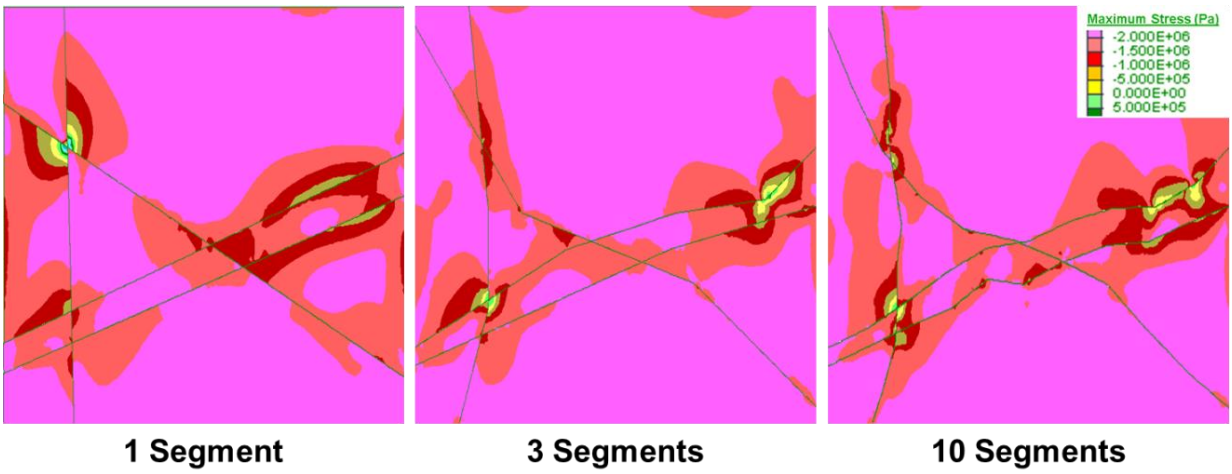

Figure 5.6. Influence of fault shape complexity (non-planarity) on maximum principal stress (σ_1) perturbations developing around a network of faults. Example shown here is from the Palabora Mine. Note that all faults were modified in this model. Compression is negative.

5.2.4. Influence of Fault Strength Contrast with Host Rock

Characterization of a fault's strength is often assessed through pit wall mapping and drill core evaluation. The intact strength is combined with a rating determined from the mapping (e.g. GSI) or drill core evaluation (e.g. RMR) and a rock mass strength is determined. In very weak or highly fractured faulted rocks, GSI values are usually estimated at around 15 to 20 while in harder, more competent rock, GSI in a fault can range up to 45 to 55. To test the sensitivity of this field estimate, a series of FLAC3D numerical models were constructed for a 600-m high slope with a 45-degree angle (Figure 4.13) using a mesh as outlined in in which the elastic and Mohr-Coulomb input values for the fault rock mass were varied relative to those for the host rock assigned an intact Young's Modulus of 49.5 GPa, a UCS of 50 MPa and a GSI of 65. The same intact properties were used for the fault, but these were scaled using different GSI values in a range encompassing typical values (Table 5.2). The fault zone in this case is modelled as dipping into the slope.

The depth of plastic shear damage within these models was estimated by recording the depth of elements which have yielded in shear behind the pit face. Extensional damage was determined by calculating the extensional strain using Equation 2.6 with a cut-off value of 5e-5. This value was chosen based on Stacey's (2003) recommendations and by reviewing the patterns observed within the models. The results from this sensitivity analysis are presented in Table 5.3, which shows that for a 600-m high slope, the depth of plastic shear damage in the footwall of the fault ranges between 130 m behind the pit face for the stronger fault

(GSI 55) to 205 m for the weaker fault rock (GSI 15). Extensional damage in the footwall side of the fault ranges between 265 to 300 m for the same fault strength values. Figure 5.7**Error! Reference source not found.** illustrates the minimum principal stress distributions around Fault Run Models 2 through 5 corresponding to GSI values of 55, 45, 35, and 25. Stress patterns and corresponding depths of extensional yield appear to be unlikely to change below a critical deformability of about 1% of the host material.

Table 5.2. FLAC3D input properties used in sensitivity analyses investigating fault strength contrast

Material	GSI Estimate	E_{rm} (GPa)	Fault E_{rm} / Host E_{rm}	Cohesion (MPa)	Friction Angle
Host	65	40.7	100%	7.3	48
Fault Run 1	15	0.18	0.4%	1.8	25
Fault Run 2	25	0.31	0.8%	2.4	28
Fault Run 3	35	0.53	1.3%	2.9	31
Fault Run 4	45	1.09	2.7%	3.5	34
Fault Run 5	55	2.03	5.0%	4.0	37

Table 5.3. FLAC3D fault strength sensitivity results

Model	Fault E_{rm} / Host E_{rm}	Maximum Depth of Plastic Damage (m)	Maximum Depth of Plastic Damage (% of slope height)	Maximum Depth of Extensional Damage (m)	Maximum Depth of Extensional Damage (% of slope height)
Fault Run 1	0.4%	206	34%	300	50%
Fault Run 2	0.8%	199	33%	300	50%
Fault Run 3	1.3%	166	28%	286	48%
Fault Run 4	2.7%	145	24%	274	46%
Fault Run 5	5.0%	130	22%	265	44%

Figure 5.7 shows the zones of potential extensional strain damage behind the pit wall face in the rock adjacent to the fault for the upper bound (GSI 55) and lower bound (GSI 15) cases. The distribution of extensional strain is similar within the hanging wall for the strength range tested. The region of the footwall adjacent to the fault undergoes a significant amount of extensional damage parallel to the fault face as the weaker material compresses and stress is cut-off within the pit toe.

When compared to the amount of damage observed within a similar pit wall without a fault, the depth of potential plastic shear and extensional strain damage was shown to increase by 13 to 26% and 21 to 26%, respectively. This suggests a moderate to high model sensitivity with respect to fault strength relative to the host rock strength.

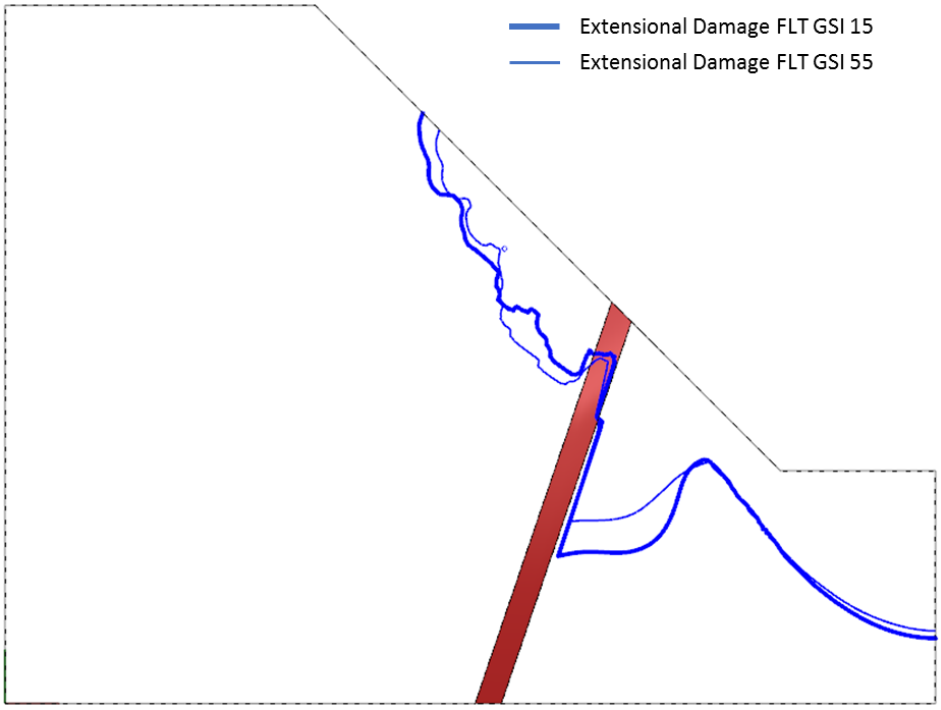

Figure 5.7. Potential extensional damage area within a 600-m high pit slope, for the bounding cases of a strong fault (GSI =55, light blue trace) and weak fault (GSI = 15, dark blue trace).

These results were further extended to consider modelled slope heights of 300 and 900 m to test the sensitivity of fault strength relative to the recent trend in designing deeper open pits (Figure 5.8). Damage depths were normalized by the overall pit depth (i.e., slope height) to return a relative percentage of expected depth of damage. This was done to determine if the larger damage depths observed in deeper pits could simply be scaled from smaller pit depth experience.

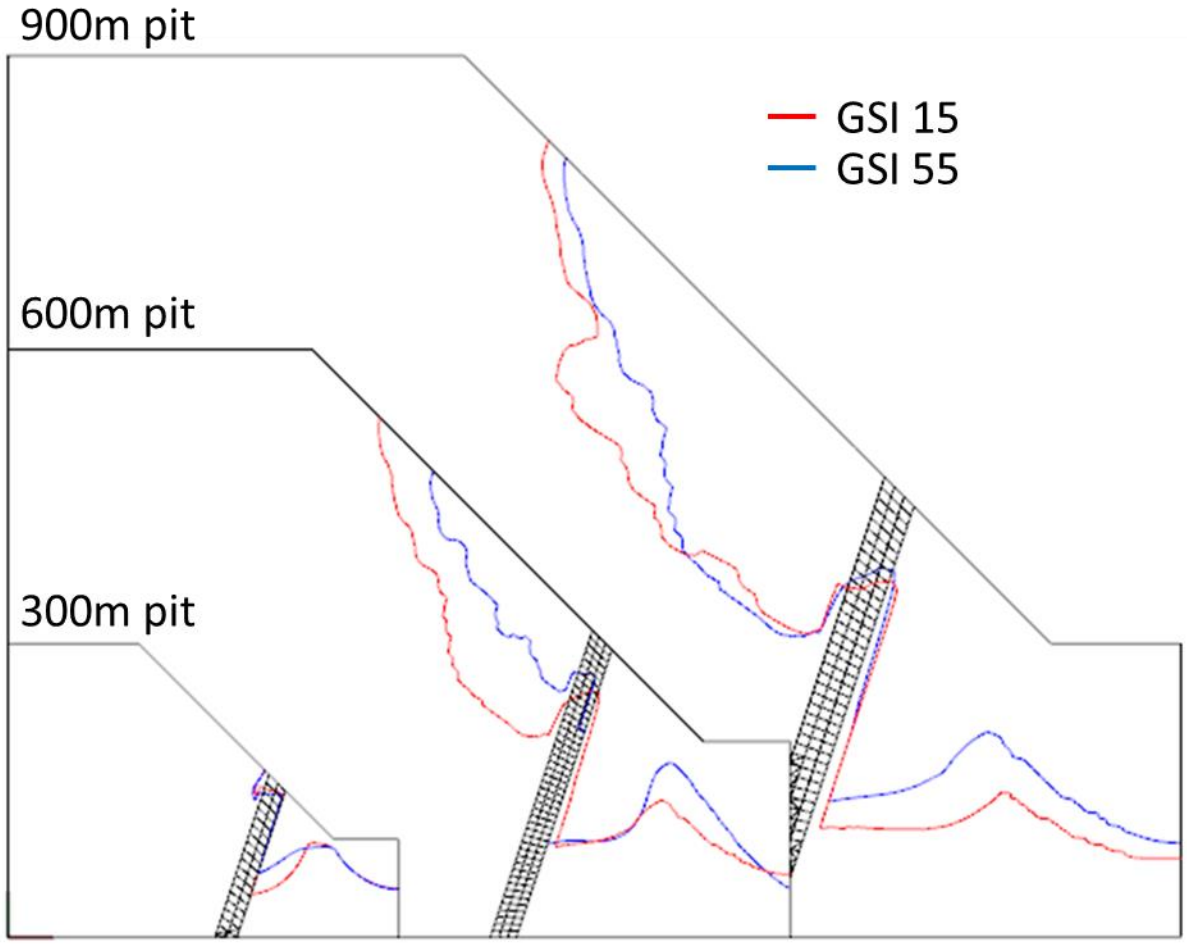

Figure 5.8. **Side by side comparison of extensional damage regions, for pit slope heights of 300, 600, and 900 m, associated with upper bound (GSI = 55, blue) and lower bound (GSI = 15, red) fault strengths.**

The model results shown in Figure 5.9 lead to several key observations, including:

- The maximum depths of plastic shear and extensional damage from pit surface can be shown to increase with slope height;
- The area affected by the pit excavation grows relative to the slope height and is not linearly scaled;
- The relative increase of plastic shear damage is far less than the extensional damage within the model;

- The increase in plastic shear damage is greater for slope heights extending above 600m, whereas the extensional damage increase is larger as the slope height extends above 300m. This suggests that increased extensional strain damage should be expected at an earlier stage of pit deepening; and

- The recognition that a fault zone is present and intersects the slope is critical (i.e., of primary importance). Only a general or rough characterization of its properties is required to gain an understanding of its importance with respect to interacting with the pit slope geometry to induce damage to the rock mass adjacent to the fault zone. Proper fault characterization is however required when the failure mechanism is believed to be influenced by the kinematics enabled by the presence of the fault.

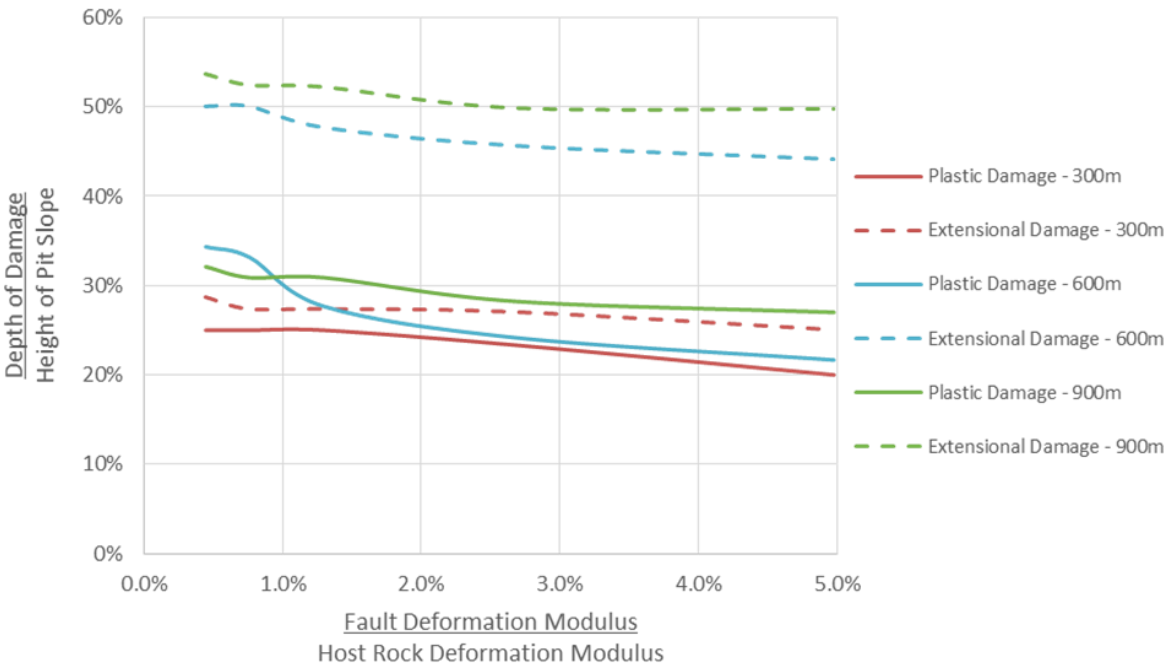

Figure 5.9. Depth of potential extensional (dashed line) and plastic shear (solid line) damage areas with respect to pit height as a function of relative fault strength and pit height.

5.2.5. Influence of Fault Thickness

Faults can be incredibly complex structures with many splays, a fault core comprised of gouge, or simply involve a highly localized discrete structure. Determining the shape, structure and thickness of faults

requires specialized geologic knowledge and field experience in pit wall mapping. Most engineers charged with operational pit face mapping and subsequent slope stability evaluations do not possess this specialized knowledge, which leads them to assume highly simplified structures. Outside of the kinematic implications this has, the simplification of fault complexity may also affect the strains observed within the slope. First, the boundaries of a fault are often difficult to determine exactly when face mapping. These boundaries are then further simplified in advanced numerical analyses. The question arises as to how important these fault boundary limits are in terms of slope behaviour. To test the sensitivity of the modelled stresses, strains and damage to fault thickness, a series of continuum models were run in which the thickness of a fault that bisects a 45-degree pit slope wall is increased using values of 10, 20, 40, 60, 80, and 100 m relative to slope heights of 600 and 900 m (Figure 5.10). Model parameters used are outlined in Table 5.4. FLAC3D input properties

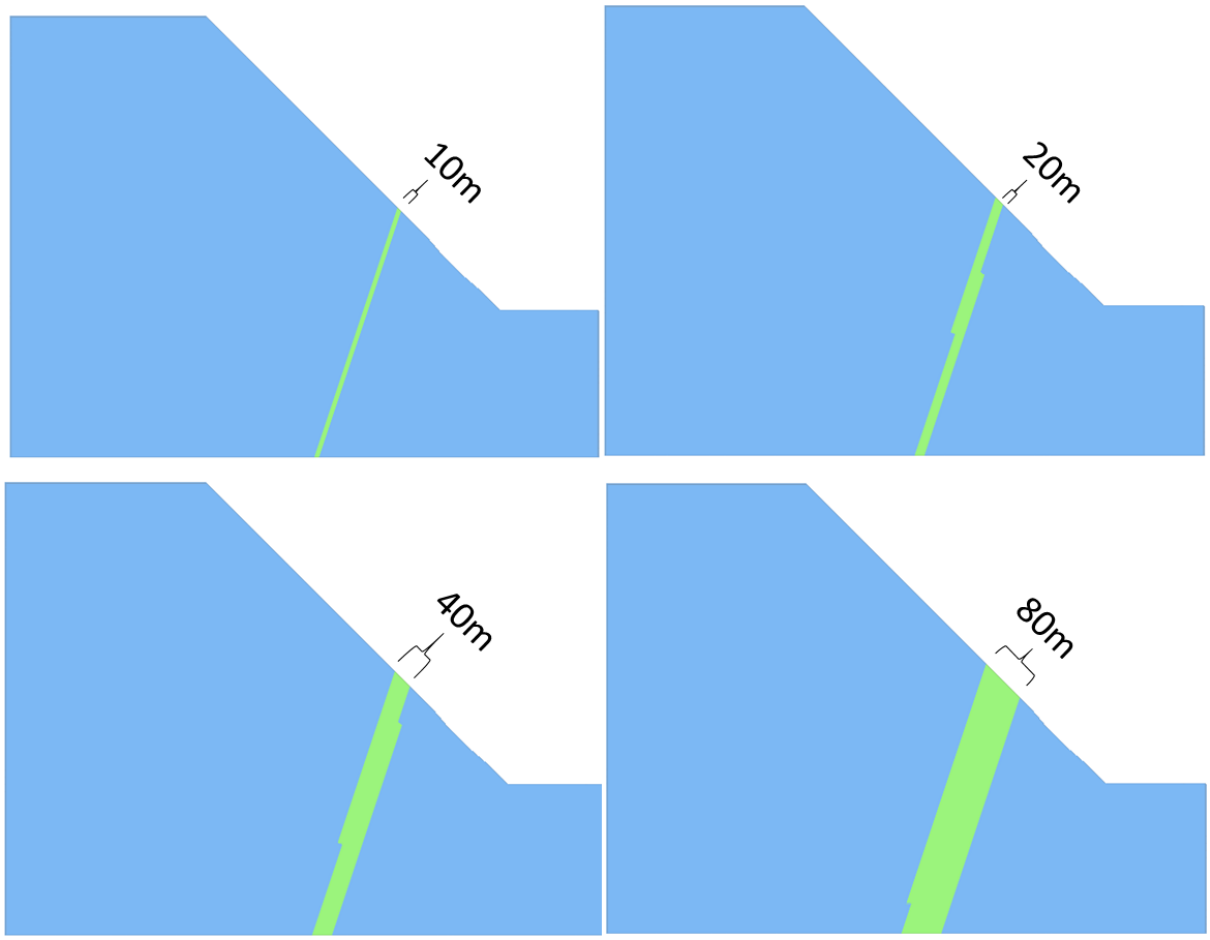

Figure 5.10. FLAC3D model set up for sensitivity analysis of fault zone thickness.

Table 5.4. FLAC3D input properties for investigation of model sensitivity to fault zone thickness

Material	Host Rock E_{rm} (GPa)	Host Rock Poisson's Ratio	Density (kg/m^3)
Host Rock	35.8	0.25	2500
Fault	0.5	0.3	2200

The fault zone is modelled as dipping into the slope. In the results presented, the fault thicknesses are expressed as a percentage value of the slope height. Example stress distributions for minimum principal stress and maximum shear stress are given for pits with 600 (Figure 5.11) and 900 m slope heights (Figure 5.12)

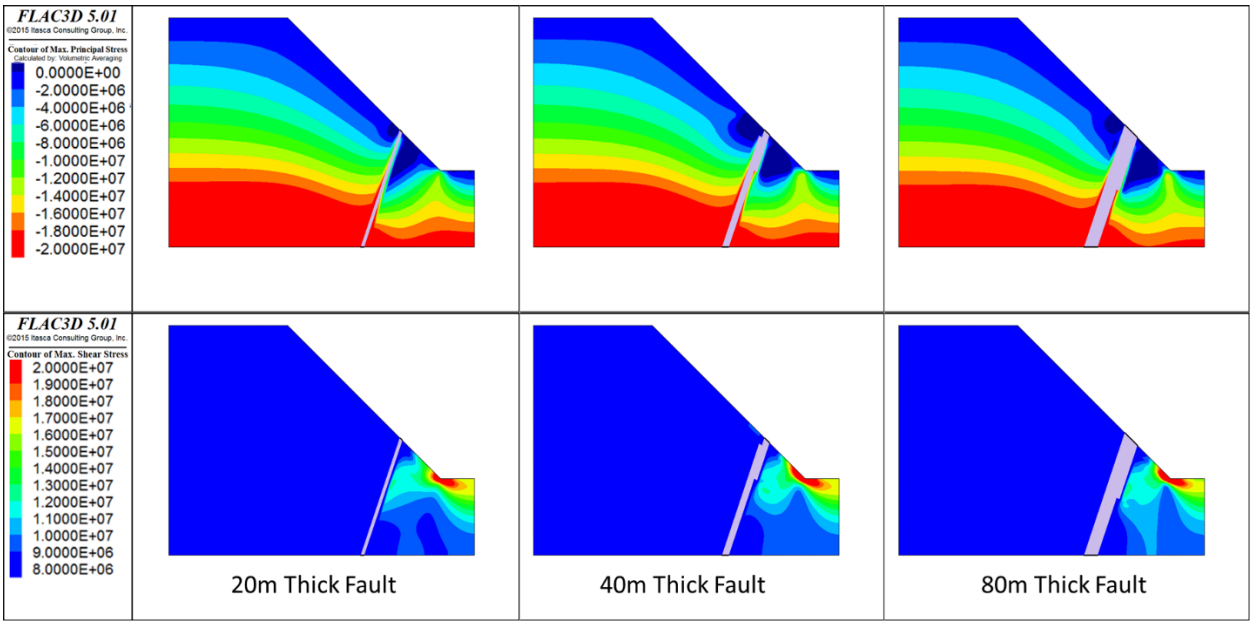

Figure 5.11. Minimum principal stresses (top) and maximum shear stress (below), in Pa, for a 600 m high pit slope comparing different fault thicknesses (10, 40m and 80m). Note that compression is negative.

Results from this parametric study indicate two very different behaviours within the footwall and hanging wall of the fault (Figure 5.13). Within the hanging wall, both extensional strain and plastic shear damage

increase with fault thickness, although this rate diminishes after a critical fault thickness of 2-3% of the slope height is reached. The thicker faults allow for increased and deeper compression of the weaker materials in the fault. The compression allows gravity driven expansion into the faulted rock. As slope height increases, the larger area and greater mass allow for more movement deeper into the weaker rock and can affect a larger portion of the slope.

In the footwall, gravity does not overly affect either the extensional or plastic shear damage process. Thus, once the critical fault thickness is reached (approximately 2-3% slope height), the effect of a thickening fault is reduced. Within the models, a slight reduction in damage depth was observed in the footwall as the fault thickened. This may be due to the fault being thickened toward the toe of the slope, which reduces the amount of damage observed. This suggests a low to moderate model sensitivity with respect to fault zone thickness.

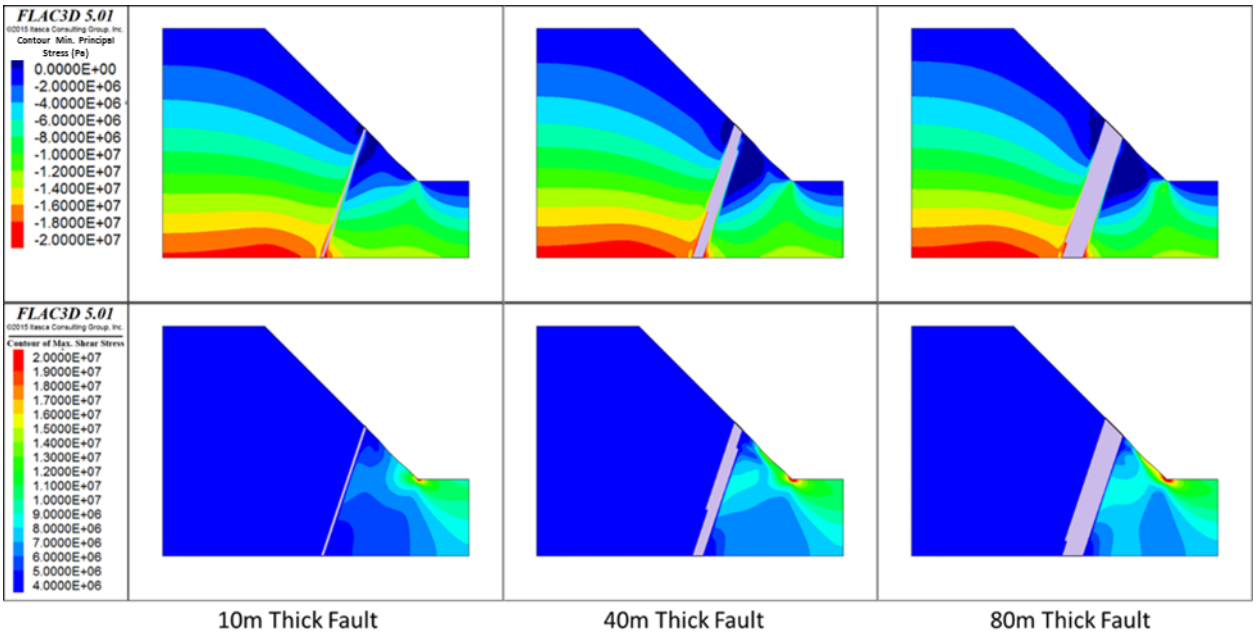

Figure 5.12. Minimum principal stress (top) and maximum shear stress (below), in Pa, for a 900 m high pit slope comparing different fault thicknesses (10, 40m and 80m). Note that compression is negative.

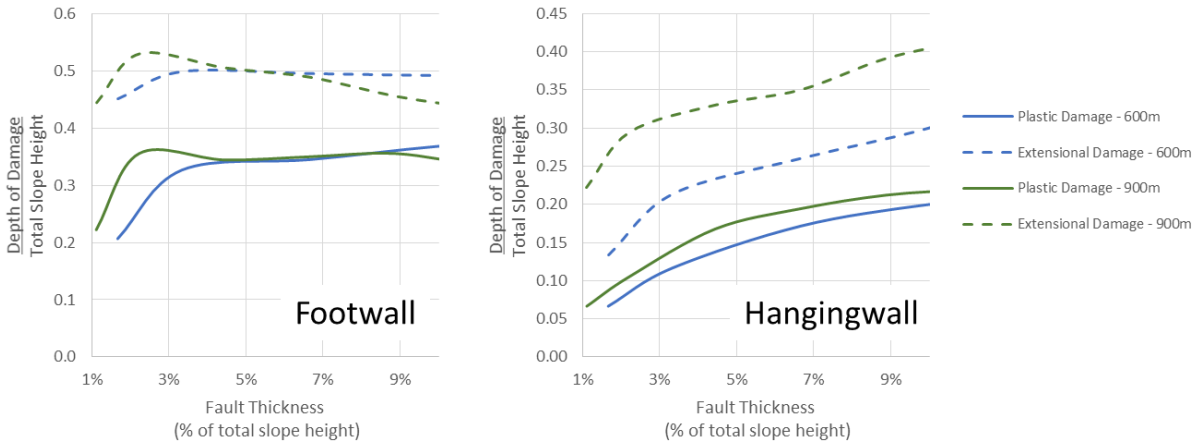

Figure 5.13. Depth of potential extensional strain (dashed line) and plastic shear (solid line) damage zones with respect to fault thickness for 600 and 900 m slope heights. Depth of damage values are reported for both the hanging wall and footwall sides of a fault dipping into the slope.

5.2.6. Influence of Fault Location Relative to its Intersection with the Pit Wall Face

Orebodies, especially large scale porphyry deposits, are often directly associated with large scale fault systems. The complex geological histories which have allowed for the deposition of the ore can lead to any number of geometric configurations. Orebodies can be either directly adjacent to a major fault or range up to several hundred meters away, which can lead to the fault zone intersecting the pit anywhere from the toe of the slope to its crest. To investigate the potential damage associated with a fault zone, continuum numerical modelling was conducted in which the fault intersection with a 45-degree slope was varied between its toe (0% of slope height) to near its crest (75% of slope length) as depicted in Figure 5.14.

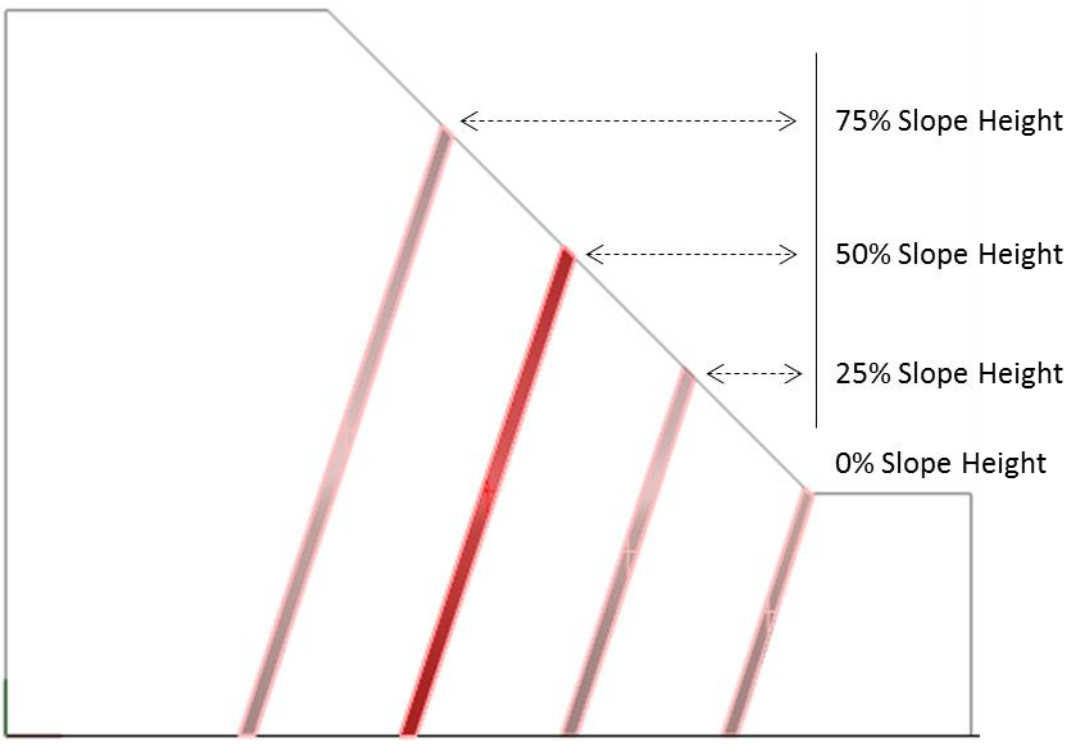

Figure 5.14. Model geometry for the FLAC3D fault intersection sensitivity analysis, showing the locations of the intersecting fault at either 0, 25, 50, or 75% of the slope height.

As before, the model slope height was also varied at 300, 600 and 900 m with the same geometry of a fault dipping into the slope. Damage depths were again normalized to the overall pit slope height to return a relative percentage of expected damage. Example stress distributions for minimum principal stress and maximum shear stress are given for a pit with a 600 m slope heights and fault intersections of 75% (top), 50% (middle) and 25% (bottom) of the slope are given in Figure 5.15.

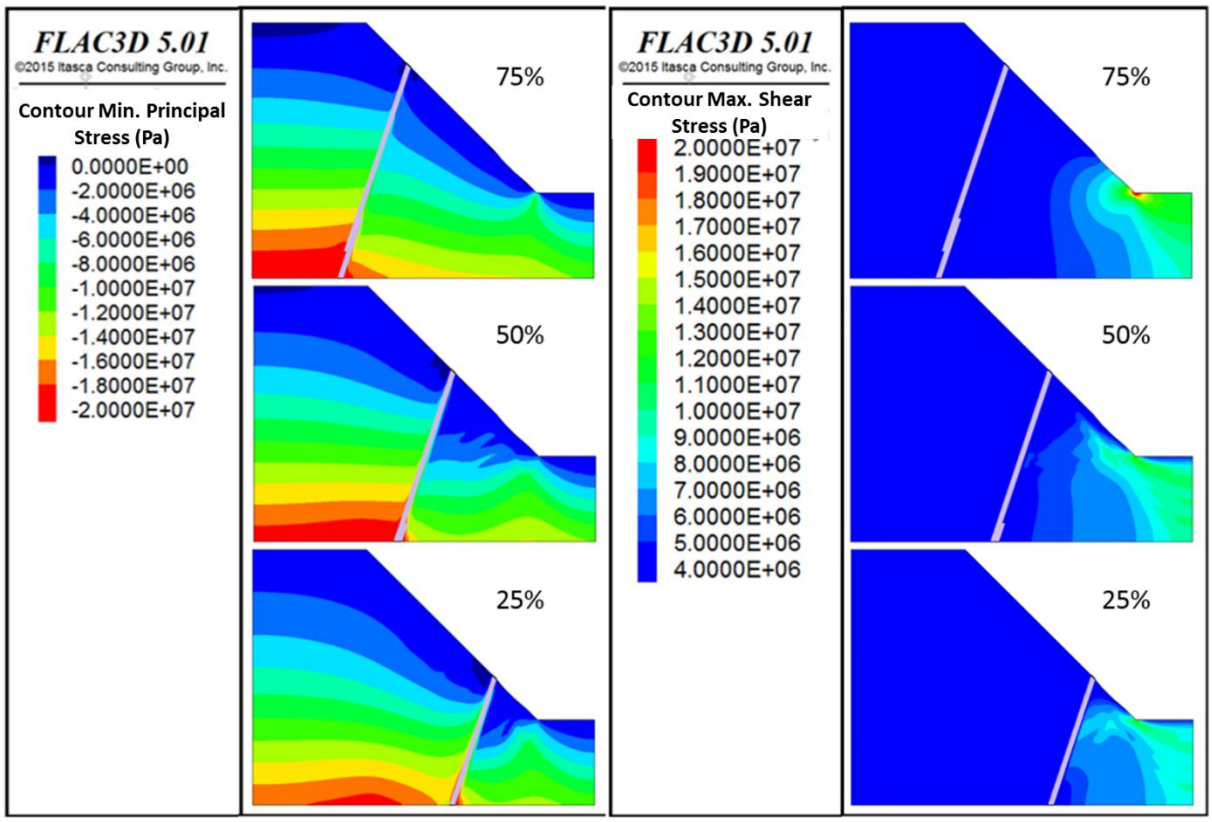

Figure 5.15. Minimum principal stress (left) and maximum shear stress (right) distributions, in Pa, with respect to fault intersection location (75, 50 and 25% slope height) for a 600m high pit slope.

The results from these models are summarized in Figure 5.16 and Figure 5.17, and lead to several key observations:

- The maximum extensional strain in the footwall occurs when the fault intersects mid-slope height (at 40 to 50% of the slope height measured from the toe);
- The maximum plastic shear damage in the footwall occurs when the fault intersects closer to the toe (at approximately 30% of the slope height);
- The pattern of extensional strain damage in the footwall is greater than the hanging wall after a slope intersection height of 10%. This contrasts with the modelled plastic shear damage, which is always greater in the footwall; and
- As the slope intersection height increases, the ratio of footwall to hanging wall damage likewise increases. This is primarily due to the increased damage that develops in the hanging wall.

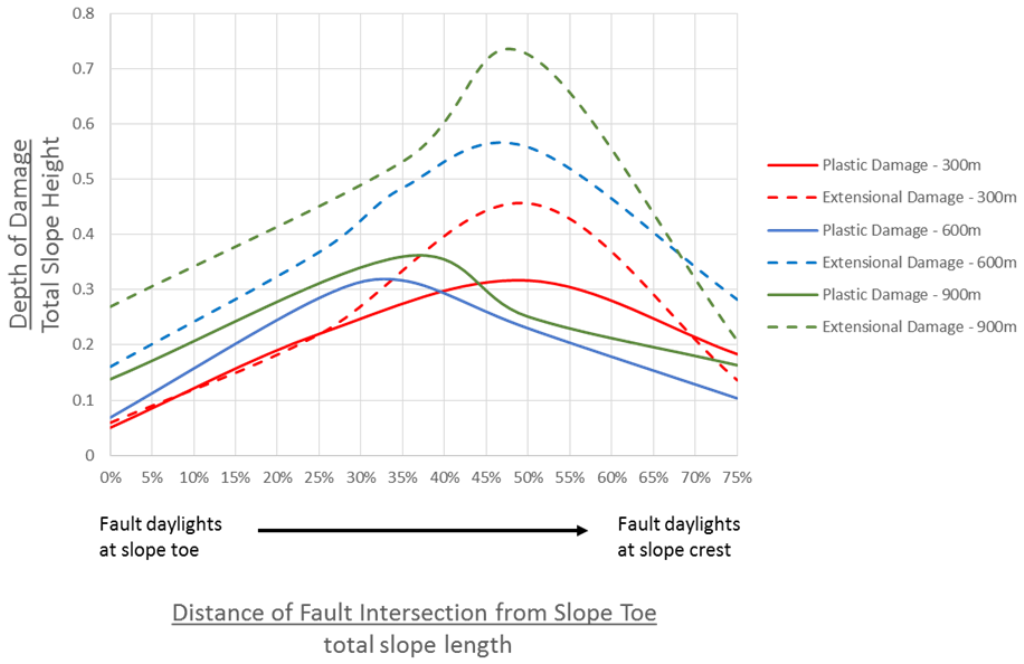

Figure 5.16. Depth of potential extensional strain (dashed line) and plastic shear (solid line) damage areas with respect to fault intersection location sensitivity and pit depth.

Figure 5.17. Ratio of depth of potential extensional strain damage in the footwall relative to the hanging wall, as a function of fault intersection location and pit slope height.

Of primary importance is that the results suggest that the rocks adjacent to the fault may undergo different types of failure (plastic shear or extensional brittle fracturing) as the location of the fault's intersection with the slope face varies, first being intersected in the toe of the slope and then migrating to the crest of the slope as the pit deepens. This migration of damage and localized failure can in turn impact the progressive failure of the slope. This suggests a moderate to high model sensitivity with respect to fault location relative to its intersection with the slope face (as well as its subsequent migration with pit deepening).

5.2.7. Influence of Fault Angle

The importance of fault angle was investigated through a FLAC3D sensitivity analysis using the parameters outlined in Table 5.4. The structural model and understanding of the structural history of a deposit can be a very difficult process, however, understanding the basic structural characteristics of the fault (trace, dip angle, etc.) can be highly beneficial to understanding the potential pit wall response and rebound effects. Continuum modelling was conducted to test the sensitivity of the model results to fault angle dips ranging from 50° to 110° in 10° increments. A pit wall angle of 45° was assumed, and slope heights of 300, 600 and 900 m were modelled. Example stress distributions for minimum principal stress and maximum shear stress are given for a pit with a 600 m slope heights and fault angles of 50°, 80°, and 110° in Figure 5.18

The results indicate that although the model trends were not as clear with respect to the influence of increasing pit depths (for similar fault angles), several clear trends can nevertheless be established (Figure 5.19):

- Plastic shear and extensional strain damage increases within the hanging wall as the angle of incidence between the fault and slope face increases to 90°; i.e., as the fault zone becomes more perpendicular to the pit face, the amount of damage in the hanging wall increases. This is likely due to a larger proportion of the hanging wall being underpinned by the weaker rock of the fault zone, which accommodates compression and additional gravitational loading;

- Plastic shear and extensional strain damage decreases within the footwall as the angle of incidence increases to 90°; i.e., as the fault zone becomes more perpendicular to the pit face, the amount of damage in the footwall decreases. This is likely due to the loss of confinement and the thinner wedge of rock mass remaining;

- Footwall and Hanging wall damage depths converge when the angle of incidence is around 90°;

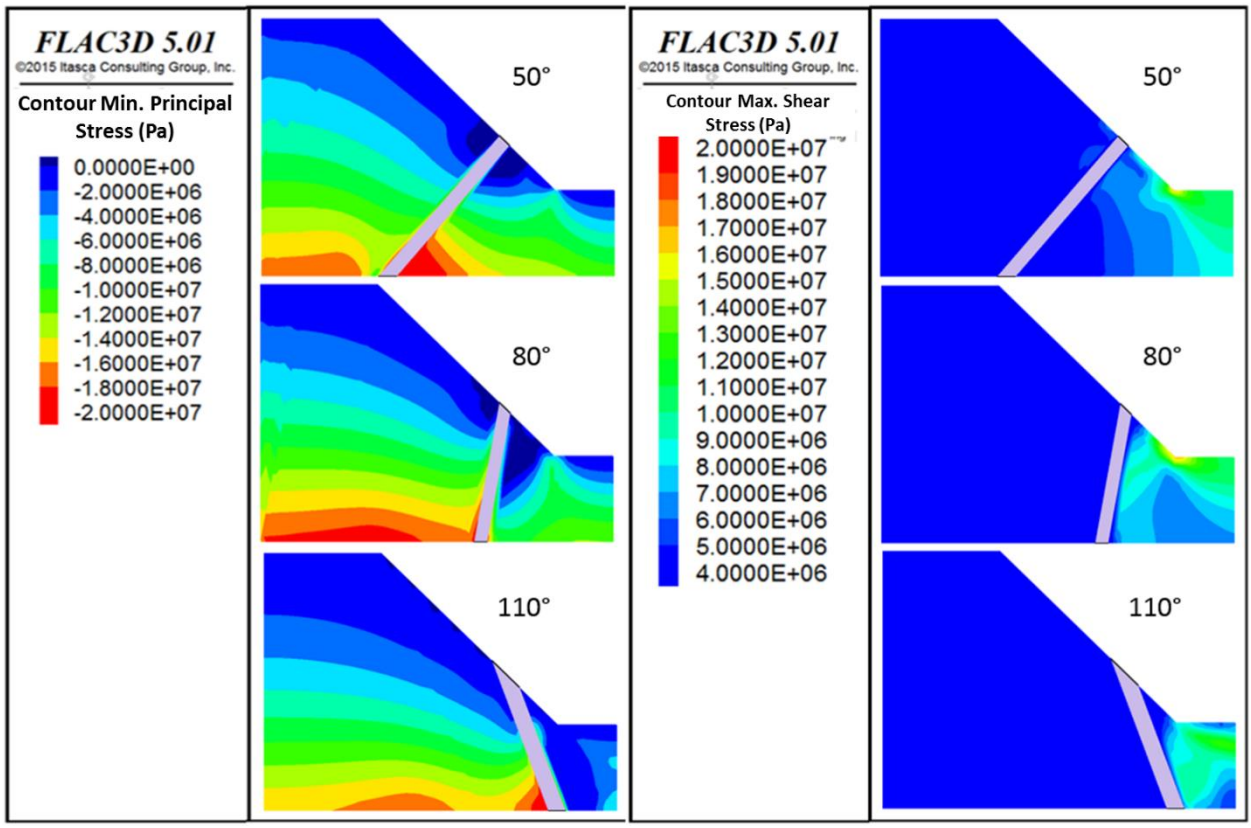

Figure 5.18. Minimum principal stress (left) and maximum shear stress (right), in Pa, with respect to fault incidence angle (50°, 80°, and 110°) for a 600 m high pit slope.

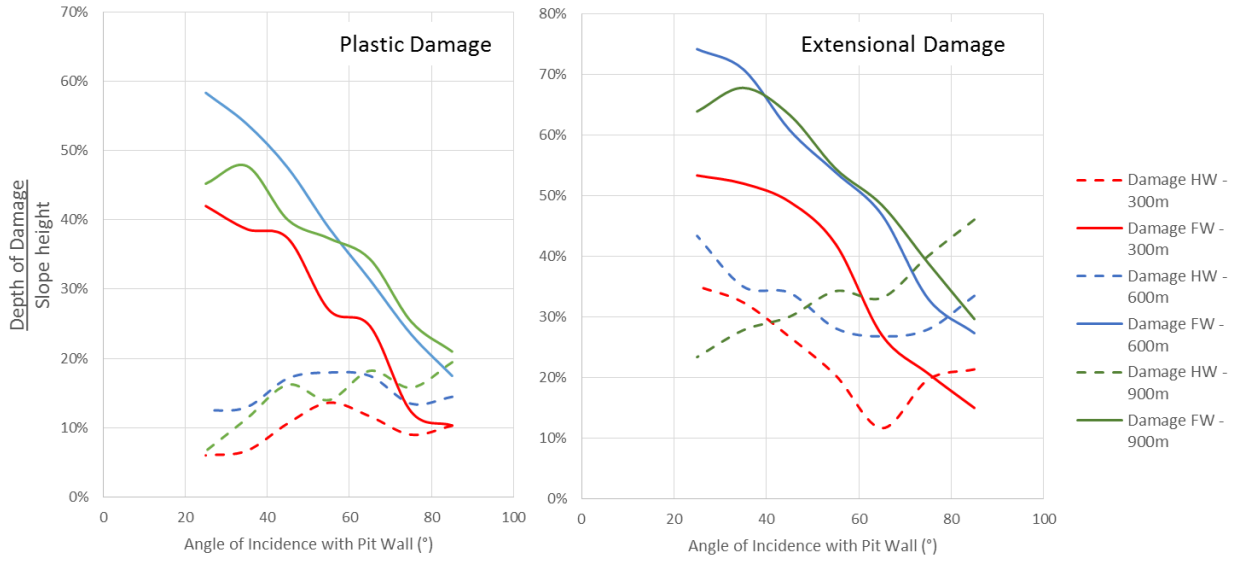

Figure 5.19. Depth of potential extensional strain (dashed line) and plastic shear (solid line) damage areas with respect to fault angle incidence and pit depth.

These results suggest a high model sensitivity with respect to the angle of incidence between the fault angle dipping into the slope and the face of the pit wall.

5.2.8. Summary of Sensitivity Analyses

The impact of the key fault characteristics and properties investigated in the previous sections on the development of stress heterogeneity is summarized in Figure 5.20. Of primary importance in the development of stress heterogeneity with respect to numerical analyses are, in order of importance:

- the angle in which the fault intersects the pit wall;
- the strength (or stiffness) contrast between the fault rock and adjacent host rock;
- the complexity (or sinuosity) of the fault zone including its irregularity relative to planarity, and the magnitude of the orientation change at these departures from planarity;
- the location of the fault intersection with the face of the slope, and its variation as the pit is deepened; and
- the composition and thickness of the fault.

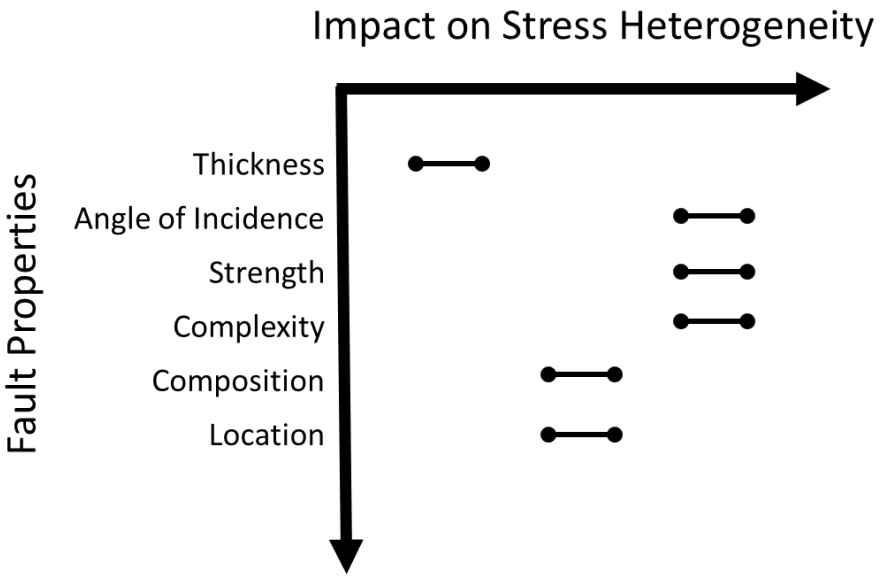

Figure 5.20. Relative impact of key fault properties on the development of stress heterogeneity within a pit slope intersected by a fault.

5.3. Modelling of Fault Development within a Numerical Slope Stability Analysis

The tectonogenesis of an ore deposit can play an important role in the distribution of in-situ stresses, including the stress heterogeneity owing to the presence of fault zones (Dight and Bogacz, 2009). Most geological environments are extremely complex with multiple deformation events, both ductile and brittle. These are not accounted for in stability analyses as the modelling of the tectonic history of a rock mass would be very time consuming and somewhat speculative due to the multiple geological interpretations possible. However, if the tectonic overprinting of an event (either recent or dominant in the local geology) is thought to be of a controlling nature to the behavior and stability of the pit slope, the analysis of the stress field generated during key tectonic events might prove valuable. This would require a numerical analysis procedure where first the initial (pre-mining) stresses are modelled relative to the tectonic event, followed then by modelling of the mining induced stresses.

In practice, this first step is replaced by assuming a highly simplified, uniform initial stress gradient. Conventional analyses will typically include the presence of a major tectonic fault zone, representing it in the model by defining the spatial limits of the fault and assigning weaker properties to the corresponding zones. Stress boundaries are applied and allowed to equilibrate resulting in a pre-mining in-situ stress state that includes reduced stresses within the weaker fault materials. However, these are very minor and the in-situ stress state is otherwise homogenous. Numerical studies do exist in which the initiation and development of faults have been modelled explicitly, with calculated shear strains being used to gain further understanding of fundamental fault processes (Cundall, 1990, Poliakov et al., 1993; Donze et al., 1994; Schopferet al., 2006). These seem promising to use fault mechanics to better represent the complexity of fault geometries and the resulting stress heterogeneity that can subsequently influence the stability and modelled response of a large open pit slope.

5.3.1. Modelling Procedure

To investigate the potential of this hypothesis, a detailed continuum analysis was carried out using the 3-D finite-difference code FLAC3D to first model the development of a major fault before analyzing the stability of the pit slope. Recent developments in pre-processing algorithms, as implemented in several industry-favoured commercial numerical-modelling codes, were exploited that allow geological units to be spatially defined using 3-D wireframe models (to be imported as .dxf files). Through this method, the staging of excavations simulating the deepening of the open pit do not have to be included within the initial model set-up but can be applied at later stages, allowing for the influence of tectonic faults and the surrounding stress field to be modelled first.

The modelling procedure and sequence developed, implemented techniques reported by Cundall (1990) in his analysis of tectonic fault processes. These were applied to explicitly model the pre-mining stress and strain state related to the presence of a complex fault system in a large open pit mine slope, which was then extended to simulate the mining of the open pit. The example used in the analysis was based on the Lornex Fault Zone in the Lornex Pit at the Teck Highland Valley Copper Mine.

5.3.1. Stage 1: Modelling of Fault Development

Figure 5.21 shows the results from the first stage of the procedure. For this model, the extensional environment responsible for the development of the Lornex Fault zone is replicated by the movement of a rotating boundary at the edge of the model. Velocities were assigned to the left side of the model as a gradient (maximum = 1e-5) and the material properties of the block were modified until a reasonable fit was achieved with reported geological and geotechnical cross sections (Figure 5.22). The input properties used are reported in Table 5.5. Figure 5.22 shows that a close fit was obtained that reproduces much of the complexity of the Lornex Fault structure. Once the various shear zones initiate, localize and fully develop, material properties more representative of the present-day faults are assigned before then proceeding with initialization of the pre-mining stress state and modelling of the open pit excavation.

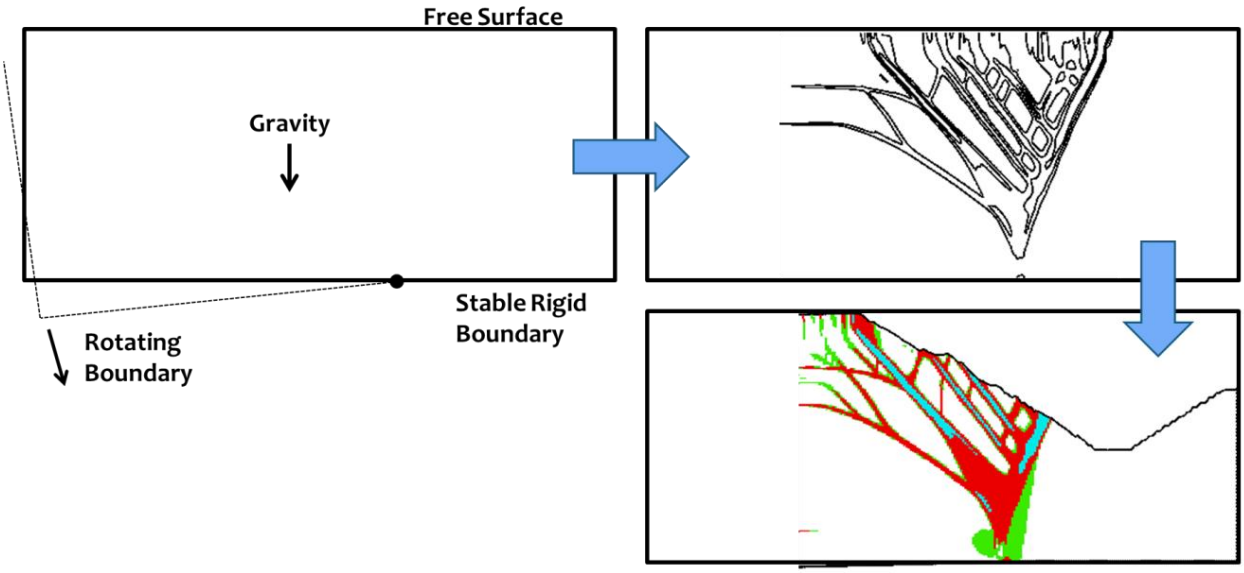

Figure 5.21. Procedure and fault generation results for modelling of fault development within the model prior to stress initialization and modelling of the open pit excavation.Contours shown are shear strain rate contours (relative contour interval 2.5 units).

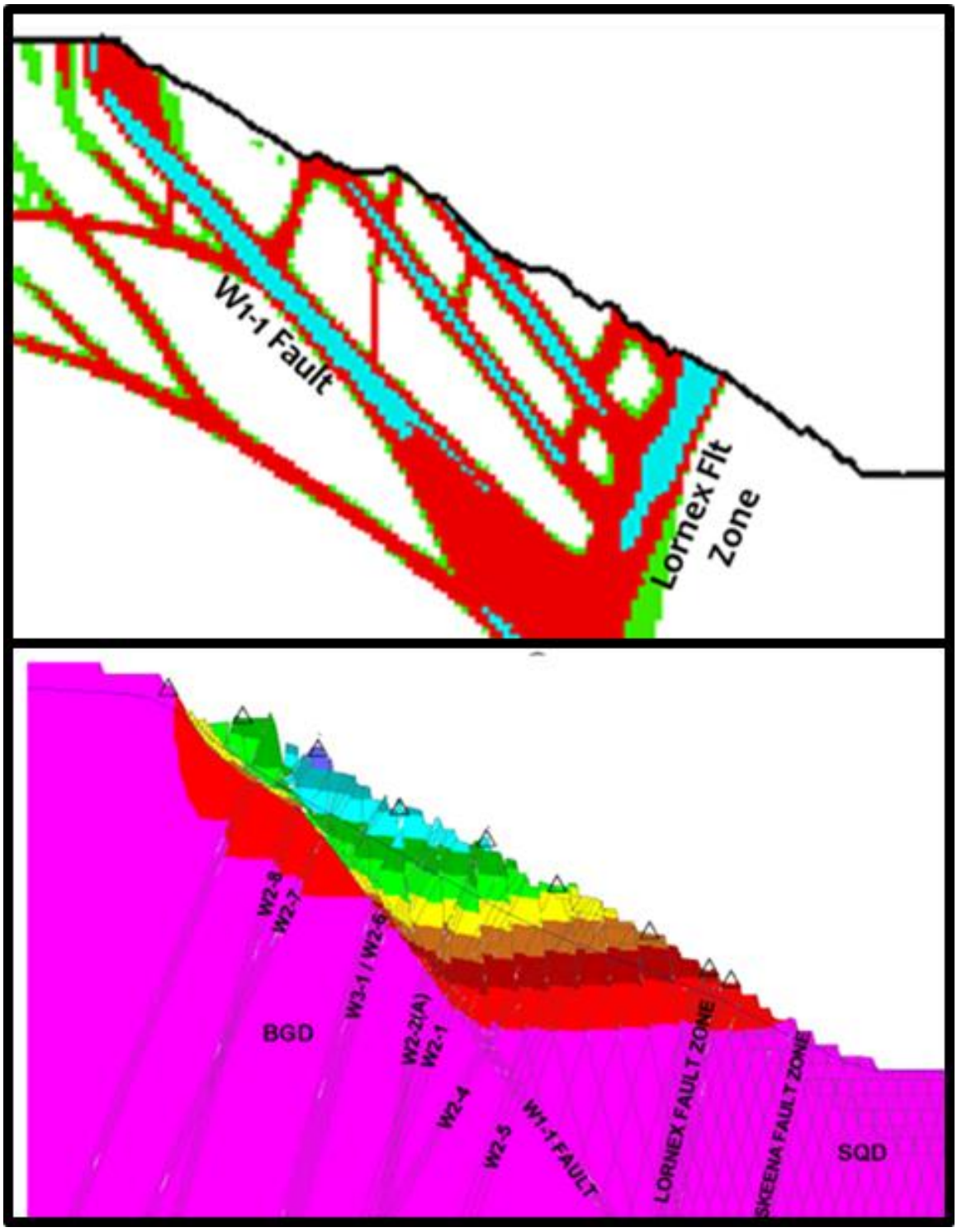

Figure 5.22. FLAC3D results of modelling of initiation and development of fault zones present in the west wall of the Lornex Pit (above), and comparison to the interpreted geotechnical section (below) reported by Piteau Associates (2005). Note that the two main faults, the Lornex and W1-1, are clearly reproduced in the modelling of fault initiation and development carried out here.

Table 5.5. FLAC3D model properties used in modelling of tectonic structures present in the Lornex west wall, and subsequent modelling of fault interaction with pre-mining stress initialization and pit slope excavation

Property	Host Rock	Fault
Deformation Modulus E_{rm} (GPa)	2.67	0.22
Host Poisson's Ratio	0.25	0.3
Cohesion – Peak (MPa)	0.681	0.112
Cohesion – Residual (MPa)	0.31	0.03
Friction – Peak (°)	55	40
Friction – Residual (°)	42	33
Tension (MPa)	0.05	0.01
Critical Strain Value	0.001	

5.3.1. Stage 2: Modelled Stress Heterogeneity and Influence on Modelled Slope Performance

The successful modelling of the fault development in the previous section can also be seen to have generated a complex stress field. Stress heterogeneity is generated during initialization of the pre-mining stress state based upon movements along the weaker faults. The resulting pre-mining stress field is significantly more complex than that based strictly on gravitational loading as would be the starting point for a conventional numerical analysis following the current state of practice. A comparison of numerical models of the stress state for the West Wall of the Lornex Pit is shown in Figure 5.23 using both the conventional approach and that where the initiation and development of the tectonic faults are first modelled. Each of the models has undergone a typical mining sequence of pushbacks to allow for stress to develop with excavation of the pit.

Of interest is the creation of low stress regions extending from surface near the faults, and of areas of relatively high stress concentrated between the faults. Near these low and high stress areas, additional damage behind the pit face can be expected, which in turn can have a significant influence on the slope deformation response and potential failure mechanism modelled.

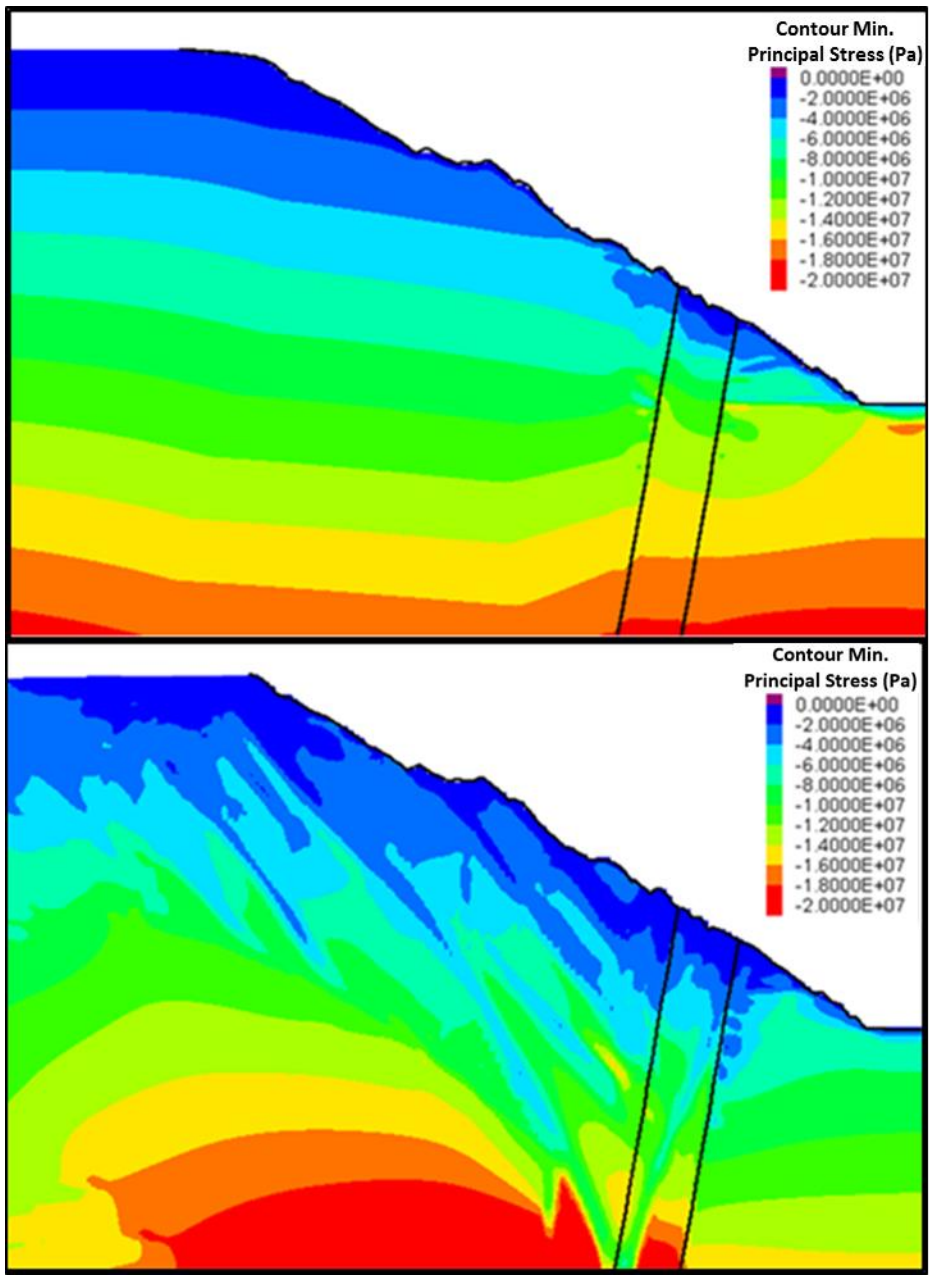

Figure 5.23. Modelled maximum principal stress field generated using a conventional numerical stress initialization approach (upper), and that where the tectonic faults are first explicitly modelled as part of the stress initialization procedure (lower).Note that the location of the Lornex Fault Zone is outlined in black for reference in both models. Compression is negative.

Stability analyses using the Shear Strength Reduction Factor method were undertaken for both the conventional gravity driven stress initialization procedure and the tectonic stress initialization procedure (as above). The models were run as strain softening with a critical strain of $1e^{-3}$ and properties for the

models are provide in Table 5.6 with fault properties within the tectonic model allowed to range between the Bethsaida Granodiorite (BGD) to the fault properties based on strain increments of $1e^{-4}$.

The model results indicate a stable slope in both cases, however, the Factor of Safety for the tectonic modelled initial stress field was calculated to be 1.75 and that for the conventional gravity driven model was 3.35 (Figure 5.24). This is a significant difference. This is likely due to the lack of a toe break plane within the continuum model, which requires the footwall material, the Skeena Quartz Diorite to be softened further for a rupture surface to localize and develop. The distinction between the results however does highlight that the level of detail in representing faults affects the outcome of the models and the stability results. The failure mechanism observed in the gravity driven model can be interpreted as a rock mass slump; however, that in the tectonic-based model shows a more significant control from the presence of the fault structure, which serves as a release surface as well as facilitating a more pronounced toe break out mechanism.

Table 5.6. FLAC3D model rock mass parameters used in the tectonic stability models

Unit	Density (kg/m^3)	Cohesion (MPa)	Friction Angle (°)	Tensile Cut-off (kPa)	Residual Cohesion (MPa)	Residual Friction Angle (°)	Residual Tensile Cut-off (kPa)	E_{rm} (GPa)
Skeena Quartz Diorite (SQD)	2700	0.261	38	100	0.20	30	0	2.5
Bethsaida Granodiorite (BGD)	2700	0.372	47	100	0.29	38	0	5.8
Fault Zone 1 (Tectonic Only)	2530	0.156	35	100	0.138	30	0	0.92
Fault Zone 2 (Tectonic Only)	2467	0.138	30	50	0.12	22	0	0.55
Fault Zone 3 (Tectonic / Gravity)	2400	0.12	22	10	0.1	20	0	0.17

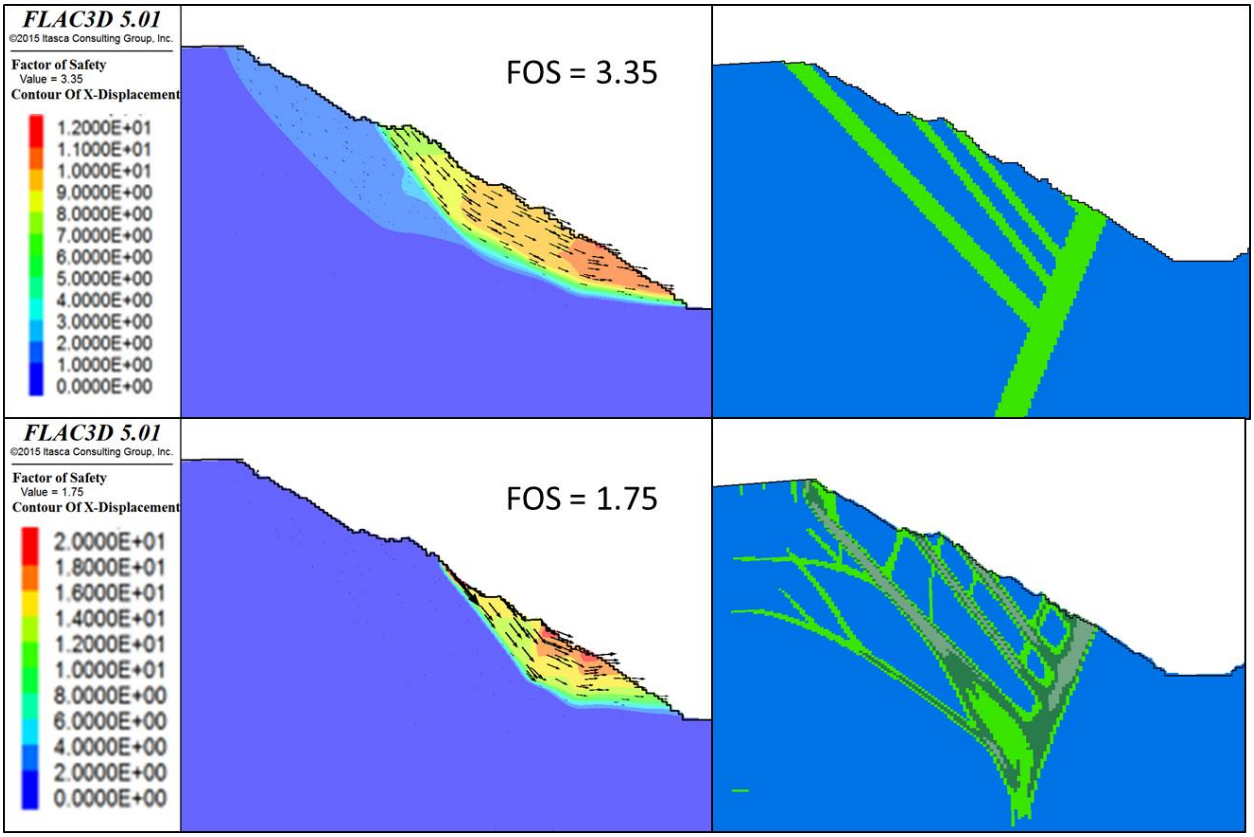

Figure 5.24. FLAC3D shear strength reduction comparative analysis of fault implementation methods. Factor of Safety (FOS) results for the THVC Lornex pit when using a conventional fault representation (above) and when using a more complex fault structure based on one that is first modelled (below).

5.4. Case History - Teck Highland Valley Copper Mine

5.4.1. Background and Pit Slope Behaviour

The Teck Highland Valley Copper (THVC) mine, as described in Section 3.2.3, is located near Kamloops in south-western British Columbia, Canada (Figure 5.25). Between 1989 and 1995, the west wall of the Lornex Pit had experienced up to 45m of displacement in the upper portion of the slope through a complex deep-seated toppling mechanism (Tosney et al., 2004). Early on, the toppling displacement was shown to occur along a set of steep faults dipping into the slope and was thought to be accommodated as the result of reduced confining stresses. Detailed numerical modelling of the west pit wall was undertaken by Rose and Schulz (2009), and they highlighted the importance of the pervasive structure and faults to the stability of the slope. A review of the slope displacement mechanism of the west wall to compare to the results of a pseudo-3-D radar monitoring experiment (Severin et al., 2013) generally agreed with Rose and Schultz's (2009) previous interpretation of the displacement mechanism. However, the new monitoring data and

interpretation highlighted the occurrence of significant bulging of the rock mass at the toe of the slope below the fault. This bulging of toe material is believed to be necessary to allow for the significant displacements observed in the upper sections of the slope which was not reflected in the earlier analyses conducted.

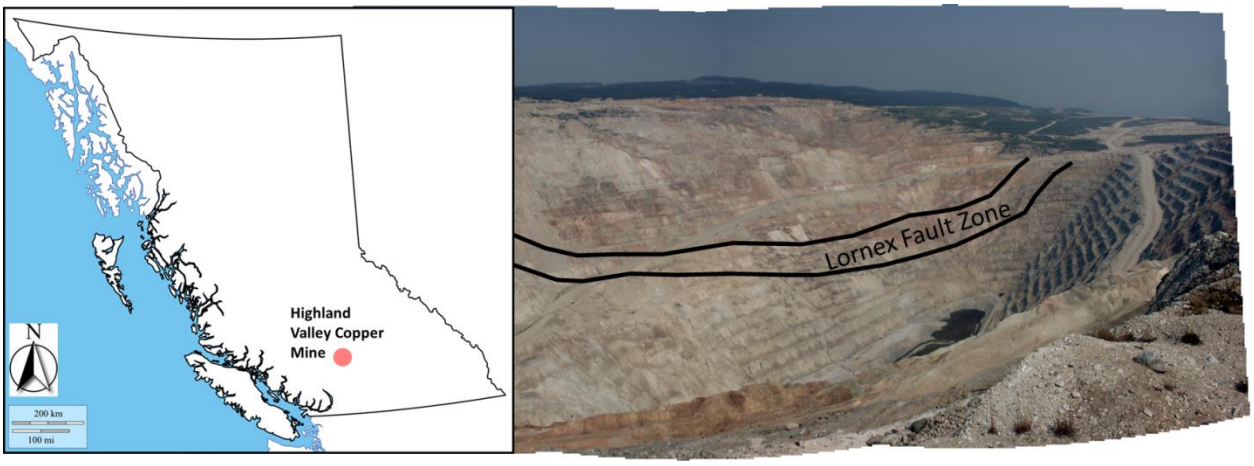

Figure 5.25. Location of Teck Highland Valley Copper mine (left) and a view of the north and west walls of the Lornex pit with the trace of the Lornex Fault Zone superimposed (right).

5.4.2. Fault Properties and Potential Damage

To examine the impact of the Lornex Fault Zone on stress and strain distribution of the slope and the potential associated damage, several 2-D distinct-element numerical models were constructed using the commercial software UDEC (Itasca, 2011). Within the models, the LFZ is represented as a 60m thick zone (comprising 7% of the overall slope height) and intersecting the slope face at approximately 25% of the slope height (measured from the toe) at an angle of incidence of 70°. The in-situ stress conditions were assumed to be hydrostatic (K=1) based on previous site investigations conducted on site (Piteau, 2005). The mining sequence used within the models included a series of 5 pushbacks with benches being excavated in 50 m intervals.

The properties for the numerical model, shown in Table 5.7, were determined through geotechnical characterization by Piteau Associates (2005). The fault deformation modulus used in the modelling was roughly 20% of the host rock material. A strain softening constitutive behaviour model was used which allows the post-peak strength to be reduced as a function of plastic shear strain. To model a brittle response, the rock mass cohesion was set to degrade sharply (friction was not softened) and the residual tensile strength was set to zero. To evaluate both the plastic shear and extensional strains, the values of each were

compared to find appropriate thresholds of plastic shear strain that would allow damage to initiate. Based on the results from the initial models, a value of 1e-3 plastic shear strain was chosen to represent the post-peak damage threshold.

Table 5.7. UDEC model input rock mass parameters for the THVC Lornex pit case study (based on Piteau, 2005)

Unit	Density (kg/m^3)	RMR/ GSI	σ_{ci} (MPa)	m_i	Cohesion (MPa)	Friction Angle (°)	Tensile Cut-off (MPa)	Residual Cohesion (MPa)
Skeena Quartz Diorite (SQD)	26	43	37.9	28	0.261	38	0.1	0.12
Bethsaida Granodiorite (BGD)	26	51	55.5	28	0.372	47	0.1	0.17
Fault Zone	22	25	20.0	28	0.156	22	0	-

Based on the conceptual sensitivity modelling presented earlier (section 5.3), the following damage states/responses might be expected. It should be noted that because the conceptual modelling was based on a 45-degree slope (the Lornex pit is a 30-degree slope), the estimated values based on these should be thought of as upper bounds.

- Fault Intersection Location: Conceptual modelling results suggest plastic shear and extensional strain damage limits of 25% and 30% of the slope height into the slope, respectively. Given the Lornex Pit slope height of 500 m, the plastic shear damage limits would extend 125 m and the extensional strain damage would extend 150 m into the slope;

- Fault Angle: Conceptual modelling results suggest a depth of plastic shear damage of approximately 15% (75 m) in the hanging wall and 25% (125 m) in the footwall. The depth of extensional strain damage would be expected to extend to 25% (125 m) in the hanging wall and 30% (150 m) in the footwall;

- Fault/Host Rock Strength Contrast: Given the relatively low contrast in deformation moduli between the fault and the host rock (0.27), plastic shear damage would be expected to extend approximately 15% (75 m) into the slope, while the extensional strain damage would be expected to extend approximately 35% (175 m) into the slope;

- Fault Thickness: The LFZ has been mapped as approximately 60 m thick, which is approximately 12% or the slope height. Expected plastic shear and extensional strain damage would be 25 and 35% in the hanging wall and 35 and 45% in the footwall.

5.4.3. Lornex Modelling Results

The results from the initial modelling of the Lornex pit are shown in Figure 5.26. These indicate the presence of zones of increased plastic shear and extensional strain in the footwall adjacent to the Lornex fault. This agrees with the conceptual sensitivity models presented previously. The volume of yielded elements within the model was determined for the final pit geometry after following the pit excavation sequencing, carried out in 9 steps. A comparison of the results without and with the fault, and in the hanging wall and footwall are provided in Figure 5.27.

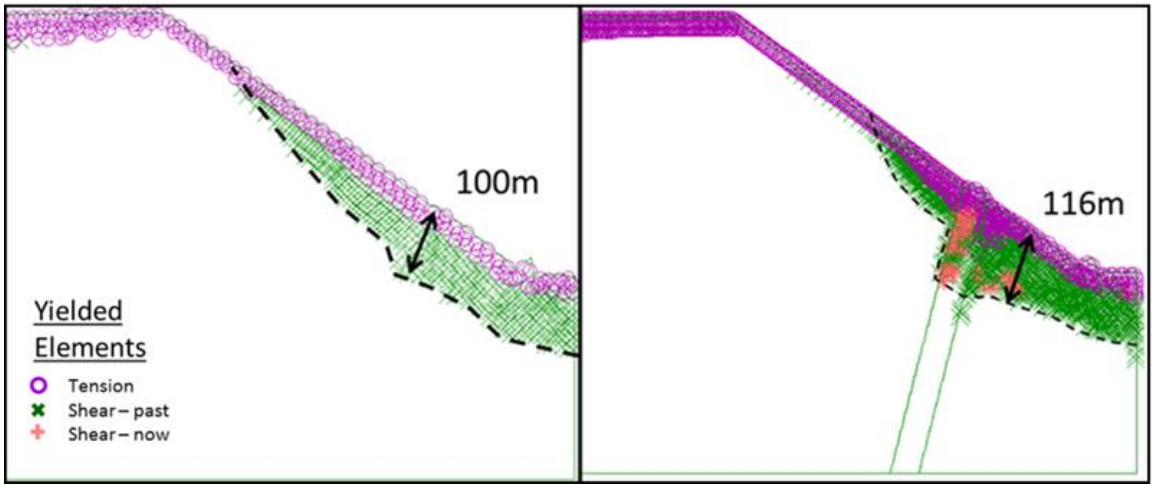

Figure 5.26. Initial UDEC model results indicating increased damage in the footwall of the fault during excavation at THVC Lornex west wall.

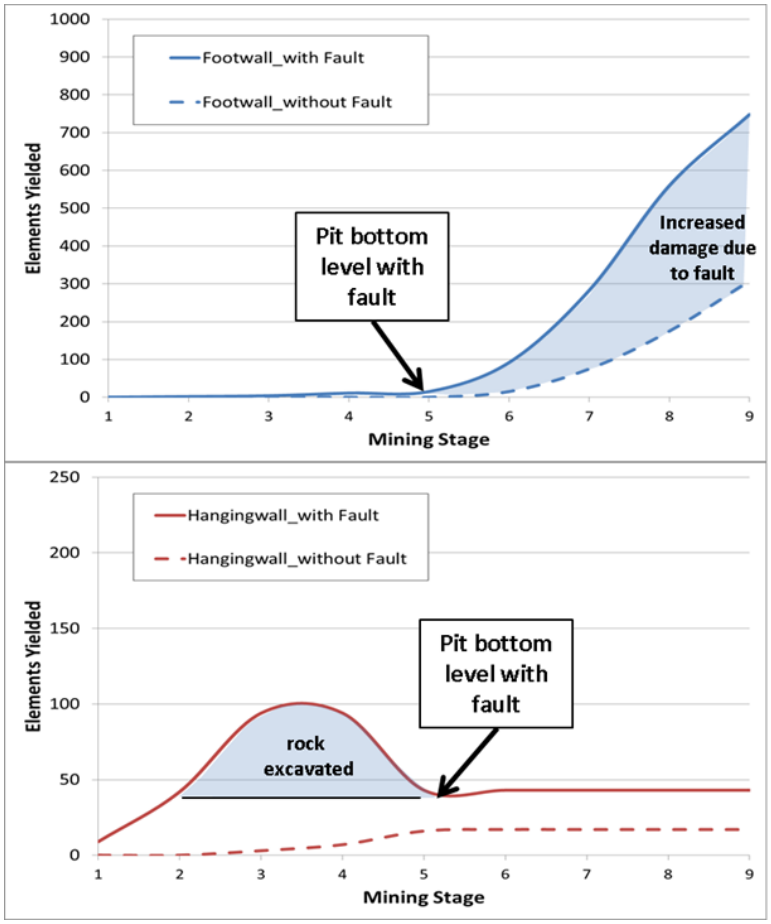

Figure 5.27. Damage (represented by yielded elements) with respect to mining stage for the footwall (above) and hanging wall (below) of the UDEC modelled Lornex Pit west wall. Results compare models that include the Lornex Fault (solid line) and those assuming a homogenous rock mass (dashed line).

A uniform mesh was used in which the elements were discretized with equal areas. This allows for the total number of elements to serve as a proxy for volume of yielded/damaged rock. Within the hanging wall, the presence of the fault allowed for a significant increase in the number of yielded elements to occur prior to the fault intersecting the pit bottom. Other than the yielding of rock in the pit floor, due to the stress concentration where the slope toe intersects the pit floor, the hanging wall appears to undergo a localized increase of yielding near the fault, but this yielding does not seem to increase as the pit continues to deepen. The rock mass within the footwall undergoes significantly more yielding when the fault is present than without the fault (200 to 300% more, both in tension and shear). The damage that initially occurs within the pit floor subsequently extends below the depth of the final pit floor elevation and the fault. The rock

mass and stress interactions that cause this increased damage situation are not well understood and are dependent on localized factors such as jointing patterns and the variation of intact rock strength.

To further evaluate the Lornex Pit west wall, a set of UDEC models were constructed in which the Lornex Fault structure was first modelled based on the findings presented in Section 5.4. Model properties were varied until a Lornex Fault with similar width developed together with splays such as the W1-1 fault defined by Rose and Scholz (2009). To this model, the detailed joint set geometries mapped in the pit (Piteau Associates, 2005) were added. A Voronoi overlay was also added to represent random degrees of freedom for potential brittle fracture paths to allow the joint-bounded blocks to fracture further. The model geometry is shown in **Error! Reference source not found.**.

The resulting stresses and development of the faults was then used as the initial pre-mining stress state and geometry for the simulation of the excavation of the open pit. The Lornex Pit was excavated following a mining sequence of 5 pushback stages with 50 m excavation steps to reflect the stress path experienced by the actual slope. 50m pushback steps were chosen to best reflect the mining history of the pit slopes.

Two constitutive models were considered to evaluate the effect of plastic shear strain and extensional strain resulting from interactions with the Lornex Fault zone on the overall stability of the west wall. These include:

- Strain-Softening Model – properties were developed by first scaling Hoek-Brown rock mass properties based on GSI and UCS properties outlined in Table 5.8 (Piteau, 2005), using the empirical relationships in Hoek et al. (2002). These were then converted to Mohr-Coulomb values, for which both upper and lower bound limits were established. The strain-softening behavior was then implemented by defining residual strength properties associated with increasing plastic shear strain values.

- Strain-Softening with Extensional Damage Model – using the same properties as those above but including weakening for areas in the model exceeding the extensional strain damage threshold. At each mining stage, extensional strains around the pit and faults were evaluated. If the value of the extensional strain was found to be greater than $5e^{-4}$, the rock mass strength in that area was weakened by applying a 'D' damage factor using the H-B criterion (see Hoek et al. 2002 for details). A 'D' factor of 0.7 was used. The value of $5e^{-4}$ was chosen to reflect a similar pattern and magnitude of extensional strain observed in the previously run Lornex models. This was implemented using a series of user-defined functions (using the program's internal language FISH), for which extensional strains are calculated and post-peak strength and deformation modulus values reduced where extensional strains exceed a set

limit. This limit and the rock mass strength reduction factors were then calibrated against the slope kinematics determined from the radar slope monitoring conducted on site.

Table 5.8 and Table 5.9 present the input properties used for the model shown in Figure 5.29. Groundwater conditions within the pit were assumed to be dry.

Table 5.8. UDEC rock mass properties for blocks in the Voronoi modelling of the Lornex Pit (THVC) case study

Model Units	Density (kg/m3)	Cohesion (MPa)	Friction Angle (degree)	Bulk Modulus (GPa)	Shear Modulus (GPa)	Tension (MPa)
Bethsaida Granodiorite (BGD) – Peak	2600	0.372	47	10	7.5	0.1
Skeena Quartz Diorite (SQD) - Peak	2600	0.498	55	1.56	0.93	0.1
Skeena Quartz Diorite (SQD) - Residual	2600	0.261	38	0.37	0.22	0.1
Skeena Quartz Diorite (SQD) – Reduced for extensional strain	2600	0.174	29	0.29	0.17	0.01
Faulted Rock	2200	0.156	22	0.85	0.59	0

Table 5.9. UDEC joint properties for discontinuities in the Voronoi modelling of the Lornex Pit (THVC) case study. The random discontinuities represent Voronoi segments along which intact rock bridge fracturing can be simulated

Structure	Dip (degree)	Dip Direction (degree)	Cohesion (MPa)	Friction Angle (degree)	Normal Stiffness (GPa/m)	Shear Stiffness (GPa/m)	Tension (MPa)
Joint Set 1	75	270	0.01	25	1	0.5	0
Joint Set 2	67	90	0.010	25	1	0.5	0
Joint Set 3	5	270	0.01	20	1	0.5	0
Random	-		0.1	35	1	0.5	0.0001
Extensional reduction			0	15	0.1	0.05	0

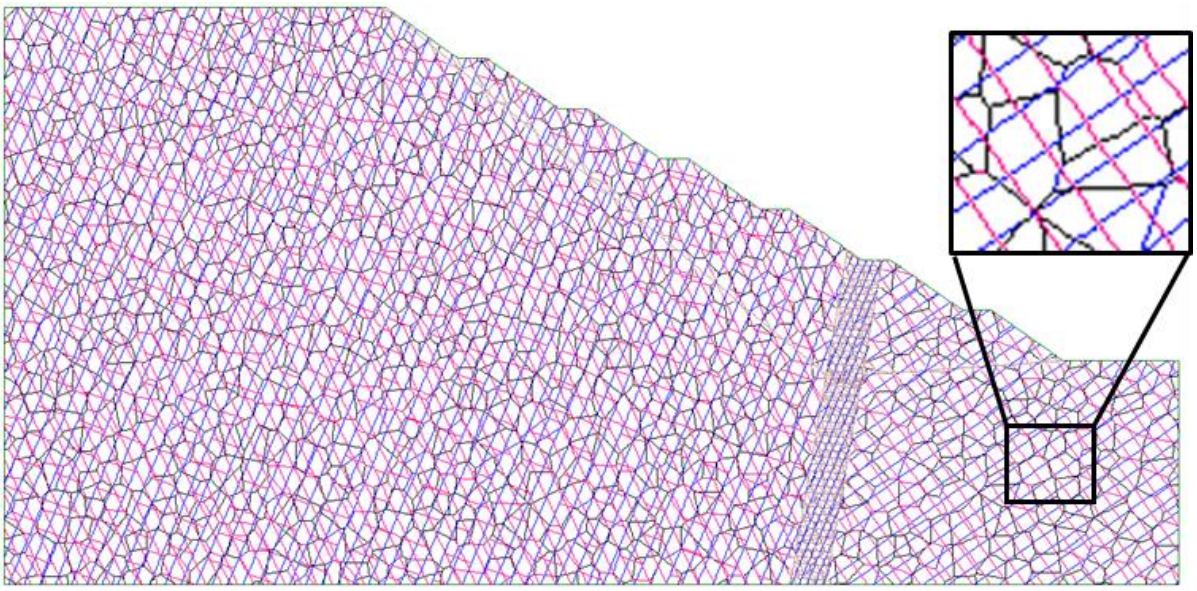

Figure 5.28 UDEC model set-up showing joint sets (red and blue) including random joints representing intact rock bridges (i.e., potential brittle fracture pathways) using voronoi tessellation (black).

The model results show that as the pit is excavated, stress interactions between the deepening toe of the slope and the complex, heterogeneous initial stress state arising from the modelling of the fault structure, results in zones of confinement loss that do not appear if the slope is modelled using a conventional approach. This leads to tensile failure and the development of extensional strain within both the hanging wall and footwall of the Lornex Fault Zone. Using the strain softening constitutive model, the stress interactions result in an area of yielded rock that extends up to approximately 120 m into the pit face. Figure 5.31 shows the depth of failure with a black dashed line, which is established from the plots of cohesion weakening and plastic shearing in the slope. Additional yielded rock near the fault within the model which includes the extensional damage is also indicated in the yielded state plot (Figure 5.31).

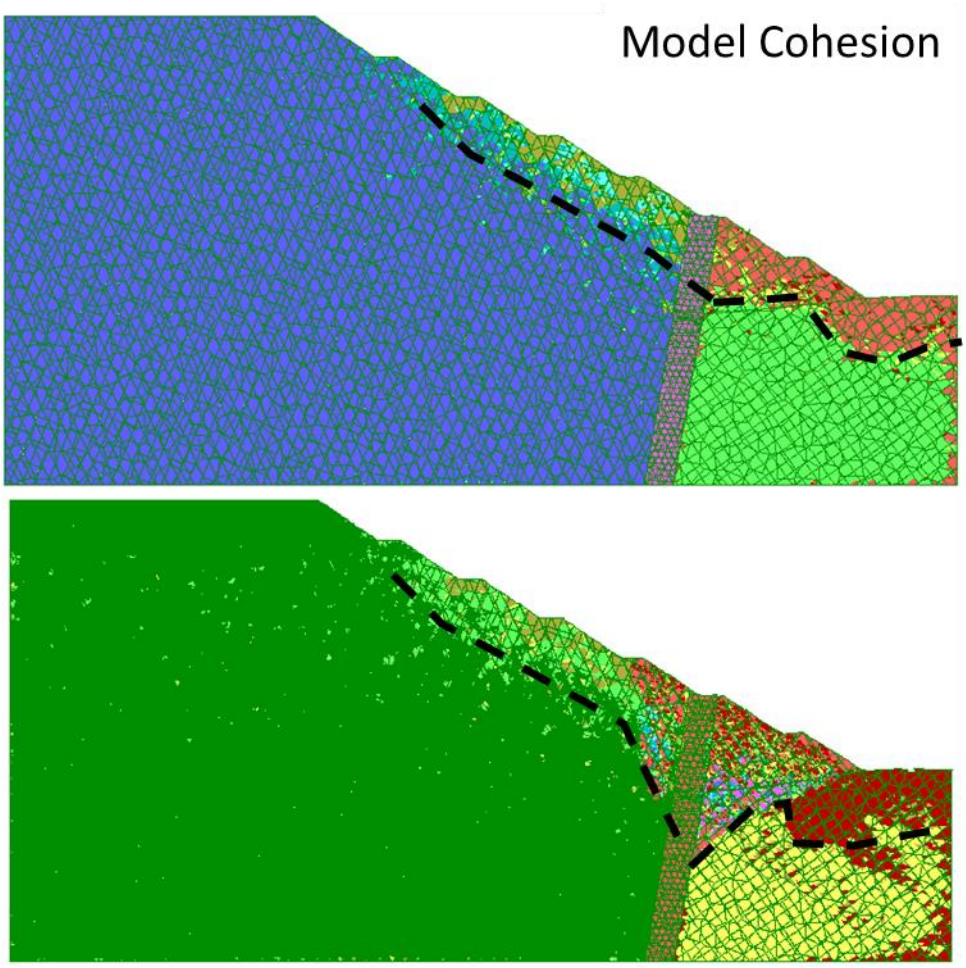

Figure 5.29 Depth of failure indicated by black line and reduced properties for strain softening model (above) and strain softening model with inclusion of reduced properties caused by extension (below) in UDEC.

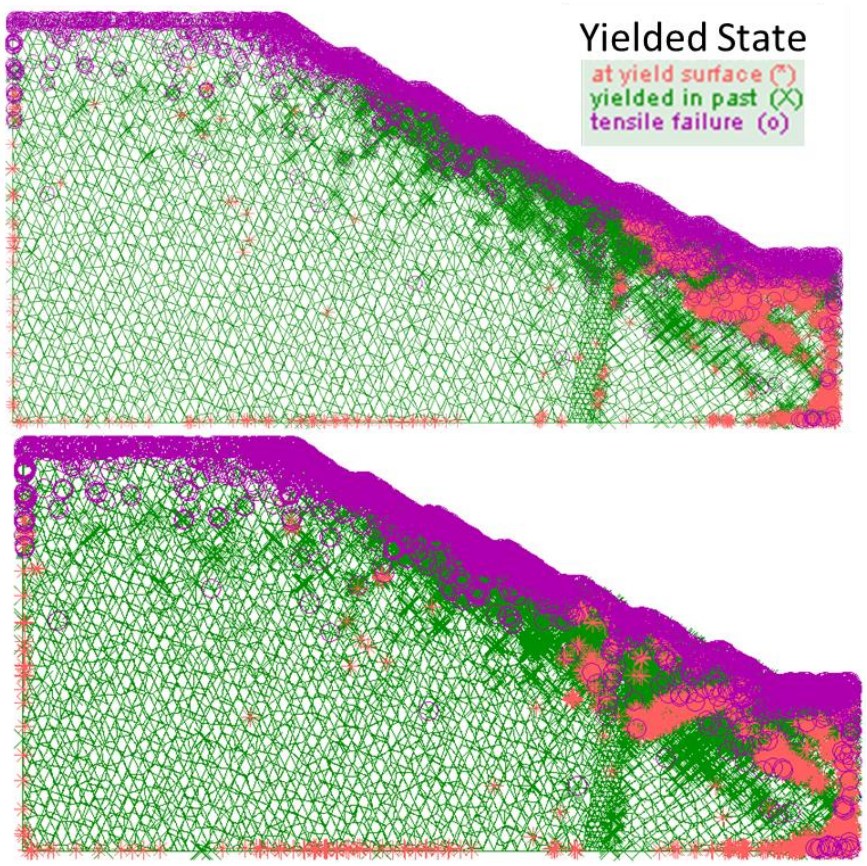

Figure 5.30 Depth of failure indicated by yielded material (pink and green) for strain softening model (above) and strain softening model with inclusion of reduced properties caused by extension (below) in UDEC.

The initial conceptual Lornex models suggested that a region of large deformation would develop between the fault and toe of the slope in response to significant yielding. However, this yield area did not undergo enough plastic shear strains to trigger the strength reduction (i.e., softening) properties and allow for mobilization of the slope. This can be observed in the x-displacements which did not exceed 2.0 m (Figure 5.31).

By including the extensional strain damage criterion, additional displacement (bulging) can be observed in the toe of the slope with a maximum displacement of up to 11 m (Figure 5.31). This bulging agrees with that detected in the radar monitoring data; the model results show that this toe bulging is required to achieve the toppling behavior observed in the upper portions of the slope. Additionally, softening of the toe of the slope allows for increased shearing along the W1-1 back fault (Figure 5.32). This shearing promotes movement within the upper blocks, producing the horst and graben structures observed at the top of the Lornex west wall. Although the models do not fully replicate the total amount of displacement observed

in the upper parts of the slope, the mechanisms and kinematics shown by including the extensional strain damage do reflect those observed in the pit. Displacement within the model may be under-predicted due to the assumption of dry hydrological conditions and the choice of 'D' factor used. Without the extensional strain criterion, the properties of the entire rock mass need to be softened to reproduce the displacements in the toe required to replicate the toppling behaviour in the upper slope. This softening of materials leads to a partial rock mass failure of the hanging wall material above the fault which allows for the movement above. This does not agree with field observations in the pit. Instead, the model results allowing for extensional strain show localization of a toe release rupture surface (Figure 5.30), followed by bulking of the toe and toppling in the upper slope.

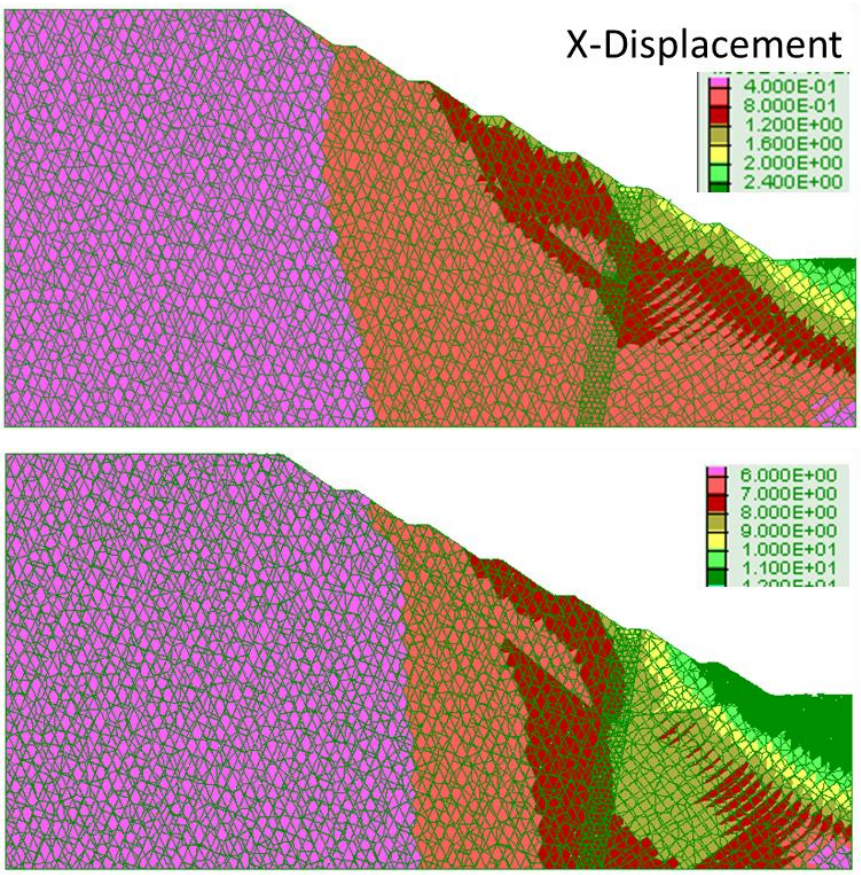

Figure 5.31. THVC Lornex pit model results indicating x-displacements (bottom) from Model 1 – Strain Softening (above) and Model 2 – Strain Softening with extensional strain (below).

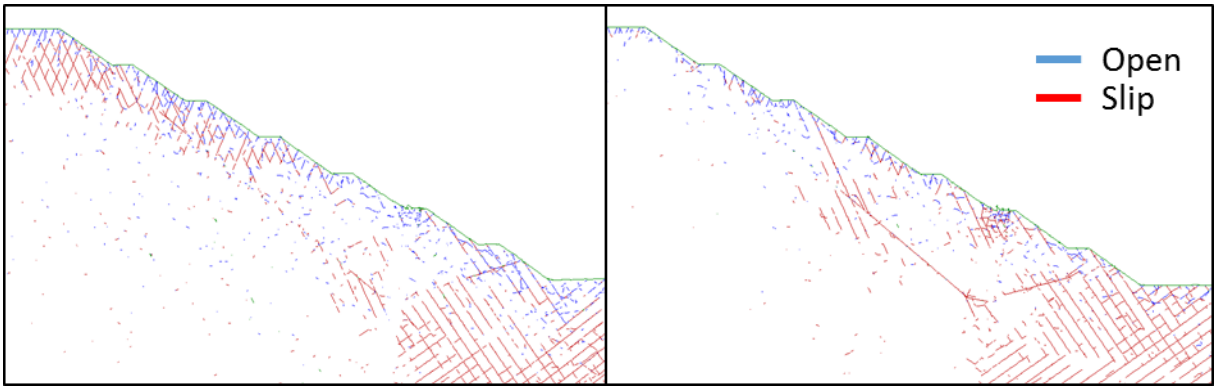

Figure 5.32. Open joints (blue) and joints undergoing shear displacement (red) for strain softening model (left) and strain softening with extensional strain (right).

Although the models do not fully replicate the amount of displacement in the upper section of the slope, the mechanisms resulting from including the extensional damage do reflect those observed in the pit as observed in the radar experiment. In previous models of the slope, the entire rock mass was softened to obtain the displacement magnitudes required to replicate the behaviour of the slope. This softening of materials leads to a partial rock mass failure of the hanging wall material above the fault which enables the movement above the fault.

5.5. Chapter Summary and Key Findings

Faults have long been identified as potential release planes and kinematic controls contributing to large, multi-bench slope failures. However, faults and fault damage zones should also be recognized for their ability to affect the regional and local rock mass and stress conditions in large open pits. Numerical modelling results presented in this chapter have identified several key fault characteristics and demonstrated the impact of these characteristics on stability analyses.

Damage surrounding fault zones within the open pit environment can be directly linked to stress heterogeneities created by the interaction between the faults and the mining induced stresses generated during excavation. The strain developed due to the stress heterogeneities include areas of high plastic shear strain near the toe of the slope and extensional strain near the fault.

Accordingly, an extensional strain criterion can be applied for assessing the impact that fault zones will have on varying slope designs to rock mass damage potential. This assessment can be undertaken quickly on basic designs prior to finalizing a pit shell by creating simple models. Similarly, an extensional strain

criterion can be used to determine if the stress state will be a consequential factor in the slope design as a project moves forward by conducting sensitivity analyses of possible in-situ stress conditions.

Based on results from the different 2-D and 3-D numerical models presented, the following key findings can be identified:

1. The choice of fault representation, including material strength and complexity, implemented in a numerical analysis can have a low to moderate effect on the orientations, magnitudes and distribution of stresses that develop in response to pit excavation;

2. Fault shape or complexity has a moderate to major impact on the development of stresses and the resultant damage within a numerical model. The style and nature of the fault should be characterized intensely during pre-mining feasibility and design studies;

3. Fault strength and deformability have a moderate to major impact on the stress redistribution in the pit slope and should be emphasized in the geotechnical characterization for pit slope stability analyses and potential pit designs;

4. Faults with deformation moduli that are less than 10% of those for the adjacent host rock mass, can have a significant impact on the principal and deviatoric shear stresses generated within a slope;

5. Both the location and the angle of the fault intersection with the pit slope have a moderate to major impact on the development of localized stresses, both high shear stresses and lower extensional stresses.

6. Increased plastic shear strain and extensional strain is expected within the toe of an open pit slope if bisected by a fault damage zone. This strain is generally unaccounted for in most numerical modelling packages used to evaluate slope stability;

7. Natural in-situ stress perturbations surrounding tectonic faults can interact with mining-induced stresses to produce damage that would otherwise not be present if the rock mass was homogeneous (i.e., no faults present);

8. Modelling fault development as an initial numerical modelling step to better capture the complexity of faults structures and stress heterogeneity, rather than simply prescribing the locations of the faults and specifying a simply initial stress distribution, shows significant value if the tectonic control is well understood and can be used to constrain fault characterization and location;

9. The effect of allowing the faults to first develop in the model can lead to differences in the final stability analysis; and

10. By accounting for extensional strain damage in the model, a reasonable distribution of down-graded rock strength can be included within the numerical model which can affect the displacement observed in the slope without downgrading the entire rock mass.

CHAPTER 6 CONCLUSIONS AND RECOMMENDATIONS FOR FURTHER WORK

6.1. Summary of Conclusions

Designing large, complex open pit slopes requires the interaction and participation of several technical leads, including mine planning, resource geology, geotechnical engineering, surface water engineering, blast engineering and many others. Understanding the impact of large fault zones on the displacement, stress, strain, and mechanics of a large open pit slope can greatly impact the geotechnical and mining recommendations used to design both interim and final pit shells to provide a safe and reliable slope that maximizes financial return for large scale projects. Unexpected inter-ramp and pit slope scale failures are the biggest geotechnical risk to an open pit operation and by increasing the stack height within the pit slopes, mining companies are in turn increasing the uncertainty of the mechanics of the slope by creating pit walls for which there is very little empirical information to compare against.

Within these large open pit slopes, one of the more significant sources of uncertainty involves the mining induced stress state. The in-situ stress conditions surrounding large porphyries that are typically exploited by large open pit or mass mining can be expected to be highly complex due to interactions between fault structures and changes during the geological history of the deposit. Local stress perturbations created through the interaction between the existing faults and the excavation of the open pit can affect the behavior of the rock mass either though increased plastic shear strain or through extensional brittle fracturing. Reliable slope designs require a solid foundation of the structural history of the area which creates the local in-situ stress as well as the interaction with the existing structures within the slope and the excavation of a free face.

Several numerical methods can be used to evaluate the potential instability and displacement mechanics of a slope, each with advantages and limitations that need to be considered prior to an analysis. Stress-induced brittle fracturing can only be captured or represented by advanced numerical techniques. Even then this representation is far from perfect. It is important to understand the role in which geological structures can affect large open pit slopes so that the geotechnical engineer can have appropriate input into the pit design by highlighting areas of potential concern to the mine planners. The response of pit slope behavior to faults and fault zones within increasingly deeper open pits was reviewed using a state-of-the-art experiment and several numerical modelling approaches. A summary of the more relevant conclusions presented in each chapter is provided below.

Chapter 2 – Background Information

A review of the current literature and state of practice highlights several key limitations in the understanding of slope behavior around fault structures, which become even more critical as stresses are increased either through tectonic stress heterogeneity or increasing pit depths. A list of the identified limitations includes:

- Traditional monitoring tools such as geodetic prisms are an absolute necessity for a base understanding of pit slope displacement. However, although this provides accurate 3-D displacement histories at specified points, displacements between sparsely placed prisms must be interpolated and important local behavior controlled by fault structures may be missed;
- Emergent technologies such as ground-based radar or InSAR have become increasingly essential in the monitoring of large pit slopes, however, they represent line-of sight displacements only and behaviour can easily be misinterpreted;
- The effect of in-situ stresses within open pits and its effect on stability is still unknown and often overlooked. However, there is enough evidence that local stress perturbations in combination with mining induced stresses can result in increased brittle fracturing within the rock; and
- Understanding the slope kinematics, potential failure mechanisms and forecasting these based on the available geotechnical data and geological history of an ore deposit, can influence the approach and tools used in stability analyses to be carried out. However, the current state of knowledge on rock slope behavior expected in deep pits or high stress pit conditions is lacking, which can lead to unexpected and complex pit slope failure modes and therefore risk.

Chapter 3 – Detection of Differential Pit Slope Displacements near Fault Structures

A first of its kind experiment involving the simultaneous deployment of two ground-based radar systems was conducted to collect continuous, line of sight displacement data in “stereo” of a large, moving open pit slope bisected by a large fault. The simultaneous monitoring with two synthetic aperture radar units has led to the construction of a high resolution, pseudo-3D displacement map of a large open pit rock slope. Analysis of the corresponding displacement vector map allowed an interpretation of the overall slope kinematics to be resolved. The 3-D radar experiment could identify localized movements related to smaller-scale geological structures and changes in pit wall slope orientation.

The radar monitoring clearly provided a significant increase in coverage above that possible using geodetic prisms, with over 25,000 common displacement points. The need to extrapolate displacements between prisms is avoided and small areas of high displacement that may pose potential safety concerns can be better identified and monitored. Furthermore, areas which cannot be monitored due to poor or dangerous access can be covered by the radar without the need to install prisms.

Understanding of the pit slope kinematics was significantly improved using the pseudo 3-D radar data. This has the potential to add significant value to a mine project where the mine plan is considering a pit wall pushback to deepen the pit. In such cases, the influence of the controlling nature of any major faults and smaller structures on the pit wall movements can be investigated and better understood with respect to pit geometry, slope deformation kinematics, evolving failure mechanisms, and ultimately geo-risk. This is the subject of ongoing research, and involves the integration of the 3-D slope deformation map with advanced 3-D numerical modeling. Modelling in Chapter 5 using the distinct element code 3DEC was carried out to further investigate and validate the kinematic model derived from the 3-D radar data. In parallel, the 3-D radar data was used to calibrate the model with respect to the controlling influence of important fault and joint properties, including location, persistence, and strength characteristics. These can then be projected for future deepening of the pit and pushback of its slopes.

The value added to radar monitoring demonstrated by these results include:

- Providing new insights with respect to kinematic controls resulting from known, or unknown, structures (e.g., as a sliding surface);
- Better resolving trends in vertical or horizontal displacements across the pit slope; and
- Identifying focal points for damage in response to stress concentrations and heterogeneity.

Chapter 4 - Influence of Stress Heterogeneity on Large Open Pit Slopes

Stress conditions within a pit slope can be affected by a range of factors, ranging from the regional scale to the pit wall scale. In-situ stress regimes, topography, pit geometry, and increased depth were seen to play an important role in the development of pit wide induced stresses contributing to zones more prone to specific types of kinematic failures or more complex failures requiring shear through intact rock bridges. Combinations of geometry and stress orientation can incur stress increases of 40% or more around the pit. As pit depths deepen, these localized concentrations of stress only increase.

Wall scale factors such as changes in lithology and large scale structures were seen to influence both stress conditions which may contribute to large, multi-bench slope failures, as well as impact the stresses within the slope. Much of the historical experience in open pit design and the influence of tectonic faults involves pit slopes that are less than 500 m in height. However, as the next generation of open pits are designed to greater depths (i.e., higher stress environments), faults and fault damage zones should also be recognized for their ability to affect the regional and local stress conditions. Numerical modelling results presented in this chapter were used to investigate these factors and the role of faults in creating stress heterogeneity, which when combined with mining induced stress and relaxation, can promote slope instability.

Based on results from the different 3-D numerical models reported, the following conclusions were drawn:

- Stress heterogeneity around open pits, especially pits greater than 300 m depth, can be affected by several factors ranging from regional to pit to slope scale;
- Open pit design and geometry can have a dramatic impact on the concentration of stresses around an open pit (up to 40%) which can influence the potential failure mechanisms observed in these areas;
- Deviatoric stresses increase dramatically in deeper open pits, suggesting these designs are more susceptible to plastic shear yielding at the toe of the slope. The increase in deformation should be accounted for in the design of the larger open pits by shallowing the inter-ramp angle rather than assuming joint-controlled kinematic behavior associated with shallower pits;
- Mining induced stresses created by the excavation of an open pit are heavily influenced by faults, whether they are relatively large faults zones, or more narrow, discrete structures;
- The stress heterogeneity created during the excavation of an open pit and its interaction with any fault zones present, can extend well behind the immediate face of the open pit slope, up to 75% of the pit diameter;
- Faults with deformation moduli that are less than 10% of those of the adjacent host rock mass, can have a significant impact on the principal and deviatoric shear stresses generated within a slope;
- Anisotropic rock masses are particularly sensitive to changes in stress orientation and magnitude;
- Small variations in stress orientations and magnitudes can have a critical effect on the yielding and shearing in the nearby rock mass, as shown through the modelling of the 10 x 10 x 10 m cubes at

the Palabora mine. Additional damage due to changes in stresses can lead to slope failure in some situations by connecting structures, especially in anisotropic rock; and

- Mine sequencing strategies should be employed, where possible, that reduce the number of horizontal pushbacks, especially if the pit wall is intersected by a fault zone. This will reduce the amount of stress heterogeneity experienced by the rock mass in the final pit wall.

Chapter 5 – Importance of Characterization and Representation of Faults and Fault Damage Zones in Large Open Pit Stability Models

The analyses carried out in Chapter 5 confirmed the increased potential of rock mass damage through increased plastic shear strain and extensional strain near fault damage zones in deep open pits. It was determined that this damage evolves with the continued excavation of an open pit or with the development of an underlying block cave. Within deeper pits, the increased in-situ stresses lead to larger potential for damage near faults.

Damage surrounding fault zones within the open pit environment can be directly linked to stress heterogeneities created by the interaction between the faults and the mining-induced stresses generated during excavation. The strain that develops in response to the stress heterogeneities include areas of high plastic shear strain near the toe of the slope and extensional strain near the fault.

The results demonstrate the application of an extensional strain criterion being applied for assessing the impact of a fault zone on varying slope designs with respect to rock mass damage potential. This assessment can be undertaken quickly on basic designs prior to finalizing a pit shell using simplified models. Similarly, extensional strain criterion can be used to determine if the stresses generated will be a critical factor in the slope design by conducting sensitivity analyses of possible in-situ stress conditions.

Based on results from the different 2-D and 3-D numerical models reported, the following conclusions can be drawn:

- The choice of fault representation, including material strength and complexity, implemented in a numerical analysis can have a significant impact on the orientations, magnitudes and distribution of stresses that develop in response to pit excavation;

- The fault shape complexity has a moderate to major impact on the development of stress and the resultant damage within a numerical model. The style and nature of the fault should be characterized thoroughly during pre-mining feasibility and design studies;
- Fault strength and deformability have a moderate to major impact on the stress redistribution around the pit, and should be emphasized in the geotechnical characterization for a pit slope stability analyses and pit design;
- Faults with deformation moduli that are of high contrast to the host rock (< 10%) have been shown to have a significant impact on the adjacent stresses (both principal and shear stresses) within a slope;
- Both the location and the angle of the fault intersection with the slope face have a moderate to major impact on the development of localized stresses, both in terms of higher plastic shear stresses and increased extensional stresses;
- Increased plastic shear strain and extensional strain damage is expected within the toe of an open pit slope if bisected by a fault zone. This strain is generally unaccounted for in most numerical modelling analyses used to evaluate slope stability;
- Natural in-situ stress perturbations surrounding tectonic faults can interact with mining-induced stresses to produce damage that would otherwise not be present if the rock mass was homogeneous (i.e., faults were not present or accounted for);
- Modelling the development of fault structures and resulting stress heterogeneity within a numerical analysis as an initial step to a stability analysis, rather than simply prescribing the fault location and gravity stress field, may prove advantageous if the tectonic controls are well understood and can be used to help constrain the fault modelling;
- The effect of allowing the faults to first develop in the numerical model can lead to differences in the final stability analysis; and
- By including extensional strain damage in a model, a reasonable distribution of weakened rock strengths can be accounted for within the numerical model, which can affect the slope displacements without the need to reduce the strengths of the entire slope to obtain observed values.

6.2. Future Work

Several areas for future research were identified during this dissertation which are listed below:

- The radar experiment conducted involved only two radar units due to the cost and limited availability of such systems. For a full 3-D radar experiment, three radar monitoring systems, simultaneously recording, would be required to construct a full 3-D vector displacement map of a pit slope.

- Additional 3D radar experiments in varying conditions, such as very hard brittle rock, or a very large pit slopes would provide insight into the controlling nature of faults on rock deformation and movement in pit slope movements not associated with large damage zones.

- Investigate the current condition of rock mass behind the pit face and compare rock mass parameters and photos to information collected prior mine excavation. This comparison could allow for a measurement of the effect of pit excavation on the rock mass strength. Choosing sites near faults and sites where large faults do not exist would allow for the damage associated between fault and pit excavation to be quantified.

- Comparing and contrasting numerical analyses for a variety of tectonic environments to can allow for knowledge to be gained on the location, amount, and style of damage expected in the pit face prior to the excavation.

- The development of an extensional based criterion that can be used quickly and reliably to determine the amount of expected damage near faults and near the excavation of a large open pit would help engineers design around expected rock mass conditions with the goal to gain confidence in pit design and potential failure mechanisms.

REFERENCES

Amadei, B. (1996). Importance of anisotropy when estimating and measuring in situ stresses in rock. *Int. Journal of Rock Mechanics and Mining Sciences and Geomechanics Abstracts.* Vol. 33, pp 293-325.

Beck, D.A., Brady, B.H.G., and Grant, D.R. (1996). Analysis of seismicity and rock deformation during open stoping of a deep orebody. In *Proceedings of ISRM International Symposium – EUROCK 96*, Turin, Italy, 2-5 September 1996. International Society for Rock Mechanics, pp. 1171-1177.

Board, M., Seldon, S., Brummer, R. and Pakalnis, R. (2000) Analysis of the failure of a large hanging wall wedge: Kidd Mine Division, Falconbridge, Ltd. CIM Bulletin 93(1043): 89-97.

Bond, D. J., Chrzanowski, A., and Kim, D. (2007). *Bringing GPS into Harsh Environments for Deformation Monitoring* (pp. 51-178). Department of Geodesy and Geomatics Engineering, University of New Brunswick.

Brown, D. W., Kalgren, P. W., Byington, C. S., and Roemer, M. J. (2007). Electronic prognostics–a case study using global positioning system (GPS). *Microelectronics Reliability*, 47(12), 1874-1881.

Brummer, R. K., Li, H., Moss, A., and Casten, T. (2006). The transition from open pit to underground mining: an unusual slope failure mechanism at Palabora. In *Proceedings of the International Symposium on Stability of Rock Slopes in Open Pit Mining and Civil Engineering*, Cape Town, South Africa (pp. 411-420).

Carnec, C., Massonnet, D., and King, C. (1996). Two examples of the use of SAR interferometry on displacement fields of small spatial extent. *Geophysical Research Letters*, 23(24), 3579-3582.

Casagli, N., Catani, F., Del Ventisette, C., and Luzi, G. (2010). Monitoring, prediction, and early warning using ground-based radar interferometry. *Landslides*, 7(3), 291-301.

Cigna, F., Osmanoğlu, B., Cabral-Cano, E., Dixon, T. H., Ávila-Olivera, J. A., Garduño-Monroy, V. H., and Wdowinski, S. (2012). Monitoring land subsidence and its induced geological hazard with Synthetic Aperture Radar Interferometry: A case study in Morelia, Mexico. *Remote Sensing of Environment*, 117, 146-161.

Cooke, D.R., Hollings, P., and Walshe, J.L. (2005). Giant porphyry deposits: Characteristics, distribution, and tectonic controls. *Economic Geology*, vol.100, no. 5. pp. 801−818.

Cox, S.F., Knackstedt, M.A., and Braun, J., (2001). Principles of structural control on permeability and fluid flow in hydrothermal systems. *Reviews in Economic Geology*, vol. 14, 1-24.

Cundall, P. A. (1990). Numerical modelling of jointed and faulted rock. In *Mechanics of jointed and faulted rock* (Vol. 12, No. 3, pp. 11-18). Balkema, Rotterdam.

Di Traglia, F., Intrieri, E., Nolesini, T., Bardi, F., Del Ventisette, C., Ferrigno, F., and Stefanelli, C. T. (2014). The ground-based InSAR monitoring system at Stromboli volcano: linking changes in displacement rate and intensity of persistent volcanic activity. *Bulletin of Volcanology*, 76(2), 1-18.

Diederichs, M. S. (2003). Manuel Rocha medal recipient rock fracture and collapse under low confinement conditions. *Rock Mechanics and Rock Engineering*, vol. 36, no.5, pp. 339-381.

Diederichs, M.S., Kaiser, P.K., and Eberhardt, E. (2004). Damage initiation and propagation in hard rock during tunneling and the influence of near-face stress rotation. *International Journal of Rock Mechanics and Mining Sciences*, vol. 41, no.5. pp. 785-812.

Dight, P.M., and Bogacz, W.V. (2009). The application of a deposit tectogenesis in pit slope geotechnical engineering: a case example, In *International Symposium on Rock Slope Stability in Open Pit and Civil Engineering*, Santiago, Chile, CD-ROM, pp. 9 pp.

Dight, P. M. (2006). JOURNAL PAPERS-Pit wall failures on 'unknown' structures. *Journal of the South African Institute of Mining and Metallurgy*, 106(7), 451-458.

Donzé, F., Mora, P., and Magnier, S. A. (1994). Numerical simulation of faults and shear zones. *Geophysical Journal International*, 116(1), 46-52.

Dunnicliff, J. (1988). Field Instrumentation for Monitoring Field Performance.

Eberhardt, E., Stead, D., Coggan, J.S., and Willenberg, H. (2003). Hybrid finite/discrete-element modelling of progressive failure in massive rock slopes. In 1*0th Congress of the International Society for Rock Mechanics*, Johannesburg. The South African Institute of Mining and Metallurgy, Johannesburg, 275-279.

Eberhardt, E., Stead, D. and Coggan, J.S. (2004). Numerical analysis of initiation and progressive failure in natural rock slopes - the 1991 Randa rockslide. *International Journal of Rock Mechanics and Mining Sciences*. Volume 41, no. 1. pp. 69-87.

Eberhardt, E., Watson, A. D., & Loew, S. (2008). Improving the interpretation of slope monitoring and early warning data through better understanding of complex deep-seated landslide failure mechanisms. In

Landslides and engineered slopes: from the past to the future, 10th Int. Symp. on Landslides and Engineered Slopes. Taylor & Francis, Xi'an (pp. 39-51).

Elmo, D., Yan, M., and Stead, D. (2007). The importance of intact rock bridges in the stability of high rock slopes. In Proce*edings of the International Symposium on Rock Slope Stability in Open Pit Mining and Civil Engineering*, Perth, Australia, 12–14 September, 2007. pp. 253– 266.

Evans, J.P. and Chester, F.M. (1995). Fluid-rock interaction in faults of the San Andreas system: Inferences from San Gabriel fault rock geochemistry and microstructures. *Journal of Geophysical Research*. Vol. 100, no. B7. pp. 13007 – 13020.

Farrar, C. R., Darling, T. W., Migliori, A., and Baker, W. E. (1999). Microwave interferometers for non-contact vibration measurements on large structures. *Mechanical Systems and Signal Processing*, 13(2), 241-253.

Faulkner, D. R., Jackson, C. A. L., Lunn, R. J., Schlische, R. W., Shipton, Z. K., Wibberley, C. A. J., and Withjack, M. O. (2010). A review of recent developments concerning the structure, mechanics and fluid flow properties of fault zones. *Journal of Structural Geology*, 32(11), 1557-1575.

Fruneau, B., Achache, J., and Delacourt, C. (1996). Observation and modelling of the Saint-Etienne-de-Tinée landslide using SAR interferometry. *Tectonophysics*, 265(3), 181-190.

Fukuzono, T. (1985). A new method for predicting the failure time of a slope. In *Proceedings of the 4th International Conference and Field Workshop in Landslides*, Tokyo (pp. 145-150).

Fujii, Y., Kiyama, T. and Ishijima, Y. (1994a). A study on tensile strain criterion. *Journal of Mineral Material Process*. Institute. Japan, vol. 110, pp. 211–214 (in Japanese)

Fujii, Y., Kiyama, T. and Ishijima, Y. (1994b). A new criterion for brittle failure of rock. In Proceedings *MMIJ/AusIMM Joint Symposium '94*, Ube, pp. 469–476

Glazer, S. (2003). Seismology: A tool for cave monitoring. Rio Tinto Internal Presentation.

Haimson, B.C. and Rummel, F. (1982). Hydrofracturing stress measurements in the Iceland drilling project drill hole at Reydasfjordur, Iceland. *J.Geophys*., Vol. 87, pp. 6631-49.

Hajiabdolmajid, V., & Kaiser, P. (2002). Slope stability assessment in strain sensitive rocks. In *ISRM International Symposium-EUROCK 2002*. International Society for Rock Mechanics.

Hamman, E. C. F., and Coulthard, M. A. (2007). Developing a numerical model for a deep open pit. In *Slope Stability 2007–Proceedings International Symposium on Rock Slope Stability in Open Pit Mining and Civil Engineering*, Potvin (ed), Australian Centre for Geomechanics.

Harries, N., Noon, D., & Rowley, K. (2006). Case studies of slope stability radar used in open cut mines. *Stability of Rock Slopes in Open Pit Mining and Civil Engineering Situations*, 335-342.

Harries, N. J., & Roberts, H. (2007). The use of slope stability radar (SSR) in managing slope instability hazards. In *First Canada-US Rock Mechanics Symposium Proceedings* (pp. 53-59).

Harrison, J.P., Xiang, J., and Latham, J.P. (2010). Stress heterogeneity in a fractured rock mass modelled with the combined finite-discrete element method. In *44th US Rock Mechanics Symposium,* Salt Lake City, USA, June, 2010.

Hebblewhite, B.K. (2003). Northparkes findings – The implications for geotechnical professionals in the mining industry. In *1st Australasian Ground Control in Mining Conference*. Sydney: UNSW Press, pp. 3-10.

Herrera, G., Davalillo, J. C., Mulas, J., Cooksley, G., Monserrat, O., and Pancioli, V. (2009). Mapping and monitoring geomorphological processes in mountainous areas using PSI data: Central Pyrenees case study. *Nat. Hazards Earth Syst. Sci*, 9, 1587-1598.

Hoek, E., and Brown, E.T. (1980) Underground Excavations in Rock. London: Institution of Mining and Metallurgy 527 pages.

Hoek, E., Read, J., Karzulovic, A., and Chen, Z. (2000). Rock slopes in civil and mining engineering. In: *Proceedings of the International Conference on Geotechnical and Geological Engineering*, Melbourne.

Hormazabal, E., Veramendi, R., Barrios, J., Zuñiga, G., Gonzalez, F. (2013). Slope design at Cuajone Pit, Peru. In *Proceedings of the International Symposium on Slope Stability in Open Pit Mining and Civil Engineering*. Brisbane, Australia, September, 2013. pp 527 – 540.

Imber, J., Holdsworth, R. E., Smith, S. A. F., Jefferies, S. P., and Collettini, C. (2008). Frictional-viscous flow, seismicity and the geology of weak faults: a review and future directions. Geological Society, London, Special Publications, 299(1), 151-173.

Itasca Consulting Group Inc. (2003) 3DEC (3-Dimensional Distinct Element Code), Version 3.0. Minneapolis, Minnesota.

Itasca Consulting Group. Inc. (2011). UDEC – Universal Dimensional Distinct Element Code, Version 5.0, Itasca, Minneapolis

Itasca Consulting Group, Inc. (2012). FLAC3D — Fast Lagrangian Analysis of Continua in Three Dimensions, Ver. 5.0. Minneapolis

Jarosz, A., and Wanke, D. (2003). Use of InSAR for monitoring of mining deformations. In *Proceedings of FRINGE 2003 Workshop*, Frascati, Italy (pp. 1-5).

Kaiser, P.K. and Kim, B.H. (2008). Rock mechanics advances for underground construction in civil excavations and mining. In *Proceedings of KRMS 2008*, Seoul, South Korea, pp 3 – 16.

Kaiser, P.K. and Kim, B.H. (2015). Characterization of strength of intact brittle rock considering confinement-dependent failure processes. *International Journal of Rock Mechanics and Mining Sciences*, vol. 48, no. 1. pp. 107-119.

Kattenhorn, S. and Marshall, S. (2006). Fault-induced perturbed stress fields and associated tensile and compressive deformation at fault tips in the ice shell of Europa: implications for fault mechanics. *Journal of Structural Geology* 28: 2204-2221.

Kirsch, G., (1898). Die theorie der elastizitat und die bedurfnisse der festigkeitslehre. Veit. Deit. Ing. Vol. 42 no. 28. pp. 797-807.

Kwaśniewski M. and Mogi K. (1990). Effect of the intermediate principal stress on the failure of a foliated anisotropic rock. In *Mechanics of Jointed and Faulted Rock*. H.-P. Rossmanith (ed.). Rotterdam: Balkema. pp 407-416.

Kwaśniewski, M. and Takahashi, M. (2010). Strain-based failure criteria for rocks: State of the art and recent advances. Rock Mechanics in Civil and Environmental Engineering. Taylor and Francis Group, London. pp 45 – 56.

Laubscher, D. H. (1993). Planning mass mining operations. Comprehensive rock engineering principles practice and projects, 2, 547-583.

Leech, S., & McGann, M. (2007). Open Pit Slope Depressurization using Horizontal Drains–a Case Study. In *Slope Stability 2007: Proceedings of the 2007 International Symposium on Rock Slope Stability in Open Pit Mining and Civil Engineering* 12-14 September 2007, Perth, Australia. Potvin, Y. (Ed.). Australian Centre for Geomechanics, The University of Western Australia.

Li, X., Wu, Z., Takahashi, M. and Yasuhara, K. (2000). An experimental study on strain-based failure criteria of brittle materials. *Journal of Applied Mechanics* Vol. 3. pp. 387–394.

Little, M. J. (2006). Slope monitoring strategy at PPRust open pit operation. In *Proceedings of the International Symposium on Stability of Rock Slopes in Open Pit Mining and Civil Engineering*.

Logan, A. S., Villaescusa, E., Stampton V. R., Struthers, M. A. and Bloss, M. l. (1993). Geotechnical instrumentation and ground behaviour monitoring at Mount Isa, In *Geotechnical instrumentation and monitoring in open pit and underground mining*, Szwedzicki, T. (ed.), A. A. Balkema, Rotterdam, Netherlands, pp. 321- 329.

Lorig, L. J. (2009). Challenges in Current Slope Stability Analysis Methods. In *International Symposium on Rock Slope Stability in Open Pit and Civil Engineering*, Santiago, Chile, CD-ROM.

Lorig, L.J. and Brady, B.H.G. (1984). A hybrid computational scheme for excavation and support design in jointed rock media. Design and performance of underground excavations. E.T. Brown and J.A. Hudson (eds). London: British Geotechnical Society. pp. 105-112.

Lorig, L.J., and Calderón Rojo, A. (2002). Modeling Time-Dependent Slope Deformation at Chuquicamata Mine. In *Proceedings of the EUROCK 2002 (ISRM International Symposium on Rock Engineering for Mountainous Regions*), Madeira, Portugal, November 2002, Lisbon: Sociedade Portuguesa de Geotecnia, 2002. pp. 137-143.

Love, A.E.H. (1927). A treatise on the mathematical theory of elasticity. New York: Dover.

Lynch, R.A. and Malovichko, D.A. (2006). Seismology and slope stability in open pit mines. In *International Symposium on Stability of Rock Slopes in Open Pit Mining and Civil Engineering*, Johannesburg, South Africa. pp. 375–389.

Maerten, L., Gillespie, P. and Pollard, D.D. (2002). Effects of local stress perturbation on secondary fault development. *Journal of Structural Geology*. vol.24, no. 1. pp. 145-153.

Maloney, S., Kaiser, P., and Vorauer, A. (2006, January). A re-assessment of in situ stresses in the Canadian Shield. In Golden Rocks 2006, The *41st US Symposium on Rock Mechanics (USRMS*). American Rock Mechanics Association.

Martin, C.D. (1990). Characterizing in situ stress domains at the AECL Underground Research Laboratory. *Canadian Geotechnical Journal*, vol. 27, no.5. pp. 631–646.

Martin, C. D., Kaiser, P. K. and Christiansson, R. (2003). Stress, instability and design of underground excavations. *International Journal of Rock Mechanics and Mineral Sciences*. Vol. 40, no. 7. pp. 1027–1047.

Martino, S., and Mazzanti, P. (2014). Integrating geomechanical surveys and remote sensing for sea cliff slope stability analysis: the Mt. Pucci case study (Italy). *Natural Hazards and Earth System Science*, 14(4), 831-848.

Massonnet, D., M. Rossi, C. Carmona, F. Adragna, G. Peltzer, K. Feigl, and T. Rabaute. (1993). The displacement field of the Landers earthquake mapped by radar interferometry, *Nature*, 364, pp. 138-142.

Massonnet, D., K. Feigl, M. Rossi and F. Adrangna. (1994). Radar interferometric mapping of deformation in the year after The Landers Earthquake, *Nature*, 369, pp. 227-230.

Mitchell, T. M., and Faulkner, D. R. (2012). Towards quantifying the matrix permeability of fault damage zones in low porosity rocks. *Earth and Planetary Science Letters*, 339, 24-31.

Monserrat, O., Crosetto, M., and Luzi, G. (2014). A review of ground-based SAR interferometry for deformation measurement. ISPRS *Journal of Photogrammetry and Remote Sensing*, 93, 40-48.

Muskhelishvili, N.I. (1953). Some basic problems of the mathematical theory of elasticity. 4th edn, translated by J.R.M. Radok. Gronigen: Noordhoff.

Myrvang, A., Hansen, S.E., and Sørensen, T. (1993). Rock stress redistribution around an open pit mine in hard rock. *International Journal of Rock Mechanics and Mining Sciences*. Vol. 30, no. 7. pp. 1001 – 1004.

Noferini, L., Mecatti, D., Macaluso, G., Pieraccini, M., and Atzeni, C. (2009). Monitoring of Belvedere Glacier using a wide-angle GB-SAR interferometer. *Journal of Applied Geophysics*, 68(2), 289-293.

Noorani, R., Ahangari, K., and Aloodari, S. (2011). The influence of horizontal stress on the failure mechanism and slope stability in Chador-Malu Iron Ore Mine. In *Proceedings Slope Stability 2011: International Symposium on Rock Slope Stability in Open Pit and Civil Engineering*, Vancouver, Canada. September, 2011.

Pariseau, W. G. (2007). Fitting failure criteria to laboratory strength tests. *International Journal of Rock Mechanics and Mining Sciences*, 44(4), 637-646.

Pieraccini, M., Noferini, L., Mecatti, D., Atzeni, C., Teza, G., Galgaro, A., and Zaltron, N. (2005). Integration of radar interferometry and laser scanning for remote monitoring of an urban site built on a sliding slope. *Geoscience and Remote Sensing*, IEEE Transactions on, 44(9), 2335-2342.

Piteau Associates Engineering Ltd., (2000) Numerical modelling of the effects of open pit deepening and block cave mining on the stability of the East and North walls. Internal Report.

Piteau Associates Engineering Ltd. (2005) Assessment of pit wall stability and slope displacement as a result of interaction between the open pit and underground mine. Internal Report.

Poliakov, A. N. B., Podladchikov, Y., and Talbot, C. (1993). Initiation of salt diapirs with frictional overburdens: numerical experiments. *Tectonophysics*, 228(3), 199-210.

Read, J and Stacey, P. (2009). Guidelines for Open Pit Slope Design. CSIRO Publishing, Collingwood.

Reeves, B., Noon, D., Stickley, G., and Longstaff, D. (1997). Monitoring rock slope deformation by radar interferometry. In *Proceedings of the Workshop on Applications of Radio Science WARS'97* (pp. 119-123). Australian Academy of Science.

Reusch, F., Beck, D., and Tyler, D. (2009). Quantitative forecasting of sidewall stability and dilution in Sub-Level Caves. In *Proceedings of the 43rd US Rock Mechanics Symposium*, Asheville. American Rock Mechanics Association.

Robotham, M. (2011). Slope design in large open pit mines. *Proceedings Slope Stability 2011: International Symposium on Rock Slope Stability in Open Pit and Civil Engineering*, Vancouver, Canada. September, 2011.

Rödelsperger, S., Läufer, G., Gerstenecker, C., and Becker, M. (2010). Monitoring of displacements with ground-based microwave interferometry: IBIS-S and IBIS-L. *Journal of Applied Geodesy*, 4(1), 41-54.

Rose, N. (2011). Investigating the effects of mining-induced strain in open pit slopes. *Proceedings Slope Stability 2011: International Symposium on Rock Slope Stability in Open Pit and Civil Engineering*, Vancouver, Canada. September, 2011.

Rose, N. D., and Hungr, O. (2007). Forecasting potential rock slope failure in open pit mines using the inverse-velocity method. *International Journal of Rock Mechanics and Mining Sciences*, 44(2), 308-320.

Rose, N. and Scholz, M. (2009). Analysis of complex deformation behaviour in large open pit mine slopes using the Universal Distinct Element Code (UDEC). In *Proceedings Slope Stability 2009: International Symposium on Rock Slope Stability in Open Pit and Civil Engineering*, Santiago, Chile. November, 2009.

Sainsbury, B., Pierce, M. and Mas Ivars, D. (2008) Analysis of caving behavior using a synthetic rock mass – ubiquitous joint rock mass modelling technique. In *Proceedings First International FLAC / DEM Symposium on Numerical Modelling*, 25–27 August, Minneapolis. Itasca.

Sainsbury, D., Pothitos, F., Finn, D. and Silva, R. (2007). Three-dimensional discontinuum analysis of structurally controlled failure mechanisms at the Cadia Hill open pit. In *Proceedings of the International Symposium on Rock Slope Stability in Open Pit Mining and Civil Engineering*, Perth, Australia, 12–14 September, 2007. pp. 307– 320.

Sassi, W. and Faure, J.L. (1997). Role of faults and layer interfaces on the spatial variation of stress regimes in basins: inferences from numerical modelling. *Tectonophysics*, vol. 166, pp. 101–119.

Savin, G.N. (1961). Stress concentrations around holes. London: Pergamon.

Schöpfer, M. P., Childs, C., and Walsh, J. J. (2006). Localisation of normal faults in multilayer sequences. *Journal of Structural Geology*, 28(5), 816-833.

Schulz, S. E., and Evans, J. P. (2000). Mesoscopic structure of the Punchbowl Fault, Southern California and the geologic and geophysical structure of active strike-slip faults. *Journal of Structural Geology*, 22(7), 913-930.

Seery, J. M. (2007). Monitoring of a Large Wall Failure at Tom Price Iron Ore Mine. In *Slope Stability 2007: Proceedings of the 2007 International Symposium on Rock Slope Stability in Open Pit Mining and Civil Engineering*, 12-14 September 2007, Perth, Australia (p. 333). Australian Centre for Geomechanics, The University of Western Australia.

Severin, J., Eberhardt, E., Ngidi, S. & Stewart, A. (2009). Importance of understanding 3-D kinematic controls in the review of displacement monitoring of deep open pits above underground mass mining operations. In *Rock Engineering in Difficult Conditions, Proceedings of the 3rd Canada–US Rock Mechanics Symposium,* Toronto. Edited by M. Diederichs & G. Grasselli. Canadian Rock Mechanics Association, e-Paper, 3914, 12 pp.

Severin, J., Eberhardt, E. and Woo, K. (2010) Influence of major fault zones on 3-D ground deformations caused by open pit - block cave interactions. In *Caving 2010, Proceedings Second International Symposium on Block and Sublevel Caving*, 20–22 April 2010, Perth.

Severin, J., and Eberhardt, E. (2012). Influence of stress path during the transition from open pit to block cave mine - a Palabora example. *Proceedings of the MassMin Conference*, Sudbury, Canada. 10-14 June 2012.

Severin, J., Eberhardt, E., and Fortin, S. (2013). Open pit numerical model calibration using a pseudo three-dimensional radar monitoring technique. *Proceedings Slope Stability 2013: International Symposium on Rock Slope Stability in Open Pit and Civil Engineering*, Brisbane, Australia. September, 2013.

Severin, J., Eberhardt, E., Leoni, L., and Fortin, S. (2014). Development and application of a pseudo-3D pit slope displacement map derived from ground-based radar. *Engineering Geology*, 181, 202-211.

Sibsone, R.H. (2001). Seismogenic framework for hydrothermal transport and ore deposition. *Reviews in Economic Geology* vol. 14, pp. 25-50.

Sillitoe, R.H. (2010). Porphyry copper systems. *Economic Geology*. vol. 105. pp 3-41.

Sjöberg, J. (1996). Large Scale Slope Stability in Open Pit Mining – A Review. Luleå University of Technology, Luleå, Sweden. Technical Report, 229 pp.

Sjoberg, J. (2013). Numerical analysis, slope design and in-situ stress. In *Proceedings Slope Stability 2013: International Symposium on Rock Slope Stability in Open Pit and Civil Engineering*, Brisbane, Australia. September, 2013.

Smith, J.V. (2013). Interpreting local critical orientations of structural weakness in relation to stress and dilatancy in rock slopes. In *Proceedings Slope Stability 2013: International Symposium on Rock Slope Stability in Open Pit and Civil Engineering*, Brisbane, Australia. September, 2013.

Stacey, T.R. (1981). A simple extension strain fracture criterion for fracture of brittle rock. *International Journal of Rock Mechanics and Mining Sciences*, vol. 18, no.6. pp. 469-474.

Stacey, T.R., and Swart, A.H. (2001) Practical rock engineering practice for shallow and opencast mines. SIMRAC. The safety of mines research advisory committee, 66 p.

Stacey, T. R., Xianbin, Y., Armstrong, R., and Keyter, G. J. (2003). New slope stability considerations for deep open pit mines. *Journal of the South African Institute of Mining and Metallurgy*, 103(6), 373-389.

Stacey, T. R. (2007). Slope stability in high stress and hard rock conditions. In *Slope Stability 2007– Proceedings International Symposium on Rock Slope Stability in Open Pit Mining and Civil Engineering*, Potvin (ed), Australian Centre for Geomechanics (pp. 12-14).

Stead, D., and Eberhardt, E. (2013). Understanding the mechanics of large landslides. *Italian Journal of Engineering Geology Environment*. Series, 6, pp. 85-112.

Stow, R. (1997). Application of SAR interferometry to the imaging and measurement of neotectonic movement applied to mining and other subsidence/downwarp modelling. ESA SP.

Su, S. (2004). Effect of fractures on in situ rock stresses studied by the distinct element method. *International Journal of Rock Mechanics and Mining Sciences*, vol. 41, no.1. pp. 159-164.

Su, S., and Stephansson, O. (1999). Effect of a fault on in situ stresses studied by the distinct element method. *International Journal of Rock Mechanics and Mining Sciences*, vol. 36, no. 8. pp. 1051-1056.

Sukurai, S. (1981). Direct strain evaluation technique in construction of underground openings. In *Proceedings of the 22nd U.S. Symposium on Rock Mechanics*, Cambridge, USA, June 29-July 2, 1981. pp. 278-282.

Talich, M., Glöckner, M., Böhm, O., Antoš, F., Soukup, L., Havrlant, J., and Šolc, J. (2014). The Application of the Ground-based InSAR technique for the deformation monitoring of concrete hydropower dam Orlík on Vltava river. In *INGEO 2014—6th International Conference on Engineering Surveying*, Prague, Czech Republic, April 3–4, 2014.

Tanno, T., Hirano, T., and Mtasui, H. (2010). Development of method for evaluation of three-dimensional distribution of in situ stress state and preliminary estimation of applicability. *Rock Stress Earthquakes*, pp. 521-526.

Tarchi, D., Casagli, N., Moretti, S., Leva, D., and Sieber, A. J. (2003). Monitoring landslide displacements by using ground-based synthetic aperture radar interferometry: Application to the Ruinon landslide in the Italian Alps. *Journal of Geophysical Research: Solid Earth*, 108(B8).

Taylor, J. D. (2001). 4 Ultra-Wideband Radar Receivers. Ultra-wideband radar technology, 75.

Tosney, J. R., Milne, D., Chance, A.V., and Amon, F. (2004). Verification of a large scale slope instability mechanism at Highland Valley Copper. *International Journal of Mining, Reclamation and Environment*. vol. 18, no. 4. pp 273 - 288.

Walker, P., Knight, P., Johnson, T., and Speight, H. (2006). Pushback 8 South – A case study in pit slope management In *Stability of Rock Slopes in Open Pit Mining and Civil Engineering Situations*. Johannesburg: SAIMM, Symposium Series S44, pp. 435–450.

Warpinski, N.R., Branagan, P., and Wilmer, R. (1985). In-situ stress measurements at US DOE's multiwall experiment site, Mesaverde group, Rifle, Colorado. *J. Petrol Technol*., Vol. 37, pp. 527-36.

Wesseloo, J. and Sweby, G.J. (2008). Microseismic Monitoring of Hard Rock Mine Slopes. In *Proceedings of SHIRMS 2008*. Perth, Australia. Australian Centre for Geomechanics. Y. Potvin (ed).

Wesseloo, J. and Dight, P. (2009) Rock mass damage in hard rock open pit mine slopes. In *Slope Stability 2009, International Symposium on Rock Slope Stability in Open Pit and Civil Engineering*, Santiago, Chile, CD ROM.

Whitehead, W.S., hunt, E.R., and Holditch, S.A. (1987). The effects of lithology and reservoir pressure on the in-situ stresses in the Waskon field, In *Proceedings SPE/DOE Joint Symp. On Low Permeability Reservoirs*, Denver, Paper SPE/DOE 16403, pp. 139-52.

Willenberg, H., Loew, S., Eberhardt, E., Evans, K. F., Spillmann, T., Heincke, B., and Green, A. G. (2008). Internal structure and deformation of an unstable crystalline rock mass above Randa (Switzerland): Part I—Internal structure from integrated geological and geophysical investigations. *Engineering Geology*, 101(1), 1-14.

Yang, D.Y., Brouwer, K.J., Sheets, R.J., St Louis, R.M., and Douglas, S.J. (2011). Large-scale slope instability at the Gold Quarry Mine, Nevada. In *Proceedings Slope Stability 2011: International Symposium on Rock Slope Stability in Open Pit and Civil Engineering*, Vancouver